UNIVERSITÀ
DEGLI STUDI DI BARI
ALDO MORO

DIPARTIMENTO INTERATENEO DI FISICA "M. MERLIN"
Dottorato di ricerca in Fisica - Ciclo XXXII
Settore Scientifico Disciplinare FIS/02

Bound states in the continuum in one-dimensional qubit arrays

Dottorando:
Domenico Pomarico

Supervisori:
Ch.mo Prof. Saverio Pascazio
Dott. Francesco V. Pepe

Coordinatore:
Ch.mo Prof. Giuseppe Iaselli

ESAME FINALE 2020

Contents

Introduction

Things that have worked for a long time are preferable - they are more likely to have reached their ergodic states. At the worst, we don't know how long they'll last

Nassim Taleb,
"The black swan"

Quantum systems display a wide variety of behaviors related in an essential way with mathematical structures. This characterization includes the complexity a physicist has to face with during experimental tests for a model: at this stage the implementation of approximations represents a key ingredient, which may affect predictions depending on the targeted coarse-grained level. In Chapter 1 two example of the latter approach are encountered, consisting in the dipolar and rotating wave approximation used to simulate the Friedrichs-Lee model [42], defined in the restricted one-excitation sector of a Hamiltonian commuting with the total number of excitations, thus representing our family of commuting observables.

Fundamental methods to characterize the eigensystem of the presented exactly solvable model are shown in Chapter 2, where the Dyson-Neumann expansion is applied to the Hamiltonian resolvent, thus yielding the definition of self-energy. Our interest for this quantity resides in its predictions about the existence of bound states in the continuum according to a non-perturbative approach. This thesis is focused in overcoming the usual approach exploited in waveguide quantum electrodynamics (WQED), based on the linearization of the dispersion relation. If, on one hand, this approximation simplifies the theoretical framework for experimental feasibility, on the other hand it misses emerging phenomena such as plasmonic bound states, associated with non propagating photons, and degeneracy lifting for bound states in the continuum. In a more appropriate terminology these new features are included through a complete characterization of the interaction form factor, which determines the

analytical structure of the complex energy plane [40], as made in Chapter 3 to test the model for a single two-level emitter.

In Chapter 4 the generation of entanglement between a pair of emitters, corresponding to a interatomic distance spanned by half-integer multiples of the emitted wavelength, appears as a benchmark for the relation linking the Friedrichs-Lee model and bound states associated with a purely point spectrum immersed in an absolutely continuous one. Renormalized propagator poles are described both numerically and according to an approximation which provides analytic expressions holding true in the weak coupling regime. Plasmonic off-resonance states are introduced, playing a key role also in Chapter 5 because they emerge in stronger coupling regimes. Indeed, in the two-excitation sector, the double atomic excitation does not involve any bound state in the continuum, but just below the energetic cutoff for photons propagation, where the plasmonic type holds. A correlated emission of photons is characterized according to the variation of the interatomic distance.

The focus on the one-excitation sector led to a complete characterization of the eigensystem for any number of two-level systems in proximity of eigenvalues corresponding to the resonance condition between interatomic distance and emitted wavelength half-integers multiples, with distances sufficiently large to make the single mode coupling effective. In Chapter 6 systems with three and four emitters are described, with a full treatment of the analytic structure imposed by the form factor, whose effect consists in removing eigenvalues degeneracy. Pole trajectories obtained in the variation of free parameters reveal a phenomenon, for small values of the distance, opposite to the splitting out of electromagnetic field in subsystems of the chain observed in the large distance regime: at some critical distances poles scatter along the real line, thus providing the emergence of new eigenstates with the bosonic field covering wider parts of the one-dimensional lattice. In Chapter 7 the complexity reduction implemented with the truncation of interactions up to nearest-neighbors characterizes the self-energy matrix as a Laplacian one associated with finite differences on graphs, which provides an eigensystem composed by spin-waves, the aforementioned multimerization phenomenon for an odd number of emitters and the presence of super-radiant states as a typification of regular graphs.

Part I

Friedrichs-Lee model simulators

Chapter 1

The Friedrichs-Lee model

It will be impossible to answer any one question completely without at the same time answering them all

Paul Dirac,
"The Quantum Theory of the Emission and Absorption of Radiation"

During the 20^{th} century the study of decay phenomena boosted an enormous amout of research in mathematics and physics [2, 25, 38, 85, 102, 120, 121, 136]: considering two major references per field we can mention E. Wigner in his foundation of random matrix theory [137], a topic involving usual tools for the analytical treatment as propagators resummations, E. Fermi with the first theoretical attempt in describing the coupling between vector currents associated with Dirac spinors [52].

The non-relativistic version of the latter approach corresponds to Lee's model, where a neutral fermionic particle decays in another fermion of lower mass and a scalar relativistic boson, with key ingredients residing in renormalization for physical quantities as mass, coupling constant and scattering amplitude. The mass of the decaying particle belongs to the free spectrum, while the complete Hamiltonian yields a dynamics not including the initial fermion as a steady state if the difference in energy associated with fermionic masses at rest is more than the scalar boson one. Viceversa, if the initial amount of energy is not sufficient, the fermionic particle remains stable with an eigenvalue not included in the continuum [85]. The interaction term involved in the Hamiltonian is an integral operator, that Friedrichs defines as a class of continuous spectra perturbation [53], displaying, with appropriate conditions, a decay inhibition for states associated with a purely point spectrum immersed in the continuum, thus providing the emergence of many-body bound states.

The presented elementary phenomenon encapsulates the non-unitary dynamics at the heart of the master equation [54], targeting the study of decay processes in the development set off for quantum technologies concerning dipolar interactions. The emerged renormalization procedure [2, 121] is currently applied for the description of dressed two-level atoms [108], whose excited and ground state play fermionic particles roles, characterized by typical lifetimes for photon dissipation. The application of the resolvent formalism allows the study of particular values assumed by model parameters that define not decaying bound eigenstates: for widely separated elements belonging to this collective state, the intrinsic nonlocality provides a secure defence with respect to local sources of decoherence, so representing a privileged platform for fault-tolerant quantum memories and information processing [67, 98].

This thesis targets the description of steady states and their stability with respect to variation of model parameters, given that experimental realizations are all affected by data inaccuracy. The basic tool employed consists in the resolvent formalism, whose analytical properties impose the complex energy plane structure: corresponding to the continuous spectrum of the Hamiltonian there is a branch cut, joining the second Riemann sheet where propagator poles lie, ruling the exponential decay at intermediate times [40, 45]. A pole placed in correspondance with the branch cut signals decay inhibition characterizing steady states, thus allowing us to choose model parameters suitable for the realization of long-lived quantum memories and to characterize typical eigenstates features, as motional states in ion traps [12, 23, 29, 86, 99, 105, 118].

1.1 Unstable vacua

The decay phenomenon described in Lee's exactly solvable model [85] concerns a vacuum state defined for the global system, defined by the initially undecayed neutral fermionic particle and the absence of scalar relativistic bosons to which it refers. Physical parameters of the model characterize uniquely each of these states. Renormalization procedures applied for the solution have been extensively studied in currently available experimental platforms in the framework of quantum technologies, referred to waveguide quantum electrodynamics (QED) [7, 18, 19, 31, 35, 37, 41, 46, 48, 49, 56, 59, 61, 66, 67, 73, 81, 89, 90, 93, 101, 103, 104, 109, 110, 114, 123, 129, 130, 143, 144, 145], because the simulation of the same degrees of freedom allows us to give precise predictions concerning the large time behavior, beyond perturbation theory limitations, according to Poincarè recurrences [40, 45].

The bare energy of the unstable vacuum state is quantified through the gap of a two-level system, prepared in an initially excited state. This decay

phenomenon naturally involves the interaction with a bosonic field, associated with a given measure space, that consists in the momentum space [92].

Our interest in the emergence of bound states in the continuum requires systems embedded in one spatial dimension, because in this way a point-like atom represents a boundary capable of limiting a field endowed with motional degrees of freedom. For this reason the Hilber space of a single-boson wavefunction is $\mathfrak{H} = L^2(\mathbb{R})$ while the states with arbitrary boson number live in the symmetrized Fock space [14]

$$\mathfrak{F}_+(\mathfrak{H}) = \bigoplus_{N\geq 0} L^2(\mathbb{R})^{\odot N}, \tag{1.1}$$

where $\mathfrak{H}^0 = \mathbb{C}$ and $\odot$ denotes a symmetrized tensor product, such that a state belonging to the N-boson subspace reads

$$\left|\xi^{(N)}\right\rangle = |\xi_1\rangle \odot |\xi_2\rangle \odot \cdots \odot |\xi_N\rangle = \frac{1}{N!}\sum_{\pi\in S_N} \left|\xi_{\pi_1}\right\rangle \otimes \left|\xi_{\pi_2}\right\rangle \otimes \cdots \otimes \left|\xi_{\pi_N}\right\rangle \ , \tag{1.2}$$

with S_N the permutation group. Now it is possible to introduce the number operator [14]

$$\hat{N}\left|\xi^{(N)}\right\rangle = N\left|\xi^{(N)}\right\rangle, \tag{1.3}$$

whose eigenspaces contain states with a fixed number N of bosons.

The wavefunction symmetry in (1.2) is selected by the bosonic algebra composed by annihilation and creation operators according to the canonical commutation relations:

$$\left[a(k), a^\dagger(k')\right] = \delta(k-k')\mathbb{1} \ , \quad [a(k), a(k')] = 0 \ , \quad \left[a^\dagger(k), a^\dagger(k')\right] = 0 \ , \tag{1.4}$$

with δ the Dirac delta function, $\mathbb{1}$ the identity operator and where k denotes boson momentum, linked via Fourier transform with the position representation. In this way, the number operator is easily identified:

$$\hat{N} = \int \mathrm{d}k \, a^\dagger(k)a(k), \tag{1.5}$$

where $a^\dagger(k)a(k)$ is the momentum density. In general operator-valued distributions are defined with the aim of inducing an amplitude for momenta occupation:

$$a(\xi) = \int \mathrm{d}k \, \xi^*(k)a(k) \ , \qquad a^\dagger(\xi) = \int \mathrm{d}k \, \xi(k)a^\dagger(k) \ , \tag{1.6}$$

characterized by the following commutation relation [14]

$$\left[a(\xi_1), a^\dagger(\xi_2)\right] = \langle \xi_1 | \xi_2 \rangle \, \mathbb{1} \, , \tag{1.7}$$

such that, considering single-boson states $|\xi\rangle = \int \xi(k) \, |k\rangle$ and associated Hermitian conjugate $\langle k|$, operators act as follow:

$$a\,(\xi) \left|\xi^{(N)}\right\rangle = \sqrt{N} \, \langle \xi | \xi_1 \rangle \, |\xi_2\rangle \odot |\xi_3\rangle \odot \cdots \odot |\xi_N\rangle \, , \tag{1.8}$$

$$a^\dagger\,(\xi) \left|\xi^{(N)}\right\rangle = \sqrt{N+1} \; |\xi\rangle \odot |\xi_1\rangle \odot \cdots \odot |\xi_N\rangle \, , \tag{1.9}$$

for $\left|\xi^{(N)}\right\rangle \in D\left(\hat{N}^{1/2}\right)$, the domain of the square root of the positive operator [112].

The definition in the number operator (1.5) of a momentum density allows us to introduce the Hamiltonian of the free bosonic field, in which a dispersion relation $\omega(k)$ is associated with each boson momentum k:

$$\Omega = \int \mathrm{d}k \, \omega(k) a^\dagger(k) a(k) \, , \tag{1.10}$$

so working as a multiplication operator in the momentum representation $\Omega \, |k\rangle = \omega(k) \, |k\rangle$. The conservation law $\left[\Omega, \hat{N}\right] = 0$ is obtained straightforwardly, entailing that the dynamics preserves the fixed number of excitation sectors of the Hilbert space: the one with single excitation provides (1.5) as a resolution of the identity, where the Friedrichs-Lee model is restricted [42, 92], otherwise an overall factor $\frac{1}{N}$ has to be introduced, linked with a projection-valued measure, formally presented in Section 2.3.

We shall now consider a two-level atom, endowed with a ground state $\left|g\right\rangle$ and an excited one $\left|e\right\rangle$, interacting with the free bosonic field. The atomic degrees of freedom correspond to a representation of the $\mathfrak{su}(2)$ algebra, with $\left|e\right\rangle\!\left\langle g\right|$ describing the two-level atom excitation process and $\left|g\right\rangle\!\left\langle e\right|$ the reversed one, thus translated in terms of Pauli matrices:

$$\left|e\right\rangle\!\left\langle g\right| = \sigma^+ = \frac{\sigma_x + \mathrm{i}\sigma_y}{2}, \qquad \left|g\right\rangle\!\left\langle e\right| = \sigma^- = \frac{\sigma_x - \mathrm{i}\sigma_y}{2}. \tag{1.11}$$

The free atom Hamiltonian accounting for the energy gap ε reads:

$$H^0_{\mathrm{at}} = \varepsilon \left|e\right\rangle\!\left\langle e\right| = \begin{pmatrix} \varepsilon & 0 \\ 0 & 0 \end{pmatrix} = \varepsilon \, \sigma^+ \sigma^- . \tag{1.12}$$

The global system is described by states living in $\mathscr{H} = \mathbb{C}^2 \otimes \mathfrak{F}_+(\mathfrak{H})$. Up to this point, the ingredients required for the definition of the non-interacting theory are introduced, thus leading to the free Hamiltonian:

$$H_0 = H^0_{\mathrm{at}} \otimes \mathbb{1} + \mathbb{1} \otimes \Omega, \tag{1.13}$$

where identity operators are referred to the different Hilbert spaces, respectively associated with bosonic and atomic degrees of freedom. A more convenient expression of the global Hilbert space is achieved by noting that the total excitation number operator, defined as:

$$\mathcal{N} = \mathcal{N}_{\rm at} + \hat{N} = \sigma^+\sigma^- + \int \mathrm{d}k\, a^\dagger(k)a(k), \tag{1.14}$$

represents a conserved quantity, according to the commutation $[H_0, \mathcal{N}] = 0$, which generalizes $\left[\Omega, \hat{N}\right] = 0$, valid for the bosonic field. In this way it is possible to fix the dynamics in a sector endowed with N excitations and look at the ground state amplitude simply as an overall phase, such that:

$$\mathscr{H} = \bigoplus_{N\geq 0} \mathscr{H}^{(N)}, \qquad \mathscr{H}^{(N)} = \left(\mathbb{C}\otimes L^2(\mathbb{R})^{\odot(N-1)}\right)\oplus L^2(\mathbb{R})^{\odot N}, \tag{1.15}$$

with $\mathscr{H}^{(0)} = \mathbb{C}$. At this stage, the theoretical ingredients involved in the definition of the free theory are completely characterized and we are ready to introduce the interaction. It has to couple the action of ladder matrices (1.11) with respectively annihilation and creation of a boson in the following way:

$$H_{\rm int} = \int \mathrm{d}k\, \left(\sigma^+\otimes F^*(k)a(k) + \sigma^-\otimes F(k)a^\dagger(k)\right) = \sigma^+\otimes a(F) + \sigma^-\otimes a^\dagger(F), \tag{1.16}$$

where $F(k)$ is the form factor, encoding in its analytical properties the structure of complex energy plane, as we will see in Sections 2.3 and 3.2.1 [40, 42, 45, 92].

Parameters concerning physical details of the model are included in the form factor as the multiplicative coupling constant, weighting the interaction strength, with the exception of the atom energy gap. In Chapters 3-7 the coupling constant will emerge as a measure of the single atom decay rate determined by the interaction with an electromagnetic field whose dispersion relation establishes a reference energy scale.

The appearance of a point spectrum embedded in the continuum is subject to conditions determined by Friedrichs [53], essentially related with the form factor, representing the kernel of an integral operator. In Sections 2.3 and 2.5 we will derive this structural correspondence concerning the single excitation sector, where (1.14) represents the decomposition of the resolution of the identity associated with a projection-valued measure, formally presented in Section 2.3, in a point spectrum for atomic excitations (in general for the multi-atom case) and in an absolutely continuous one which considers bosonic excitations, corresponding to photons for the system defined in Section 1.4.

In the $\mathcal{N} = 1$ sector, the Hilbert space corresponds to $\mathscr{H}^{(1)} = \mathbb{C} \oplus L^2(\mathbb{R})$, whose states have the following form:

$$\big|\psi\big\rangle = a\,|e\rangle \otimes |\mathrm{vac}\rangle + \big|g\big\rangle \otimes |\xi\rangle = \begin{pmatrix} a \\ |\xi\rangle \end{pmatrix}, \tag{1.17}$$

with $a \in \mathbb{C}$, $|a|^2 + \|\xi\|^2 = 1$ and $|\mathrm{vac}\rangle$ the vacuum of the bosonic field ($a(\xi)\,|\mathrm{vac}\rangle = 0$ for every ξ), thus motivating the possibility of studying unstable vacuum state which corresponds to an atom initially prepared in the excited state. In this sector, the Hamiltonian assumes a simple matrix form [42, 92]:

$$H = H_0 + H_{\mathrm{int}} = \begin{pmatrix} \varepsilon & \langle F| \\ |F\rangle & \Omega \end{pmatrix}, \tag{1.18}$$

valid also in the multi-excitations case, acting on (1.17) according to the usual matrix indices contraction.

1.2 Minimal coupling

The dipolar interaction represents a low-energy approximation of the physics of multi-level system (atoms, molecules, artificial structures, ...) coupled to electromagnetic radiation [33, 45, 51, 94]. Its expression refers to the coupling between two subsystems: the electromagnetic field and an ensemble of charged particles. At the classical level, the study of Lorentz equations of motion for charged particles interacting with the electromagnetic field, resulting in the coupled Maxwell-Lorentz equations, provides the minimal coupling to include a longitudinal momentum component yielded by charge density as source of Coulomb interactions [25]. The system is described by the classical conserved energy:

$$H(t) = \frac{1}{2}\sum_{j=1}^{n} m_j \boldsymbol{v}_j^2(t) + \frac{\epsilon_0}{2}\int \mathrm{d}^3\boldsymbol{r}\,\Big(\boldsymbol{E}^2(\boldsymbol{r},t) + c^2\boldsymbol{B}^2(\boldsymbol{r},t)\Big), \tag{1.19}$$

where $j = 1, \ldots, n$ runs over charged particles label endowed with mass m_j and velocity $\boldsymbol{v}_j$, $(\boldsymbol{r}, t)$ represent position and time coordinates, $\boldsymbol{E}$ and $\boldsymbol{B}$ stand for electric and magnetic fields, ϵ_0 vacuum dielectric constant and c the speed of light, according to SI units, as in Sections 1.3 and 1.4. The aforementioned key ingredients are represented by the separation of the electromagnetic field degrees of freedom in transverse and longitudinal ones. This is achieved by means of the Coulomb gauge, imposing that the magnetic field $\boldsymbol{B}(\boldsymbol{r}, t)$ is transverse

with respect to the propagation direction:

$$\begin{cases} \nabla \cdot \boldsymbol{A}(\boldsymbol{r},t) = 0, \\ \boldsymbol{E}_{\perp}(\boldsymbol{r},t) = -\dot{\boldsymbol{A}}(\boldsymbol{r},t), \\ \boldsymbol{E}_{\parallel}(\boldsymbol{r},t) = -\nabla\varphi(\boldsymbol{r},t), \end{cases} \tag{1.20}$$

where $\boldsymbol{A}(\boldsymbol{r},t)$ is the vector potential, introduced to exploit the degree of freedom charcterizing gauge invariance. Its curl provides the magnetic field, while $\Delta\varphi(\boldsymbol{r},t) = -\rho(\boldsymbol{r},t)/\epsilon_0$ for the electrostatic potential, with $\rho(\boldsymbol{r},t)$ the charge density. The definition of the two contribution for the electric field is better expressed in the Fourier transform:

$$\widetilde{\boldsymbol{E}}(\boldsymbol{k},t) = \int \frac{\mathrm{d}^3\boldsymbol{r}}{(2\pi)^{3/2}} \boldsymbol{E}(\boldsymbol{r},t)\mathrm{e}^{\mathrm{i}\boldsymbol{k}\cdot\boldsymbol{r}}, \tag{1.21}$$

where the longitudinal and transverse parts can be identified as

$$\widetilde{\boldsymbol{E}}_{\parallel}(\boldsymbol{k},t) = \left(\hat{\boldsymbol{k}}\cdot\widetilde{\boldsymbol{E}}(\boldsymbol{k},t)\right)\hat{\boldsymbol{k}}, \qquad \widetilde{\boldsymbol{E}}_{\perp}(\boldsymbol{k},t) = \widetilde{\boldsymbol{E}}(\boldsymbol{k},t) - \left(\hat{\boldsymbol{k}}\cdot\widetilde{\boldsymbol{E}}(\boldsymbol{k},t)\right)\hat{\boldsymbol{k}}, \tag{1.22}$$

where $\hat{\boldsymbol{k}} = \boldsymbol{k}/k$, with $k = |\boldsymbol{k}|$. In this way, exploiting Parseval's identity and the orthogonality $\widetilde{\boldsymbol{E}}^{*}_{\parallel}(\boldsymbol{k},t)\cdot\widetilde{\boldsymbol{E}}_{\perp}(\boldsymbol{k},t) = 0$, we can identify the transverse contribution of the electromagnetic field to the energy:

$$H_{\perp}(t) = \frac{\epsilon_0}{2}\int \mathrm{d}^3\boldsymbol{r}\,\left(\boldsymbol{E}^2_{\perp}(\boldsymbol{r},t) + c^2\boldsymbol{B}^2(\boldsymbol{r},t)\right). \tag{1.23}$$

Considering the Maxwell equation related to the Gauss law, we obtain in the Fourier space $\widetilde{\boldsymbol{E}}_{\parallel}(\boldsymbol{k},t) = -\mathrm{i}\boldsymbol{k}\widetilde{\rho}(\boldsymbol{k},t)/\left(\epsilon_0 k^2\right)$, such that the longitudinal energy contribution translates in:

$$H_{\parallel}(t) = \frac{1}{2\epsilon_0}\int_{k\le k_c}\mathrm{d}^3\boldsymbol{k}\,\frac{\widetilde{\rho}^{*}(\boldsymbol{k},t)\widetilde{\rho}(\boldsymbol{k},t)}{k^2} = \frac{1}{8\pi\epsilon_0}\sum_{l\neq j}\frac{q_j q_l}{\left|\boldsymbol{r}_j(t)-\boldsymbol{r}_l(t)\right|} + \sum_j \frac{q_j^2 k_c}{4\pi^2\epsilon_0} \tag{1.24}$$

where point-like particles $\rho(\boldsymbol{r},t) = \sum_j q_j\delta(\boldsymbol{r}-\boldsymbol{r}_j(t))$ are considered, whose Fourier transform $\widetilde{\rho}(\boldsymbol{k},t) = \sum_j \frac{q_j}{(2\pi)^{3/2}}\mathrm{e}^{-\mathrm{i}\boldsymbol{k}\cdot\boldsymbol{r}_j(t)}$ provides the result. The second term is called Coulomb self-energy, representing a divergence cured by the introduction of an ultraviolet cutoff k_c, related to point-like charges making fields vary across arbitrarily small regions [25].

Another conserved quantity is in the total momentum of the system:

$$\boldsymbol{P}(t) = \sum_j m_j\boldsymbol{v}_j(t) + \boldsymbol{P}_{\parallel}(t) + \boldsymbol{P}_{\perp}(t)\,, \tag{1.25}$$

where

$$\boldsymbol{P}_{\parallel(\perp)}(t) = \epsilon_0 \int \mathrm{d}^3\boldsymbol{r}\ \boldsymbol{E}_{\parallel(\perp)}(\boldsymbol{r},t) \wedge \boldsymbol{B}(\boldsymbol{r},t) = \epsilon_0 \int \mathrm{d}^3\boldsymbol{k}\ \widetilde{\boldsymbol{E}}_{\parallel(\perp)}(\boldsymbol{k},t) \wedge \widetilde{\boldsymbol{B}}^*(\boldsymbol{k},t). \quad (1.26)$$

The last integrand is evaluated according to $\widetilde{\boldsymbol{B}}^*(\boldsymbol{k},t) = -\mathrm{i}\boldsymbol{k} \wedge \widetilde{\boldsymbol{A}}^*(\boldsymbol{k},t)$, thus yielding

$$\frac{\boldsymbol{k} \wedge \left(\boldsymbol{k} \wedge \widetilde{\boldsymbol{A}}^*(\boldsymbol{k},t)\right)}{k^2} = \left(\hat{\boldsymbol{k}} \cdot \widetilde{\boldsymbol{A}}^*(\boldsymbol{k},t)\right)\hat{\boldsymbol{k}} - \widetilde{\boldsymbol{A}}^*(\boldsymbol{k},t) \quad (1.27)$$

with a vanishing first term because of an absent longitudinal component for the vector potential. Applying again the hypothesis of point-like charges the minimal coupling expression is obtained:

$$\boldsymbol{P}(t) = \sum_j \left(m_j \boldsymbol{v}_j(t) + q_j \boldsymbol{A}(\boldsymbol{r}_j(t),t)\right) + \boldsymbol{P}_\perp(t) = \sum_j \boldsymbol{p}_j(t) + \boldsymbol{P}_\perp(t), \quad (1.28)$$

replacing the expression of $\boldsymbol{p}_j$ in the energy (1.19), one obtains the Hamiltonian [25, 33, 51, 94]:

$$H(t) = \sum_j \frac{1}{2m_j}\left(\boldsymbol{p}_j(t) - q_j \boldsymbol{A}(\boldsymbol{r}_j(t),t)\right)^2 + H_\parallel(t) + H_\perp(t). \quad (1.29)$$

From the canonical coordinates $(\boldsymbol{r}_j, \boldsymbol{p}_j)$, one can obtain equations of motion by applying Hamilton equations and according to canonical Poisson brackets

$$\left\{r_{j,\alpha}, p_{l,\beta}\right\}_{PB} = \delta_{j,l}\delta_{\alpha,\beta}, \quad (1.30)$$

where greek indices run over spatial dimensions $\alpha, \beta = x, y, z$. The application of Hamilton equations of motion provides a set of Newton-Lorentz equations for the acceleration of each particle in presence of the electromagnetic field. [25]

1.2.1 Canonical quantization

To proceed towards electromagnetic field quantization we need equations of motion and canonical brackets. Let us consider dynamical variables associated with conjugated $(\boldsymbol{A}, \boldsymbol{\Pi})$, for clarity in absence of any source, defined according to Lagrangian density:

$$\mathcal{L}_\perp\left(\boldsymbol{A}(\boldsymbol{r},t), \dot{\boldsymbol{A}}(\boldsymbol{r},t)\right) = -\frac{\epsilon_0}{2}\left(\boldsymbol{E}_\perp^2(\boldsymbol{r},t) - c^2\boldsymbol{B}^2(\boldsymbol{r},t)\right), \quad (1.31)$$

such that:

$$\boldsymbol{\Pi}(\boldsymbol{r},t) = \frac{\partial \mathcal{L}_\perp\left(\boldsymbol{A}(\boldsymbol{r},t), \dot{\boldsymbol{A}}(\boldsymbol{r},t)\right)}{\partial \dot{\boldsymbol{A}}(\boldsymbol{r},t)} = -\epsilon_0 \boldsymbol{E}_\perp(\boldsymbol{r},t), \quad (1.32)$$

assuming identities in (1.20), as in the Legendre transformation for the Hamiltonian density $\mathcal{H}_\perp\left(\boldsymbol{A}(\boldsymbol{r},t),\boldsymbol{\Pi}(\boldsymbol{r},t)\right)=\boldsymbol{\Pi}(\boldsymbol{r},t)\dot{\boldsymbol{A}}(\boldsymbol{r},t)-\mathcal{L}_\perp\left(\boldsymbol{A}(\boldsymbol{r},t),\dot{\boldsymbol{A}}(\boldsymbol{r},t)\right)$.

Hamilton equations of motion are obtained considering (1.23) as a functional for $\left(\widetilde{\boldsymbol{A}},\widetilde{\boldsymbol{\Pi}}\right)$ in the Fourier space and according to Radon-Nikodym (i.e. functional, distributional, weak) derivative [63, 97]:

$$\begin{cases}\dot{\widetilde{\boldsymbol{A}}}(\boldsymbol{k},t)=\dfrac{\delta H_\perp\left(\widetilde{\boldsymbol{A}}(\boldsymbol{k}',t),\widetilde{\boldsymbol{\Pi}}(\boldsymbol{k}',t),t\right)}{\delta\widetilde{\boldsymbol{\Pi}}(\boldsymbol{k},t)}=-\widetilde{\boldsymbol{E}}_\perp(\boldsymbol{k},t),\\[2ex]\dot{\widetilde{\boldsymbol{\Pi}}}(\boldsymbol{k},t)=-\dfrac{\delta H_\perp\left(\widetilde{\boldsymbol{A}}(\boldsymbol{k}',t),\widetilde{\boldsymbol{\Pi}}(\boldsymbol{k}',t),t\right)}{\delta\widetilde{\boldsymbol{A}}(\boldsymbol{k},t)}=-\mathrm{i}\,\epsilon_0\,c^2\,\boldsymbol{k}\wedge\widetilde{\boldsymbol{B}}(\boldsymbol{k},t),\end{cases}\tag{1.33}$$

where the first equation determines $\boldsymbol{E}_\perp$ in terms of $\boldsymbol{A}$, while the second one, using $\widetilde{\boldsymbol{B}}(\boldsymbol{k},t)=\mathrm{i}\boldsymbol{k}\wedge\widetilde{\boldsymbol{A}}(\boldsymbol{k},t)$ and the identity:

$$\frac{\delta\left(\boldsymbol{k}'\wedge\widetilde{\boldsymbol{A}}(\boldsymbol{k}',t)\right)^2}{\delta\widetilde{\boldsymbol{A}}(\boldsymbol{k},t)}=2\left[k'^2\widetilde{\boldsymbol{A}}(\boldsymbol{k}',t)-\left(\boldsymbol{k}'\cdot\widetilde{\boldsymbol{A}}(\boldsymbol{k}',t)\right)\boldsymbol{k}'\right]\delta(\boldsymbol{k}-\boldsymbol{k}'),\tag{1.34}$$

leads to the Ampére-Maxwell law. Let us emphasize that results in (1.33) are obtained by means of partial derivatives with respect to dynamical variables of the Hamiltonian density $\mathcal{H}_\perp\left(\widetilde{\boldsymbol{A}}(\boldsymbol{k},t),\widetilde{\boldsymbol{\Pi}}(\boldsymbol{k},t)\right)$ in momentum space as in (1.32): the definition of Radon-Nikodym derivative requires the introduction of an inner product characterizing Hilbert spaces, in the spirit of a directional derivative in a functional space.

The imposition of the Coulomb gauge $\boldsymbol{k}\cdot\boldsymbol{A}(\boldsymbol{k},t)=0$ in (1.34) and the introduction of the dispersion relation $\omega(k)=ck$ sets the equivalence between the electromagnetic field and an infinite collection of harmonic oscillators representing transverse modes [25]:

$$\begin{cases}\dot{\widetilde{\boldsymbol{A}}}(\boldsymbol{k},t)=-\widetilde{\boldsymbol{E}}_\perp(\boldsymbol{k},t),\\[2ex]\dot{\widetilde{\boldsymbol{E}}}_\perp(\boldsymbol{k},t)=\omega^2\,\widetilde{\boldsymbol{A}}(\boldsymbol{k},t).\end{cases}\tag{1.35}$$

The solution is provided by decoupled normal variables, which diagonalize the free transverse field:

$$\boldsymbol{\alpha}(\boldsymbol{k},t)=-\mathrm{i}\sqrt{\frac{\epsilon_0}{2\hbar\,\omega(k)}}\left(\widetilde{\boldsymbol{E}}_\perp(\boldsymbol{k},t)+\mathrm{i}\omega(k)\widetilde{\boldsymbol{A}}(\boldsymbol{k},t)\right).\tag{1.36}$$

The conjugated momenta to $\boldsymbol{\alpha}(\boldsymbol{k})$ are proportional to their complex conjugates, therefore the Hamilton equations of motion read

$$\dot{\boldsymbol{\alpha}}(\boldsymbol{k},t)+\mathrm{i}\omega(k)\boldsymbol{\alpha}(\boldsymbol{k},t)=0,\tag{1.37}$$

that is solved by $\boldsymbol{\alpha}(\boldsymbol{k},t) = \boldsymbol{\alpha}(\boldsymbol{k},0)\mathrm{e}^{-\mathrm{i}\omega(k)t}$.

Sources can be included in (1.33) by means of (1.29), where the functional derivative of the minimal coupling term, with the substitution $\boldsymbol{p}_j - q_j\boldsymbol{A} = m_j\boldsymbol{v}_j$, provides the source in the Ampére-Maxwell law:

$$\dot{\widetilde{\boldsymbol{E}}}_\perp(\boldsymbol{k},t) = \mathrm{i}c^2\,\boldsymbol{k}\wedge\widetilde{\boldsymbol{B}}(\boldsymbol{k},t) - \frac{\widetilde{\boldsymbol{J}}(\boldsymbol{k},t)}{\epsilon_0}, \tag{1.38}$$

where $\widetilde{\boldsymbol{J}}(\boldsymbol{k},t) = \sum_j \frac{q_j\boldsymbol{v}_j(t)}{(2\pi)^{3/2}}\mathrm{e}^{-\mathrm{i}\boldsymbol{k}\cdot\boldsymbol{r}_j(t)}$. The definition of normal variables still obeys the form dictated by (1.36), but now the description is enriched by the decomposition along two polarization unit vectors $\boldsymbol{\varepsilon}(\boldsymbol{k})$ and $\boldsymbol{\varepsilon}'(\boldsymbol{k})$, feasible also in the free case, orthogonal with respect to the propagation axis $\boldsymbol{k}$ and to each other, such that $\boldsymbol{\alpha}(\boldsymbol{k},t)\cdot\boldsymbol{\varepsilon}(\boldsymbol{k}) = \alpha_{\boldsymbol{\varepsilon}}(\boldsymbol{k},t)$ implies the evolution equation [25]:

$$\dot{\alpha}_{\boldsymbol{\varepsilon}}(\boldsymbol{k},t) + \mathrm{i}\omega(k)\alpha_{\boldsymbol{\varepsilon}}(\boldsymbol{k},t) = \mathrm{i}\frac{\widetilde{\boldsymbol{J}}(\boldsymbol{k},t)\cdot\boldsymbol{\varepsilon}(\boldsymbol{k})}{\sqrt{2\hbar\,\epsilon_0\omega(k)}}. \tag{1.39}$$

For $\boldsymbol{\varepsilon}(\boldsymbol{k}) \in \mathbb{R}$ the polarization is linear, so the current is decomposed along directions parallel to the polarization, as we will apply in Section 1.4.

The normalization constant introduced in (1.36) is better understood by looking at the free Hamiltonian for transverse components. We already proved that in the Coulomb gauge $\widetilde{\mathcal{H}}_\perp(t) = \frac{\epsilon_0}{2}\left|\widetilde{\boldsymbol{E}}_\perp + \mathrm{i}\omega\widetilde{\boldsymbol{A}}\right|^2$, using the normalization factor, one obtains

$$H_\perp(t) = \int \mathrm{d}^3\boldsymbol{k}\,\hbar\omega(k)\sum_{\boldsymbol{\varepsilon}}|\alpha_{\boldsymbol{\varepsilon}}(\boldsymbol{k},t)|^2\,. \tag{1.40}$$

The expression for the momentum carried by radiation requires the inversion of (1.36):

$$\widetilde{\boldsymbol{A}}(\boldsymbol{k},t) = \sqrt{\frac{\hbar}{2\epsilon_0\omega(k)}}\sum_{\boldsymbol{\varepsilon}}\left(\boldsymbol{\varepsilon}(\boldsymbol{k})\alpha_{\boldsymbol{\varepsilon}}(\boldsymbol{k},t) + \boldsymbol{\varepsilon}^*(-\boldsymbol{k})\alpha^*_{\boldsymbol{\varepsilon}}(-\boldsymbol{k},t)\right), \tag{1.41}$$

$$\widetilde{\boldsymbol{E}}_\perp(\boldsymbol{k},t) = \mathrm{i}\sqrt{\frac{\hbar\omega(k)}{2\epsilon_0}}\sum_{\boldsymbol{\varepsilon}}\left(\boldsymbol{\varepsilon}(\boldsymbol{k})\alpha_{\boldsymbol{\varepsilon}}(\boldsymbol{k},t) - \boldsymbol{\varepsilon}^*(-\boldsymbol{k})\alpha^*_{\boldsymbol{\varepsilon}}(-\boldsymbol{k},t)\right). \tag{1.42}$$

Following a similar procedure to (1.26), we get

$$\boldsymbol{P}_\perp(t) = -\mathrm{i}\epsilon_0\int \mathrm{d}^3\boldsymbol{k}\,\left(\widetilde{\boldsymbol{E}}_\perp(\boldsymbol{k},t)\cdot\widetilde{\boldsymbol{A}}^*(\boldsymbol{k},t)\right)\boldsymbol{k} = \int \mathrm{d}^3\boldsymbol{k}\,\hbar\boldsymbol{k}\sum_{\boldsymbol{\varepsilon}}|\alpha_{\boldsymbol{\varepsilon}}(\boldsymbol{k},t)|^2\,. \tag{1.43}$$

Adopting the definition of conjugate variables with Poisson brackets, as made in (1.30), in the extension exploiting functional derivatives [63], normal variables

take a central role in the quantization of the electromagnetic radiation, which is based on the equal-time Poisson brackets

$$\left\{\alpha_{\boldsymbol{\mathfrak{E}}}(\boldsymbol{k},t), \mathrm{i}\hbar\alpha^*_{\boldsymbol{\mathfrak{E}}'}(\boldsymbol{k}',t)\right\}_{PB} = \delta_{\boldsymbol{\mathfrak{E}},\boldsymbol{\mathfrak{E}}'}\,\delta(\boldsymbol{k}-\boldsymbol{k}'). \tag{1.44}$$

The quantization procedure looks at (1.44) as an Heisenberg algebra [32], thus mimicking the evolution of classical dynamical variables in terms of non commuting operators. The promotion of normal variables at the level of quantum operators on the Fock space reads:

$$\left[a_{\boldsymbol{\mathfrak{E}}}(\boldsymbol{k}), a^\dagger_{\boldsymbol{\mathfrak{E}}'}(\boldsymbol{k}')\right] = \delta_{\boldsymbol{\mathfrak{E}},\boldsymbol{\mathfrak{E}}'}\,\delta(\boldsymbol{k}-\boldsymbol{k}'), \tag{1.45}$$

representing an example of (1.7) in presence of continuous indices. Inserting normal mode operators in (1.41) and (1.42) provides time-0 quantized fields

$$\boldsymbol{A}(\boldsymbol{r}) = \int \frac{\mathrm{d}^3\boldsymbol{k}}{(2\pi)^{3/2}}\,\sqrt{\frac{\hbar}{2\epsilon_0\omega(k)}}\sum_{\boldsymbol{\mathfrak{E}}}\left(\boldsymbol{\mathfrak{e}}(\boldsymbol{k})a_{\boldsymbol{\mathfrak{E}}}(\boldsymbol{k})\,\mathrm{e}^{\mathrm{i}\boldsymbol{k}\cdot\boldsymbol{r}} + \boldsymbol{\mathfrak{e}}^*(\boldsymbol{k})a^\dagger_{\boldsymbol{\mathfrak{E}}}(\boldsymbol{k})\,\mathrm{e}^{-\mathrm{i}\boldsymbol{k}\cdot\boldsymbol{r}}\right), \tag{1.46}$$

$$\boldsymbol{E}_\perp(\boldsymbol{r}) = \mathrm{i}\int \frac{\mathrm{d}^3\boldsymbol{k}}{(2\pi)^{3/2}}\,\sqrt{\frac{\hbar\omega(k)}{2\epsilon_0}}\sum_{\boldsymbol{\mathfrak{E}}}\left(\boldsymbol{\mathfrak{e}}(\boldsymbol{k})a_{\boldsymbol{\mathfrak{E}}}(\boldsymbol{k})\,\mathrm{e}^{\mathrm{i}\boldsymbol{k}\cdot\boldsymbol{r}} - \boldsymbol{\mathfrak{e}}^*(\boldsymbol{k})a^\dagger_{\boldsymbol{\mathfrak{E}}}(\boldsymbol{k})\,\mathrm{e}^{-\mathrm{i}\boldsymbol{k}\cdot\boldsymbol{r}}\right), \tag{1.47}$$

satisfying an Heisenberg algebra between conjugate momenta, as in (1.32):

$$\left[A_j(\boldsymbol{r}), \Pi_\ell(\boldsymbol{r}')\right] = \mathrm{i}\hbar\,\delta^\perp_{j,\ell}(\boldsymbol{r}-\boldsymbol{r}') = \mathrm{i}\hbar\int\frac{\mathrm{d}^3\boldsymbol{k}}{(2\pi)^3}\,\mathrm{e}^{\mathrm{i}\boldsymbol{k}\cdot(\boldsymbol{r}-\boldsymbol{r}')}\left(\delta_{j,\ell} - \hat{\boldsymbol{k}}_j\hat{\boldsymbol{k}}_\ell\right), \tag{1.48}$$

which represents the projector onto the subspace of transverse fields in the reciprocal space, starting from the relation $\sum_{j,\ell}\boldsymbol{\mathfrak{e}}_j\boldsymbol{\mathfrak{e}}_\ell = \delta_{j,\ell} - \hat{\boldsymbol{k}}_j\hat{\boldsymbol{k}}_\ell$ [25]. The requirement of additional terms in the transverse Dirac delta can be understood by taking the divergence of both sides with respect to $\boldsymbol{r}$ or $\boldsymbol{r}'$ and applying the chosen Coulomb gauge (1.20).

1.3 Dipole Hamiltonian and Rotating waves

We will start by considering, for definiteness, a hydrogen-like atom, made up of an electron with charge $-e$ and mass m_e in a potential $H_\parallel(\mathbf{r})$, generated by a nucleus endowed with an infinite mass, whose Hamiltonian follows from the minimal coupling prescription (1.29), without the inclusion of contributions for electromagnetic field transverse components:

$$H_{\mathrm{at}} = \frac{1}{2m_e}(\boldsymbol{p}+e\boldsymbol{A})^2 + H_\parallel(\boldsymbol{r}) = H^0_{\mathrm{at}} + \frac{e}{m_e}\boldsymbol{p}\cdot\boldsymbol{A} + \frac{e^2}{2m_e}\boldsymbol{A}^2 = H^0_{\mathrm{at}} + H^{(1)}_{\mathrm{int}} + H^{(2)}_{\mathrm{int}}, \tag{1.49}$$

with $H^0_{\rm at} = \boldsymbol{p}^2/2m_e + H_{\parallel}(\boldsymbol{r})$, $\boldsymbol{r}$ and $\boldsymbol{p}$ the canonically conjugated position and momentum of the electron, as in (1.30). The transverse choice $\boldsymbol{\nabla}\cdot\boldsymbol{A} = 0$ for the vector potential makes the ordering with respect to $\boldsymbol{p}$ immaterial, since $[p_\alpha, \boldsymbol{A}(r_\alpha)] = \mathrm{i}\hbar\frac{\partial \boldsymbol{A}(r_\alpha)}{\partial r_\alpha}$ implies $\boldsymbol{p}\cdot\boldsymbol{A} = \boldsymbol{A}\cdot\boldsymbol{p}$ [33, 41, 45, 51, 94].

It is possible to compare the orders of magnitude characterizing the two interaction terms:

$$\frac{H^{(2)}_{\rm int}}{H^{(1)}_{\rm int}} \approx \frac{e^2A^2}{e\,pA} = \frac{e\,pA}{p^2} \approx \frac{H^{(1)}_{\rm int}}{H^0_{\rm at}}, \tag{1.50}$$

namely $H^{(2)}_{\rm int}$ is small compared to $H^{(1)}_{\rm int}$ if the latter is small compared to the free Hamiltonian [25].

In general for charged particles endowed with spin, an additional term is present in the Hamiltonian, describing the interaction between spin and magnetic field:

$$H^{(s)}_{\rm int} = \frac{e\,g_e}{4m_e}\boldsymbol{\sigma}\cdot\boldsymbol{B}(\boldsymbol{r}), \tag{1.51}$$

where g_e is the gyromagnetic ratio of the electron and $\boldsymbol{\sigma} = \left(\sigma_x, \sigma_y, \sigma_z\right)$ are the Pauli matrices. The order of magnitude of spin is well estimated by the reduced Planck constant $\hbar$, thus providing:

$$\frac{H^{(s)}_{\rm int}}{H^{(1)}_{\rm int}} \approx \frac{e\,\hbar B}{e\,pA} \approx \frac{hkA}{2\pi pA} \approx \frac{a_0}{\lambda}, \tag{1.52}$$

with k the dominant wavenumber and $\lambda = \frac{2\pi}{k}$ the associated wavelength, $a_0 = \frac{4\pi\epsilon_0}{e^2m_e}$ the Bohr radius. Considering atomic optical transition ranging in the energy scale 1 eV, the radiation wavelength is $\lambda \approx 5\times10^{-7}$m, therefore $a_0/\lambda \approx 10^{-4}$ [25]. Confining our attention to this parameter range, the main contribution in the interaction Hamiltonian is entirely attributed to $H^{(1)}_{\rm int}$, which will be the only contribution we will consider henceforth. This analysis targets the achievement of a model in the exactly solvable form (1.16) using as a bosonic field the electromagnetic one, supported by the dipolar and rotating wave approximations.

The first one is focused on the substitution of the dynamical variable describing the position of the electron as argument of the vector potential, as in (1.29), with a non dynamical center-of-mas of the global dipole. For this purpose let us include the whole set of degrees of freedom for the hydrogen-like atom, introducing the notation $(\boldsymbol{r}_N, \boldsymbol{p}_N)$ for nucleus canonical coordinates and $(\boldsymbol{r}_e, \boldsymbol{p}_e)$ for the electron ones, characterized by masses m_N, m_e and opposite charges. The center-of-mass and relative coordinate are defined as

$$\boldsymbol{r}_0 = \frac{m_N\boldsymbol{r}_N + m_e\boldsymbol{r}_e}{m_N + m_e}, \qquad \boldsymbol{r} = \boldsymbol{r}_N - \boldsymbol{r}_e. \tag{1.53}$$

Their introduction allows us to implement a Taylor expansion for the vector potential with respect to the position variable:

$$\boldsymbol{A}(\boldsymbol{r}_e) = \boldsymbol{A}(\boldsymbol{r}_0) + \nabla \boldsymbol{A}(\boldsymbol{r}_0) \cdot (\boldsymbol{r}_e - \boldsymbol{r}_0) + \dots \tag{1.54}$$

These terms are compared according to a ratio of the same order as (1.52)

$$\frac{|\nabla \boldsymbol{A}(\boldsymbol{r}_0) \cdot (\boldsymbol{r}_e - \boldsymbol{r}_0)|}{|\boldsymbol{A}(\boldsymbol{r}_0)|} \approx \frac{kAa_0}{A} \approx \frac{a_0}{\lambda}, \tag{1.55}$$

thus negligible in the regime of optical transitions.

Let us introduce the total and the relative momentum

$$\boldsymbol{p}_0 = \boldsymbol{p}_N + \boldsymbol{p}_e, \qquad \boldsymbol{p} = m_r \left(\frac{\boldsymbol{p}_N}{m_N} - \frac{\boldsymbol{p}_e}{m_e} \right), \tag{1.56}$$

with $m_r = \frac{m_N\, m_e}{m_N + m_e} \approx m_e$ the reduced mass. These momenta are canonically conjugated with the coordinates (1.53):

$$[\boldsymbol{r}_0, \boldsymbol{p}_0] = [\boldsymbol{r}, \boldsymbol{p}] = \mathrm{i}\hbar, \quad [\boldsymbol{r}_0, \boldsymbol{p}] = [\boldsymbol{r}, \boldsymbol{p}_0] = 0. \tag{1.57}$$

The above relations yield the separation of the free Hamiltonian in two commuting contributions:

$$H^0_{\mathrm{at}} = \frac{\boldsymbol{p}_N^2}{2m_N} + \frac{\boldsymbol{p}_e^2}{2m_e} + H_{\parallel}(\boldsymbol{r}_N - \boldsymbol{r}_e) = \frac{\boldsymbol{p}_0^2}{2(m_N + m_e)} + \frac{\boldsymbol{p}^2}{2m_r} + H_{\parallel}(\boldsymbol{r}), \tag{1.58}$$

while the dipolar interaction reads

$$H^{(dip)}_{\mathrm{int}} = e \left(\frac{\boldsymbol{p}_N}{m_N} - \frac{\boldsymbol{p}_e}{m_e} \right) \cdot \boldsymbol{A}(\boldsymbol{r}_0) = \frac{e}{m_r}\, \boldsymbol{p} \cdot \boldsymbol{A}(\boldsymbol{r}_0). \tag{1.59}$$

The rotating wave approximation emerges in the time evolution of terms composing the dipolar interaction [32]. This implies the introduction of the evolution operator with respect to the free Hamiltonian (1.13) of the global system, which will induce relative dynamical phases, thus selecting slowly varying terms with respect to rapidly oscillating ones.

Let us consider for clarity the hydrogen-like atom, neglecting the center-of-mass degrees of freedom. For our purposes, we will approximate it as a two-level quantum emitter, a setup in which the energy scales, as the coupling with the field, make this approximation valid. We denote with $|g\rangle$ the ground state, with $|e\rangle$ the excited one and we will set for simplicity $H^0_{\mathrm{at}} |g\rangle = 0$ and $H^0_{\mathrm{at}} |e\rangle = \hbar\varepsilon |e\rangle$, as presented in (1.12). In this way, our model includes in one parameter the Coulomb self-energy divergence presented in Section 1.2. We

assume that the valence electron undergoes the available energetic transition, e.g. between an S orbital and a P one. The incident radiation is characterized by a linear polarization along the z axis of a reference frame, aligned with respect to the coupled atomic P_z orbital. The interaction Hamiltonian matrix elements read:

$$H_{\text{int}}^{(dip)} = \frac{eA_z(\boldsymbol{r}_0)}{m_e}\Big[\langle g|p_z|g\rangle\,\sigma^-\sigma^+ + \langle e|p_z|e\rangle\,\sigma^+\sigma^- + \langle g|p_z|e\rangle\,\sigma^- + \langle e|p_z|g\rangle\,\sigma^+\Big]. \tag{1.60}$$

The expression is simplified by the vanishing expectation values of momentum in the eigenstates of the free Hamiltonian, see Section 3.1. Moreover, the canonical commutation relation can be used to obtain:

$$\langle e|p_z|g\rangle = \frac{\mathrm{i}m_e}{\hbar}\left\langle e\middle|[H_{\text{at}}^0, z]\middle|g\right\rangle = \mathrm{i}m_e\varepsilon\,\langle e|z|g\rangle =: \mathrm{i}m_e\varepsilon z_{eg} = \mathrm{i}m_e\varepsilon|z_{eg}|e^{\mathrm{i}\theta_{eg}}, \tag{1.61}$$

which cancels the mass m_e from the interaction Hamiltonian, that takes the form of a coupling between the dipole moment

$$D_{eg} = e\left|z_{eg}\right|, \tag{1.62}$$

and the electric field. We can define new canonically conjugated field operators:

$$b(k) := e^{-\mathrm{i}(\theta_{eg}+\pi/2)}a(k), \tag{1.63}$$

which satisfy the same bosonic algebra as $a(k)$ in the Friedrichs-Lee model [41].

To implement the observable evolution, let us consider Heisenberg equation of motion determined by the free Hamiltonian [94]

$$\frac{\mathrm{d}}{\mathrm{d}t}\sigma^-(t) = \frac{\mathrm{i}}{\hbar}\left[H_0, \sigma^-(t)\right], \tag{1.64}$$

$$\frac{\mathrm{d}}{\mathrm{d}t}b(k,t) = \frac{\mathrm{i}}{\hbar}\left[H_0, b(k,t)\right], \tag{1.65}$$

representing the extension of classical dynamical variables evolution according to Poisson brackets. Considering the adjoint representation of the Lie algebra [70] associated with the presented commutator map $[H_0, \cdot] = \mathrm{ad}_{H_0}\cdot$, it is possible to introduce the observables evolution implemented by $U_0(t) = \mathrm{e}^{-\mathrm{i}H_0t/\hbar}$, such that $\sigma^-(t) = U_0^\dagger(t)\sigma^-U_0(t)$ and $b(k,t) = U_0^\dagger(t)b(k)U_0(t)$, whose time derivative at $t = 0$ provides respectively (1.64) and (1.65).

These algebraic expression lead to the rotating frame [54], whose simple explicit form is obtained applying the series expansion of the observables evolution:

$$\sigma^-(t) = \sum_n \frac{(\mathrm{i}\varepsilon t/\hbar)^n}{n!}\left(\mathrm{ad}_{\sigma_z}\right)^n\sigma^- = \mathrm{e}^{-\mathrm{i}\varepsilon t/\hbar}\sigma^-, \tag{1.66}$$

$$b(k,t) = \sum_n \frac{(\mathrm{i}\omega(k)t/\hbar)^n}{n!}\left(\mathrm{ad}_{b^\dagger(k)b(k)}\right)^n b(k) = \mathrm{e}^{-\mathrm{i}\omega(k)t/\hbar}b(k), \tag{1.67}$$

where the latter resembles the classical result (1.37). These results derive respectively from the expression $\sigma^+\sigma^- = (\mathbb{1} + \sigma_z)/2$, with $\mathrm{ad}_{\mathbb{1}}\sigma^- = 0$ and $(\mathrm{ad}_{\sigma_z})^n \sigma^- = (-1)^n\sigma^-$, and integrating time by time the Dirac delta over momenta, with $\left(\mathrm{ad}_{b^\dagger(k)b(k)}\right)^n b(k) = (-1)^n b(k)$.

In the explicit computation of (1.59) in time evolution there are two rotating wave terms $b(k)\sigma^+ e^{i(\varepsilon-\omega(k))t}$ and $b^\dagger(k)\sigma^- e^{-i(\varepsilon-\omega(k))t}$, that near to resonance ($\omega(k) \approx \varepsilon$) behave as not dynamical, while the other two counter-rotating terms $b(k)\sigma^- e^{-i(\varepsilon+\omega(k))t}$ and $b^\dagger(k)\sigma^+ e^{i(\varepsilon+\omega(k))t}$ vary rapidly, such that for time of interest larger than typical lifetimes, they average to zero and are safely negligible. The resulting rotating wave approximation is valid in the weak coupling regime, conforming to a well-posed evolution driven by the free Hamiltonian, as made in (1.64) and (1.65), with a non-vanishing energy gap ε representing the reference energy scale [94].

1.4 Waveguide QED in a nutshell

The controllability for available energies carried by photons and the ability in constraining quantum system in quasi one-dimensional embeddings make waveguides a promising platform in quantum optics and quantum information. Some applications regard quantum information storage and processing, quantum energy transport, single photon on-demand and many-body phenomena [37, 127]. The quantum technology perspective exploits interactions between the photonic field and typical quantum systems composed by artificial atoms, assumed to obey a two-level approximation for the artificial "electron" transition, such that we retain only the ground state $|g\rangle$ and the first excited state $|e\rangle$ [41], endowed with the merit of tunable energy gaps [93, 114]. There are two main families referred to quantum dots [77] and superconducting qubits.

The former includes nanoparticles with controllable material, dimension and shape. The latter is mainly exploited to predict the coupling with respect to fixed linear polarization directions, where the electric field vibration causes charge migration, i.e. along the semi-major axis of an ellipsoid. The nanoparticle dimension rules the number of valence and conducting bands electrons: if on one hand this exalts the dipole moment value, on the other it causes thermal weakness for lifetimes, representing the main defect characterizing the family, measured in the order of 1 *ns* [87]. Finally, the material engineering is focused on semiconductors or metals.: it is due to different fabrication procedures, as the modelling precision or features linked to the targeted application [89, 134].

The superconducting family shows a wide variety of realizations, so we will mention just two examples associated with flux and charge qubits. An overall characterization regards the presence of a collective wavefunction spreaded on

the whole device, because of cryogenic temperatures required for superconductors [24]. This experimental setup makes the family more resilient with respect to thermal noise, so lifetimes are extremely better suited for quantum computing applications, in the order of 1 μs, in some cases reaching 1 ms. SQUIDs (Superconducting QUantum Interference Devices) represent an example of ring-shaped flux qubits, whose two-level behavior is achieved by means of setting an half magnetic flux quantum, such that two degenerate clockwise and counter-clockwise collective currents are obtained. Cooper-pair boxes are related with charge qubits, where electrons are condensed in pairs, endowed with a dissociation energy representing the energy gap: further developments of this technology are currently exploited for transmons [93, 114], providing aforementioned lifetimes, otherwise limited as in quantum dots cases.

The coupling of these elements with the waveguide electromagnetic field is achieved in multiple ways, depending on the atoms trapped inside the optical fiber or lying near the external surface, thus interacting with the evanescent field [127]. As we are going to show in Section 1.4.1, the coupling with a structured bath corresponds to the definition of a form factor, which can also contain an explicit dependence on the dispersion relation. A variety of models consider acoustic waveguides characterized by a upper and lower bounded $\omega(k)$. Our treatment will include the complete analytic structure [40] induced by the form factor, thus describing emerging new features.

1.4.1 Quasi-1D free field and interaction Hamiltonian

We will consider an artificial atom coupled to a single mode of a non-leaky waveguide, neglecting the coupling with other modes [122]. In the spirit of Section 1.3, we will consider a fixed polarization direction, parallel with the oscillating electric field of the considered waveguide mode. We will identify the single mode with indices $(1,0)$, meaning that it covers with half-wavelength the major side, quantified by L_y, of the rectangular cross section, while there are no oscillations along the minor side. The latter is quantized by introducing the field operators:

$$\boldsymbol{A}^{(1,0)}(\boldsymbol{r}) = \int \mathrm{d}k \left(\frac{\hbar}{2\pi\epsilon\omega_{1,0}(k)L_yL_z}\right)^{\frac{1}{2}} \sin\left(\frac{\pi y}{L_y}\right)\left[a(k)e^{\mathrm{i}kx} + a^\dagger(k)e^{-\mathrm{i}kx}\right]\hat{u}_z, \tag{1.68}$$

$$\boldsymbol{E}^{(1,0)}(\boldsymbol{r}) = \mathrm{i}\int \mathrm{d}k \left(\frac{\hbar\omega_{1,0}(k)}{2\pi\epsilon L_yL_z}\right)^{\frac{1}{2}} \sin\left(\frac{\pi y}{L_y}\right)\left[a(k)e^{\mathrm{i}kx} - a^\dagger(k)e^{-\mathrm{i}kx}\right]\hat{u}_z, \tag{1.69}$$

with $[a(k), a^\dagger(k')] = \delta(k-k')$ and $\hat{u}_z = (0,0,1)$. The electric field energy operator associated to the mode thus reads:

$$\mathcal{E}_{el}^{(1,0)} = \frac{\epsilon}{2}\int \mathrm{d}\boldsymbol{r} :\left(E_z^{(1,0)}(\boldsymbol{r})\right)^2 := \frac{1}{2}\int \mathrm{d}k\,\hbar\omega_{1,0}(k)\Big[a^\dagger(k)a(k) - \frac{a(k)a(-k)+a^\dagger(k)a^\dagger(-k)}{2}\Big] \tag{1.70}$$

with $:(...):$ denoting normal ordering and $\omega_{1,0}(k) = v\sqrt{k^2+\left(\frac{\pi}{L_y}\right)^2}$, while the magnetic field energy can be evaluated using the relation $\boldsymbol{B}^{(1,0)} = \boldsymbol{\nabla}\times\boldsymbol{A}^{(1,0)}$:

$$\begin{aligned}\mathcal{E}_{mag}^{(1,0)} &= \frac{\epsilon}{2}\int \mathrm{d}\boldsymbol{r} :\left(\partial_y A_z^{(1,0)}(\boldsymbol{r})\right)^2 + \left(-\partial_x A_z^{(1,0)}(\boldsymbol{r})\right)^2: \\ &= \frac{1}{2}\int \mathrm{d}k\,\hbar\omega_{1,0}(k)\Big[a^\dagger(k)a(k) + \frac{a(k)a(-k)+a^\dagger(k)a^\dagger(-k)}{2}\Big].\end{aligned} \tag{1.71}$$

The free Hamiltonian for the electromagnetic field takes the diagonal form:

$$H^{(1,0)} = \mathcal{E}_{el}^{(1,0)} + \mathcal{E}_{mag}^{(1,0)} = \int \mathrm{d}k\,\hbar\omega_{1,0}(k)a^\dagger(k)a(k) = \hbar v\int \mathrm{d}k\,\sqrt{k^2+\left(\frac{\pi}{L_y}\right)^2}\,a^\dagger(k)a(k). \tag{1.72}$$

It is worth noticing that the analogy with a massive boson is not limited to the dispersion relation. Indeed, the quantum theory of the mode can be mapped onto a real scalar theory in one dimension, by introducing the operators:

$$\begin{aligned}\alpha(x) &= \int \mathrm{d}k\,\sqrt{\frac{\hbar}{2(2\pi)\omega_{1,0}(k)}}\left[a(k)e^{\mathrm{i}kx} + a^\dagger(k)e^{-\mathrm{i}kx}\right], \\ \Pi(x) &= -\mathrm{i}\int \mathrm{d}k\,\sqrt{\frac{\hbar\omega_{1,0}(k)}{2(2\pi)}}\left[a(k)e^{\mathrm{i}kx} - a^\dagger(k)e^{-\mathrm{i}kx}\right],\end{aligned} \tag{1.73}$$

satisfying

$$[\alpha(x), \Pi(x')] = \mathrm{i}\hbar\delta(x-x') \tag{1.74}$$

and related to the vector potential and the electric field by multiplication. The Hamiltonian can be expressed in terms of the field operator $\alpha(x)$ and its canonically conjugated momentum $\Pi(x')$ as:

$$H^{(1,0)} = \frac{1}{2}\int \mathrm{d}x :\Big[(\Pi(x))^2 + v^2\left(\partial_x\alpha(x)\right)^2 + v^4\left(\frac{m}{\hbar}\right)^2\left(\partial_x\alpha(x)\right)^2\Big]: \tag{1.75}$$

with $m := \frac{\pi\hbar}{vL_y}$, which also allows to identify a Hamiltonian density $\mathcal{H}(x)$ such that $H^{(1,0)} = \int \mathrm{d}x\,\mathcal{H}(x)$, which corresponds to the one ruling in Lee's model the relativistic scalar boson [85].

Furthermore, we apply a small coupling approximation to the interaction term, which enable one to neglect the $O(e^2)$ contribution [25] and to apply a dipolar approximation to the $O(e)$ term, as explained in Section 1.3. The position operator $\boldsymbol{r}$ is replaced by a non dynamical center-of-mass position $\boldsymbol{r}_0$, according to (1.59). Considering bosonic operators (1.63) and retaining only the rotating-wave terms $b(k)\sigma^+$ and $b^\dagger(k)\sigma^-$, we obtain the interaction operator:

$$H_{\text{int}}^{(dip,RW)} = \frac{\sqrt{\hbar v \mu}\ \varepsilon D_{eg}}{\sqrt{2\pi L_y L_z}} \int \frac{\mathrm{d}k}{\sqrt[4]{k^2 + (vm/\hbar)^2}} \left[b(k)\sigma^+ e^{ikx_0} + b^\dagger(k)\sigma^- e^{-ikx_0} \right], \tag{1.76}$$

where $y_0 = L_y/2$ has been used, implying the center-of-mass placed corresponding to the maximum of the transverse electric field.

Chapter 2

The resolvent formalism

If that keyboard is infinite, then on that keyboard there is no music you can play

Alessandro Baricco,
"Novecento"

2.1 Resolvent operator

The formalism introduced by Dirac to include the non-commutativity of quantum observables, naturally involves the theory of linear operators [80, 128]. The representation of these q(uantum)-numbers in this matricial framework depends on associated spectral typologies [33], whose combination is at the basis of the emergence of bound states in the continuum [53].

A detailed description of quantum systems temporal behavior requires the adoption of non-perturbative methods, such that the interaction is included at all orders in its weight, the coupling constant [40, 45]. These techniques are strictly related in their foundations with complex analysis [80], given the possibility to study the spectrum $\sigma(H)$ of an operator H by means of its resolvent set $\rho(H) = \mathbb{C} \setminus \sigma(H)$. The latter is the domain of the resolvent operator

$$G(z) = \frac{1}{z - H} \,, \tag{2.1}$$

with $z \in \rho(H)$ [25, 40, 45, 69, 80, 112, 128].

At the algebraic level, a polynomial mapping $p(z) \to p(H)$ is a homomorphism, thus preserving sum and multiplication rules [80], extendable for holomorphic functions endowed with an infinite convergent series, imposing

bounded operators as their arguments. The operator multiplication rule yields the implementation of projectors on eigenspaces of H exploiting the residue calculus:

$$P_j = \frac{1}{2\pi \mathrm{i}} \oint_{\Gamma_j} \mathrm{d}z \, G(z) \,, \tag{2.2}$$

where Γ_j represents an anticlockwise contour enclosing an eigenvalue E_j of H, which will be considered, for the sake of clarity, belonging to the discrete spectrum and isolated [40, 45]. Exploiting this algebraic basis, it is possible to express a generic function of an observable according to the holomorphic functional calculus:

$$f(H) = \frac{\mathrm{i}}{2\pi} \oint_{\Gamma} \mathrm{d}z \, \frac{f(z)}{z - H} \,, \tag{2.3}$$

where Γ is a closed contour lying in the region of analyticity of f and winding once around the spectrum $\sigma(H)$ in the clockwise direction [68]. This general expression will turn out to be extremely useful in the implementation of Fourier-Laplace transform.

In order to introduce non-perturbative methodologies capable of describing the evolution of a quantum system at all times, we have to identify the central role played by the Hamiltonian observable, which incorporates the internal structure of each free and independent element of the system together with their mutual interaction. Starting from the definition of these two separate contributions, the resolvent (2.1) will be characterized as a geometric series, so requiring the introduction of a norm to determine the convergence domain. The required operator norm corresponds to the sup norm [40, 45, 112, 128]:

$$\|G(z)\|_\infty = \sup_{\|\psi\|=1} \left\|G(z)\psi\right\| = \sup_{E\in\sigma(H)} \left|\frac{1}{z-E}\right| , \tag{2.4}$$

where in the second equality $\left\|G(z)\psi\right\| = \langle\psi|G(z)\psi\rangle$ is applied [80] and $\sigma(H)$ has to display an Hausdorff topology, that is any two distinct points have disjoint neighborhoods [128]. The Hamiltonian is conveniently separated as $H = H_0 + H_{\mathrm{int}}$, where H_0 represents the free Hamiltonian and H_{int} the interaction part. Introducing the free Hamiltonian resolvent as $G_0(z) = (z - H_0)^{-1}$, the relation [25, 40, 45]

$$G(z) = G_0(z)(1 + H_{\mathrm{int}}G(z)) \tag{2.5}$$

is solved by iteration, yielding the Dyson-Neumann expansion

$$G(z) = G_0(z) \sum_n (H_{\mathrm{int}}G_0(z))^n . \tag{2.6}$$

The absolute convergence of this geometric series regards the domain satisfying $\|H_{\text{int}}\|_\infty < \|G_0(z)\|_\infty^{-1} = \inf_{E^{(0)}\in\sigma(H_0)} \left|z - E^{(0)}\right|$ [40, 45], which is physically associated with the interaction strength and energy scales of the system.

2.2 Schrödinger equation

The Schrödinger equation [119] determines the dynamics of closed quantum systems, defining a one-parameter unitary group whose generator is a self-adjoint Hamiltonian [69, 112, 128]:

$$\mathrm{i}\,\frac{\mathrm{d}}{\mathrm{d}t}\left|\psi(t)\right\rangle = H\left|\psi(t)\right\rangle. \tag{2.7}$$

The solution of (2.7) for $\left|\psi(t=0)\right\rangle = \left|\psi_0\right\rangle$ is written as $\left|\psi(t)\right\rangle = U(t)\left|\psi_0\right\rangle$, where $U(t) = \mathrm{e}^{-\mathrm{i}Ht}$. In the general case, the evolution operator from t' to t reads $U(t,t') = U(t)U^\dagger(t')$ [25]. From now on we will consider natural units, as made in Section 1.1.

We can interpret the unitary transformation as a single-variable function of the Hamiltonian, such that, exploiting (2.3)

$$U(t) = \frac{\mathrm{i}}{2\pi}\oint_\Gamma \mathrm{d}z\,\frac{\mathrm{e}^{-\mathrm{i}zt}}{z-H}, \tag{2.8}$$

$$G(z) = -\,\mathrm{i}\int_0^{\mathrm{sgn}(\mathrm{Im}\ z)\infty} \mathrm{d}t\,\mathrm{e}^{\mathrm{i}(z-H)t}, \tag{2.9}$$

for $t > 0$ [40, 45]. This notation enables us to introduce the notion of forward and backward propagator [25]. For $\mathrm{Im}\ z > 0$ and $t > 0$ the convergence of (2.8) is related to a contour Γ called the Bromwich path. Its definition aims at the inclusion of the spectrum $\sigma(H)$ inside the contour just for positive times, thus naming the associated (2.9) forward propagator. In this way a Fourier-Laplace transform is implemented along an horizontal path lying above the real axis corresponding to the constant $\mathrm{Im}\ z$, then closing the contour to ensure convergence in the lower half-plane. Viceversa for $t < 0$ the backward propagator is linked to a closed contour in the upper half-plane, without including any singularity of the spectrum [40, 45]. Attributed names consisting in retarded and advanced Green's functions are motivated because of a non vanishing contribution just for positive or negative times [25].

The property of Fourier-Laplace transform concerning convolutions [40, 45]

$$G_0(z)G(z) \longleftrightarrow \int_0^t \mathrm{d}\tau\ U_0(t-\tau)U(\tau), \tag{2.10}$$

where $U_0(t) = \mathrm{e}^{-\mathrm{i}H_0 t}$, is applied to (2.5) to obtain

$$U(t) = U_0(t) - \mathrm{i}\int_0^t \mathrm{d}\tau\; U_0(t-\tau)H_{\mathrm{int}}U(\tau). \tag{2.11}$$

The complete treatment involves the Dyson-Neumann expansion (2.6), which is better suited in the interaction picture, where Green's functions read $V(t) = U_0^\dagger(t)U(t)$ and the evolved interaction term $H_{\mathrm{int}}(t) = U_0^\dagger(t)H_{\mathrm{int}}U_0(t)$ runs according to the free evolution [54]. Using $V(t)$ we can express (2.11) as

$$V(t) = \mathbb{1} - \mathrm{i}\int_0^t \mathrm{d}\tau\; H_{\mathrm{int}}(\tau)V(\tau), \tag{2.12}$$

consisting in a Volterra equation, whose iterative solution yields the Dyson's perturbative expansion

$$\begin{aligned} V(t) &= \sum_{n=0}^{\infty}(-\mathrm{i})^n \int_0^t \mathrm{d}\tau_1 \int_0^{\tau_1} \mathrm{d}\tau_2 \cdots \int_0^{\tau_{n-1}} \mathrm{d}\tau_n\; H_{\mathrm{int}}(\tau_1)H_{\mathrm{int}}(\tau_2)\ldots H_{\mathrm{int}}(\tau_n) \\ &= \mathcal{T}\,\mathrm{e}^{-\mathrm{i}\int_0^t \mathrm{d}\tau\; H_{\mathrm{int}}(\tau)}, \end{aligned} \tag{2.13}$$

where $\mathcal{T}$ represents the time-ordering of operator products, required by the absence of commutativity at different times [40, 45, 106].

2.3 Survival amplitude

The quantization procedure presented in Section 2.1 is applied in functional analysis to the implementation of a projection-valued measure, defined as a map P from elements of a Borel σ-algebra $\Omega \subseteq \mathbb{R}$ to the algebra of bounded operators $P(\Omega)$, with respect to a norm like (2.4). These operators have to satisfy orthogonal projections properties $P^\dagger(\Omega) = P(\Omega)$, $P^2(\Omega) = P(\Omega)$ and the following conditions: (i) $P(\varnothing) = 0$ and $P(\mathbb{R}) = \mathbb{1}$, (ii) $\sum_n P(\Omega_n)\left|\psi\right\rangle = P\left(\bigcup_n \Omega_n\right)\left|\psi\right\rangle$ for every $\left|\psi\right\rangle \in \mathscr{H}$, with $\Omega_n \cap \Omega_m = \varnothing$, $n \neq m$ [69, 112, 128].

In order to introduce the spectral theorem based on the uniqueness of the projection-valued measure for a self-adjoint operator, it is necessary to define the resolution of the identity associated with each projection-valued measure

$$P(\lambda) = P((-\infty, \lambda]), \tag{2.14}$$

which is an orthogonal projection. For every distribution function $\mu(\lambda) = \langle\psi|P(\lambda)|\psi\rangle$ there is a unique Borel measure $\mu_\psi(\Omega) = \langle\psi|P(\Omega)|\psi\rangle$, such that the integration

$$H = \int_{\mathbb{R}} \lambda \mathrm{d}P(\lambda) = \sum_j E_j P(\Omega_j) \tag{2.15}$$

is uniquely determined with respect to the projection-valued measure [69, 128]. The holomorphic functional calculus presented in Section 2.1 preserves the spectral mapping theorem, such that $\sigma(f(H)) = f(\sigma(H))$.

The inversion of the map (2.15) is expressed by means of the resolvent (2.1), whose quadratic form corresponds to the propagator of $|\psi\rangle$

$$G_\psi(z) = \langle\psi|G(z)|\psi\rangle = \int_{\mathbb{R}} \frac{1}{z-\lambda} \mathrm{d}\mu_\psi(\lambda), \tag{2.16}$$

known as the Borel transform of the measure $\mu_\psi(\lambda)$ [128]. This Herglotz function maps holomorphically the upper (respectively lower) half-plane to itself [92, 128]. The reconstruction of the measure is provided by the inversion formula

$$\mu_\psi(\lambda) = \lim_{\delta,\eta\downarrow 0} \frac{1}{\pi} \int_{-\infty}^{\lambda+\delta} \mathrm{d}E \, \mathrm{Im}\Big(G_\psi(E+\mathrm{i}\eta)\Big), \tag{2.17}$$

called spectral measure corresponding to $|\psi\rangle$ [53, 128], whose integrand represents the spectral density, a byproduct of the Herglotz functions property $G^*_\psi(z) = G_\psi(z^*)$ analyzed in Section 3.2.2.

The propagator (2.16) covers a central role in the definition of survival amplitude, as expressed in (2.8):

$$a_\psi(t) = \langle\psi|U(t)|\psi\rangle = \frac{\mathrm{i}}{2\pi} \oint_\Gamma \mathrm{d}z \, \mathrm{e}^{-\mathrm{i}zt} G_\psi(z), \tag{2.18}$$

where the introduction of (2.16) and the application of residue theorem yields

$$a_\psi(t) = \int_{\mathbb{R}} \mathrm{d}\lambda \, \varpi_\psi(\lambda) \, \mathrm{e}^{-\mathrm{i}\lambda t}, \tag{2.19}$$

with the spectral density defined by $\mathrm{d}\mu_\psi(\lambda) = \varpi_\psi(\lambda)\mathrm{d}\lambda$, with $\mathrm{supp}\left(\varpi_\psi\right) = \sigma(H)$. The unique decomposition with respect to the Lebesgue measure reads:

$$\mathrm{d}\mu_\psi = \mathrm{d}\mu^{ac}_\psi + \mathrm{d}\mu^{sc}_\psi + \mathrm{d}\mu^{pp}_\psi, \tag{2.20}$$

where $\mathrm{d}\mu^{ac}_\psi$ represents the component absolutely continuous with respect to Lebesgue measure, while $\mathrm{d}\mu^{sc}_\psi$ and $\mathrm{d}\mu^{pp}_\psi$ compose the singular component supported on sets with zero Lebesgue measure, respectively known as singular continuous (e.g. devil's staircase on Cantor set) and pure point (e.g. cavity field) part [69, 112, 128]. In the development of Friedrichs-Lee model simulators we will not meet the singular continuous component.

The same decomposition holds true in the direct sum form for Hilbert spectral subspaces and in the set union form for the different kind of spectra

[69, 112, 128]. In absence of the singular part, the Riemann-Lebesgue lemma ensures

$$\lim_{t\to\infty} a_\psi(t) = 0, \tag{2.21}$$

which constitutes the definition of quantum unstable states, conforming to the interpretation of infinitely long return periods in Poincaré recurrences [40] mentioned in Section 1.1.

2.4 Fermi golden rule

Transition amplitudes are extensively used in scattering and decay theory [45], defined similar to the survival amplitude (2.18), but the matrix element involves different initial and final states, that we will indicate as $|i\rangle$ and $|f\rangle$, which we consider to be eigenstates of H_0 with eigenvalues E_i and E_f, observed at time t_i and t_f, respectively.

Starting from (2.11), the perturbation theory is developed, with important hypotheses about time scales, which require a careful treatment. Let us consider terms up to the second order in H_{int} in the expansion of the integral equation solution:

$$U\left(t_f - t_i\right) = U_0\left(t_f - t_i\right) + \sum_{n=1}^{\infty} U^{(n)}\left(t_f - t_i\right), \tag{2.22}$$

where the dipendence just on time separation of

$$U^{(n)}\left(t_f - t_i\right) = -\mathrm{i}\int_{t_i}^{t_f} \mathrm{d}\tau\, U_0\left(t_f - \tau\right) H_{\text{int}} U^{(n-1)}\left(\tau - t_i\right), \tag{2.23}$$

is allowed by a time independent operator H. The presented result provides scattering matrix elements:

$$S_{f,i} = \left\langle f\middle|U\left(t_f - t_i\right)\middle|i\right\rangle = \mathrm{e}^{-\mathrm{i}\left(E_f t_f - E_i t_i\right)}\left(\delta_{f,i} + \sum_{n=1}^{\infty} S_{f,i}^{(n)}\right), \tag{2.24}$$

whose diagonal part represents survival amplitudes and the first term reads:

$$S_{f,i}^{(1)} = -\left\langle f|H_{\text{int}}|i\right\rangle \frac{\mathrm{e}^{\mathrm{i}\left(E_f - E_i\right)t_f} - \mathrm{e}^{-\mathrm{i}\left(E_f - E_i\right)t_i}}{E_f - E_i}. \tag{2.25}$$

Choosing initial and final times $t_f = -t_i = t/2$ symmetrical with respect to the origin, it is possible to write the result in term of the function

$$\delta_t\left(E_f - E_i\right) = \frac{\sin\left(E_f - E_i\right)t/2}{\pi\left(E_f - E_i\right)}, \tag{2.26}$$

which, since $\int \mathrm{d}E\ \delta_t(E) = 1$, represents an approximation of the Dirac delta.

This function characterizes each term in (2.24) because of the free propagator at both ends of the iterated kernel in the integral equation solution, thus providing the expression of the S-matrix:

$$S_{f,i} = \mathrm{e}^{-\mathrm{i}\left(E_f+E_i\right)\frac{t}{2}}\left[\delta_{f,i} - 2\pi\mathrm{i}\ \delta_t\left(E_f - E_i\right)\left(\langle f|H_{\mathrm{int}}|i\rangle + \sum_{j\neq i}\frac{\langle f|H_{\mathrm{int}}|j\rangle\langle j|H_{\mathrm{int}}|i\rangle}{E_i - E_j} + \dots\right)\right], \tag{2.27}$$

which will be discussed at all orders with Feynman diagrams in Section 2.5, while in this analysis we will retain terms up to the first order [25].

To obtain the Fermi golden rule we need to introduce the notion of density of states, strictly related with an absolutely continuous part of the spectrum, e.g. photons belonging to a bath in the three-dimensional space. Let us define the subspace associated with this part of the spectrum as $\mathfrak{D} \subseteq \mathbb{R}^3$, with generalized eigenvalue equation for states $H_0|\boldsymbol{k}\rangle = \omega(\boldsymbol{k})|\boldsymbol{k}\rangle$, $\boldsymbol{k} = (k_1, k_2, k_3)$ and $\langle \boldsymbol{k}|\boldsymbol{k}'\rangle = \prod_{\ell=1}^{3}\delta(k_\ell - k'_\ell)$. We introduce the survival probability as the square modulus of the amplitude (2.18), but here expressed according to states normalization condition:

$$P_i(t) = |a_i(t)|^2 = 1 - P_{\mathfrak{D},i}(t) - \sum_{j\neq i} P_{j,i}(t), \tag{2.28}$$

where in $P_{j,i}(t) = \left|\langle j|U(t)|i\rangle\right|^2$ the index j labels remaining eigenstates associated with the singular spectrum components, e.g. excited states of a multi-level system, while $P_{\mathfrak{D},i}(t) = \int_{\mathfrak{D}} \mathrm{d}^3\boldsymbol{k}\,|\langle \boldsymbol{k}|U(t)|i\rangle|^2$. The transition probability obeys the integrated squared modulus of the first order S-matrix element:

$$P_{\mathfrak{D},i}(t) \approx 4\pi^2 \int_{\mathfrak{D}} \mathrm{d}^3\boldsymbol{k}\ |\langle \boldsymbol{k}|H_{\mathrm{int}}|i\rangle|^2\,\delta_t^2(\omega(\boldsymbol{k}) - E_i). \tag{2.29}$$

Considering for clarity that the point spectrum includes only the initial state, the completeness relation reads

$$|i\rangle\langle i| + \int_{\mathfrak{D}} \mathrm{d}^3\boldsymbol{k}\ |\boldsymbol{k}\rangle\langle \boldsymbol{k}| = \mathbb{1}, \tag{2.30}$$

which, inserted in the Hamiltonian variance, yields

$$\left\langle \Delta H^2\right\rangle_i = \left\langle i\left|H^2\right|i\right\rangle - \langle i|H|i\rangle^2 = \int_{\mathfrak{D}} \mathrm{d}^3\boldsymbol{k}\ |\langle \boldsymbol{k}|H_{\mathrm{int}}|i\rangle|^2\,. \tag{2.31}$$

Applying the expansion for $\delta_t(E) \overset{t\to 0}{\approx} \frac{t}{2\pi}$, the survival probability reads

$$P_i(t) = 1 - P_{\mathfrak{D},i}(t) \approx 1 - t^2\left\langle \Delta H^2\right\rangle_i, \tag{2.32}$$

thus defining the Zeno time $\tau_Z = \langle \Delta H^2 \rangle_i^{-1}$ [40, 45]. For $t \gg \frac{2\pi}{E_i}$

$$\int_{\mathfrak{D}} \mathrm{d}^3\boldsymbol{k}\; f(\boldsymbol{k})\, \delta_t^2(\omega(\boldsymbol{k}) - E_i) \approx \frac{t}{2\pi} \int_{\mathfrak{D}} \mathrm{d}^3\boldsymbol{k}\; f(\boldsymbol{k})\, \delta\left(\omega(\boldsymbol{k}) - E_i\right), \tag{2.33}$$

valid for arbitrary integrable functions $f(\boldsymbol{k})$. This result enables one to express the survival probability in this time range as

$$P_i(t) \approx 1 - \Gamma_i t, \tag{2.34}$$

where

$$\Gamma_i = 2\pi \int_{\mathfrak{D}} \mathrm{d}^3\boldsymbol{k}\; |\langle \boldsymbol{k}|H_{\mathrm{int}}|i\rangle|^2\, \delta(\omega(\boldsymbol{k}) - E_i) = 2\pi\kappa_i(E_i) \tag{2.35}$$

is the transition rate that defines the Fermi golden rule [40, 45], with

$$\kappa_i(E) = \int_{\mathfrak{D}} \mathrm{d}^3\boldsymbol{k}\; |\langle \boldsymbol{k}|H_{\mathrm{int}}|i\rangle|^2\, \delta(\omega(\boldsymbol{k}) - E), \tag{2.36}$$

proportional to the density of states around the initial energy E_i in the assumption of interaction Hamiltonian matrix element independent on the final state on-shell energy. The approximated form (2.34) of the survival probability is valid provided

$$\frac{2\pi}{E_i} \ll t \ll \frac{1}{\Gamma_i}. \tag{2.37}$$

Considering Γ_i as a constant transition rate leads to the exponential approximation $P_i(t) \approx e^{-\Gamma_i t}$ of the transition probability. The exact description of dynamics at all times requires a non-perturbative approach, based on the renormalization implemented by the self-energy function in Section 2.5. The object presented here as proportional to states density in (2.36) will be formally introduced as a spectral density associated with a Borel transform, as made in (2.16), and the Fermi golden rule (2.35) will emerge as propagator poles approximation in Section 3.2.1 [40].

2.5 Diagrammatics and Self-energy

Among the techniques based on Feynman diagrams we are interested in the representation through vertices of the operation of indices contraction between matrices. As presented in Section 2.1 this operation may involve integrals, instead of sums, using characteristic values belonging to a continuous spectrum [33]. For clarity we will start the discussion in the framework of discrete spectra [25, 40, 45]. These two cases are related by considering the system enclosed

in a finite-size cavity, thus imposing a discrete spectrum, while in the infinite volume limit a discrete spectrum part can merge in a continuum [40].

We will follow the notation of Section 2.4, indicating with $|i\rangle$ the initial state whose survival amplitude (2.18) requires the expression of the propagator (2.16), expanded according to the Dyson resummation procedure [38]. With this aim, we introduce the free propagator and the interaction Hamiltonian matrix:

$$G_i^0(z) = \langle i|G_0(z)|i\rangle = \frac{1}{z - E_i}, \qquad H_{\text{int}}^{\ell,j} = \langle \ell|H_{\text{int}}|j\rangle\,, \tag{2.38}$$

which are required to define the edges of the diagrammatic representation and the vertices connecting them, respectively as shown in Figure 2.1(a). With the imposition that sums for an index in contraction, for intermediate free propagator of a state different from i, do not cover the value i ($j, \ell, \cdots \neq i$), it is possible to explicitly compute the diagonal matrix element $G_i(z)$, using the Dyson-Neumann expansion (2.6):

$$\begin{aligned} G_i(z) = {} & G_i^0 + G_i^0 H_{\text{int}}^{i,i} G_i^0 + \sum_{j\neq i} G_i^0 H_{\text{int}}^{i,j} G_j^0 H_{\text{int}}^{j,i} G_i^0 + G_i^0 H_{\text{int}}^{i,i} G_i^0 H_{\text{int}}^{i,i} G_i^0 \\ & + \sum_{j,\ell\neq i} G_i^0 H_{\text{int}}^{i,j} G_j^0 H_{\text{int}}^{j,\ell} G_\ell^0 H_{\text{int}}^{\ell,i} G_i^0 + \sum_{j\neq i} G_i^0 H_{\text{int}}^{i,j} G_j^0 H_{\text{int}}^{j,i} G_i^0 H_{\text{int}}^{i,i} G_i^0 \\ & + \sum_{j\neq i} G_i^0 H_{\text{int}}^{i,i} G_i^0 H_{\text{int}}^{i,j} G_j^0 H_{\text{int}}^{j,i} G_i^0 + G_i^0 H_{\text{int}}^{i,i} G_i^0 H_{\text{int}}^{i,i} G_i^0 H_{\text{int}}^{i,i} G_i^0 + \dots \end{aligned} \tag{2.39}$$

where the index i is not contracted and the dependence on z is related to free propagators [40, 45]. The summation of these terms is characterized by a self-similar structure, which allows to rearrange them as:

$$\begin{aligned} G_i(z) = {} & G_i^0 \left[H_{\text{int}}^{i,i} + H_{\text{int}}^{i,j} G_j^0 H_{\text{int}}^{j,i} + H_{\text{int}}^{i,j} G_j^0 H_{\text{int}}^{j,\ell} G_\ell^0 H_{\text{int}}^{\ell,i} + \dots \right] G_i^0 \\ & + G_i^0 \left[H_{\text{int}}^{i,i} + H_{\text{int}}^{i,j} G_j^0 H_{\text{int}}^{j,i} + \dots \right] G_i^0 \left[H_{\text{int}}^{i,i} + H_{\text{int}}^{i,j} G_j^0 H_{\text{int}}^{j,i} + \dots \right] G_i^0 + \dots \end{aligned} \tag{2.40}$$

thus obtaining (2.5) once the self-energy function

$$\Sigma_i(z) = H_{\text{int}}^{i,i} + H_{\text{int}}^{i,j} G_j^0(z) H_{\text{int}}^{j,i} + H_{\text{int}}^{i,j} G_j^0(z) H_{\text{int}}^{j,\ell} G_\ell^0(z) H_{\text{int}}^{\ell,i} + \dots \tag{2.41}$$

is introduced. The self-energy is characterized by the relation:

$$\begin{aligned} G_i(z) &= G_i^0(z) + G_i^0(z)\Sigma_i(z)G_i^0(z) + G_i^0(z)\Sigma_i(z)G_i^0(z)\Sigma_i(z)G_i^0(z) + \dots \\ &= G_i^0(z) + G_i^0(z)\Sigma_i(z)G_i(z). \end{aligned} \tag{2.42}$$

This algebraic equation, whose solution is the renormalized propagator:

$$G_i(z) = \frac{1}{z - E_i - \Sigma_i(z)}, \tag{2.43}$$

is the fundamental tool of non-perturbative methods [40, 108]. Given the characterization of the propagator as a Herglotz function of Section 2.3, the same property holds true also for the self-energy function, i.e. $\Sigma_e^*(z) = \Sigma_e(z^*)$.

It is possible to drastically simplify the self-energy expression (2.41) adopting the off-diagonal decomposition [40]. It starts by defining the projector on the initial state $|i\rangle$, supposed to be an eigenstate of H_0, and the orthogonal complement

$$P = |i\rangle\langle i|, \qquad Q = \mathbb{1} - P, \tag{2.44}$$

such that all diagonal contributions of the interaction are absorbed in the following decomposition of the total Hamiltonian:

$$H = H_0^i + H_{\text{int}}^i, \tag{2.45}$$

where

$$H_0^i = PHP + QHQ = H_0 + PH_{\text{int}}P + QH_{\text{int}}Q, \tag{2.46}$$

$$H_{\text{int}}^i = PHQ + QHP = H_{\text{int}} - PH_{\text{int}}P - QH_{\text{int}}Q, \tag{2.47}$$

with the right-hand sides deduced by the diagonality of H_0 with respect to the (P, Q) decomposition. The initial state represents still an eigenvector of H_0^i, with its eigenvalues shifted by $H_{\text{int}}^{i,i}$, as well as eigenvectors belonging to the complementary subspace.

The rearrangement of interaction terms imposes that the only nonvanishing off-diagonal elements of H_{int}^i are those between $|i\rangle$ and $|j\rangle$ with $j \neq i$, such that for every $j, \ell \neq i$ we have $\left\langle j\middle|H_{\text{int}}^i\middle|\ell\right\rangle = 0$. From now on, we will drop the superscript and include in the definition of H_0 all the diagonal part of interactions, thus absorbing the Coulomb self-energy presented in Section 1.2.

The self-energy in (2.41) is so reduced to just its second order term:

$$\Sigma_i(z) = \sum_{j\neq i} \frac{\left|H_{\text{int}}^{j,i}\right|^2}{z - E_j} = \int \mathrm{d}E\, \frac{\kappa_i(E)}{z - E}, \tag{2.48}$$

where the spectral density, mentioned in Section 2.4 as a states density, emerges as subjected to a Borel transform:

$$\kappa_i(E) = \sum_{j\neq i} \left|\langle j|H_{\text{int}}|i\rangle\right|^2 \delta(E - E_j), \tag{2.49}$$

with $\text{supp}\,(\kappa_i) = \sigma(H)$, in this case associated with a discrete spectrum, but generally supposed to be lower bounded [40].

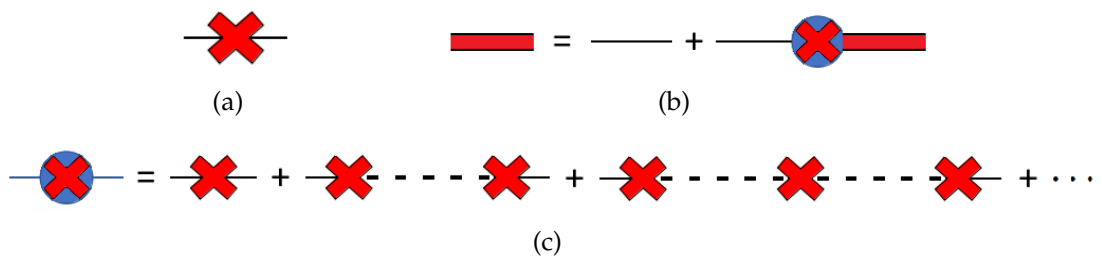

Figure 2.1: The cross in panel (a) represents the interaction Hamiltonian matrix in the eigenbasis of the free Hamiltonian H_0, with legs corresponding to the indices. In panel (b) the recurrence relation (2.42) is represented diagrammatically: the thin edge corresponds to $G_i^0(z)$, the thick red edge to $G_i(z)$ and the circled cross to the self-energy (2.41), shown in (c), whose legs are related to the matricial form of the level shift operator (2.57) and where dashed edges stand for $G_j^0(z)$ with $j \neq i$.

2.6 Projection of the resolvent in a subspace

In the following we will consider sets of identical two-level emitters, coupled to a guided field. The analysis of the evolution of their excited states will require the extension of the results obtained in Section 2.5 to the case in which P is the projector on a degenerate eigenspace of H_0. The starting point resides in the straightforward identity

$$(z - H_0 - H_{\text{int}})G(z) = \mathbb{1}, \tag{2.50}$$

following from the definition of resolvent. Multiplying it by P or Q to the left and by P to the right, inserting the completeness relation $P + Q = \mathbb{1}$ before $G(z)$ and exploiting the idempotence property, one gets [40]

$$(z - PHP)PG(z)P - PH_{\text{int}}QQG(z)P = P, \tag{2.51}$$
$$-QH_{\text{int}}PPG(z)P + (z - QHQ)QG(z)P = 0. \tag{2.52}$$

The solution of the latter, involving transition amplitudes in the complementary subspace of the degenerate one, reads

$$QG(z)P = \frac{Q}{z - QHQ}H_{\text{int}}PPG(z)P, \tag{2.53}$$

which, inserted in (2.51), provides

$$\left(z - PHP - PH_{\text{int}}\frac{Q}{z - QHQ}H_{\text{int}}P\right)PG(z)P = P. \tag{2.54}$$

We can invert the expression (2.43) to obtain the restriction of the resolvent to the subspace of the initial states, spanned by P:

$$PG(z)P = \frac{P}{z - PH_0P - PR(z)P}, \tag{2.55}$$

with the level shift operator $R(z)$ determined by

$$R(z) = H_{\text{int}} + H_{\text{int}}\frac{Q}{z - QHQ}H_{\text{int}}. \tag{2.56}$$

It is possible to apply a perturbative expansion to recover the diagrammatic expression in Figure 2.1(c)

$$R(z) = H_{\text{int}} + H_{\text{int}}\frac{Q}{z - QH_0Q}\sum_{n=0}^{\infty}\left(\frac{H_{\text{int}}}{z - QH_0Q}\right)^n QH_{\text{int}} = H_{\text{int}} + H_{\text{int}}\frac{Q}{z - QH_0Q}R(z), \tag{2.57}$$

where, considering the one dimensional case $P = |i\rangle\langle i|$ of Section 2.5, it is evident that intermediate states must be orthogonal to $|i\rangle$. Considering the off-diagonal decomposition, the coupling among the latter vanishes, thus yielding

$$R(z) = H_{\text{int}} + H_{\text{int}}\frac{Q}{z - H_0}H_{\text{int}}, \tag{2.58}$$

such that in the aforementioned one dimensional case (2.48) is recovered [40], with

$$\Sigma_i(z) = \langle i|R(z)|i\rangle\,. \tag{2.59}$$

Chapter 3

Single emitter decay

If our small minds, for some convenience, divide this glass of wine, this universe, into parts – physics, biology, geology, astronomy, psychology, and so on – remember that nature does not know it!

Richard Feynman,
"The Feynman Lectures on Physics"

Decay phenomena targeted in our quantum optics framework are included in the absent unitary dynamics for the reduced qubit system once the electromagnetic field is traced out. This lacking of a self-adjoint Hamiltonian as generator translates in energy eigenvalues that cease to be real and thus require to be associated with generalized eigenfunctions that are no more square integrable. Unstable states defined by (2.21) perfectly match with this condition, because aformentioned complex eigenvalues cannot belong to the singular spectrum.

A complete characterization through propagator poles will be given, underlining the resulting Fermi's golden rule from the self-energy series expansion around the bare energy gap. For increasing coupling values a not decaying eigenstate emerges outside the continuum as a non-perturbative effect in waveguides.

3.1 Selection rules

A multi-level system coupled with the electromagnetic field is already presented in its basic ingredients in Section 1.3. Here we will discuss more detailed insights about the dipolar approximation. To understand the generality

of this framework, we will start from the three-dimensional case [3, 21]. Let us consider (1.59) in its explicit form

$$H_{\text{int}} = \frac{e}{m_e}\sqrt{\frac{\hbar}{2\epsilon_0}}\int \frac{\mathrm{d}^3\boldsymbol{k}}{\sqrt{(2\pi)^3\omega(\boldsymbol{k})}}\sum_{\boldsymbol{\mathfrak{e}}} \boldsymbol{\mathfrak{e}}(\boldsymbol{k})\cdot\boldsymbol{p}\left[a_{\boldsymbol{\mathfrak{e}}}(\boldsymbol{k})e^{i\boldsymbol{k}\cdot\boldsymbol{r}_0} + a^\dagger_{\boldsymbol{\mathfrak{e}}}(\boldsymbol{k})e^{-i\boldsymbol{k}\cdot\boldsymbol{r}_0}\right], \tag{3.1}$$

where from now on we will omit the superscript (*dip*). The commonly quantized hydrogen-like atom orbitals are labelled as $|n,\ell,m\rangle$, respectively the principal, angular and magnetic quantum numbers. Considering Heisenberg equations of motion for relative coordinates, approximated by the electron ones in Section 1.3, we can substitute the momentum operator with the position operator in each matrix element $\sigma^{n,\ell,m}_{n',\ell',m'} = |n,\ell,m\rangle\langle n',\ell',m'|$ associated with internal degrees of freedom [131], which implements transitions between energy levels:

$$\left\langle n,\ell,m\middle|\frac{\boldsymbol{p}}{m_e}\middle|n',\ell',m'\right\rangle = \frac{\mathrm{i}}{\hbar}\left\langle n,\ell,m\middle|\left[H^0_{\text{at}},\boldsymbol{r}\right]\middle|n',\ell',m'\right\rangle = \mathrm{i}\Delta_{n,n'}\langle n,\ell,m|\boldsymbol{r}|n',\ell',m'\rangle\,, \tag{3.2}$$

where $\Delta_{n,n'} = \frac{Z^2e^4m_e}{32\pi^2\epsilon_0^2\hbar^2}\left(\frac{1}{n'^2}-\frac{1}{n^2}\right)$ represents the energy shift between considered states, with Z the atomic number. The decomposed of circular polarization according to spherical basis unit vectors reads

$$\boldsymbol{\mathfrak{e}}(\boldsymbol{k}) = (\boldsymbol{\mathfrak{e}}_+(\boldsymbol{k}),\boldsymbol{\mathfrak{e}}_-(\boldsymbol{k}))\,, \qquad \boldsymbol{\mathfrak{e}}_q(\boldsymbol{k}) = \left|\boldsymbol{\mathfrak{e}}_q(\boldsymbol{k})\right| \times \begin{cases} -\frac{\hat{x}+\mathrm{i}\hat{y}}{\sqrt{2}} & \text{for } q=+, \\ \frac{\hat{x}-\mathrm{i}\hat{y}}{\sqrt{2}} & \text{for } q=-, \end{cases} \tag{3.3}$$

where we assume that the dependence on $\boldsymbol{k}$ is related just to the modulus. According to atomic internal degrees of freedom the interaction matrix assumes the following form:

$$\left\langle n,\ell,m\middle|\sum_{\boldsymbol{\mathfrak{e}}}\frac{\boldsymbol{\mathfrak{e}}(\boldsymbol{k})\cdot\boldsymbol{p}}{m_e}\middle|n',\ell',m'\right\rangle\sigma^{n,\ell,m}_{n',\ell',m'} = \mathrm{i}\Delta_{n,n'}\sum_{q=\pm}(-1)^q\boldsymbol{\mathfrak{e}}_q(\boldsymbol{k})\left\langle r_{-q}\right\rangle^{n,\ell,m}_{n',\ell',m'}\sigma^{n,\ell,m}_{n',\ell',m'}, \tag{3.4}$$

with $\left\langle r_{-q}\right\rangle^{n,\ell,m}_{n',\ell',m'} = \left\langle n,\ell,m\middle|r_{-q}\middle|n',\ell',m'\right\rangle$ and where radial position components in the spherical basis $\boldsymbol{r} = (r_+,r_-)$ exploit spherical harmonics $\mathrm{Y}^m_\ell(\hat{\boldsymbol{n}}) = \langle\hat{\boldsymbol{n}}|\ell,m\rangle$, with $|\hat{\boldsymbol{n}}\rangle$ for polar and azimuthal angle coordinates representation

$$r_q = r\sqrt{\frac{4\pi}{3}}\mathrm{Y}^q_1(\hat{\boldsymbol{n}}), \tag{3.5}$$

where $q=\pm1$, such that following (1.62) the dipole matrix reads:

$$D^{n,\ell,m}_{n',\ell',m'} = e\sqrt{\frac{4\pi}{3}}\left|\sum_{q=\pm}(-1)^q\boldsymbol{\mathfrak{e}}_q(\boldsymbol{k})\left\langle n,\ell,m\middle|r\mathrm{Y}^{-q}_1(\hat{\boldsymbol{n}})\middle|n',\ell',m'\right\rangle\right|. \tag{3.6}$$

Further elaborations of this expression require the explicit integration in the three-dimensional space of the sandwiched factor, separated in its radial and angular part. The latter leads to the introduction of Clebsch-Gordan coefficients, which impose selection rules $\Delta\ell = 0, \pm 1$ and $\Delta m = \pm 1, 0$, where vanishing variation in both is forbidden, holding true for targeted dipole transitions.

The dipole matrix shows vanishing diagonal elements if the interaction Hamiltonian is parity invariant. In general for a unitary parity transformation $\mathcal{P}$, its eigenvalues are ± 1, so $\mathcal{P}^2 = \mathbb{1}$. It reverses both position and momentum:

$$\mathcal{P}\boldsymbol{r}\mathcal{P} = -\boldsymbol{r}, \qquad \mathcal{P}\boldsymbol{p}\mathcal{P} = -\boldsymbol{p}, \tag{3.7}$$

as for photons momentum, such that the invariance reads:

$$\mathcal{P}H_{\text{int}}\mathcal{P} = H_{\text{int}}, \tag{3.8}$$

holding true with our choice of momentum dependence just in modulus of circular polarizations in (3.3) if $|\boldsymbol{\varepsilon}(\boldsymbol{k})| = |\boldsymbol{\varepsilon}(-\boldsymbol{k})|$, while the sign is opposite for remaining vectorial quantities. Spherical harmonics implement the sign change for atomic orbitals:

$$\langle \boldsymbol{r}|\mathcal{P}|n,\ell,m\rangle = \langle -\boldsymbol{r}|n,\ell,m\rangle = R_{n,\ell}(r)\mathrm{Y}_\ell^m(-\hat{\boldsymbol{n}}) = R_{n,\ell}(r)(-1)^\ell \mathrm{Y}_\ell^m(\hat{\boldsymbol{n}}), \tag{3.9}$$

because we can reverse just the direction. In general if we are dealing with nanostructures presented in Section 1.4, the eigenvalue equation $\mathcal{P}|e\rangle = \pm|e\rangle$ implies:

$$\langle e|\boldsymbol{p}|e\rangle = \left\langle e\middle|\mathcal{P}^2\boldsymbol{p}\mathcal{P}^2\middle|e\right\rangle = -\langle e|\boldsymbol{p}|e\rangle = 0. \tag{3.10}$$

A higher precision in the determination of dipole matrix elements is achievable including the spin quantum number, while for applications described in Section 1.4 atomic orbitals should be replaced by molecular ones and predictions of band theory [87].

3.1.1 Approximations summary

The interaction Hamiltonian (3.1) involves the whole set of degrees of freedom characterizing the problem, represented by internal states, translational (center-of-mass) and electromagnetic field degrees of freedom. This means that the global system Hilbert space is spanned by the vectors

$$|\boldsymbol{p}_0\rangle \otimes |\boldsymbol{j}\rangle \otimes |\boldsymbol{k}_1, \boldsymbol{\varepsilon}_1; \ldots; \boldsymbol{k}_N, \boldsymbol{\varepsilon}_N\rangle\,, \tag{3.11}$$

where $\boldsymbol{p}_0$ is the center-of-mass momentum, $\boldsymbol{j}$ is a general multi-index for internal states and $(\boldsymbol{k}, \boldsymbol{\varepsilon})$ are momentum and polarization of each photon characterizing the n-photon basis (Fock) state. The transition between internal states is

accompanied by a recoil of the center-of-mass, implemented by

$$e^{i\boldsymbol{k}\cdot\boldsymbol{r}_0}\,|\boldsymbol{p}_0\rangle = |\boldsymbol{p}_0 + \hbar\boldsymbol{k}\rangle\,. \tag{3.12}$$

The center-of-mass momentum translation is linked with the multipole expansion in the original frame [45]

$$e^{i\boldsymbol{k}\cdot\boldsymbol{r}} = 1 + i\boldsymbol{k}\cdot\boldsymbol{r} - \frac{(\boldsymbol{k}\cdot\boldsymbol{r})^2}{2!} + \ldots, \tag{3.13}$$

where the second term is associated with dipolar transitions discussed in Section 3.1, while higher order terms employ selection rules with larger variations of angular momenta.

Following the approach of Section 1.3 we can estimate the orders of magnitude exploiting an approximate description. The fine structure constant, defined as

$$\alpha = \frac{e^2}{4\pi\epsilon_0\hbar c} \approx \frac{1}{137}, \tag{3.14}$$

plays a central role in the expression of Bohr's energy levels

$$E_n = -\frac{Z^2\alpha\hbar c}{2a_0 n^2} = -\frac{Z^2\alpha^2 m_e c^2}{2n^2}, \tag{3.15}$$

where Bohr's radius, introduced in Section 1.3, reads

$$a_0 = \frac{4\pi\epsilon_0\hbar^2}{e^2 m_e} = \frac{\hbar}{\alpha m_e c}. \tag{3.16}$$

These quantities allow us to evaluate the relative ratio of multipole expansion terms, starting from the observation that emitted and absorbed radiation by atoms has a large wavelength compared to the atomic orbital extension a_0. Considering a linear dispersion relation $\omega(\boldsymbol{k}) = ck$, the wavelength for a generic transition is well estimated from (3.15) for a small principal quantum number by $(\alpha^2 m_e c)^{-1}$, such that $|\boldsymbol{k}\cdot\boldsymbol{r}| \approx \alpha \ll 1$ [45]. Instead, for high energy transitions, an explicit dependence on Z and n has to be taken into account.

Our one-dimensional embedding, mainly referred to waveguides, is still described by (3.1), but two of the three continuous degrees of freedom for photons momenta become discrete to label the waveguide modes. As already introduced in Section 1.4 our model will deal with just the lowest energy mode, selected through an adequate choice of the energy gap characterizing quantum systems, approximated as endowed with just two-levels.

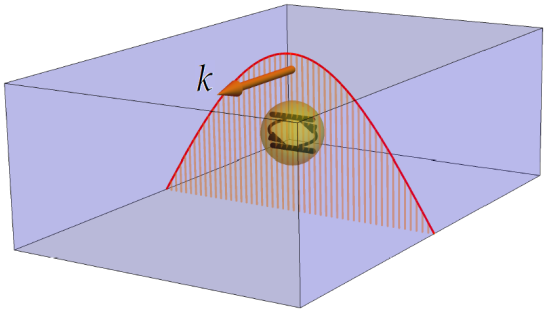

Figure 3.1: Pictorial representation of the atomic transition between the excited state $|e\rangle$ and the ground state $|g\rangle$ coupled only to the lowest energy mode of the waveguide, whose profile is shown in red.

3.2 Spontaneous photon emission

The study of typical properties for the qubit of our one dimensional platform has to characterize first of all the single coupled two-level emitter. Dipolar and rotating wave approximations presented in Section 1.3 enable us to map the QED dynamics onto a Friedrichs-Lee Hamiltonian in the one excitation sector, in which states take the form (1.17). The main issue concerns the identification of the form factor, whose solution is written in (1.76) and where the bosonic algebra introduced in (1.63) appears. Adopting from now on natural units, the field model is ruled by the following Hamiltonian

$$H = H_0 + H_{\text{int}}, \tag{3.17}$$

$$H_0 = \varepsilon\sigma^+\sigma^- + \int \mathrm{d}k\, \omega(k) b^\dagger(k) b(k), \tag{3.18}$$

$$H_{\text{int}} = \int \mathrm{d}k \left[F^*(k) b(k) \sigma^+ + F(k) b^\dagger(k) \sigma^- \right], \tag{3.19}$$

where the emitter is placed in the origin $x_0 = 0$ and the form factor reads

$$F(k) = \sqrt{\frac{\gamma}{2\pi\omega(k)}}. \tag{3.20}$$

It is possible to recognize the off-diagonal decomposition presented in Section 2.5, because the interaction is not endowed with a diagonal part in the adopted basis (1.17) for the one-excitation sector. The expression of the self-energy is

obtained through the eigenvalue equation:

$$Ea = \varepsilon a + \int \mathrm{d}k\, F^*(k)\xi(k), \tag{3.21}$$

$$E\xi(k) = \omega(k)\xi(k) + F(k)a, \tag{3.22}$$

whose solutions are related to the kernel of the inverse propagator associated with the initial excited state of the qubit

$$G_e^{-1}(E)\, a = \Big(E - \varepsilon - \Sigma_e(E)\Big)\, a = 0, \tag{3.23}$$

where the self-energy for the initial excited state reads

$$\Sigma_e(E) = \int_{-\infty}^{+\infty} \mathrm{d}k\, \frac{|F(k)|^2}{E - \omega(k)}. \tag{3.24}$$

In this case, we have a straightforward extension of (2.48) for a continuous spectrum, associated with propagating photons. The absence of eigenstates immersed in the continuum is signaled by the integrand divergence for real energies in $E = \omega(k)$ not compensated by a vanisking spectral density, formally presented in Section 2.5. As explained in Section 3.2.1, this translates in a not vanishing imaginary part for the self-energy in proximity of the real axis.

In the case of an atom coupled to a waveguide mode, with dispersion relation $\omega(k) = \sqrt{k^2 + m^2}$, one obtains the spectral density

$$\kappa_e(\omega) = \frac{\gamma}{\pi\sqrt{\omega^2 - m^2}}\, \chi_{[m,\infty)}(\omega), \tag{3.25}$$

characterized by a square-root divergence at the lower bound of the absolutely continuous spectrum.

An explicit expression for the self-energy (3.24) for waveguide QED is achieved employing the analytical continuation to the complex k plane of the integrand function:

$$\Sigma_e(z) = \frac{\gamma}{2\pi} \int_{-\infty}^{+\infty} \mathrm{d}k\, \frac{1}{\sqrt{k^2 + m^2}\Big(z - \sqrt{k^2 + m^2}\Big)}. \tag{3.26}$$

Notice that $\Sigma_e(z)$ is well-defined only if $\mathrm{Im}(z) \neq 0$ or $\mathrm{Re}(z) < m$. We define a semicircular contour $C_\rho = \left\{\rho \mathrm{e}^{\mathrm{i}\phi} | \phi \in [0, \pi]\right\}$ of arbitrary radius ρ, lying in the upper half plane, such that the integration contour $\Gamma_\rho = \mathbb{R} \cup C_\rho \cup \Gamma_\rho^{\mathrm{cut}}$, where $\Gamma_\rho^{\mathrm{cut}}$ represents the contour sorrounding the cut of the complex plane along $[\mathrm{i}m, \mathrm{i}\rho)$,

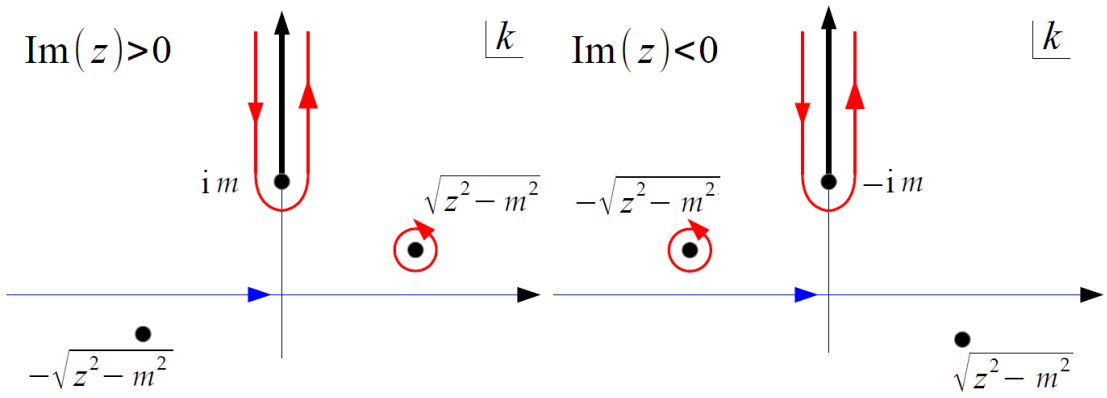

Figure 3.2: Integration contours (red) in the complex k plane for the computation of the integral in (3.26) with $\mathrm{Im}(z) > 0$ (left panel) and $\mathrm{Im}(z) < 0$ (right panel).

shown with the reversed orientation in Figure 3.2. In the limit $\rho \to \infty$, the latter is involved in the following identity:

$$\Sigma_e(z) = \frac{\gamma}{2\pi} \oint_{\Gamma_\infty} \mathrm{d}k \, \frac{1}{\sqrt{k^2+m^2}\left(z - \sqrt{k^2+m^2}\right)} - \frac{\gamma}{2\pi} I_{\mathrm{cut}}(z), \tag{3.27}$$

where $I_{\mathrm{cut}}(z)$ represents the integration along $\Gamma_\infty^{\mathrm{cut}}$, inversely oriented with respect to Figure 3.2.

The residue theorem provides the first term in (3.27),

$$\lim_{k \to \sqrt{z^2-m^2}} \frac{\left(k - \sqrt{z^2-m^2}\right)\left(z + \sqrt{k^2+m^2}\right)}{\sqrt{k^2+m^2}\,(z^2-m^2-k^2)} = -\frac{z+\sqrt{z^2}}{2\sqrt{z^2}\sqrt{z^2-m^2}} = \begin{cases} \frac{-1}{\sqrt{z^2-m^2}}, & \mathrm{Re}(z) > 0 \\ 0, & \mathrm{Re}(z) < 0 \end{cases} \tag{3.28}$$

where we considered $\sqrt{z^2} = \mathrm{sgn}\big(\mathrm{Re}(z)\big)\, z$. The result (3.28) holds true for $\mathrm{Im}(z) > 0$, while the opposite is obtained otherwise. Let us introduce the notation:

$$\mathcal{I}^{\pm}_{\mathrm{cut}}(z,k) = \lim_{x \to 0^{\pm}} \frac{1}{\sqrt{(x+\mathrm{i}y)^2+m^2}\left(z - \sqrt{(x+\mathrm{i}y)^2+m^2}\right)}, \tag{3.29}$$

where $\sqrt{(\mathrm{i}y + 0^{\pm})^2 + m^2} = \pm \mathrm{i}\sqrt{y^2-m^2}$, such that, integrating along the cut:

$$I_{\mathrm{cut}}(z) = \int_{\mathrm{i}m}^{\mathrm{i}\infty} \mathrm{d}k \left(\mathcal{I}^{-}_{\mathrm{cut}}(z,k) - \mathcal{I}^{+}_{\mathrm{cut}}(z,k)\right) = \int_m^{\infty} \mathrm{d}y \, \frac{2z}{\sqrt{y^2-m^2}\left(m^2-y^2-z^2\right)}. \tag{3.30}$$

The self-energy in (3.27) is characterized by a "pole" and a "cut" contribution:

$$\Sigma_e(z) = \Sigma_e^{\text{pole}}(z) + \Sigma_e^{\text{cut}}(z) \tag{3.31}$$
$$= \operatorname{sgn}\Big(\operatorname{Im}(z)\Big)\frac{-\mathrm{i}\gamma\,\Theta\Big(\operatorname{Re}(z)\Big)}{\sqrt{z^2-m^2}} - \frac{\gamma z\,\operatorname{sgn}\Big(\operatorname{Re}(z)\Big)}{\pi}\int_m^\infty \mathrm{d}y\,\frac{\operatorname{sgn}\Big(\operatorname{Re}(z)\Big)}{\sqrt{y^2-m^2}\Big(m^2-y^2-z^2\Big)},$$

with the second term integral

$$\int_m^\infty \mathrm{d}y\,\frac{\operatorname{sgn}\Big(\operatorname{Re}(z)\Big)}{\sqrt{y^2-m^2}\Big(m^2-y^2-z^2\Big)} = \left[\frac{1}{z\sqrt{z^2-m^2}}\operatorname{arctanh}\left(-\frac{\operatorname{sgn}\Big(\operatorname{Re}(z)\Big)yz}{\sqrt{y^2-m^2}\,\sqrt{z^2-m^2}}\right)\right]_m^\infty, \tag{3.32}$$

yielding

$$\Sigma_e^{\text{cut}}(z) = -\frac{\gamma}{\pi}\,\frac{\operatorname{sgn}\Big(\operatorname{Re}(z)\Big)}{\sqrt{z^2-m^2}}\,\operatorname{Log}\left(\frac{\operatorname{sgn}\Big(\operatorname{Re}(z)\Big)\,z - \sqrt{z^2-m^2}}{m}\right), \tag{3.33}$$

where $\operatorname{Re}\Big(\operatorname{sgn}\Big(\operatorname{Re}(z)\Big)\,z - \sqrt{z^2-m^2}\Big) > 0$ for every z.

3.2.1 Analytical continuation

The inverse propagator (3.23) is generally defined for a complex energy z, according to which unstable or metastable states are endowed with a lifetime shorter or longer than the non-interacting one and thus cannot be characterized as stable steady eigenstates. Poles of the propagator (2.16) are associated with real eigenvalues in the case of eigenstates, while complex poles $z_p = E_p - \mathrm{i}\gamma_p/2$ in the second Riemann sheet of the propagator yield the decay law (2.18).

The first procedure involves distribution limits [40, 95] in the following form

$$\lim_{\gamma_p\to 0}\frac{E_p-\omega}{(E_p-\omega)^2+\gamma_p^2/4} = \frac{\text{P.V.}}{E_p-\omega}, \tag{3.34}$$

$$\lim_{\gamma_p\to 0}\frac{\gamma_p}{(E_p-\omega)^2+\gamma_p^2/4} = 2\pi\delta(E_p-\omega), \tag{3.35}$$

where P.V. stands for principal value. The absolutely continuous part of the Hamiltonian spectrum is not modified by the interaction with a discrete spectrum [53]: the complex plane associated with the integration in (2.18) is endowed with a cut lying on the real axis corresponding to this part of the spectrum. In the case of a waveguides mode the branching point is at $z = m$, with

a branch cut extending to $z \to \infty$, such that the Sokhotski-Plemelj formula [40] reads

$$\Sigma_e(E \pm \mathrm{i}0^+) = \int \mathrm{d}\omega \, \frac{\kappa_e(\omega)}{E \pm \mathrm{i}0^+ - \omega} = \fint \mathrm{d}\omega \, \frac{\kappa_e(\omega)}{E \pm \mathrm{i}0^+ - \omega} \mp \mathrm{i}\pi \int \mathrm{d}\omega \, \kappa_e(\omega)\delta(E - \omega), \tag{3.36}$$

where $\fint = \text{P.V.} \int$ for the principal value integral. Thus, the discontinuity at the cut reads

$$\Sigma_e(E - \mathrm{i}0^+) - \Sigma_e(E + \mathrm{i}0^+) = 2\pi\mathrm{i}\kappa_e(E). \tag{3.37}$$

The analytical continuation of the self-energy in the lower complex half-plane is based on the imposition of continuity $\Sigma_e(E + \mathrm{i}0^+) = \Sigma_e^{\mathrm{II}}(E - \mathrm{i}0^+)$ yielding

$$\Sigma_e^{\mathrm{II}}(z) = \Sigma_e(z) - 2\pi\mathrm{i}\kappa_e(z) = \Sigma_e(z) - \frac{2\gamma\mathrm{i}}{\sqrt{z^2 - m^2}}, \tag{3.38}$$

immediately leading to the analytical continuation of the inverse propagator

$$\left(G_e^{\mathrm{II}}\right)^{-1}(z) = z - \varepsilon - \Sigma_e^{\mathrm{II}}(z). \tag{3.39}$$

The definition for its kernel is a straightforward extension of (3.23), providing

$$z_p = E_p - \mathrm{i}\frac{\gamma_p}{2} = \varepsilon + \Sigma_e(z_p) - 2\pi\mathrm{i}\kappa_e(z_p), \tag{3.40}$$

decomposed for real and imaginary part as

$$E_p = \varepsilon + \int \mathrm{d}\omega \, \frac{(E_p - \omega)\kappa_e(\omega)}{\left|z_p - \omega\right|^2} + 2\pi \, \mathrm{Im}\left(\kappa_e(z_p)\right), \tag{3.41}$$

$$\frac{\gamma_p}{2}\left(1 + \int \mathrm{d}\omega \, \frac{\kappa_e(\omega)}{\left|z_p - \omega\right|^2}\right) = 2\pi \, \mathrm{Re}\left(\kappa_e(z_p)\right). \tag{3.42}$$

These expression can be treated by means of different perturbative approaches, to obtain the results presented in Section 2.4. Considering first order terms in the expansion with respect to the spectral density (hence, to the squared coupling constant) yields

$$E_p = \varepsilon + \fint \mathrm{d}\omega \, \frac{\kappa_e(\omega)}{\varepsilon - \omega} + O(\gamma^2), \tag{3.43}$$

$$\gamma_p = 2\pi\kappa_e(\varepsilon) + O(\gamma^2), \tag{3.44}$$

where the latter equation corresponds to the Fermi golden rule (2.35).

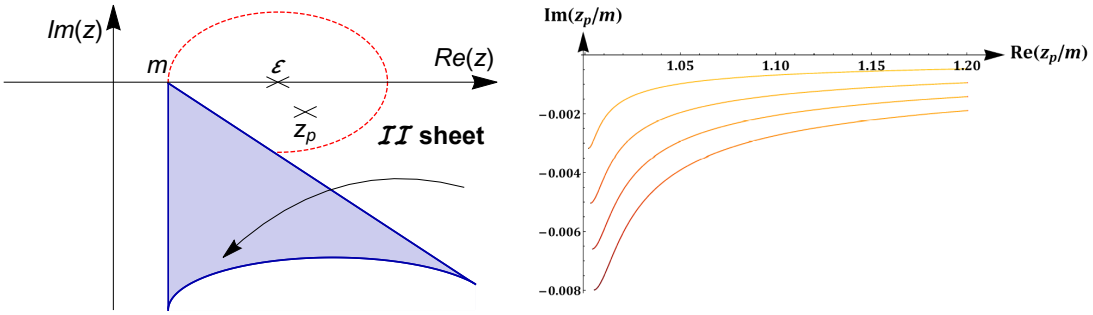

(a) (b)

Figure 3.3: Representation of the complex plane with the branching cut and radius of convergence of the Breit-Wigner expansion (3.45) in (a). Trajectories of the pole z_p for the waveguide model in (b), given by numerical solutions of (3.40) associated with the variation in ε, while graded colors refer to couplings $\gamma = \pi \times 10^{-4}m^2$, $\gamma = 2\pi \times 10^{-4}m^2$, $\gamma = 3\pi \times 10^{-4}m^2$, $\gamma = 4\pi \times 10^{-4}m^2$.

The second procedure is called the Breit-Wigner approximation [40] and it involves a series expansion of the self-energy function around the bare energy

$$\Sigma_e^{\mathrm{II}}(z) = \Sigma_e^{\mathrm{II}}(\varepsilon - \mathrm{i}0^+) + \left.\frac{\mathrm{d}\Sigma_e^{\mathrm{II}}}{\mathrm{d}z}\right|_{z=\varepsilon-\mathrm{i}0^+}(z-\varepsilon) + O(\gamma^3). \tag{3.45}$$

The radius of convergence $r_c = \varepsilon - m$ coincides with the distance from the singularity at the branching point, as shown in Figure 3.3(a). In the weak-coupling limit, the pole lies inside the convergence region $\left|z_p - \varepsilon\right| \approx \gamma\varepsilon \ll r_c$, such that the condition defining the kernel of (3.39) is expressed as

$$z_p - \varepsilon = \Sigma_e(\varepsilon + \mathrm{i}0^+) + \left.\frac{\mathrm{d}\Sigma_e}{\mathrm{d}z}\right|_{z=\varepsilon-\mathrm{i}0^+}(z-\varepsilon) + O(\gamma^3), \tag{3.46}$$

where we exploit the continuity between $\Sigma_e^{\mathrm{II}}(z)$ and $\Sigma_e(z)$ along the branch cut. Considering only the first term of the Breit-Wigner expansion and using its expression according to (3.36), level shift (3.43) and Fermi golden rule (3.44) are obtained.

3.2.2 Weisskopf-Wigner approximation

In Section 2.3 we already presented the propagator as a Herglotz function, whose property entails the expression (2.17). Let us apply (3.37) to the propagator:

$$G_e(E - \mathrm{i}0^+) - G_e(E + \mathrm{i}0^+) = 2\pi\mathrm{i}\omega_e(E), \tag{3.47}$$

obtaining the spectral density [40]

$$\varpi_e(E) = -\frac{1}{\pi}\,\mathrm{Im}\Big(G_e(E+\mathrm{i}0^+)\Big), \tag{3.48}$$

whose sign is an overall phase with no physical meaning with respect to the Fourier transform (2.19) of the probability amplitude it is associated with. An explicit expression for this density is achievable using (3.36) to identify real and imaginary part for the self-energy:

$$\Sigma_e(E \pm \mathrm{i}0^+) = \Delta_e(E) \mp \frac{\mathrm{i}}{2}\Gamma_e(E), \tag{3.49}$$

which also admits operatorial expressions [25, 40] following (2.58)

$$\Delta_e(E) = \mathrm{P.V.}\left\langle e\middle|H_{\mathrm{int}}\frac{Q}{E-QH_0Q}H_{\mathrm{int}}\middle|e\right\rangle = \fint \mathrm{d}\omega\,\frac{\kappa_e(\omega)}{E-\omega}, \tag{3.50}$$

$$\Gamma_e(E) = 2\pi\left\langle e\middle|H_{\mathrm{int}}Q\,\delta\Big(E-QH_0Q\Big)\,QH_{\mathrm{int}}\middle|e\right\rangle = 2\pi\kappa_e(E). \tag{3.51}$$

Here we exploited the off-diagonal form of (1.18) with respect to $P = |e\rangle\langle e|$ and $Q = \mathbb{1} - P$. The introduced notation allows us to obtain the interesting explicit form of the spectral density:

$$\varpi_e(E) = -\frac{1}{\pi}\,\mathrm{Im}\left[\frac{1}{E-\varepsilon-\Delta_e(E)+\frac{\mathrm{i}}{2}\Gamma_e(E)}\right] = \frac{\Gamma_e(E)}{2\pi}\,\frac{1}{\Big(E-\varepsilon-\Delta_e(E)\Big)^2+\Big(\frac{\Gamma_e(E)}{2}\Big)^2}, \tag{3.52}$$

consisting in a Lorentzian distribution with energy-dependent coefficients, whose variation within the peak affects the decay time behavior. In the limit of constant coefficients, not varying with respect to their value corresponding to the bare energy, a pure exponential decay is observed, given by:

$$\varpi_e^{(BW)}(E) = \frac{\Gamma_e(\varepsilon)}{2\pi}\,\frac{1}{\Big(E-\varepsilon-\Delta_e(\varepsilon)\Big)^2+\Big(\frac{\Gamma_e(\varepsilon)}{2}\Big)^2}, \tag{3.53}$$

known as the Breit-Wigner spectrum. The purely exponential decay is obtained by integrating (2.18) with the approximated spectral density (3.53), neglecting other poles and the branch cut contribution, which causes large-time power-law behaviors. This procedure is equivalent to the approximation

$$G_e^{\mathrm{II}}(z) \approx \frac{1}{z-\varepsilon-\Sigma_e^{\mathrm{II}}(z_p)} = \frac{1}{z-z_p}, \tag{3.54}$$

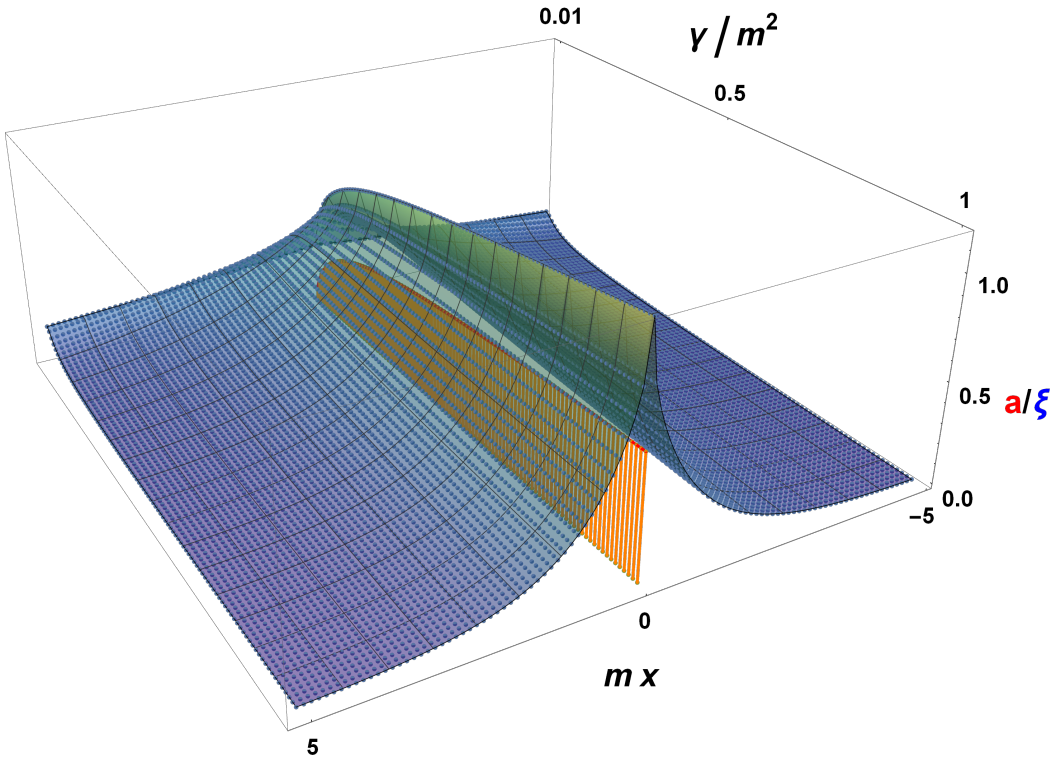

Figure 3.4: Behavior of the plasmonic eigenstate excited state amplitude (red) and exponentially localized photon wavefunction (blue) with $\varepsilon = 1.1\ m$ with respect to a variation in the coupling constant γ.

where the equality holds true by (3.40). Weisskopf-Wigner approximation thus describes a pure exponential behavior $a(t) = e^{-iz_p t}$, without short and long time corrections [40].

The photon dissipation associated with the decay of a single two-level emitter in a single-mode waveguide is described in Figure 3.3(b) concerning intermediate time scales, where the exponential approximation holds. Even if the rich analytic structure linked with the branch cut is not considered, variations in the decay rate are observed, whose knowledge requires the complete treatment moving near the energetic cutoff for propagating photons.

3.2.3 Plasmonic eigenstates

The key role played by the form factor strongly influences perturbative and non-perturbative system dynamics. In particular eigenstates associated with evanescent field modes, with energy below the threshold m can emerge. Such states are characterized by the photon exponentially localized near the quantum

emitter and are named "plasmonic" [26]. This fast decrease property of the photon wavefunction is essential to ensure the global state normalizability.

Let us start with the singularity condition expressed by (3.40), where the analytical continuation is based on the spectral density $\kappa_e(E)$, characterized by a support on the real axis starting from the threshold m, like the self-energy imaginary part $\Gamma_e(E)$. This means that poles associated with evenescent modes below the cutoff lie on the first Riemann sheet and are real because $\mathrm{Im}\,(\Sigma_e(E)) = 0$ for $E < m$, so representing eigenstates.

An analytic expression of the energy of plasmonic modes is achievable by considering in (3.31) the real cut contribution, such that (3.32) becomes for energies below the cutoff,

$$\Sigma_e^{\mathrm{cut}}(E) = -\frac{\gamma}{2\pi}\frac{\pi + 2\arctan\left(\frac{E}{\sqrt{m^2-E^2}}\right)}{\sqrt{m^2-E^2}}. \tag{3.55}$$

The singularity condition $E - \varepsilon = \Sigma_e^{\mathrm{cut}}(E)$ is translated into the intersection of the straight line $E - \varepsilon$, with $\varepsilon > 0$, and the monotonically decreasing real self-energy, yielding a single simple pole. This solution is displaced by an increasing distance from m for increasing coupling γ and fixed ε, while a reversed behavior of these parameters pushes the pole towards m. If the emitter gap is much larger than the threshold, it is possible to apply a perturbative expansion, thus providing $E \approx \varepsilon + \Sigma_e^{\mathrm{cut}}(\varepsilon)$, otherwise numerical solutions are required.

In the weak coupling limit the probability to find the excitation settled in the two-level system vanishes in practice: this is caused by an extremely spreaded photon wavefunction, because the "penetration depth" is $(m^2 - E^2)^{-1/2}$. Indeed for $\gamma/m^2 = 10^{-2}$ and $\varepsilon = 1.1\ m$ in Figure 3.4, we obtain $E \approx 0.996\ m$, where the state is widely spreaded.

The explicit expression of the photon wavefunction is obtained following the same strategy of Section 3.2. Using Fourier transform, the position representation of the field amplitude reads

$$\xi(x) = a\sqrt{\frac{\gamma}{2\pi}}\oint \frac{\mathrm{d}k}{\sqrt{2\pi}}\,\frac{\mathrm{e}^{-\mathrm{i}kx}}{\sqrt[4]{k^2+m^2}\left(E - \sqrt{k^2+m^2}\right)}, \tag{3.56}$$

whose contour closure lies in the lower (upper) half-plane depending on positive (negative) x, which sorrounds a pole in $\pm\mathrm{i}\sqrt{m^2-E^2}$. Including the contour orientation we obtain

$$\mp 2\pi\mathrm{i}\lim_{k\to\mp\mathrm{i}\sqrt{m^2-E^2}}\frac{\left(k \pm \mathrm{i}\sqrt{m^2-E^2}\right)\mathrm{e}^{-\mathrm{i}kx}\left(E + \sqrt{k^2+m^2}\right)}{\sqrt[4]{k^2+m^2}\,(E^2-m^2-k^2)} = -2\pi\sqrt{\frac{E}{m^2-E^2}}\,e^{-\sqrt{m^2-E^2}|x|}, \tag{3.57}$$

while the cut contribution is expressed as

$$J_{\text{cut}}(x,E) = \int_{im}^{i\infty} \mathrm{d}k \left(\mathcal{J}^{-}_{\text{cut}}(E,k) - \mathcal{J}^{+}_{\text{cut}}(E,k)\right) = \frac{1}{\pi}\sqrt{\frac{\gamma}{2}} \int_{m}^{\infty} \mathrm{d}y \, \frac{\mathrm{e}^{-y|x|}\left(\sqrt{y^2-m^2}-E\right)}{\sqrt[4]{y^2-m^2}\left(E^2+y^2-m^2\right)}, \tag{3.58}$$

where $\mathcal{J}^{\pm}_{\text{cut}}(E,k) = \xi(0^{\pm} + \mathrm{i}y)\ \mathrm{e}^{-y|x|}$ and $\sqrt[4]{m^2-y^2} = \sqrt[4]{y^2-m^2}\ \mathrm{e}^{\pm \mathrm{i}\pi/4}$ along cut sides. The residue theorem yields these contributions, so the wavefunction in position representation reads:

$$\xi(x) = (-a)\left[\sqrt{\frac{\gamma E}{m^2-E^2}}\ \mathrm{e}^{-\sqrt{m^2-E^2}|x|} + J_{\text{cut}}(x,E)\right], \tag{3.59}$$

with the cut contribution relevant only in proximity of the two-level emitter, because of the exponential factor in the integral. The excited state population is deduced using the normalization condition and (3.22):

$$|a|^2 = \left(1 + \sqrt{\frac{\gamma}{2\pi}}\ \frac{2\sqrt{m^2-E^2} + E\left(\pi + 2\arctan(E)\right)}{\left(m^2-E^2\right)^{3/2}}\right)^{-1}, \tag{3.60}$$

consisting in an analytic expression defined for $E \in (-m, m)$ matching the remaining portion of the real line available for plasmonic eigenstates and whose dependence on the coupling is shown in Figure 3.4 with the red curve, while the associated photon wavefunction in position representation corresponds to the blue surface.

The plasmonic eigenstate is non perturbative because it always exists independently of the coupling constant, due to the divergent spectral density (3.25) [26]: the cutoff m represents its asymptote, such that every straight line in the presented form $E - \varepsilon$, with $\varepsilon > 0$, will have an intersection with $\Sigma_e(E)$. In this way the unstable pole, for energies immersed in the continuum, is accompanied by a plasmonic eigenstate, belonging to the singular spectrum lying below the threshold.

Part II

Emitters pair: bound states and their dissociation

Chapter 4

Entangled bound states generation

Living matter evades the decay to equilibrium

Erwin Schrödinger,
"What is life?"

The physics of effectively one-dimensional systems is recently attracting increasing attention, thanks to the unprecedented possibilities offered by modern quantum technologies [115]. A number of interesting and versatile experimental platforms are available nowadays, to implement an efficient dimensional reduction [55, 82] and enable photon propagation in one-dimension.

These schemes differ in scope and make use of diverse physical systems, such as optical fibers [6, 132], cold atoms [36, 88, 146], superconducting qubits [5, 34, 73, 89, 123, 130, 133], photonic crystals [28, 37, 50, 56, 61], quantum dots in photonic nanowires [13, 113], in cavity [8, 25, 71, 72, 107] and circuit QED [11, 141]. Light propagation in these systems is characterized by different energy dispersion relations and interaction form factors, yielding novel, drastically dimension-dependent features, that affect dynamics, decay and propagation [124, 125].

A system composed by two atoms in the single-excitation sector provides the emergence of bound states in the continuum subject to the condition linked to their distance partitioned by a half-integer multiple of the emitted wavelength. This optical path selects the parity characterizing the bound state: the emerging opposition in phase for the atom pair positions provides a destructive interference for the photon wavefunction lying outside the edge joining them, thus confining the electromagnetic field. In this sector the Friedrichs-Lee model is characterized by a self-energy endowed with a compact expression achievable with Dyson geometric series [41].

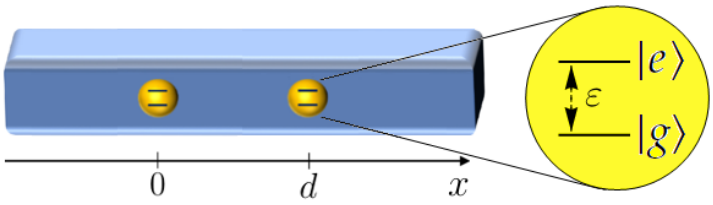

Figure 4.1: Pictorial representation of two atoms A and B, modeled as two-level fixed quantum emitters, embedded in a linear waveguide at a distance d from each other. The atoms have identical excitation energy ε, and we assume that the atomic transition between the excited state $|e\rangle$ and the ground state $|g\rangle$ is coupled only to one mode of the waveguide.

4.1 Resonant bound states in the continuum

We describe the dynamics of two two-level atoms A and B, situated in an infinite waveguide of rectangular cross section, with sides $L_y > L_z$, see Figure 4.1. When longitudinal propagation occurs with long wavelength compared to the transverse size, interaction between atoms and field can be reduced to a coupling with the lowest-cutoff-energy $\mathrm{TE}_{1,0}$ mode, in which the electric field vibrates along the z direction and has a sine modulation in the y direction [79]. In this situation, the electromagnetic field is effectively scalar and massive. The interacting atoms and photons are described, in dipolar and rotating wave approximations, by the Hamiltonian:

$$H = H_0 + H_{\mathrm{int}} = \varepsilon\left(\sigma_A^+\sigma_A^- + \sigma_B^+\sigma_B^-\right) + \int \mathrm{d}k\,\omega(k)b^\dagger(k)b(k) + \sqrt{\frac{\gamma}{2\pi}}\int \frac{\mathrm{d}k}{\sqrt{\omega(k)}}\left[\sigma_A^+ b(k) + \sigma_B^+ b(k)\mathrm{e}^{\mathrm{i}kd} + \mathrm{H.c.}\right], \tag{4.1}$$

where ε is the bare energy separation between the atomic ground $|g\rangle$ and first-excited states $|e\rangle$, γ is the coupling constant (see Chapter 3), d is the A-B distance, $\omega(k)$ is the photon dispersion relation, and $b(k)$ ($b^\dagger(k)$) is the annihilation (creation) field operator, satisfying the canonical commutation relation $[b(k), b^\dagger(k')] = \delta(k-k')$ defined with (1.63). Henceforth, we will focus on the dispersion $\omega(k) = \sqrt{k^2+m^2}$ of the $\mathrm{TE}_{1,0}$ mode in the waveguide, characterized by a mass $m \propto L_y^{-1}$. However, as discussed in Section 4.4, our approach is applicable to a wide class of one-dimensional dispersion relations. The effective mass m provides a natural cutoff to the coupling. The Hamiltonian (4.1) commutes

with the excitation number:

$$\mathcal{N} = \mathcal{N}_{\text{at}} + \int \mathrm{d}k\, b^\dagger(k) b(k), \tag{4.2}$$

where $\mathcal{N}_{\text{at}} = \sigma_A^+\sigma_A^- + \sigma_B^+\sigma_B^-$ is the atomic excitation number. The $\mathcal{N} = 0$ sector is 1-dimensional and is spanned by the bare ground state $\left|g_A, g_B; \text{vac}\right\rangle$. We shall focus instead on the dynamics in the $\mathcal{N} = 1$ sector, where the states read:

$$\left|\psi\right\rangle = \left(a_A \left|e_A, g_B\right\rangle + a_B \left|g_A, e_B\right\rangle\right) \otimes \left|\text{vac}\right\rangle + \left|g_A, g_B\right\rangle \otimes \left|\xi\right\rangle \tag{4.3}$$

where $\left|\xi\right\rangle := \int \mathrm{d}k\, \xi(k) b^\dagger(k) \left|\text{vac}\right\rangle$ is a one-photon state as presented in Section 1.1, and the normalization condition holds $|a_A|^2 + |a_B|^2 + \int \mathrm{d}k |\xi(k)|^2 = 1$.

In the small-coupling regime, an isolated excited atom with $\varepsilon \gtrsim m$ would decay to the ground state. In the following we shall demonstrate that, when two atoms are considered, a resonance effect emerges, yielding a bound state. Using the expansion (4.3) the eigenvalue equation, $H\left|\psi\right\rangle = E\left|\psi\right\rangle$, reads:

$$Ea_A = \varepsilon a_A + \sqrt{\frac{\gamma}{2\pi}} \int \mathrm{d}k \frac{\xi(k)}{\omega(k)^{1/2}}, \tag{4.4}$$

$$Ea_B = \varepsilon a_B + \sqrt{\frac{\gamma}{2\pi}} \int \mathrm{d}k \frac{\xi(k)\mathrm{e}^{\mathrm{i}kd}}{\omega(k)^{1/2}}, \tag{4.5}$$

$$\xi(k) = \sqrt{\frac{\gamma}{2\pi\omega(k)}} \frac{a_A + a_B\mathrm{e}^{-\mathrm{i}kd}}{E - \omega(k)}. \tag{4.6}$$

The field amplitude $\xi(k)$ has two simple poles at $k = \pm\bar{k} = \pm\sqrt{E^2 - m^2}$. Thus, when $E > m$, the integrals in (4.4)-(4.5) are finite only if $a_A + a_B\mathrm{e}^{\pm i\bar{k}d} = 0$, yielding $\bar{k}d = \nu\pi$ for $\nu \in \mathbb{N}$. This implies that a bound state can exist only for discrete values of the interatomic distance d. Moreover, in the first component of such an eigenstate (4.3), the atoms are in a maximally entangled (singlet or triplet) state, namely $a_A = (-1)^{\nu+1} a_B$. To determine the distances at which the bound state exists, let us first compute the energy eigenvalue

$$E = \varepsilon + \frac{\gamma}{2\pi} \int \mathrm{d}k \frac{1 - (-1)^\nu \mathrm{e}^{-\mathrm{i}kd}}{\omega(k)(E - \omega(k))}, \tag{4.7}$$

where the integral can be evaluated by complex plane integration, as predicted by the procedure (3.27):

$$\int \mathrm{d}k \frac{1 - (-1)^\nu \mathrm{e}^{-\mathrm{i}kd}}{\omega(k)(E - \omega(k))} = \oint \mathrm{d}k \frac{1 - (-1)^\nu \mathrm{e}^{-\mathrm{i}kd}}{\omega(k)(E - \omega(k))} - \int_m^\infty \mathrm{d}y \, \frac{2E\left(1 - (-1)^\nu \mathrm{e}^{-yd}\right)}{\sqrt{y^2 - m^2}\,(m^2 - E^2 - y^2)}. \tag{4.8}$$

The residue contribution vanishes because of the resonance condition, while the integral evaluated along the cut is estimated according to:

$$2E\int_m^\infty \frac{\mathrm{d}y}{\sqrt{y^2-m^2}\,(E^2+y^2-m^2)} = \frac{2\,\mathrm{sgn}(E)}{\sqrt{E^2-m^2}}\mathrm{Log}\left(\frac{\mathrm{sgn}(E)E+\sqrt{E^2-m^2}}{m}\right)\approx\frac{2}{m}, \tag{4.9}$$

where the approximation holds true for $E-m \ll m$. The remaining contribution is exponentially suppressed with the distance. After the resonance condition, the energy eigenvalue is the solution of

$$E = \varepsilon + \frac{\gamma}{m\pi}\left[1+O\left(\frac{E-m}{m}\right)+O\left(\mathrm{e}^{-md}\right)\right], \tag{4.10}$$

whose right hand side corrections are negligible, in the considered small coupling regime, if $\varepsilon - m \ll m$, representing also the condition for a self-consistent single-mode approximation. This will result as a special case of the ensuing analysis of the complex poles of the resolvent, as shown in (4.47) and following ones. Thus, near the cutoff m, a bound state with $E > m$ is present only if the distance d takes one of the discrete values

$$d_\nu = \frac{\nu\pi}{\bar{k}}, \quad \text{with} \quad \bar{k} := \sqrt{\left(\varepsilon+\frac{\gamma}{m\pi}\right)^2 - m^2}, \tag{4.11}$$

and if the wavenumber $\bar{k}$ is real ($\varepsilon > m-\gamma/m\pi$). We shall discuss in the following the properties of states with $E < m$, to which an imaginary wavenumber can be associated.

To complete the characterization of the bound state, we shall analyze the atomic populations and the field energy density. The former can be immediately obtained using the normalization condition on the states (4.3) as

$$1 = 2\,|a_A^{(\nu)}|^2\left(1+\frac{\gamma}{2\pi}\int \mathrm{d}k \frac{1-(-1)^\nu\cos(kd_\nu)}{\omega(k)(E-\omega(k))^2}\right), \tag{4.12}$$

Where we use the shorthands $a_A^{(\nu)}, a_B^{(\nu)}$ to indicate the coefficients of the bound state with $d = d_\nu$. Defining $p_\nu := |a_A^{(\nu)}|^2 + |a_B^{(\nu)}|^2$ as the probability associated with the $\mathcal{N}_{\mathrm{at}} = 1$ sector, derived explicitly in Section 4.1.3, one gets:

$$p_\nu \approx \left(1+\nu\pi\frac{\gamma m}{\bar{k}^3}\right)^{-1}. \tag{4.13}$$

Notice that, despite being apparently of order γ, the correction to unity is given by the ratio between powers of two small quantities, namely the effective coupling constant γ/m^2, and the wavenumbers ratio $\bar{k}/m$. The resulting number

can be of order one, even at small coupling constants. Observe that the probability vanishes like $\bar{k}^3/\nu$ at very small $\bar{k}$: this behavior is physically motivated by the fact that, as the energy approaches the cutoff, the distance between the atoms must increase to infinity in all bound states. Let us finally analyze the Fourier transform of the photon amplitude:

$$\begin{aligned}\xi_\nu(x) &= \int \frac{\mathrm{d}k}{\sqrt{2\pi}}\, \xi_\nu(k) \mathrm{e}^{\mathrm{i}kx} \\ &= a_A^{(\nu)} \sum_{j=1}^{2} (-1)^{(\nu+1)(j-1)} \left(\frac{\sqrt{\gamma E}}{\bar{k}(E)} \sin\Big(\bar{k}(E)\,\big|x-(j-1)d_\nu\big|\Big) - J_{\mathrm{cut}}\Big(\,\big|x-(j-1)d_\nu\big|\,\Big)\right),\end{aligned} \tag{4.14}$$

where neglecting the cut contribution, exponentially suppressed with distance,

$$\xi_\nu(x) \approx a_A^{(\nu)} \frac{\sqrt{\gamma E}}{\bar{k}(E)} \sin\Big(\bar{k}(E)\,|x|\,\Big), \tag{4.15}$$

for $x \in [0, d_\nu]$, which turns out to be related to the energy density of the electromagnetic field as:

$$\mathcal{E}_\nu(x) \approx E|\xi_\nu(x)|^2 \approx \frac{\gamma p_\nu}{2} \left(\frac{E}{\bar{k}}\right)^2 \sin(\bar{k}\,|x|)^2, \tag{4.16}$$

and $\mathcal{E}_\nu(x) \approx 0$ outside the emitters pair. Thus, the field is confined between the two atoms, and modulated with periodicity $\pi/\bar{k}$, with nodes at the positions of the atoms which act as mirrors. This explains the occurrence of such bound states for discrete values (4.11) of the interatomic distance.

4.1.1 Entanglement by relaxation

Let us recall that the structure of the bound state is

$$\big|\psi_\nu\big\rangle = \sqrt{p_\nu}\,|\Psi^s\rangle \otimes |\mathrm{vac}\rangle + \big|g_A, g_B\big\rangle \otimes |\xi_\nu\rangle\,, \tag{4.17}$$

where $s = (-1)^{\nu+1}$ and $|\Psi^\pm\rangle = \Big(\big|e_A, g_B\big\rangle \pm \big|g_A, e_B\big\rangle\Big) / \sqrt{2}$ are (maximally entangled) Bell states. This is a key feature which enables entanglement generation by atom-photon interaction. Indeed, suppose that $d = d_\nu$: a factorized initial state, say $\big|\psi(0)\big\rangle = \big|e_A, g_B\big\rangle \otimes |\mathrm{vac}\rangle$, can be expanded into a "stable" and a "decaying" part as

$$\big|e_A, g_B; \mathrm{vac}\big\rangle = \sqrt{\frac{p_\nu}{2}}\,\big|\psi_\nu\big\rangle + \sqrt{1-\frac{p_\nu}{2}}\,\big|\psi_\nu^\perp\big\rangle\,, \tag{4.18}$$

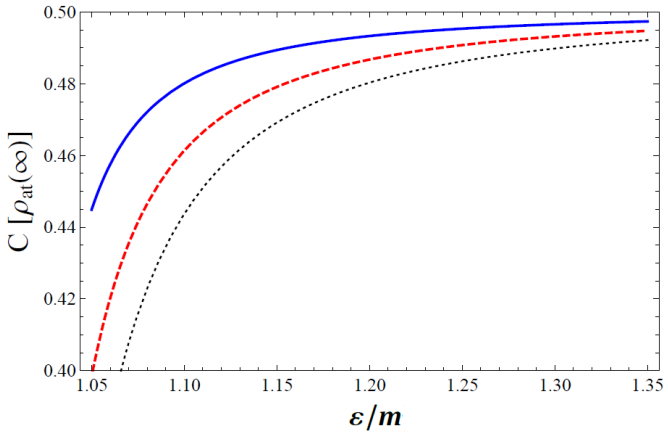

Figure 4.2: Behavior of the concurrence $C = p_\nu^2/2$ of the asymptotic states $\rho_{\rm at}(\infty)$ as a function of the atomic excitation energy, for $\gamma/m^2 = 2\pi \times 10^{-4}$ and a factorized initial state. The solid (blue) line, dashed (red) line and dotted (black) line are referred to the resonant states with $\nu = 1, 2, 3$, respectively.

with $\left\langle \psi_\nu^\perp \middle| \psi_\nu \right\rangle = 0$ and a phase is included in the definition of $\left|\psi_\nu^\perp\right\rangle$. After a transient of the order of $\left|\psi_\nu^\perp\right\rangle$'s lifetime (see discussion in the following), the atomic density matrix $\rho_{\rm at}(t) := {\rm Tr}_{\rm field} \left|\psi(t)\right\rangle \left\langle\psi(t)\right|$ approaches

$$\rho_{\rm at}(\infty) = \frac{p_\nu^2}{2} \left|\Psi^s\right\rangle \left\langle\Psi^s\right| + \left(1 - \frac{p_\nu^2}{2}\right) \left|g_A, g_B\right\rangle \left\langle g_A, g_B\right|, \tag{4.19}$$

in which the atoms have a finite probability, determined by (4.13), to be maximally entangled. In Figure 4.2 we display the atomic entanglement in the asymptotic state, as measured by the concurrence [139]. However, one could also measure the photon state and obtain, with a finite probability, a maximally entangled atomic state. The strategy is therefore the following: one prepares a factorized state, and measures whether a photon is emitted. If (after a few lifetimes) no photon has been observed, the atomic state is projected over the maximally entangled Bell state $|\Psi^s\rangle$. This can be achieved with higher probabilities for larger values of ε. In realistic scenarios this simplified picture is challenged by the presence of losses, such that it is no longer possible to prepare an exact Bell state. Nevertheless, if losses occur on sufficiently long timescales (as compared to the decay rate of the fast pole — see Section 4.2 below), and provided the detector efficiency is high enough, it remains possible to achieve with high fidelity a Bell state.

4.1.2 Energy density

Using the scalar Hamiltonian density defined in Section 1.4.1, so using SI units, and the normal ordering introduced in (1.70), one can compute the energy density

$$\begin{aligned}\langle\psi|\,\mathcal{H}(x)\,|\psi\rangle &= \frac{1}{2}\Big[\langle\psi|:(\Pi(x))^2:|\psi\rangle + v^2\langle\psi|:(\partial_x\alpha(x))^2:|\psi\rangle \\ &\quad + v^4\left(\frac{m}{\hbar}\right)^2\langle\psi|:(\partial_x\alpha(x))^2:|\psi\rangle\Big] \\ &= \left|\int \mathrm{d}k\sqrt{\frac{\hbar\omega_{1,0}(k)}{2(2\pi)}}\xi(k)e^{ikx}\right|^2 + \left|\int \mathrm{d}k\frac{\hbar v k}{\sqrt{2(2\pi)\hbar\omega_{1,0}(k)}}\xi(k)e^{ikx}\right|^2 \\ &\quad + \left|\int \mathrm{d}k\frac{v^2 m}{\sqrt{2(2\pi)\hbar\omega_{1,0}(k)}}\xi(k)e^{ikx}\right|^2 . \end{aligned} \tag{4.20}$$

This stucture can be simplified if one assumes that the dominant contribution to the integrals comes from the poles of $\xi(k) \sim A_+(k-k_0)^{-1} + A_-(k+k_0)^{-1}$, with $k_0 = \sqrt{\varepsilon^2 - m^2}$. Neglecting the corrections yielded by square-root branch-cut integration, one obtains

$$\langle\psi|\,\mathcal{H}(x)\,|\psi\rangle \approx \hbar\omega_{1,0}(k_0)\left|\int \frac{\mathrm{d}k}{\sqrt{2\pi}}\xi(k)e^{ikx}\right|^2 =: \hbar\omega_{1,0}(k_0)\,|\xi(x)|^2\,, \tag{4.21}$$

which is used to compute the energy density for the resonant states in (4.16).

4.1.3 Atomic population

Complex integration techniques provide a suitable estimation for emitters population, as expressed by (4.13). Let us start from the direct elaboration of the normalization condition (4.12):

$$p_\nu = \left(1 + \frac{\gamma}{4\pi}\int \mathrm{d}k\frac{2-(-1)^\nu\left(\mathrm{e}^{\mathrm{i}kd_\nu} + \mathrm{e}^{-\mathrm{i}kd_\nu}\right)}{\omega(k)(E-\omega(k))^2}\right)^{-1} = \left(1 + \frac{\gamma}{4\pi}\mathcal{K}^{(\nu)}(E)\right)^{-1}, \tag{4.22}$$

whose integral becomes the half-sum:

$$\mathcal{K}^{(\nu)}(E) = \frac{1}{2}\left(\int_{-\infty+\mathrm{i}0^+}^{\infty+\mathrm{i}0^+}\mathrm{d}k\frac{2-(-1)^\nu\left(\mathrm{e}^{\mathrm{i}kd_\nu} + \mathrm{e}^{-\mathrm{i}kd_\nu}\right)}{\omega(k)(E-\omega(k))^2} + \int_{-\infty-\mathrm{i}0^+}^{\infty-\mathrm{i}0^+}\mathrm{d}k\frac{2-(-1)^\nu\left(\mathrm{e}^{\mathrm{i}kd_\nu} + \mathrm{e}^{-\mathrm{i}kd_\nu}\right)}{\omega(k)(E-\omega(k))^2}\right). \tag{4.23}$$

Evaluating exponential terms singularly, it is possible to exploit the identity:

$$\int_{-\infty+\mathrm{i}0^+}^{\infty+\mathrm{i}0^+} \mathrm{d}k \frac{\mathrm{e}^{\mathrm{i}kd_\nu}}{\omega(k)(E-\omega(k))^2} = \int_{-\infty-\mathrm{i}0^+}^{\infty-\mathrm{i}0^+} \mathrm{d}k \frac{\mathrm{e}^{-\mathrm{i}kd_\nu}}{\omega(k)(E-\omega(k))^2}, \tag{4.24}$$

valid for $E \in \mathbb{R}$, given that the dispersion relation fulfills $\omega(k) = \omega(-k)$, thus yielding

$$\mathcal{K}^{(\nu)}(E) = \int_{-\infty+\mathrm{i}0^+}^{\infty+\mathrm{i}0^+} \mathrm{d}k \frac{1-(-1)^\nu \mathrm{e}^{\mathrm{i}kd_\nu}}{\omega(k)(E-\omega(k))^2} + \int_{-\infty-\mathrm{i}0^+}^{\infty-\mathrm{i}0^+} \mathrm{d}k \frac{1-(-1)^\nu \mathrm{e}^{\mathrm{i}kd_\nu}}{\omega(k)(E-\omega(k))^2} = \mathcal{K}_1^{(\nu)}(E) + \mathcal{K}_2^{(\nu)}(E), \tag{4.25}$$

along contours closed in the upper half-plane. By deforming the second contribution into the first one, two second order poles in $\pm\bar{k}(E) = \pm\sqrt{E^2-m^2}$ provide the associated residue contribution:

$$\begin{aligned} &2\pi\mathrm{i} \lim_{k\to\pm\bar{k}(E)} \frac{\mathrm{d}}{\mathrm{d}k} \left[\left(k \mp \sqrt{E^2-m^2}\right)^2 \frac{1-(-1)^\nu \mathrm{e}^{\mathrm{i}kd_\nu}}{\sqrt{k^2+m^2}\left(E-\sqrt{k^2+m^2}\right)^2} \right] \\ &= 2\pi\mathrm{i} \lim_{k\to\pm\bar{k}(E)} \frac{\mathrm{d}}{\mathrm{d}k} \left[\frac{\left(1-(-1)^\nu \mathrm{e}^{\mathrm{i}kd_\nu}\right)\left(E+\sqrt{k^2+m^2}\right)^2}{\sqrt{k^2+m^2}\left(k \pm \sqrt{E^2-m^2}\right)^2} \right] = 2\pi d_\nu \frac{E}{E^2-m^2}. \end{aligned} \tag{4.26}$$

The targeted integral reads:

$$\mathcal{K}^{(\nu)}(E) = 2\mathcal{K}_1^{(\nu)}(E) + 4\pi d_\nu \frac{E}{E^2-m^2}, \tag{4.27}$$

where, due to the absence of poles inside the contour, the first term becomes a cut contribution:

$$\mathcal{K}_1^{(\nu)}(E) = \int_{\mathrm{i}m}^{\mathrm{i}\infty} \mathrm{d}k \left(\mathcal{K}_{\mathrm{cut}}^{(\nu)+}(k,E) - \mathcal{K}_{\mathrm{cut}}^{(\nu)-}(k,E) \right) \tag{4.28}$$

with

$$\mathcal{K}_{\mathrm{cut}}^{(\nu)\pm}(y,E) = \pm \frac{1-(-1)^\nu \mathrm{e}^{-yd_\nu}}{\mathrm{i}\sqrt{y^2-m^2}\left(E \mp \mathrm{i}\sqrt{y^2-m^2}\right)^2}, \tag{4.29}$$

obtained following the same strategy shown in Section 3.2. The final form of the integral is:

$$\mathcal{K}_1^{(\nu)}(E) = 2\int_m^\infty \mathrm{d}y \frac{\left(1-(-1)^\nu \mathrm{e}^{-yd_\nu}\right)(E^2-y^2+m^2)}{\sqrt{y^2-m^2}\,(E^2+y^2-m^2)^2}, \tag{4.30}$$

subject to a further decomposition:

$$\mathcal{K}_1^{(\nu)}(E) = 4E^2 \int_m^\infty \mathrm{d}y \, \frac{\left(1-(-1)^\nu \mathrm{e}^{-yd_\nu}\right)}{\sqrt{y^2-m^2}\,(E^2+y^2-m^2)^2} - 2\int_m^\infty \mathrm{d}y \, \frac{\left(1-(-1)^\nu \mathrm{e}^{-yd_\nu}\right)}{\sqrt{y^2-m^2}\,(E^2+y^2-m^2)}, \tag{4.31}$$

which we will estimate up to the exponentially suppressed contribution. Keeping only the unity in both numerators, the result is:

$$\begin{aligned}\mathcal{K}_1^{(\nu)}(E) \approx 4E^2 \Bigg[&-\frac{1}{2E^2(E^2-m^2)} + \frac{2E^2-m^2}{2E^3(E^2-m^2)^{3/2}} \operatorname{Log}\left(\frac{\operatorname{sgn}(E)E + \sqrt{E^2-m^2}}{m}\right)\Bigg] \\ &- 2\frac{\operatorname{sgn}(E)}{E\sqrt{E^2-m^2}} \operatorname{Log}\left(\frac{\operatorname{sgn}(E)E + \sqrt{E^2-m^2}}{m}\right),\end{aligned} \tag{4.32}$$

where the last term coincides with the integral of the self-energy cut contribution in Section 3.2. The order of these last expressions is well approximated in the limit of energies near the cutoff m by

$$\mathcal{K}_1^{(\nu)}(E) \approx -\frac{2}{E^2-m^2} + 2\frac{2E^2-m^2}{Em(E^2-m^2)} - \frac{2}{Em} = \frac{2}{m(E+m)}, \tag{4.33}$$

such that the atomic population reads

$$p_\nu \approx \left(1 + \gamma \frac{\nu\pi E}{\bar{k}^3(E)} + \frac{\gamma}{\pi m(E+m)}\right)^{-1}. \tag{4.34}$$

4.2 Time evolution and bound state stability

Let us now study the general evolution of an initial state in the atomic sector $\mathcal{N}_{\mathrm{at}} = 1$. We will use the resolvent formalism [25, 95] to illustrate that the system relaxes towards the bound state, and to quantify the robustness of the bound state against small variations in the model parameters (such as the A-B distance). We remark that the usefulness of the resolvent formalism goes beyond the analysis of stable states, in that it provides crucial information on the relevant timescales of the problem. Indeed, the entanglement-by-relaxation protocol described in Section 4.1 relies on the fast decay of the unstable Bell state. The analysis of the resolvent enables to determine the lifetime of this unstable state, which must be much shorter than the typical timescales of waveguide or atomic losses, as well as the inevitably finite lifetime of the bound state (due for example to imperfect control of the A-B distance). Whenever these

conditions are met, the effectiveness of the protocol is guaranteed and a long-lived entangled state may be prepared by relaxation.

The resolvent $G(z) = (z - H)^{-1}$, with z the complex energy variable, has singularities only on the real axis (in the first Riemann sheet) and the study of additional singularities (in the other Riemann sheets, as explained in Section 3.2.1) yields crucial information about the dynamical stability of the system: in particular, a pole with a non-vanishing imaginary component signals an exponential decay process. The resolvent approach yields results that are consistent with those obtained from the analysis of the Laplace transform of the time evolution [122].

For $\gamma = 0$, the free resolvent $G_0(z) = (z - H_0)^{-1}$, restricted to the one-excitation sector, has a pole on the real axis, at $z = \varepsilon$, corresponding to the excited states of atoms A or B. When interaction is turned on, this singularity splits into two simple poles, which generally migrate into the second Riemann sheet. We shall see from a non-perturbative analysis that, under the resonance conditions (4.11), one of the poles falls on the real axis (and is therefore very long-lived), while the other one has a very short lifetime. Let $G(z)$ and $G_0(z)$ be the restrictions to the $\mathcal{N}_{\text{at}} = 1$ sector of the interacting and free resolvent, respectively. In the basis $\left\{\left|e_A, g_B\right\rangle, \left|g_A, e_B\right\rangle\right\}$ one gets:

$$G_0(z) = \frac{1}{z - \varepsilon}\begin{pmatrix} 1 & 0 \\ 0 & 1 \end{pmatrix} \tag{4.35}$$

and

$$G(z) = \left[G_0(z)^{-1} - \Sigma(z)\right]^{-1} = \left[z - \varepsilon - \Sigma(z)\right]^{-1}, \tag{4.36}$$

where

$$\Sigma(z) = \begin{pmatrix} \Sigma_{AA}(z) & \Sigma_{AB}(z) \\ \Sigma_{BA}(z) & \Sigma_{BB}(z) \end{pmatrix} \tag{4.37}$$

is the matrix form of the self energy presented in Section 2.6.

The resolvent $G(z)$ is analytic in the whole complex energy plane, except, in general, at points on the real axis that belong to the spectrum of the Hamiltonian H. As shown in Section 3.2.2, we are interested in poles of the resolvent that physically correspond to unstable states with energy and decay rates given by their real and imaginary part, respectively.

The particular form of the interaction Hamiltonian H_{int} in (4.1) enables one to exactly evaluate the self energy:

$$\Sigma_{AA}(z) = \Sigma_{BB}(z) = \frac{\gamma}{2\pi}\int \mathrm{d}k \frac{1}{\omega(k)(z - \omega(k))}, \tag{4.38}$$

$$\Sigma_{AB}(z) = \Sigma_{BA}(z) = \frac{\gamma}{2\pi}\int \mathrm{d}k \frac{\cos(kd)}{\omega(k)(z - \omega(k))}. \tag{4.39}$$

Due to the excitation energy degeneracy and the symmetric structure of the self energy, the propagator can be diagonalized as

$$G(z) = \frac{|\Psi^+\rangle\langle\Psi^+|}{z-\varepsilon-\Sigma_+(z)} + \frac{|\Psi^-\rangle\langle\Psi^-|}{z-\varepsilon-\Sigma_-(z)}, \tag{4.40}$$

where

$$\Sigma_s(z) = \int_m^\infty \mathrm{d}\omega\, \frac{\kappa_s(\omega)}{z-\omega}, \qquad s = \pm, \tag{4.41}$$

with spectral densities

$$\kappa_\pm(\omega) = \frac{\gamma}{\pi}\frac{1 \pm \cos\left(\sqrt{\omega^2-m^2}d\right)}{\sqrt{\omega^2-m^2}}\chi_{[m,\infty)}(\omega). \tag{4.42}$$

The self-energy functions $\Sigma_\pm(z)$ are analytic in the cut complex energy plane $\mathbb{C}\setminus[m,+\infty)$ and have a purely imaginary discontinuity across the cut proportional to the spectral density:

$$\Sigma_s(E-\mathrm{i}0^+) - \Sigma_s(E+\mathrm{i}0^+) = 2\pi\mathrm{i}\kappa_s(E). \tag{4.43}$$

During the continuation process into the second Riemann sheet through the cut, the self energy (4.41) will thus get an additional term

$$\Sigma_s(z) \longrightarrow \Sigma_s^{\mathrm{II}}(z) = \Sigma_s(z) - 2\pi\mathrm{i}\kappa_s(z), \qquad z\in\mathbb{C}. \tag{4.44}$$

Note that the new term has in general a nonvanishing imaginary part and is the analytical continuation of the discontinuity of the self-energy function across the cut. Now, a pole

$$z_p = E_p - \mathrm{i}\gamma_p/2 \tag{4.45}$$

of $G(z)$ on the second sheet must satisfy the equation

$$z_p = \varepsilon + \Sigma_s^{\mathrm{II}}(z_p), \tag{4.46}$$

for $s=\pm$. By plugging (4.44) and (4.42) into (4.46) we get

$$z_p = \varepsilon + \Sigma_\pm(z_p) - 2\gamma\mathrm{i}\frac{1 \pm \cos\left(\sqrt{z_p^2-m^2}\,d\right)}{\sqrt{z_p^2-m^2}}. \tag{4.47}$$

It is evident from (4.47) how the energetic degeneracy at $\gamma = 0$ is lifted by interactions.

The last ingredient we need in order to get a closed expression for the complex energy poles is the evaluation of $\Sigma_s(z)$ in (4.47). Thus, let us rewrite (4.41) as an integral over k:

$$\Sigma_{\pm}(z) = \int_{-\infty}^{+\infty} \frac{\mathrm{d}k}{\sqrt{k^2+m^2}} \frac{1 \pm e^{\mathrm{i}kd}}{z - \sqrt{k^2+m^2}}. \tag{4.48}$$

The integrand function can be analytically continued to the complex k plane using the principal determination of the square root, which has nonnegative real part for all values of its argument, and is characterized by a branch cut for $k^2 + m^2 < 0$, that is

$$k = \pm \mathrm{i}y, \quad \text{with } y \in (m, \infty). \tag{4.49}$$

Two first-order poles, symmetric with respect to the origin of the k plane, are also present whenever $\mathrm{Re}(z) > 0$:

$$k = \pm k_0(z) = \pm \sqrt{z^2 - m^2}. \tag{4.50}$$

By deforming the integration contours as in Figure 3.2 and applying Jordan's theorem, Σ_s is split in two terms

$$\Sigma_s(z) = \Sigma_s^{\mathrm{cut}}(z) + \Sigma_s^{\mathrm{pole}}(z). \tag{4.51}$$

coming from the upper branch cut and from one of the two poles (see Figure 3.2). Specifically, when $\mathrm{Im}(z) > 0$, the pole $k_0(z)$ lies in the upper half plane, and the computation of the integral involves the residue

$$\Sigma_{\pm}^{\mathrm{pole}}(z) = \mathrm{i}\gamma \lim_{k \to k_0(z)} \frac{(k - k_0(z))(1 \pm e^{\mathrm{i}kd})}{\sqrt{k^2+m^2}\left(z - \sqrt{k^2+m^2}\right)} = -\mathrm{i}\gamma \frac{1 \pm e^{\mathrm{i}\sqrt{z^2-m^2}d}}{\sqrt{z^2-m^2}} \Theta\Big(\mathrm{Re}(z)\Big). \tag{4.52}$$

Instead, when $\mathrm{Im}(z) < 0$, the deformed contour in the upper plane encircles $-k_0(z)$, where the residue yields

$$\Sigma_{\pm}^{\mathrm{pole}}(z) = \mathrm{i}\gamma \lim_{k \to -k_0(z)} \frac{(k + k_0(z))(1 \pm e^{\mathrm{i}kd})}{\sqrt{k^2+m^2}\left(z - \sqrt{k^2+m^2}\right)} = \mathrm{i}\gamma \frac{1 \pm e^{-\mathrm{i}\sqrt{z^2-m^2}d}}{\sqrt{z^2-m^2}} \Theta\Big(\mathrm{Re}(z)\Big). \tag{4.53}$$

Finally, the integrals along the cut read

$$\begin{aligned} \Sigma_{\pm}^{\mathrm{cut}}(z) &= -\frac{\gamma z}{\pi} \int_m^{\infty} \mathrm{d}y \, \frac{1 \pm e^{-yd}}{\sqrt{y^2-m^2}\,(z^2+y^2-m^2)} \\ &= -\frac{\gamma}{\pi} \frac{\mathrm{sgn}\Big(\mathrm{Re}(z)\Big)}{\sqrt{z^2-m^2}} \mathrm{Log}\left(\frac{\mathrm{sgn}\Big(\mathrm{Re}(z)\Big)\, z - \sqrt{z^2-m^2}}{m} \right) \pm O(e^{-md}), \end{aligned} \tag{4.54}$$

where the contribution from e^{-yd}, for which an explicit closed form in terms of simple functions is available in Section 6.4.1, is exponentially suppressed and can be neglected for large values of md.

We are now able to recognize the real resonant poles as special solutions of (4.47), where we have to specify the choice of $\mathrm{sgn}\Big(\mathrm{Im}(z_p)\Big) = -1$ for all square roots concerning numerical solutions, as shown in Figure 4.3. Indeed, assuming that the complex energy pole (4.45) is far from the branching point $z = m$ and that its imaginary part is almost vanishing, one can decouple the real and imaginary parts of (4.47) and obtain from (4.51)-(4.54):

$$E_p \approx \varepsilon - \frac{\gamma}{\pi k_p}\mathrm{Log}\left(\frac{E_p - k_p}{m}\right) \pm \gamma\frac{\sin(k_p d)}{k_p}, \tag{4.55}$$

$$\frac{\gamma_p}{2} \approx \gamma\frac{1 \pm \cos(k_p d)}{k_p}, \tag{4.56}$$

where $k_p = \sqrt{E_p^2 - m^2}$. Hence, we find that the poles in the second Riemann sheet have a cyclic behavior with respect to d [41, 60].

In particular, when the resonance condition is satisfied with $d = d_v$, as defined in (4.11), the real part of the pole equations is solved by $E_p = \sqrt{\bar{k}^2 + m^2}$. In this case, one of the poles corresponds to the entangled bound state, and has vanishing imaginary part, while the other signals an unstable state with associated decay rate

$$\gamma_p^{(u)} = 4\gamma/\bar{k} \tag{4.57}$$

Even if, strictly speaking, bound states only occur for discrete values of d, it can be readily checked that while the energy shift is linear, the decay rate of the stable pole is quadratic for $d \to d_v$

$$\gamma_p^{(s)} \approx \gamma\bar{k}(d - d_v)^2, \tag{4.58}$$

implying that the state $|\psi_v\rangle$ remains very long-lived close to resonance and quantifying through (4.58) the robustness of the bound states against variations of the parameter d. Note how (4.57) and (4.58) provide essential information on the feasibility and effectiveness of the entanglement generation protocol: first, it is necessary that the condition $\gamma_p^{(s)} \ll \gamma_p^{(u)}$, equivalent to $\bar{k}^2(d - d_v)^2 \ll 1$ is satisfied. Second, $\gamma_p^{(u)}$ must be much larger than any decay rate associated with loss processes (e.g. waveguide losses). Even though approximate analytical expressions such as (4.57)-(4.58) are extremely valuable, we emphasize that our methodology is capable of capturing the *exact* behaviour of the poles against variations in the model parameters. To illustrate this, in Figure 4.3 we show the

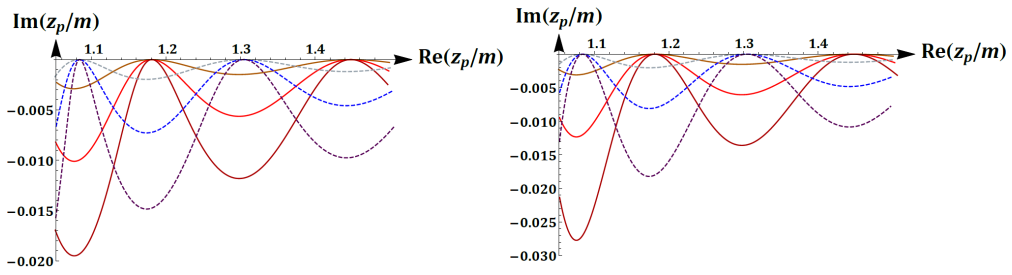

(a) (b)

Figure 4.3: Trajectories of the poles $E_p^{(+)} - i\gamma_p^{(+)}/2$ (solid lines) and $E_p^{(-)} - i\gamma_p^{(-)}/2$ (dashed lines) on the second Riemann sheet of the complex energy plane, for $md = 15$, with varying $1.05 \leq \varepsilon/m \leq 1.5$. In (a) exact numerical results are shown, while in (b) trajectories are obtained through the decoupling approximation. The trajectories are tangent to the real axis (they touch it whenever condition (4.11) is satisfied), showing that the approximate bound states are robust against variation of ε. Graded colors are referred to respectively $\gamma/m^2 = 2\pi \times 10^{-4}$, $\gamma/m^2 = 8\pi \times 10^{-4}$ and $\gamma/m^2 = 18\pi \times 10^{-4}$.

trajectories of the poles (4.45) in the complex energy plane, obtained by fixing m and d and varying the bare excitation energy ε. On the one hand, we are thus able to assess quantitatively the robustness of bound states against variations in ε. On the other hand, Figure 4.3 demonstrates how our methodology allows one to interpolate seamlessly between perturbative and non-perturbative regimes. Pole trajectories are continuous for considered couplings using the determination of square root for the lower half-plane. With this choice, trajectories show a smaller imaginary part for unstable states poles than the results deduced by means of the decoupling approximation in Figure 4.3(b).

4.3 Off-resonant bound states

Let us briefly discuss the behavior of bound states with $E < m$. In this case, following the perturbation theory, the atoms are not expected to decay. Nonetheless, they interact by coupling to the evanescent modes of the waveguide. Scrutiny of (4.4)-(4.5) shows that there are bound states for all d, whose energy satisfy

$$\begin{pmatrix} E - \omega_0 - \alpha(E) & -\beta(E) \\ -\beta(E) & E - \omega_0 - \alpha(E) \end{pmatrix} \begin{pmatrix} a_A \\ a_B \end{pmatrix} = 0, \tag{4.59}$$

with

$$\alpha(E) = -\frac{\gamma}{2\pi\sqrt{m^2-E^2}}\left(\pi + 2\arctan\frac{E}{\sqrt{m^2-E^2}}\right), \tag{4.60}$$

$$\beta(E) = -\frac{\gamma}{\sqrt{m^2-E^2}}\, e^{-\sqrt{m^2-E^2}d}. \tag{4.61}$$

where we have again neglected the $O(e^{-md})$ contributions from branch-cut integration in the complex k plane, explicitly analyzed in Section 6.4.1. If the coupling is small and the excitation energy ε is far from the threshold m for photon emission, the above equations reduce to an effective Hamiltonian eigenvalue equation in the $\mathcal{N}_{\text{at}} = 1$ sector. The eigenvalues read:

$$E^{(\pm)} = \varepsilon + \alpha(\varepsilon) \pm \beta(\varepsilon) + O(\gamma^2), \tag{4.62}$$

with $a_A = a_B$ for the plus sign (ground state) and $a_A = -a_B$ for the minus sign. These bound states are not associated to any resonant distance. It is also possible to see that the electromagnetic energy density falls like $\mathrm{e}^{-\sqrt{m^2-E^2}|x|}$ away from the atoms, as introduced in Section 3.2.3. Let's apply the approach exploited for the single two-level emitter plasmonic eigenstate addressed in Section 3.2.3:

$$\xi(x) = \sqrt{\frac{\gamma}{2\pi}}\int \frac{\mathrm{d}k}{\sqrt{2\pi}}\, \frac{\mathrm{e}^{\mathrm{i}kx}\left(a_A + a_B\mathrm{e}^{-\mathrm{i}kd}\right)}{\sqrt[4]{k^2+m^2}\left(E - \sqrt{k^2+m^2}\right)}, \tag{4.63}$$

where the condition $a_A = \pm a_B$ has to hold corresponding to $\bar{k} = \sqrt{E^2-m^2}$. The complex integration provides

$$\xi(x) = -a_A \sum_{j=1}^{2} s^{j-1}\left(\sqrt{\frac{\gamma E}{m^2-E^2}}\,\mathrm{e}^{-\sqrt{m^2-E^2}|x-(j-1)d|} + J_{\text{cut}}\Big(x-(j-1)d, E\Big)\right), \tag{4.64}$$

represented in Figure 4.4. In panel (b) we can see that the appearance of the antisymmetric state is restricted to different values for the coupling constant: a symmetric plasmonic eigenstate always exists because of the spectral density divergence [26], while this is not true in the other parity sector. More precisely the self-energy expression below the cutoff for the antisymmetric case is $\alpha(E) - \beta(E)$, which in the limit $E \to m$, yields

$$\gamma \lim_{E\to m} \frac{\mathrm{e}^{-d\sqrt{m^2-E^2}} - \frac{1}{2\pi}\left(\pi + 2\arctan\frac{E}{\sqrt{m^2-E^2}}\right)}{\sqrt{m^2-E^2}} = -\gamma\left(d - \frac{1}{m\pi}\right). \tag{4.65}$$

This means that each straight line $E-\varepsilon$ has to reach in m a value greater than or equal to this limit as a condition for the emergence of the antisymmetric bound state below threshold, thus defining a critical value of the coupling constant:

$$\gamma_c \approx \frac{\varepsilon - m}{d - \frac{1}{m\pi}}. \tag{4.66}$$

This value holds true for sufficiently large distances, but it is not exact because of the missing cut contribution (4.54) in the self-energy, which will be indicated from now on as

$$b_s(E) = sE \int \mathrm{d}y \, \frac{e^{-yd}}{\sqrt{y^2 - m^2}(E^2 + y^2 - m^2)}, \tag{4.67}$$

such that the exact critical coupling reads

$$\gamma_c = \frac{\varepsilon - m}{d - \frac{1}{m\pi}\left(1 + \frac{b_-(m)}{m}\right)}. \tag{4.68}$$

Antisymmetric eigenstates below cutoff can still be treated with a perturbative appoach, while the singularity characterizing the symmetric sector shows a non-perturbative behavior. The antisymmetric solution approximates the dark eigenstate $|\Psi^-\rangle\otimes|\mathrm{vac}\rangle$ occurring for $d = 0$. The triplet, instead, survives as a real eigenstate even for all ε. However, since $a_A = a_B$ implies that the integrals over the field become divergent in this limit, the population in the $\mathcal{N}_{\mathrm{at}} = 1$ sector must be suppressed to fulfill normalization, and the contribution of this pole to the expansion (4.18) can be safely neglected.

The limiting condition (4.68) is useful to study the limit $d \to 0$, a value of the distance parameter which corresponds to the first dark resonant state associated with a fixed point of the evolution operator in the antisymmetric sector. This is realized by means of a divergent (4.68) in $d = 0$ for any $\varepsilon \neq m$, while, for a free energy gap which coincides with the propagating photon cutoff, the value $\gamma_c = 0$ is obtained because the free energy gap has to coincide with the energy eigenvalue.

We can exploit the expression for atomic population (4.22) to describe the excitation trapping in eigenstates associated with non-propagating photons. The residue calculation now involves poles lying on the imaginary axis in $\pm\bar{k}(E) = \pm\mathrm{i}\sqrt{m^2 - E^2}$, with a slightly more difficult procedure than the one in Section 4.1.3, due to the absence of any constraint related to the resonance condition. This means that we have to abandon the use of the integer ν, as in (4.26), and the parity label s is no longer associated with a discrete set of

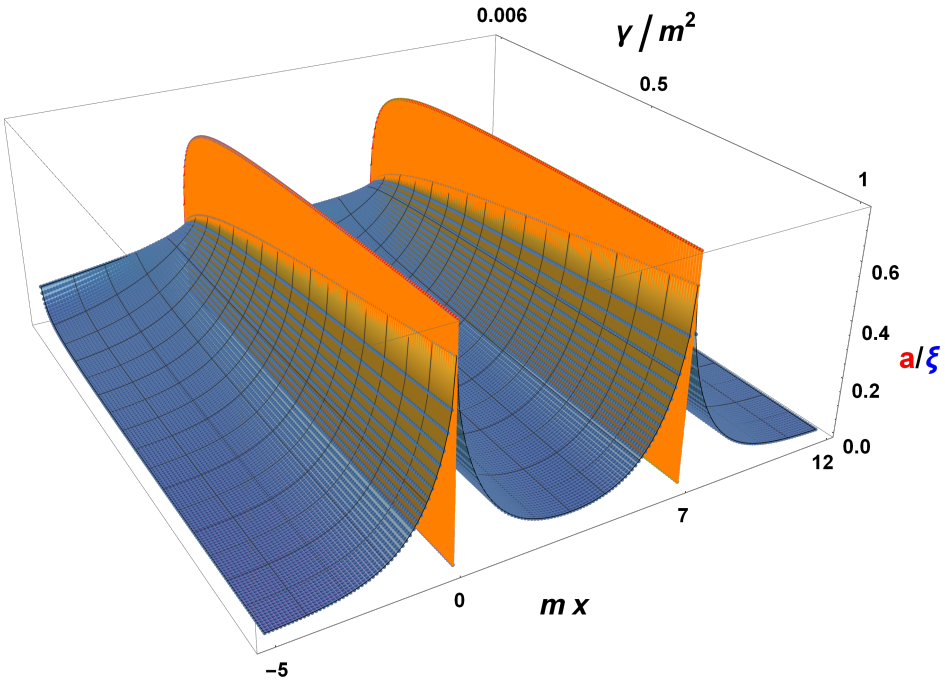

(a)

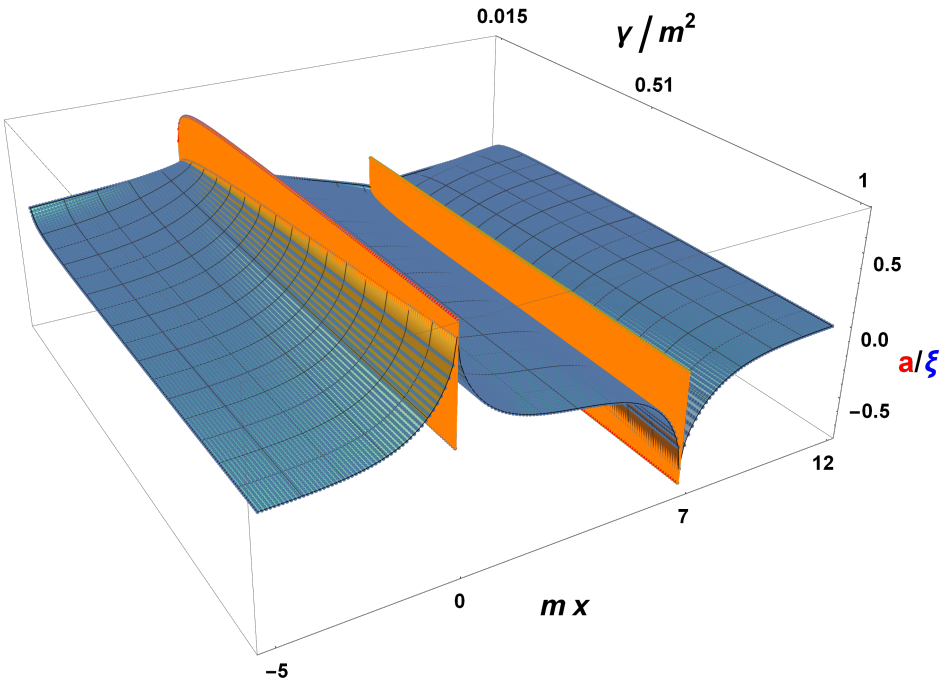

(b)

Figure 4.4: Panels (a) and (b) are show respectively the behavior of the symmetric and antisymmetric plasmonic eigenstate amplitude (red) and exponentially localized photon wavefunction (blue) with $\varepsilon = 1.1\ m$ and $md = 7$ with respect to a variation in the coupling constant γ.

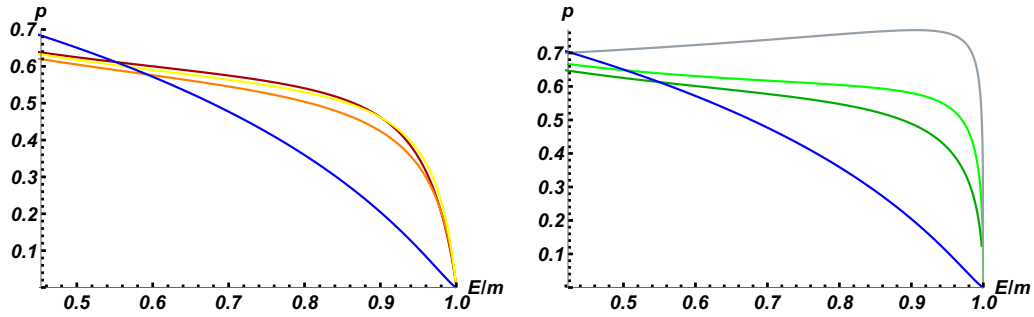

(a) (b)

Figure 4.5: In both panels the blue curve describes the single qubit population for $E < m$ as expressed by (3.60). The symmetric and antisymmetric state are shown in respectively (a) and (b), following the predicted population (4.70) with graded colors for $md = 10$, $md = 4$, $md = 0.7$ from the darker tone. Curves are obtained increasing the coupling constant starting from $\gamma = 10^{-4}\ m^2$ and with fixed $\varepsilon = 1.1\ m$. In (b) the case $md = 0.7$ requires couplings $\gamma/m^2 > 1$ to reach energies $E \lesssim 0.9\ m$.

energies:

$$
\begin{aligned}
&2\pi \mathrm{i} \lim_{k\to\bar{k}(E)} \frac{\mathrm{d}}{\mathrm{d}k}\left[\left(k-\mathrm{i}\sqrt{m^2-E^2}\right)^2 \frac{1+s\,\mathrm{e}^{\mathrm{i}kd_v}}{\sqrt{k^2+m^2}\left(E-\sqrt{k^2+m^2}\right)^2}\right] \\
&= 2\pi \mathrm{i} \lim_{k\to\bar{k}(E)} \frac{\mathrm{d}}{\mathrm{d}k}\left[\frac{\left(1+s\,\mathrm{e}^{\mathrm{i}kd_v}\right)\left(E+\sqrt{k^2+m^2}\right)^2}{\sqrt{k^2+m^2}\left(k+\mathrm{i}\sqrt{m^2-E^2}\right)^2}\right] \\
&= 2\pi \frac{2E\left(1+s\,\mathrm{e}^{-d\sqrt{m^2-E^2}}\left(1+d\sqrt{m^2-E^2}\right)\right)}{2(m^2-E^2)^{3/2}},
\end{aligned}
\tag{4.69}
$$

which has to be accounted twice, since it is included in both closed contours, thus yielding

$$
p = \frac{1}{2}\left(1+\gamma\,\frac{2E\left(1+s\,\mathrm{e}^{-d\sqrt{m^2-E^2}}\left(1+d\sqrt{m^2-E^2}\right)\right)}{2(m^2-E^2)^{3/2}}\right)^{-1}, \tag{4.70}
$$

up to a negligible cut contribution. The different behavior of these atomic populations for vanishing distances is shown in Figure 4.5, while they converge to the same curve for large separations. The excitation is shared by a larger

amount on the bound state for energies lying immediately below the threshold with respect to the single emitter case analyzed in Section 3.2.3.

Since the eigenstates of the effective Hamiltonian are Bell states, the evolution of an initially factorized state is characterized by oscillations between two orthogonal maximally entangled states with period $2\pi/\beta(\varepsilon)$. Compared to entanglement by relaxation, this mechanism yields unit concurrence [122]. On the other hand, the process can be very slow, since the energy splitting is exponentially suppressed with the interatomic distance, and requires the fine tuning of an optimal time to stop the interactions, which is not required in the spontaneous entanglement process described in Section 4.1.

4.4 Extension to generic dispersion relations

While we have examined in detail the case of a rectangular waveguide, we emphasize that our methods can be applied to a generic dispersion relation $\omega(k)$. We start by noticing that (4.4)-(4.6) lead in full generality to the implicit condition

$$E = \varepsilon + \frac{\gamma}{2\pi}\int \mathrm{d}k \frac{1-(-1)^{\nu}\mathrm{e}^{-\mathrm{i}kd}}{\omega(k)(E-\omega(k))}, \tag{4.71}$$

which must be satisfied by the bound state energy E. For the existence of a resonant (i.e. above threshold) bound state, it is evident that also the condition $\bar{k}d = \nu\pi$, $\nu \in \mathbb{N}$ must hold, where $\bar{k} > 0$ satisfies $E = \omega(\pm\bar{k})$. If this were not the case, the right hand side of (4.71) would diverge. We assume that such $\bar{k}$ exists and is unique. This is the case, for example, when $\omega(k)$ is an increasing lower-bounded function of $|k|$. Moreover, the possibility of non-resonant eigenstates below threshold follows as in the case of a rectangular waveguide.

Moving on to the complex energy plane, the analysis of poles proceeds along the same lines as in Section 4.2, albeit the existence of compact analytical expressions will rely on the specific functional form of $\omega(k)$. The pole contribution to the self energies can be generalized by replacing the denominators in (4.52)-(4.53) with $\omega(k_0)\omega'(k_0)$, and the square root in the exponentials with k_0. In the perturbative regime, this change does not affect formally the ratio of the decay rates of stable and unstable poles close to a resonance, namely (see (4.57)-(4.58))

$$\frac{\gamma_p^{(s)}}{\gamma_p^{(u)}} = \frac{1}{4}\bar{k}^2(d-d_\nu)^2, \tag{4.72}$$

where $d_\nu = \nu\pi/\bar{k}$. We can see that quantitative differences between models arise in the inversion of the dispersion relation as a function of the energy. The quantity in (4.72) gives a clear indication of the potential of a given model to

generate entanglement by relaxation. While losses would inevitably degrade the quality of the achievable entangled state, (4.72) may be seen as posing a fundamental limit to the entangling capabilities of a given system, a limit which would persist even in an idealized lossless scenario.

Chapter 5

Correlated photon emission by two excited atoms in a waveguide

The miracle of the appropriateness of the language of mathematics for the formulation of the laws of physics is a wonderful gift which we neither understand nor deserve

Eugene Wigner,
"The unreasonable effectiveness of
mathematics in the natural sciences"

The single-excitation sector contains, for a proper choice of the dispersion relation and for selected interatomic distances, a nontrivial atom–photon bound state [41, 47], characterized by a finite probability to find the atomic excitation in a singlet or triplet state. In the double-excitation sector the dissociation of such kind of bound states is obtained and exploited for applications. Considering initially both excited atoms, a proper treatment of the system will require a suitable renormalization scheme for the vertex of the propagator. In the computational perspective, the Breit-Wigner expansion is required in the weak coupling limit to avoid an otherwise divergent amplitude in the asymptotic two photon state, caused by a plasmonic bound state. The adoption of the renormalized propagator reveals effects unpredictable according to the perturbative approach, even if the coupling energy scale is much smaller than atoms energy gap [46].

5.1 The two-excitation sector

We will assume that the atoms presented in Figure 4.1 are both excited and are effectively coupled to a single mode of the waveguide, characterized by the dispersion relation $\omega(k)$. Hence, at the Fermi golden rule level, the excitation frequency ε must be larger than the low-energy cutoff $m := \min_k \omega(k)$ of the mode, to enable propagation along the guide. Other modes can be neglected, either because they do not couple efficiently to the $e \leftrightarrow g$ transition (g and e denoting the ground and excited atomic states, respectively), or because their energy cutoff is larger than ε. Both conditions are easily satisfied in a lossless linear rectangular waveguide with sides $L_y > L_z$, where the dispersion relation of the $TE_{1,0}$ mode reads $\omega(k) = \sqrt{k^2 + m^2}$, with $m \propto L_y^{-1}$ [79], with all the other modes characterized by a larger cutoff. We will consider this dispersion relations also in this Chapter, but will otherwise keep our discussion as general as possible.

The initial state is expected to relax towards an asymptotic configuration with both atoms in their ground state and two propagating photons. We will show how the emission properties are strongly influenced by interatomic distance, coupling and excitation energy. In particular, we will focus on and compare the probabilities of parallel and antiparallel emission. If two photon detectors placed at each end of the waveguide, only one detector will click in the case of parallel emission, detecting both photons, while both detectors will click in the antiparallel case. The experimental measurement of correlations can be exploited to detect properties of the atomic pair, such as their distance, the strenght of interactions with the waveguide field, asymmetries in their excitation frequency and other kinds of impurities. The initial state, in which both atoms are excited, can be prepared by a scattering process, in which a photon wave packet shines the atoms.

Assuming the dipolar and rotating-wave approximations, the Hamiltonian of the system corresponds to (4.1). We shall assume

$$\omega(k) = \omega(-k), \quad F(k) = F(-k), \tag{5.1}$$

where $F(k)$ is the form factor, defined in (4.1). Now we will consider the $\mathcal{N} = 2$ sector. In particular, we will study the evolution of the initial state

$$|e_A, e_B\rangle := |e_A\rangle \otimes |e_B\rangle \otimes |\text{vac}\rangle = \sigma_A^+ \sigma_B^+ |0\rangle\,, \tag{5.2}$$

with $\sigma_A^+ = \sigma^+ \otimes \mathbb{1}$, $\sigma_B^+ = \mathbb{1} \otimes \sigma^+$ for the tensor product of qubits Hilbert spaces and $|0\rangle = |g_A\rangle \otimes |g_B\rangle \otimes |\text{vac}\rangle$ the global vacuum of the non interacting theory, annihilated by all the b operators we are going to introduce.

In the following, it will be convenient to express the interaction Hamiltonian (4.1) in terms of coupling of the symmetric and antisymmetric combinations of atomic operators:

$$H_{\rm int} = \int \mathrm{d}k\, F(k) \left(\frac{1 + e^{\mathrm{i}kd}}{\sqrt{2}} b_+ + \frac{1 - e^{\mathrm{i}kd}}{\sqrt{2}} b_- \right) b^\dagger(k) + \text{H.c.} \tag{5.3}$$

where the new operators $b_\pm^\dagger$ create either a triplet $|\Psi^+\rangle$ or singlet $|\Psi^-\rangle$ atomic Bell state from the vacuum:

$$\left|\Psi^\pm\right\rangle = b_\pm^\dagger |0\rangle = \frac{\sigma_A^+ \pm \sigma_B^+}{\sqrt{2}} |0\rangle = \frac{\left|e_A, g_B\right\rangle \pm \left|g_A, e_B\right\rangle}{\sqrt{2}}. \tag{5.4}$$

Since $(\sigma_{A,B}^\pm)^2 = 0$ and $[\sigma_A^\pm, \sigma_B^\pm] = 0$, it is easy to check that $b_+ b_- = 0$ and $|e_A, e_B\rangle = \pm (b_\pm^\dagger)^2 |0\rangle$. The pure states belonging to the $\mathcal{N} = 2$ sector have the form:

$$\left|\psi\right\rangle = a_{AB} |e_A, e_B\rangle + \sum_{s=\pm} \int \mathrm{d}k\, \xi_s^{(1)}(k) |\Psi^s; k\rangle + \frac{1}{\sqrt{2}} \int \mathrm{d}k\, \mathrm{d}k'\, \xi^{(2)}(k, k') |k, k'\rangle\,, \tag{5.5}$$

with $|\Psi^s; k\rangle = b_s^\dagger\, b^\dagger(k) |0\rangle$, $|k, k'\rangle = b^\dagger(k) b^\dagger(k') |0\rangle$, and $\xi^{(2)}(k, k') = \xi^{(2)}(k', k)$, as presented in Section 1.1. The coefficients must satisfy the normalization conditions

$$|a_{AB}|^2 + \sum_{s=\pm} \int \mathrm{d}k\, |\xi_s^{(1)}(k)|^2 + \frac{1}{2} \int \mathrm{d}k\, \mathrm{d}k'\, |\xi^{(2)}(k, k')|^2 = 1. \tag{5.6}$$

Unlike the $\mathcal{N} = 1$ case, the sector Hamiltonian is not expressed in a off-diagonal Friedrichs-Lee form, since the one-photon states $|\Psi^s; k\rangle$, directly coupled to $|e_A, e_B\rangle$, are also indirectly coupled to each other through the two-photon states $|k, k'\rangle$. Hence, the self energy of the initial state $|e_A, e_B\rangle$ cannot be evaluated in a closed form. However, in the following we shall discuss a partial resummation of the self energy, in order to investigate the lifetime of the initial $|e_A, e_B\rangle$ state, the emission spectrum and the two-photon correlations.

5.2 Self-energy and decay rate of double excitations

To study the evolution of the initial state $|e_A, e_B\rangle$, we will analyze the resolvent (2.1), which determines the evolution through a Fourier-Laplace transform:

$$\left|\psi(t)\right\rangle = \mathrm{e}^{-\mathrm{i}tH} |e_A, e_B\rangle = \frac{\mathrm{i}}{2\pi} \int_{-\infty+\mathrm{i}\eta}^{+\infty+\mathrm{i}\eta} \mathrm{d}z \frac{\mathrm{e}^{-\mathrm{i}zt}}{z - H} |e_A, e_B\rangle\,, \tag{5.7}$$

with $\eta > 0$ [25]. Since in general it is not possible to compute $G(z)$ exactly, we consider its Dyson-Neumann expansion (2.6) and resum the relevant diagrams. The basic building blocks of the matrix elements of the expanded resolvent (2.6) are given by free propagators:

$$\left\langle e_A, e_B \left| \frac{1}{z - H_0} \right| e_A, e_B \right\rangle = \frac{1}{z - 2\varepsilon} = G_2^{(0)}(z), \tag{5.8}$$

$$\left\langle \Psi^{s'}; k' \left| \frac{1}{z - H_0} \right| \Psi^{s}; k \right\rangle = G_1^{(0)}(z, k)\, \delta_{s,s'} \delta(k - k'),$$

$$G_1^{(0)}(z, k) = \frac{1}{z - \varepsilon - \omega(k)}, \tag{5.9}$$

$$\left\langle k_1', k_2' \left| \frac{1}{z - H_0} \right| k_1, k_2 \right\rangle = G_0^{(0)}(z, k_1, k_2)\Big(\delta(k_1 - k_1')\delta(k_2 - k_2') + \delta(k_1 - k_2')\delta(k_2 - k_1')\Big),$$

$$G_0^{(0)}(z, k_1, k_2) = \frac{1}{z - \omega(k_1) - \omega(k_2)}, \tag{5.10}$$

and by the interaction vertices

$$\langle \Psi^s; k | H_{\text{int}} | e_A, e_B \rangle = s\, v_s(k), \tag{5.11}$$

$$\langle k_1, k_2 | H_{\text{int}} | \Psi^s; k \rangle = v_s(k_1)\delta(k_2 - k) + v_s(k_2)\delta(k_1 - k), \tag{5.12}$$

$$v_s(k) = F(k)\frac{1 + s\mathrm{e}^{\mathrm{i}kd}}{\sqrt{2}}, \tag{5.13}$$

with $s = \pm 1$. Since the interaction Hamiltonian is off-diagonal, no $O(H_{\text{int}})$ terms appear in the decomposition of the propagator

$$G_2(z) = \langle e_A, e_B | G(z) | e_A, e_B \rangle = \frac{1}{z - 2\varepsilon - \Sigma_2(z)}, \tag{5.14}$$

where $\Sigma_2(z)$ is the self-energy of $|e_A, e_B\rangle$. The smallest-order contribution to (5.14) comes from the process of emission and reabsorption of a photon, through an intermediate state $|\Psi^s, k\rangle$. In this process, represented in Fig. 5.1(a), it is clear from (5.9) that the atomic excitation cannot switch its sign s during the intermediate free evolution, before the photon is reabsorbed. Transitions can generally occur only in higher-order diagrams, such as the $O(H_{\text{int}}^4)$ terms in Fig. 5.1(b)-(c)-(d). However, a diagram in which a photon is emitted and then reabsorbed takes the general form

$$\int \mathrm{d}k\, F^2(k) \frac{(1 + s'\mathrm{e}^{-\mathrm{i}kd})(1 + s\mathrm{e}^{\mathrm{i}kd})}{2}\, \Phi_{ss'}(z, \omega(k)), \tag{5.15}$$

where s (s') is the sign of the atomic excitation attached to the emission (absorption) vertex, and the function Φ is related to the particular structure of the

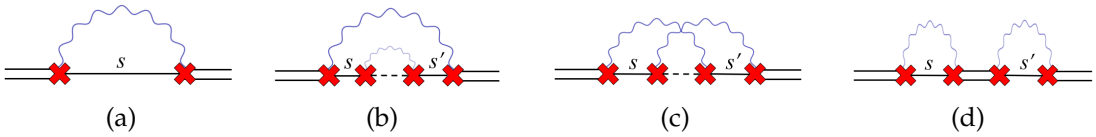

Figure 5.1: Contributions of order $H^2_{\rm int}$ (diagram (a)) and $H^4_{\rm int}$ (diagrams (b), (c) and (d)) to the double-excitation propagator $G_2(z)$ in (5.14). The diagrams (a), (b) and (c), without external legs, represent the $O(H^4_{\rm int})$ contributions to the self energy $\Sigma_2(z)$. The wavy lines represent photons; the double horizontal line represents the free propagator $G_2^{(0)}(z)$ in (5.8); the single horizontal line with a wavy line represents the free propagator (5.9) of $|\Psi^s;k\rangle$, the single excitation with sign s and a photon; the dashed line with two wavy lines represents the free propagator $G_1^{(0)}(z,k)$ in (5.10). The crosses represent one of the vertices $v_s(k)$ in (5.11)–(5.13). Processes (b) and (c), preserve the sign s (i.e., $s' = s$), while in diagram (c) the relative sign of s and s' is arbitrary.

diagram. Since we have assumed in (5.1) that both the dispersion relation and the form factor are even functions, only terms with $s = s'$ survive integration over k and contribute, for instance, to the diagrams in Figure 5.1(b)-(c); no constraint on the relative sign exists, instead, for the diagram (d).

The diagrams (b) and (c) in Figure 5.1 are both contributions of order $H^4_{\rm int}$ to the self energy of $|e_A, e_B\rangle$, but they qualitatively differ. In (b), the emission and reabsorption of a second photon is dressing the intermediate one-excitation propagator, while this is not the case in (c), where, since the first emitted photon is absorbed before the second one, two photon lines cross. Diagrams with crossings can be interpreted as a renormalization of the vertex between the double-excitation state $|e_A, e_B\rangle$ and the states $|\Psi^s;k\rangle$. Notice that, since we consider the dynamics in the $\mathcal{N} = 2$ sector, where at most two photons can be present in an intermediate state, each photon line can cross at most two other lines before being re-absorbed. The self energy appearing in (5.14), containing the sum of all the intermediate diagrams between the two double-excitation states, can be resummed as

$$\Sigma_2(z) = \sum_{s=\pm} \int \mathrm{d}k\, F^2(k) \frac{(1 + X_s(k,z))(1 + s\cos(kd))}{z - \varepsilon - \omega(k) - \Sigma_s(z - \omega(k))}, \tag{5.16}$$

where Σ_s is the self-energy of the one-excitation state $|\Psi^s\rangle$

$$\Sigma_s(z) = \int \mathrm{d}k\, F^2(k) \frac{1 + s\cos(kd)}{z - \omega(k)}. \tag{5.17}$$

which we already encountered in (4.41). Observe that, in (5.16), the argument of Σ_s is shifted by the energy $\omega(k)$ of the additional propagating photon [41], and

notice that $\Sigma_s(z-\omega(k))$ does *not* coincide with the self-energy function of $|\Psi^s;k\rangle$. The vertex renormalization X_s is implicitly defined by the integral equation, obtained in Section 5.2.1:

$$X_s(k,z) = \int \mathrm{d}q\, F^2(q) \frac{(1+X_s(q,z))(1+s\cos(qd))}{(z-\varepsilon-\omega(q)-\Sigma_s(z-\omega(q)))\,(z-\omega(q)-\omega(k))}. \tag{5.18}$$

The renormalization of the atomic double excitation propagator $G_2(z)$ is graphically represented in Figure 5.2.

The evaluation of the renormalized vertex requires an approximation procedure, that will be detailed in the next section, where it will be crucial for the consistent evaluation of the two-photon amplitude and spectrum.

In order to characterize the lifetime of the double excitation, it is sufficient to consider the lowest order of the self energy, by neglecting $X_s(k,z)$ and $\Sigma_s(z-\omega(k))$ in its integral expression (5.16), namely

$$\Sigma_2^{(2)}(z) = \sum_{s=\pm} \Sigma_s(z-\omega_0) = \int \mathrm{d}k \frac{2F^2(k)}{z-\varepsilon-\omega(k)}. \tag{5.19}$$

By evaluating the self energy on shell, $\Sigma_2(2\varepsilon)$, in the propagator (5.14) we can infer, as a first approximation, that the lifetime of the double excitation,

$$\tau_2 \approx -\frac{1}{2\mathrm{Im}\left(\Sigma_2^{(2)}(2\varepsilon+\mathrm{i}0)\right)}, \tag{5.20}$$

is half the lifetime of a single *isolated* excited atom. It is evident from (5.19) that the lowest-order contribution to the lifetime of $|e_A,e_B\rangle$ is insensitive to the interatomic distance, and *a fortiori*, to the existence of resonant bound states in the $\mathcal{N}=1$ sector. This result is physically in accord with the fact that photon exchanges between the two atoms are neglected at $O(H_{\mathrm{int}}^2)$ of the self energy, and is consistent with the oscillating behavior of the lifetimes of $|\Psi^{\pm}\rangle$ in the one-excitation sector [41]: the state $|e_A,e_B\rangle$ has two decay modes, and when one of them is close to a resonant bound state, the antiresonant mode has twice the lifetime of an isolated atom. The effects related to interatomic distance will emerge in the analysis of the photon pair emitted by the double-excitation state, that will be the topic of the following section.

Finally, it is worth noticing that, since the self-energy functions $\Sigma_s(z)$ in (5.17) are characterized by a branch cut along the half line $[m,\infty)$ on the real axis, the $O(H_{\mathrm{int}}^2)$ contribution to the self-energy (5.19) has a cut in correspondence of $[m+\varepsilon,\infty)$. However, considering the exact expression (5.16), one finds that the branch cut of the self energy (and of the propagator $G_2(z)$ as well) actually starts from $2m$. This result, as we will show in the following, is consistent with the integrability of the asymptotic two-photon distribution.

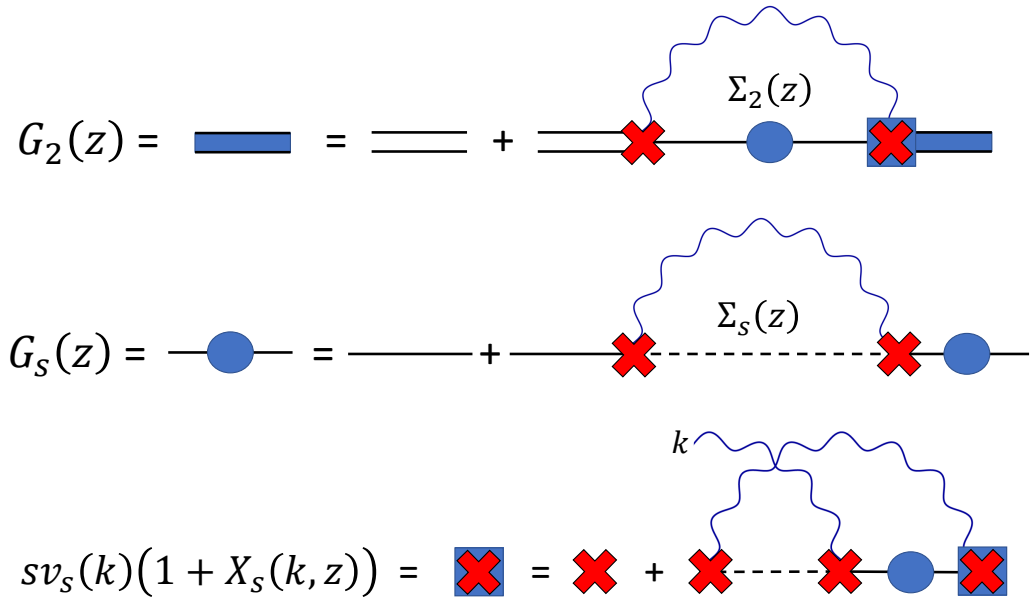

Figure 5.2: Renormalization scheme for the two-excitation state propagator $G_2(z)$.

5.2.1 Fredholm integral equations

The vertex renormalization (5.18) is expressed in a recurrent form highlighting the absence of a closed expression typifying the simple off-diagonal Friedrichs-Lee renormalization presented in Section 2.5. As already explained, our initial state consists in a double-atomic excitation, which does not interact directly with the two photon state. This latter interacts with the single-atomic excitation, representing another decayed state in the terminology of the off-diagonal decomposition in Section 2.5 and 2.6, thus yielding a forbidden interaction for the renormalization scheme.

It is possible to recognize the different structure of the Hamiltonian in this sector with respect to the one characterizing (1.18), exploited also for the free degenerate subspace of Chapter 4, by using the following matrix expression

$$H = \begin{pmatrix} 2\varepsilon & \langle v_+| & \langle v_-| & 0 \\ |v_+\rangle & \varepsilon + \Omega & 0 & \langle v_+| \\ |v_-\rangle & 0 & \varepsilon + \Omega & \langle v_-| \\ 0 & |v_+\rangle \odot & |v_-\rangle \odot & \Omega \end{pmatrix}, \quad |\psi\rangle = \begin{pmatrix} a_{AB} \\ \left|\xi_+^{(1)}\right\rangle \\ \left|\xi_-^{(1)}\right\rangle \\ \left|\xi^{(2)}\right\rangle \end{pmatrix} \in \mathscr{H}^{(2)} = \mathbb{C} \oplus \Big(\mathbb{C}^2 \otimes L^2(\mathbb{R})\Big) \oplus L^2(\mathbb{R})^{\odot 2}, \tag{5.21}$$

following the notation of (5.5), where $\left(\left|\xi_+^{(1)}\right\rangle, \left|\xi_-^{(1)}\right\rangle\right) \in \mathbb{C}^2 \otimes L^2(\mathbb{R})$ for the single

atomic excitation and one photon. It is evident the absent diagonal form for the block acting on decayed components.

The explicit expression for the renormalized vertex (5.18) is obtained through the eigenvalue equation for the Hamiltonian:

$$Ea_{AB} = 2\varepsilon a_{AB} + \sum_{s=\pm} \left\langle v_s \middle| \xi_s^{(1)} \right\rangle, \tag{5.22}$$

$$E\xi_s^{(1)}(k) = a_{AB} v_s(k) + \Big(\varepsilon + \omega(k)\Big)\xi_s^{(1)}(k) + \left\langle v_s \middle| \xi^{(2)} \right\rangle, \tag{5.23}$$

$$E\xi^{(2)}(k,k') = \sum_{s=\pm} \Big(v_s(k)\xi_s^{(1)}(k') + v_s(k')\xi_s^{(1)}(k)\Big) + \Big(\omega(k) + \omega(k')\Big)\xi^{(2)}(k,k'), \tag{5.24}$$

where the substitution of the latter in the two equation for single-atomic excitation amplitudes provides two decoupled singular Fredholm integral equations of the second kind [135]. More precisely, let us expand the scalar product:

$$\left\langle v_s \middle| \xi^{(2)} \right\rangle = \xi_s^{(1)}(k) \int \mathrm{d}q \, \frac{\left|v_s(q)\right|^2}{E - \omega(k) - \omega(q)} + v_s(k) \int \mathrm{d}q \, \frac{v_s^*(q)\xi_s^{(1)}(q)}{E - \omega(k) - \omega(q)}, \tag{5.25}$$

where the first term corresponds to the diagonalized self-energy (4.41), while in the second term $\left\langle \Psi^s \middle| \Psi^{s'} \right\rangle = \delta_{s,s'}$ provides the typical form:

$$\xi_s^{(1)}(k) = f_s(k) + \int \mathrm{d}q \, K(k,q)\xi_s^{(1)}(q). \tag{5.26}$$

with

$$f_s(k) = \frac{a_{AB} v_s(k)}{E - \varepsilon - \omega(k) - \Sigma_s(E - \omega(k))}, \tag{5.27}$$

$$K(k,q) = \frac{v_s(k)v_s^*(q)}{\Big(E - \varepsilon - \omega(k) - \Sigma_s(E - \omega(k))\Big)\Big(E - \omega(k) - \omega(q)\Big)}, \tag{5.28}$$

the latter characterizing the equation as singular, according to the non factored two photon free propagator in a product of separate dependencies on k and q. We apply the method of successive approximation, based on the definition of iterated kernels, as made in Section 2.4 for the Volterra integral equation of the evolution operator:

$$K_j(k,q) = \int \mathrm{d}q_{j-1} \, K_{j-1}(k,q_{j-1})K(q_{j-1},q), \quad K_1(k,q) = K(k,q), \tag{5.29}$$

which provide the solution according to the resolvent expansion $\sum_{j=1}^{\infty} K_j(k,q)$:

$$\xi_s^{(1)}(k) = f_s(k) + \sum_{j=1}^{\infty} \int \mathrm{d}q \, K_j(k,q) f_s(q). \tag{5.30}$$

This expression for the solution includes the explicit form of (5.18):

$$X_s(k,E) = \sum_{\ell=1}^{\infty} \int \prod_{j=1}^{\ell} \mathrm{d}q_j \, \frac{\left|v_s(q_j)\right|^2}{\Big(E-\varepsilon-\omega(q_j)-\Sigma_s(E-\omega(q_j))\Big)\Big(E-\omega(q_{j-1})-\omega(q_j)\Big)}\Bigg|_{q_0=k} \tag{5.31}$$

finally yielding the single-atomic excitation amplitude:

$$\xi_s^{(1)}(k) = a_{AB} v_s(k) \frac{1+X_s(k,E)}{E-\varepsilon-\omega(k)-\Sigma_s(E-\omega(k))}, \tag{5.32}$$

whose substitution in (5.22) defines the self-energy (5.16).

5.3 Two-photon amplitude

One of the most interesting features of the evolution dynamics of the initial state $|e_A, e_B\rangle$ under the action of the Hamiltonian (4.1) are correlations and interference effects involving the emission of two photons. Unlike the lifetime of the initial state, such effects are deeply influenced by the existence of resonant bound states in the $\mathcal{N}=1$ sector. The properties of the two-photon amplitude at a generic time t

$$\xi^{(2)}(k_1,k_2,t) = \langle k_1,k_2|\, \mathrm{e}^{-\mathrm{i}tH}\, |e_A,e_B\rangle \tag{5.33}$$

are determined through (5.7) by its representation in the energy domain, which, following the same resummation procedure as for the self energy (5.16), reads

$$\xi^{(2)}(k_1,k_2,z) = \left\langle k_1,k_2 \left| \frac{1}{z-H} \right| e_A,e_B \right\rangle = \frac{\widetilde{\xi^{(2)}}(k_1,k_2,z)}{z-\omega(k_1)-\omega(k_2)}, \tag{5.34}$$

with

$$\widetilde{\xi^{(2)}}(k_1,k_2,z) = \sum_{s=\pm} \frac{s v_s(k_1) v_s(k_2)}{z-2\varepsilon-\Sigma_2(z)} \sum_{j=1,2} \frac{1+X_s(k_j,z)}{z-\varepsilon-\omega(k_j)-\Sigma_s(z-\omega(k_j))}. \tag{5.35}$$

See the Feynman diagrams in Figure 5.3.

In order to characterize the properties of the two-photon amplitude, we will specialize our analysis to the case of a pair of atoms coupled to a massive guided mode, characterized by the following dispersion relation and form factor [41]

$$\omega(k) = \sqrt{k^2+m^2}, \quad F(k) = \sqrt{\frac{\gamma}{2\pi\omega(k)}}, \tag{5.36}$$

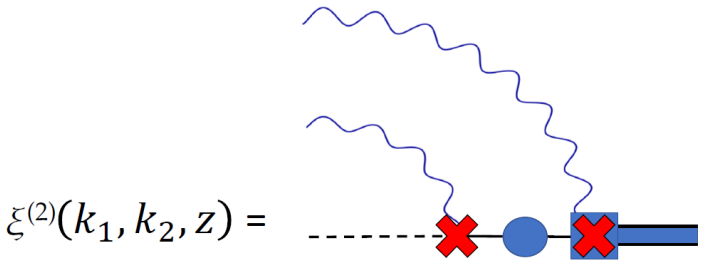

Figure 5.3: Diagrammatic representation of the two-photon ampliude $\xi^{(2)}(k_1, k_2, z) = \langle k_1, k_2 | \, (z - H)^{-1} \, | e_A, e_B \rangle$. The dressed propagators and the dressed vertex are defined in (5.16)-(5.18) and represented in Figure 5.2.

where the units are chosen in a way that the speed of light in the waveguide is equal to one. We also introduce for convenience the on-shell quantities $k_0 > 0$, c_0 and F_0:

$$\omega(k_0) = \varepsilon, \quad c_0 = \frac{\mathrm{d}\omega}{\mathrm{d}k}\Big|_{k=k_0}, \quad F_0 = \sqrt{\frac{\gamma}{2\pi\varepsilon}}. \tag{5.37}$$

Since the relevance of the one-excitation self-energy functions $\Sigma_s(z)$, with $s = \pm$, is manifest in (5.34)-(5.35), let us review their properties before discussing the two-photon amplitude. In the case (5.36), the self energy can be analytically evaluated for $\mathrm{Re}(z) > 0$ on the first Riemann sheet, where it reads [41]

$$\Sigma_s(z) = \frac{\gamma}{\pi\sqrt{z^2 - m^2}}\left[(1 + s\lambda(z)) \log\left(\frac{z + \sqrt{z^2 - m^2}}{m}\right) - \mathrm{i}\pi\left(1 + s\mathrm{e}^{\mathrm{i}\sqrt{z^2-m^2}d}\right)\right], \tag{5.38}$$

where the first term coincides with (4.54) and $\lambda(z) = O(\mathrm{e}^{-md})$ is a real-valued function for real z. Notice the square-root divergence at the branching point $z = m$, that depends on the diverging density of states close to the threshold m for photon propagation. The existence of bound states for special values of the interatomic distance is related to the oscillating behavior of the imaginary part of (5.38). In particular, considering the lowest order in $\sqrt{\gamma}$ and neglecting the $O(\mathrm{e}^{-md})$ corrections, the energy shift and decay rate of $|\Psi^s\rangle$ can be written as

$$\delta_s = \mathrm{Re}(\Sigma_s(\varepsilon + \mathrm{i}0^+)) \approx \delta_0 + 2\pi s\frac{F_0^2}{c_0}\sin(k_0 d), \tag{5.39}$$

$$\gamma_s = -2\mathrm{Im}(\Sigma_s(\varepsilon + \mathrm{i}0^+)) = 4\pi s\frac{F_0^2}{c_0}(1 + s\cos(k_0 d)), \tag{5.40}$$

respectively, with δ_0 independent of the distance d. Notice that the above results are generalizable to the case of different dispersion relations and form factors,

provided the on-shell parameters are defined as in (5.37). When the interatomic distance satisfies $k_0 d = n\pi$, with n a positive integer, the lifetime of state $|\Psi^s\rangle$ with $s = (-1)^{n+1}$, becomes infinite, since $\gamma_s = 0$. On the other hand, when $k_0 d = (n + 1/2)\pi$, the symmetric and antisymmetric atomic excitations have the same lifetime, which is equal to that of an isolated atom. In all cases, the sum of the two decay rates is twice the decay rate of an isolated excited atom. Based on the consideration of the previous section, it is evident that the lowest-order on-shell contribution to the self energy of $|e_A, e_B\rangle$ reads

$$\sigma_2 = \Sigma_2^{(2)}(2\varepsilon + \mathrm{i}0^+) \approx 2\delta_0 - 4\pi \mathrm{i} \frac{F_0^2}{c_0}, \tag{5.41}$$

where, as expected, the on-shell decay rate of the double excitation is twice the rate for a single atom.

5.4 Two-photon correlated emission

Knowledge of $\xi^{(2)}(k_1, k_2, z)$ enables one to compute, through (5.33) and (5.7), the photon correlation function at any time t. This function will feature damped contributions, due to the cuts along the real axis on the single- and double-excitation propagators, and asymptotically stable terms, approaching, at large times (larger than the lifetimes of the excitations), the form

$$\xi_\infty^{(2)}(k_1, k_2, t) = \widetilde{\xi^{(2)}}\,(k_1, k_2, \omega(k_1) + \omega(k_2))\, \mathrm{e}^{-\mathrm{i}(\omega(k_1)+\omega(k_2))t} + \xi_{\mathrm{bt}}^{(2)}(k_1, k_2, t), \tag{5.42}$$

where $\widetilde{\xi^{(2)}}$ is defined in (5.35) and is the dominant contribution, given by the residue of the bare two-photon pole $z = \omega(k_1) + \omega(k_2)$ appearing in (5.34), while the term $\xi_{\mathrm{bt}}^{(2)}$ (below threshold) arises due to real poles below the branching points of the renormalized propagators and vertices, and represents a small correction in the weak-coupling regime. For instance, for the dispersion relation (5.36), the single-excitation propagator $(z-\varepsilon-\omega(k)-\Sigma_+(z-\omega(k)))^{-1}$ diverges at $z - \omega(k) = E_p$, with

$$E_p \approx m\left(1 - \frac{2\gamma^2}{m^2(\varepsilon - m)^2}\right), \tag{5.43}$$

with a residue that scales like γ^2, while no pole below threshold is present in the propagator of the antisymmetric excitation, at least for small coupling. In the special cases in which, in the $\mathcal{N} = 1$ sector, a bound state with energy $E > m$ exists, it would be necessary to include an additional asymptotic contribution to (5.42). However, the contributions to the amplitude (5.35) stemming from resonant bound states are suppressed, since the peaks of the corresponding

residues are compensated by the numerators $(1+se^{ikd})$, that vanish at $k=\bar{k}$ such that $E=\omega\left(\bar{k}\right)$. From the large-time limit of the two-photon amplitude, one can also determine the two-photon spectral probability

$$P(k_1,k_2)=\lim_{t\to\infty}|\xi^{(2)}(k_1,k_2,t)|^2, \tag{5.44}$$

$\xi^{(2)}$ being the full two-photon amplitude (5.33). Notice that $P(k_2,k_1)$ is symmetric in its arguments, due to the bosonic nature of the two-photon wavefunction ($|k_1,k_2\rangle$ and $|k_2,k_1\rangle$ represent the same state).

Before extending the numerical computation to a wider range of couplings, let us discuss the analytical results when $\gamma\to 0$. As the coupling vanishes, the asymptotic two-photon amplitude $\widetilde{\xi^{(2)}}(k_1,k_2,\omega(k_1)+\omega(k_2))$ in (5.42) becomes concentrated around regions of linear size $O(\gamma)$ around the four points $\omega(k_1)=\omega(k_2)=\varepsilon$ in the two-photon momentum space, while the additional pole contributions $\xi^{(2)}_{\rm bs}$ becomes vanishingly small. For symmetry reasons, it is enough to focus on the points (k_0,k_0) and $(k_0,-k_0)$, around which $\widetilde{\xi^{(2)}}(k_1,k_2,\omega(k_1)+\omega(k_2))$ is well approximated by

$$\widetilde{\xi^{(2)}_{\Leftrightarrow}}(k_1,k_2)=\sum_{s=\pm}s(1+s\mathrm{e}^{\mathrm{i}k_0d})^2Q_s(k_1-k_0,k_2-k_0), \tag{5.45}$$

$$\widetilde{\xi^{(2)}_{\rightleftharpoons}}(k_1,k_2)=\sum_{s=\pm}s|1+s\mathrm{e}^{\mathrm{i}k_0d}|^2Q_s(k_1-k_0,-k_2-k_0), \tag{5.46}$$

respectively, where parallel ($\Leftrightarrow$) and antiparallel ($\rightleftharpoons$) arrows denote photons emitted in the same and opposite direction, and with

$$Q_s(k_1,k_2)=\frac{\gamma}{4\pi\varepsilon}\frac{1}{c_0(k_1+k_2)-\sigma_2}\left(\frac{1}{c_0k_1-\sigma_s}+\frac{1}{c_0k_2-\sigma_s}\right), \tag{5.47}$$

where $\sigma_s=\delta_0+\delta_s-\mathrm{i}\gamma_s/2$ are defined in (5.39)-(5.40) and σ_2 is introduced in (5.41). From these results, we can obtain the following approximate expression for the asymptotic probability density (5.44) close to the on-shell points,

$$\begin{aligned}P(k_1,k_2)=16\Bigg\{&\cos^4\left(\frac{k_0d}{2}\right)|Q_+(k_1-k_0,\pm k_2-k_0)|^2+\sin^4\left(\frac{k_0d}{2}\right)|Q_-(k_1-k_0,\pm k_2-k_0)|^2\\&\pm\frac{1}{2}\sin^2(k_0d)\mathrm{Re}\Big[Q_+^*(k_1-k_0,\pm k_2-k_0)Q_-(k_1-k_0,\pm k_2-k_0)\Big]\Bigg\},\end{aligned} \tag{5.48}$$

where + and − is for photons emitted in the same (parallel) and opposite (antiparallel) directions, respectively. In the limit $\gamma\to 0$, the integrals over the

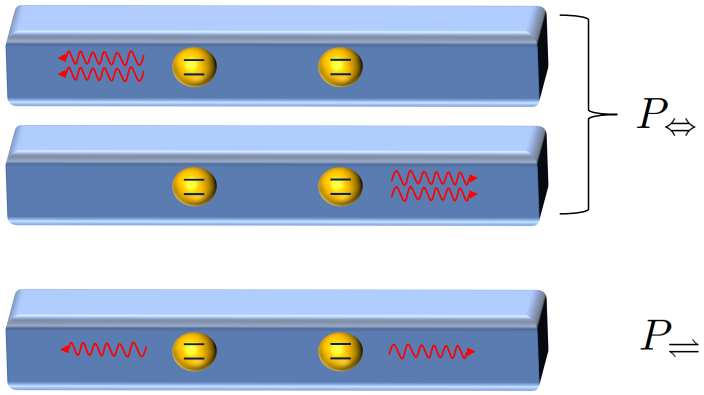

Figure 5.4: Representation of the processes that contribute to the probability of parallel ($P_{\Leftrightarrow}$) and antiparallel ($P_{\rightleftharpoons}$) photon pair emission.

different quadrants of the (k_1, k_2) plane can be evaluated with arbitrary accuracy, leading to the result

$$P_{\Leftrightarrow} = \frac{1}{2}\int_{D_{\Leftrightarrow}} \mathrm{d}k_1 \mathrm{d}k_2 P(k_1, k_2) = \frac{1}{2}\left(1 + \frac{\sin^2(k_0 d)}{1 + \sin^2(k_0 d)}\right), \tag{5.49}$$

$$P_{\rightleftharpoons} = \frac{1}{2}\int_{D_{\rightleftharpoons}} \mathrm{d}k_1 \mathrm{d}k_2 P(k_1, k_2) = \frac{1}{2}\left(1 - \frac{\sin^2(k_0 d)}{1 + \sin^2(k_0 d)}\right), \tag{5.50}$$

where $D_{\Leftrightarrow} = \{(k_1, k_2) \in \mathbb{R}^2 | \, k_1 k_2 > 0\}$ and $D_{\rightleftharpoons} = \{(k_1, k_2) \in \mathbb{R}^2 | \, k_1 k_2 < 0\}$. The factor $1/2$ has been introduced to remove redundancy with respect to momentum exchange. The processes contributing to $P_{\Leftrightarrow}$ and $P_{\rightleftharpoons}$ are pictorially represented in Figure 5.4.

The ratio of asymptotic probabilities to observe parallel and antiparallel photon pairs reads

$$R(\lambda)\big|_{\lambda \to 0} = \frac{P_{\Leftrightarrow}}{P_{\rightleftharpoons}} = 1 + 2\sin^2(k_0 d), \tag{5.51}$$

being minimal and equal to one at resonance, when the two photons are emitted in states with the same spatial symmetry, characterized by equal weights of the parallel and antiparallel configurations. The limiting value of R is universal, in the sense that it depends only on the dimensionless product between interatomic distance and momentum of the emitted photon, and not on the dispersion relation, the atomic excitation energy or the speed of propagation. Nonetheless, it is crucially determined by the dynamics, through the relation between the phase shifts and the linewidths in (5.39)-(5.40). The maximal value $R = 3$ corresponds to the off-resonant points $\sin(k_0 d) = \pm 1$, where construc-

tive interference between photon states with opposite spatial symmetry favors parallel photon emission.

This effect is similar to the photon bunching occurring in a Hong-Ou-Mandel (HOM) interferometer [74], with the role of the input photons played by the initial double atomic excitation. Indeed, neglecting dynamical effects, in the off-resonant case $k_0 d = (n + 1/2)\pi$ the atom pair is expected to behave like the beam splitter in the HOM experiment, fully suppressing the possibility of antiparallel emission (i.e., $R \to \infty$). However, the two-photon emission differs from the HOM case in two aspects, both related to dynamics: first, the emitted photons are characterized by a typical momentum distribution, and the relative phase between spatially symmetric and antisymmetric photons depends on momentum; second, the difference in the energy shifts $\delta_\pm$ (see (5.39)) lifts the degeneracy between the symmetric and antisymmetric atomic excitations. The combination of such effects regularize the ratio to a nontrivial finite value, as in (5.51). Notice that a different expression of δ_s and γ_s would lead to generally different value of R. The effect of interference between symmetric and antisymmetric states on the structure of the parallel and antiparallel peaks is displayed in Figure 5.5.

In order to compute the two-photon amplitude in the case of larger couplings, some approximations are needed. In particular, it is not possible to express the vertices $X_s(k, z)$, defined in (5.18) and represented in Figure 5.2, in a closed form. We choose to truncate the expansion of X_s at the first diagram, thereby regularizing the intermediate single-excitation propagator with its on-shell self energy $\sigma_s = \Sigma_s(\varepsilon + \mathrm{i}0^+)$. Namely, we approximate the vertex corrections as

$$\begin{aligned} X_s(k, z) &\approx \int \mathrm{d}q \frac{F^2(q)(1 + s\cos(qd))}{(z - \omega(k) - \omega(q))(z - \varepsilon - \omega(q) - \sigma_s)} \\ &= \frac{\Sigma_s(z - \varepsilon - \sigma_s) - \Sigma_s(z - \omega(k))}{\varepsilon + \sigma_s - \omega(k)}. \end{aligned} \tag{5.52}$$

Some relevant results are displayed in Figure 5.6. In general, the plots show that $R(\lambda)$ is a decreasing function of the coupling strength, and the effect of increasing the coupling are more relevant in the off-resonance cases ($k_0 d = (n + 1/2)\pi$). However, if one considers $d \in [(n - 1/2)\pi/k_0, (n + 1/2)\pi/k_0]$, R remains an increasing function of the distance $|d - n\pi/k_0|$ from the resonance value. The decrease of R with $\sqrt{\gamma}$ is mitigated by the discrepancy of the excitation energy ε with respect to the propagation cutoff m, and enhanced by the distance d, if one considers the cases $k_0 d = (n + \alpha)\pi$ with α real and fixed. These effects are due to a different behavior of the peak widths in the parallel and antiparallel cases, and to the emergence of strong-coupling effects due to the poles below

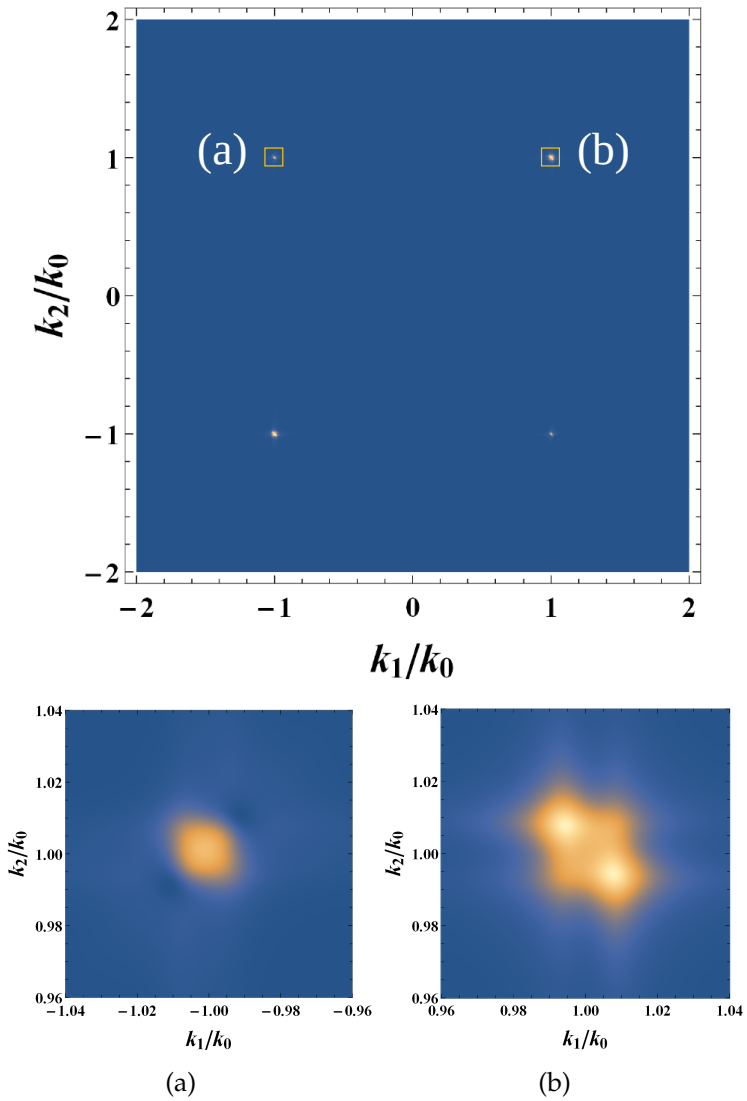

(a) (b)

Figure 5.5: The upper panel displays the density plot of the two-photon distribution $P(k_1, k_2)$, normalized to its maximal value, for $\varepsilon = 1.1m$, $\gamma/m^2 = 2\pi \times 10^{-4}$ and $k_0 d = \pi/2$. Colors range from blue (normalized density equal to 0) to white (normalized density equal to 1). It is evident that the probability is concentrated in very small areas of linear size $O(\gamma)$ around the on-shell points. The lower panels (a) and (b) represent magnifications of the on-shell peaks highlighted in the upper plot, around $(-k_0, k_0)$ and (k_0, k_0), respectively. The different shape of these peaks is due to the fact that emission with intermediate symmetric and antisymmetric atomic states interfere constructively in the parallel case (b), and destructively in the antiparallel case (a). For such choice of parameters, the ratio $R(\lambda)$ between the total parallel and antiparallel emission is close to 3.

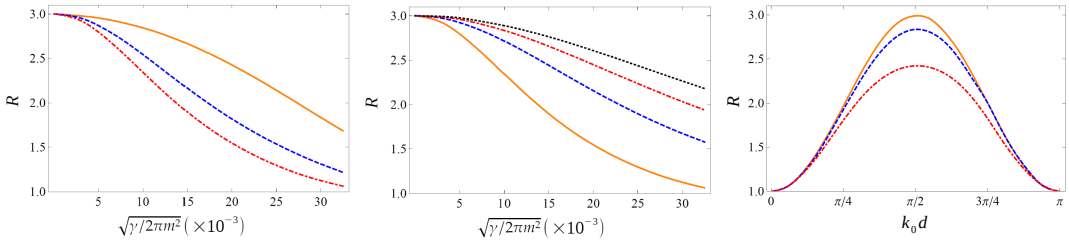

(a) (b) (c)

Figure 5.6: Plots of the ratio $R = P_{\Leftrightarrow}/P_{\rightleftharpoons}$ in different conditions. Panel (a): dependence of R on $\sqrt{\gamma}$ at fixed $\varepsilon = 1.1m$, for $d = \pi/(2k_0)$ (solid orange line), $d = 3\pi/(2k_0)$ (dashed blue line) and $d = 5\pi/(2k_0)$ (dot-dashed red line). Panel (b): dependence of R on $\sqrt{\gamma}$ in the case $d = 5\pi/(2k_0)$ for $\varepsilon = 1.1m$ (solid orange line), $\varepsilon = 1.2m$ (dashed blue line), $\varepsilon = 1.3m$ (red dot-dashed line) and $\varepsilon = 1.4m$ (dotted black line). Panel (c): dependence of R on $k_0 d$, at fixed $\varepsilon = 1.1m$, for $\gamma/m^2 = 2\pi \times 10^{-6}$ (solid orange line), $\gamma/m^2 = 2\pi \times 10^{-4}$ (dashed blue line) and $\gamma/m^2 = 8\pi \times 10^{-4}$ (red dot-dashed line).

threshold, that are correctly taken into account in the computation. Since the distance, the coupling strength and the excitation energy are fully independent parameters, the results suggest that correlated two-photon emission in a linear waveguide can be possibly used to determine one of them, when the other two are known. In particular, in the small coupling regime, the relation (5.51) depends only on a relation between d and ε.

5.4.1 Breit-Wigner self-energy expansion

The numerical procedure targeting coupling regimes beyond the perturbative limit requires to approximate the vertex renormalization (5.18). With this aim, the Breit-Wigner expansion of the analytical self-energy (5.16) together with the truncation (5.52) must be applied in (5.35). An exact normalization constraint is no longer satisfied, nevertheless it still holds approximately in the weak coupling limit. For increasing values of γ, the population of the plasmonic off-resonant state becomes no longer negligible, as observed in Section 3.2.3, but its description is hindered by the loss of normalization.

The techniques presented in Section 3.2.1 represent most important ingredients, essential for the expansion (3.46) near the on-shell condition

$$\Sigma_s(z - \omega(k)) = \Sigma_s(\varepsilon + \mathrm{i}0^+) + \frac{\mathrm{d}\Sigma_s}{\mathrm{d}z}(\varepsilon + \mathrm{i}0^+)(z - \varepsilon - \omega(k)) + O(\gamma^3) \tag{5.53}$$

holding true for $\mathrm{Im}\, z > 0$ and inserting it in the truncated $\Sigma_2(z)$ (without $X_s(k,z)$) to estimate the error

$$\begin{aligned}\Sigma_2(z) &\approx \sum_s \int \mathrm{d}k\, F^2(k) \frac{1 + s\cos kd}{z - \varepsilon - \omega(k) - \Sigma_s(z - \omega(k))} \\ &\approx \Sigma_{\mathrm{BW}}(z) + \sum_s \frac{\mathrm{d}\Sigma_s}{\mathrm{d}z}(\varepsilon + \mathrm{i}0^+) \int \mathrm{d}k\, F^2(k)\, \frac{(1 + s\cos kd)(z - \varepsilon - \omega(k))}{(z - \varepsilon - \omega(k) - \sigma_s)^2},\end{aligned} \tag{5.54}$$

where σ_s was defined in (5.47) and

$$\Sigma_{\mathrm{BW}}(z) = \sum_s \Sigma_s\Big(z - \varepsilon - \sigma_s\Big), \tag{5.55}$$

representing the lowest-order Breit-Wigner approximation deduced through the on-shell single-atomic excitation self-energy.

The same scheme is applied to (5.52), whose series expansion yields:

$$X_s(k,z) \approx \frac{\Sigma_s(z - \varepsilon - \sigma_s) - \Sigma_s(z - \omega(k))}{\varepsilon + \sigma_s - \omega(k)} + \delta X_s(k,z)\, \frac{\mathrm{d}\Sigma_s}{\mathrm{d}z}(\varepsilon + \mathrm{i}0^+), \tag{5.56}$$

providing an error estimation depending on

$$\delta X_s(k,z) = \int \mathrm{d}q\, F^2(q)\, \frac{(1 + s\cos qd)(z - \varepsilon - \omega(q))}{(z - \omega(q) - \omega(k))(z - \varepsilon - \omega(q) - \sigma_s)^2}. \tag{5.57}$$

The renormalized propagator for the double atomic excitation with $\Sigma_2(z)$ is rearranged as

$$\frac{1}{z - 2\varepsilon - \Sigma_{\mathrm{BW}}(z)} \left(1 + \frac{\sum_s \delta\Sigma_s(z)\, \frac{\mathrm{d}\Sigma_s}{\mathrm{d}z}(\varepsilon + \mathrm{i}0^+)}{z - 2\varepsilon - \Sigma_{\mathrm{BW}}(z)}\right), \tag{5.58}$$

where we introduced

$$\delta\Sigma_s(z) = \int \mathrm{d}k\, F^2(k)\, \frac{(1 + s\cos kd)(z - \varepsilon - \omega(k))}{(z - \varepsilon - \omega(k) - \sigma_s)^2}. \tag{5.59}$$

We assume that the single-atomic excitation self-energy derivative takes the form

$$\frac{\mathrm{d}\Sigma_s}{\mathrm{d}z}(\varepsilon + \mathrm{i}0^+) = \frac{\gamma}{2\pi}\, C_s(\varepsilon)\, \frac{\varepsilon}{(\varepsilon^2 - m^2)^{3/2}}, \tag{5.60}$$

with the overall factor

$$\begin{aligned}C_s(\varepsilon) = {} & 2\mathrm{i}\pi \left(1 + s\mathrm{e}^{\mathrm{i}d\sqrt{\varepsilon^2 - m^2}} - \mathrm{i}sd\sqrt{\varepsilon^2 - m^2}\mathrm{e}^{\mathrm{i}d\sqrt{\varepsilon^2 - m^2}}\right) + 2\,(1 + s\lambda(\varepsilon))\, \frac{\sqrt{\varepsilon^2 - m^2}}{\varepsilon} \\ & - 2\left(1 + s\lambda(\varepsilon) - s\, \frac{\varepsilon^2 - m^2}{\varepsilon}\lambda'(\varepsilon)\right) \mathrm{Log}\left(\frac{\varepsilon + \sqrt{\varepsilon^2 - m^2}}{m}\right).\end{aligned} \tag{5.61}$$

The asymptotic probability density (5.44) assumes the second-order approximate expression, without including the term with the squared derivative:

$$P(k_1,k_2) \approx P_{BW}(k_1,k_2)\left|1+\frac{\gamma\,\varepsilon\,C\Big(\varepsilon,\omega(k_1)+\omega(k_2)\Big)}{2\pi\left(\varepsilon^2-m^2\right)^{3/2}}\right|^2+\left|\frac{\gamma\,\varepsilon\,C_X\Big(\varepsilon,\omega(k_1)+\omega(k_2),k_1,k_2\Big)}{2\pi\left(\varepsilon^2-m^2\right)^{3/2}}\right|^2$$
$$+\left(\frac{\gamma\,\varepsilon}{2\pi\left(\varepsilon^2-m^2\right)^{3/2}}\right)^2\left(C_X^*\,C\,\widetilde{\xi_{BW}^{(2)}}+\widetilde{\xi_{BW}^{(2)}}^*\,C^*\,C_X\right)$$
$$+\left(\frac{\gamma\,\varepsilon}{2\pi\left(\varepsilon^2-m^2\right)^{3/2}}\right)\left(C_X^*\,\widetilde{\xi_{BW}^{(2)}}+\widetilde{\xi_{BW}^{(2)}}^*\,C_X\right), \tag{5.62}$$

where $P_{BW}(k_1,k_2)$ represents the probability density obtained using lowest order Breit-Wigner approximation, implemented in Figure 5.5-5.6, with the compact notation:

$$C(\varepsilon,z)=\sum_s\frac{C_s(\varepsilon)\,\delta\Sigma_s(z)}{z-2\varepsilon-\Sigma_{\mathrm{BW}}(z)}, \tag{5.63}$$

$$C_X(\varepsilon,z,k_1,k_2)=\sum_s\frac{v_s(k_1)v_s(k_2)}{z-2\varepsilon-\Sigma_{BW}(z)}\sum_{j=1,2}\frac{C_s(\varepsilon)\,\delta X_s(k_j,z)}{z-\varepsilon-\omega(k_j)-\Sigma_s(z-\omega(k_j))}. \tag{5.64}$$

The values $\gamma^*(\varepsilon)$ of the coupling for which

$$P_{BW}=\int \mathrm{d}k_1\,\mathrm{d}k_2\,P_{BW}(k_1,k_2), \tag{5.65}$$

falls below $\alpha\in(0,1]$ can be searched numerically. In the investigated coupling regime, the probability density is still concentrated on-shell $\omega(k_1)+\omega(k_2)=2\varepsilon$, so we can study just the variation according to the energy gap of $C(\varepsilon,2\varepsilon)$ and $C_X(\varepsilon,2\varepsilon,\sqrt{\varepsilon^2-m^2})$. Imposing the condition $P_{BW}=\alpha P$ leads to the relation:

$$\frac{\gamma^*(\varepsilon)\,\varepsilon}{2\pi(\varepsilon^2-m^2)^{3/2}}\approx\frac{-B-2\alpha\,\mathrm{Re}(C)+\sqrt{(B+2\alpha\,\mathrm{Re}(C))^2+4(1-\alpha)\left(A+|C_X|^2+\alpha\,|C|^2\right)}}{2\left(A+|C_X|^2+\alpha\,|C|^2\right)}, \tag{5.66}$$

where $A=C_X^*\,C\,\widetilde{\xi_{BW}^{(2)}}+\widetilde{\xi_{BW}^{(2)}}^*\,C^*\,C_X$ and $B=C_X^*\,\widetilde{\xi_{BW}^{(2)}}+\widetilde{\xi_{BW}^{(2)}}^*\,C_X$.

The extension to stronger coupling regimes requires the inclusion of the plasmonic state populations, lying below the cutoff, whose energy does not fall in the convergence circle of the Breit-Wigner expansion.

Part III

Many-body bound states

Chapter 6

Bound states in the continuum for an array of quantum emitters

Humans see what they look for

Richard Hamming,
"The Unreasonable
Effectiveness of Mathematics"

Although the physics of *single* quantum emitters in waveguides is well understood [1, 36, 84, 91, 117, 130, 138], novel phenomena arise when *two* [19, 41, 47, 59, 60, 83, 93, 103, 111, 114, 122, 144, 145] or *more* [7, 9, 17, 18, 31, 35, 48, 49, 56, 61, 65, 66, 81, 84, 90, 101, 104, 109, 110, 117, 124, 129, 142, 143] emitters are present, since the dynamics is influenced by photon-mediated quantum correlations. In this and similar contexts, sub- and super-radiant states often emerge. However, while standard (Dicke) superradiance effects occur at light wavelength much larger than typical interatomic distances [3, 21, 30, 64], considering wavelengths comparable to the interatomic distance brings to light a number of interesting quantum resonance effects [75].

The application of the resolvent formalism [25] allows us to study the existence of single-excitation bound states in the continuum in a system of n quantum emitters. In these states, the excitation is shared in a stable way between the emitters and the field, even though the energy would be sufficient to yield photon propagation. The case of $n = 2$ emitters has already been considered in Chapters 4-5, both in the one- and two-excitation sectors [41, 46]. Here, we extend the results to general n, under the assumption of large interatomic spacing compared to the inverse infrared cutoff of the waveguide mode. We will then consider how the corrections to such approximation crucially affect the physical picture of the system, by explicitly analyzing the cases of $n = 3$

and $n = 4$ emitters. The existence of nonperturbative eigenstates, that emerge when the interatomic spacing is smaller than a critical value, depending on the number n, is characterized, even if the high energy involved obstacles their experimental observation in single coupled mode framework.

6.1 Physical system and Hamiltonian

We shall consider a system of n two-level emitters, equally spaced at a distance d and characterized by the same excitation energy ε. Henceforth, we shall occasionally refer to the emitters as "atoms". The ground and excited state of each emitter will be denoted by $\left|g_j\right\rangle$ and $\left|e_j\right\rangle$, respectively, with $j = 1, \ldots, n$. The emitter array is coupled to a structured one-dimensional photon continuum (e.g., a waveguide mode), characterized by a dispersion relation $\omega(k) \geq 0$, with $k \in \mathbb{R}$, and represented by the canonical field operators $b(k)$ and $b^\dagger(k)$, satisfying $[b(k), b^\dagger(k')] = \delta(k - k')$. To obtain the multi-qubit generalization of the Hamiltonian (4.1), let us consider that, in absence of interactions, the Hamiltonian of the system reads

$$H_0 = \varepsilon \sum_{j=1}^{n} \sigma_j^+ \sigma_j^- + \int \mathrm{d}k\, \omega(k) b^\dagger(k) b(k). \tag{6.1}$$

When the total Hamiltonian $H = H_0 + H_{\mathrm{int}}$ is considered, the interacting dynamics generally does not preserve the total number of excitations

$$\mathcal{N} = \sum_{j=1}^{n} \sigma_j^+ \sigma_j^- + \int \mathrm{d}k\, b^\dagger(k) b(k), \tag{6.2}$$

unless a rotating-wave approximation is applied. In this case, the interaction Hamiltonian reads

$$H_{\mathrm{int}} = \sum_{j=1}^{n} \int \mathrm{d}k \Big[F(k) \mathrm{e}^{\mathrm{i}(j-1)kd} \sigma_j^+ b(k) + \mathrm{H.c.} \Big], \tag{6.3}$$

where $F(k)\mathrm{e}^{\mathrm{i}(j-1)kd}$ is the form factor describing the strength of the coupling of the jth emitter standing at $x = (j-1)d$ with a photon of momentum k, and H can be diagonalized in orthogonal sectors characterized by a fixed eigenvalue of $\mathcal{N}$. The system is sketched in Figure 6.1.

The zero-excitation sector, $\mathcal{N} = 0$, is spanned by the ground state of H_0, $\left|G^{(n)}\right\rangle \otimes |\mathrm{vac}\rangle$, with

$$\left|G^{(n)}\right\rangle = \bigotimes_{j=1}^{n} \left|g_j\right\rangle \tag{6.4}$$

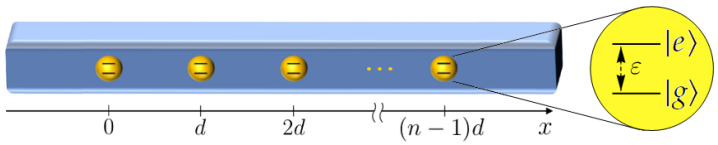

Figure 6.1: The system: n two-level emitters, placed at a relative distance d and characterized by excitation energy ε.

and $|\text{vac}\rangle$ being the vacuum photon state, $b(k)\,|\text{vac}\rangle = 0$ for all k's.

We will focus on the search of bound states in the one-excitation sector, $\mathcal{N} = 1$, whose vectors have the form

$$\left|\psi\right\rangle = \sum_{j=1}^{n} a_j \left|E_j^{(n)}\right\rangle \otimes |\text{vac}\rangle + \left|G^{(n)}\right\rangle \otimes \int \mathrm{d}k\, \xi(k) b^\dagger(k)\,|\text{vac}\rangle\,, \tag{6.5}$$

with

$$\left|E_j^{(n)}\right\rangle = \left|g_1\right\rangle \otimes \cdots \otimes \left|g_{j-1}\right\rangle \otimes \left|e_j\right\rangle \otimes \left|g_{j+1}\right\rangle \otimes \cdots \otimes \left|g_n\right\rangle. \tag{6.6}$$

In particular, we will consider a photon continuum with the massive dispersion relation introduced in Section 1.4

$$\omega(k) = \sqrt{k^2 + m^2}, \tag{6.7}$$

and the form factor (3.20) determined by the $\boldsymbol{p}\cdot\boldsymbol{A}$ interaction of QED [25], with γ a coupling constant with the dimensions of squared energy.

The Hamiltonian defined by the dispersion relation (6.7) and by the form factor (3.20), depends on the four parameters ε, m, d and γ, all with physical dimension.

6.2 Bound states in the continuum

We are interested in bound states in the continuum of the one-excitation sector, with $E > m$. By considering the Hamiltonian defined by (6.1) and (6.3), and the expansion of the state vectors (6.5), the eigenvalue equation in the one-excitation sector reads

$$\begin{cases} (\varepsilon - E) a_j = -\displaystyle\int \mathrm{d}k\, \mathrm{e}^{-\mathrm{i}(j-1)kd}\, F(k)^*\, \xi(k), \\[2ex] (\omega(k) - E)\, \xi(k) = -\displaystyle\sum_{l=1}^{n} a_\ell\, \mathrm{e}^{\mathrm{i}(\ell-1)kd}\, F(k). \end{cases} \tag{6.8}$$

From the second equation

$$\xi(k) = -\sum_{\ell=1}^{n} a_\ell \, \mathrm{e}^{\mathrm{i}(\ell-1)kd} \frac{F(k)}{\omega(k) - E}, \tag{6.9}$$

one infers that, since $\xi(k)$ must be normalizable for a bound state, the vanishing of the denominator, occurring when $\omega(k) = E$, i.e. at $k = \pm\bar{k}$, with

$$\bar{k}(E) = \sqrt{E^2 - m^2}, \tag{6.10}$$

for $E > m$, must be compensated by the vanishing of the numerator at the same points. Therefore, the atomic excitation amplitudes and the energy eigenvalue of bound states in the continuum necessarily satisfy the constraint

$$\sum_{\ell=1}^{n} a_\ell \mathrm{e}^{\pm\mathrm{i}(\ell-1)\bar{k}d} = 0. \tag{6.11}$$

By using the expression (6.9), one obtains the relation

$$(\varepsilon - E)a_j = \sum_{l=1}^{n} \int \mathrm{d}k \frac{a_\ell \, \mathrm{e}^{\mathrm{i}(\ell-j)kd} \, |F(k)|^2}{\omega(k) - E}, \tag{6.12}$$

involving only the atomic excitation amplitudes and the eigenvalue E. Equation (6.12) can be expressed in the compact form

$$\mathrm{G}^{-1}(E)\, \boldsymbol{a} = \boldsymbol{0}, \tag{6.13}$$

with $\boldsymbol{a} = (a_1, a_2, \ldots, a_n)^T$ and G^{-1} the inverse propagator matrix in the single-atomic-excitation subspace, generally defined for a complex energy z by

$$\mathrm{G}^{-1}(z) = (\varepsilon - z)\mathbb{1} - \Sigma(z), \tag{6.14}$$

where the self-energy matrix Σ has elements

$$\Sigma_{j\ell}(z) = \int \mathrm{d}k \frac{|F(k)|^2}{\omega(k) - z} \mathrm{e}^{-\mathrm{i}(j-\ell)kd}. \tag{6.15}$$

The self-energy and the inverse propagator are well defined for non-real arguments and for $z < m$, with a discontinuity across the continuum spectrum $z \in [m, \infty)$, where generally

$$\Sigma(E + \mathrm{i}0^+) - \Sigma(E - \mathrm{i}0^+) \neq 0, \qquad E \in [m, \infty), \tag{6.16}$$

with $\Sigma(E \pm \mathrm{i}0^+) = \lim_{\eta \downarrow 0} \Sigma(E \pm \mathrm{i}\eta)$.

Therefore, the equality of the upper and lower boundary value is a necessary condition for (6.13) to be well defined and, *a fortiori*, for E to be an eigenvalue. Finally, notice that (6.13) always admits a trivial solution, which correspond, due to (6.9), to the null vector. If $\mathsf{G}^{-1}(E)$ is well defined, the equation

$$\det \mathsf{G}^{-1}(E) = 0 \tag{6.17}$$

provides a necessary and sufficient condition for E to be an eigenvalue with a nontrivial solution $\boldsymbol{a} \neq \mathbf{0}$, providing the atomic excitation amplitudes of the corresponding eigenstate.

The integrals that define the elements of the self-energy in (6.15) can be evaluated for $z = E \pm \mathrm{i}0^+$ with $E > m$ by analytic continuation in the complex k-plane, yielding

$$\Sigma_{jl}(E \pm \mathrm{i}0^+) = \frac{\pm \mathrm{i}\gamma'}{\bar{k}(E)} \left(\mathrm{e}^{\pm \mathrm{i}|j-l|\bar{k}(E)d} \pm \mathrm{i}\, b_{|j-l|}(E) \right), \tag{6.18}$$

where the first term derives from integration around one of the poles at $k = \pm\bar{k}$ and the second one

$$b_j(E) = \frac{\bar{k}(E)}{\pi} \int_m^\infty \mathrm{d}\kappa \frac{\mathrm{e}^{-j\kappa d}}{\sqrt{\kappa^2 - m^2}} \frac{E}{E^2 + \kappa^2 - m^2} \tag{6.19}$$

from integration around one of the branch cuts, $(\mathrm{i}m, \mathrm{i}\infty)$ or $(-\mathrm{i}\infty, \mathrm{i}m)$, of the analytic continuation in the complex k-plane. The original and modified integration contours are shown in Figure 3.2 in Chapter 3. Notice that the functions b_j are real for $E > m$.

In the case $j = 0$, the integral can be evaluated analytically and yields

$$b_0(E) = -\frac{1}{\pi} \mathrm{Log}\left(\frac{E - \sqrt{E^2 - m^2}}{m} \right). \tag{6.20}$$

In the general case, the cut contribution must be evaluated numerically. However, a relevant property follows from the definition (6.19),

$$\frac{|b_j(E)|}{|b_0(E)|} \leq \exp(-jmd) \quad \text{for } E > m, \tag{6.21}$$

implying that, for $md \gg 1$, the terms $b_{j>0}$ are exponentially suppressed and can be neglected as a first approximation.

In the following, we will show that, interestingly, the inclusion of such terms in the analysis on one hand entails selection rules that remove the degeneracy

of bound states in the continuum, on the other hand displaces by orders $O(\mathrm{e}^{-md})$ the energies, resonance distances and amplitudes that satisfy the constraint in (6.11).

The photon eigenfunction (6.9) in the position representation reads

$$\xi(x) = -\int \frac{\mathrm{d}k}{\sqrt{2\pi}} \frac{F(k)}{\omega(k) - E} \sum_{\ell=1}^{n} a_\ell \mathrm{e}^{-\mathrm{i}k(x-(\ell-1)d)} = \sum_{\ell=1}^{n} a_\ell \, \xi_1\Big(x - (\ell-1)d\Big) \tag{6.22}$$

with

$$\xi_1(x) = -\fint \frac{\mathrm{d}k}{\sqrt{2\pi}} \frac{F(k)}{\omega(k) - E} \mathrm{e}^{-\mathrm{i}kx} = \frac{\sqrt{\gamma E}}{\bar{k}} \Big[\sin(\bar{k}|x|) - \eta(x)\Big], \tag{6.23}$$

according to the principal value introduced in (3.36) and where

$$\eta(x) = \frac{1}{\pi} \frac{\bar{k}}{\sqrt{2E}} \int_m^\infty \mathrm{d}y \, \frac{\mathrm{e}^{-y|x|}}{\sqrt[4]{y^2 - m^2}} \frac{\sqrt{y^2 - m^2} - E}{E^2 + y^2 - m^2} \tag{6.24}$$

is the $O(\mathrm{e}^{-m|x|})$ cut contribution. Notice that the principal value prescription $\fint$ is required in the definition of ξ_1 for $E > m$, while the integral in $\xi(x)$ is regularized by the constraint (6.11).

6.3 Eigenvalues and eigenstates

6.3.1 Block-diagonal representation of the propagator

Given the form (6.13) of the eigenvalue equation for the atomic amplitude vector $\boldsymbol{a}$ and the dependence of the propagator on the inter-atomic distance d and the transition energy ε, it is convenient to introduce the matrix $A_n(\theta, \chi, \boldsymbol{b})$, depending on $n + 1$ real parameters, $\theta, \chi \in \mathbb{R}$, $\boldsymbol{b} \in \mathbb{R}^{n-1}$, and defined as

$$[A_n(\theta, \chi, \boldsymbol{b})]_{j\ell} = \begin{cases} 1 + \mathrm{i}\chi, & \text{for } j = \ell \\ \mathrm{e}^{\mathrm{i}|j-\ell|\theta} + \mathrm{i}b_{|j-\ell|}, & \text{for } j \neq \ell \end{cases} \tag{6.25}$$

with $j, \ell = 1, \ldots, n$, that is

$$A_n(\theta, \chi, \boldsymbol{b}) = \begin{pmatrix} 1 + \mathrm{i}\chi & \mathrm{e}^{\mathrm{i}\theta} + \mathrm{i}b_1 & \mathrm{e}^{\mathrm{i}2\theta} + \mathrm{i}b_2 & \ldots \\ \mathrm{e}^{\mathrm{i}\theta} + \mathrm{i}b_1 & 1 + \mathrm{i}\chi & \mathrm{e}^{\mathrm{i}\theta} + \mathrm{i}b_1 & \\ \mathrm{e}^{\mathrm{i}2\theta} + \mathrm{i}b_2 & \mathrm{e}^{\mathrm{i}\theta} + \mathrm{i}b_1 & 1 + \mathrm{i}\chi & \\ \mathrm{e}^{\mathrm{i}3\theta} + \mathrm{i}b_3 & \mathrm{e}^{\mathrm{i}2\theta} + \mathrm{i}b_2 & \mathrm{e}^{\mathrm{i}\theta} + \mathrm{i}b_1 & \\ \vdots & & & \ddots \end{pmatrix}. \tag{6.26}$$

The inverse propagator reads

$$\mathrm{G}^{-1}(E) = -\frac{\mathrm{i}\gamma}{\bar{k}(E)} A_n\Big(\theta(E), \chi(E), \boldsymbol{b}(E)\Big), \tag{6.27}$$

with

$$\theta(E) = \bar{k}(E)d, \tag{6.28}$$

$$\chi(E) = \frac{\varepsilon - E}{\gamma}\bar{k}(E) + b_0(E), \tag{6.29}$$

and $\bar{k}(E)$, $b_{j>0}(E)$ and $b_0(E)$ as defined in (6.10), (6.19) and (6.20), respectively.

The matrix A_n can be recast in block-diagonal form by exploiting the invariance of the Hamiltonian with respect to spatial reflections at the midpoint $x = (n-1)d/2$, transforming the local-excitation basis $\left|E_j^{(n)}\right\rangle$ in (6.6) by the unitary transformation

$$\mathcal{U}_n \left|E_j^{(n)}\right\rangle = \begin{cases} \frac{\left|E_j^{(n)}\right\rangle - \left|E_{n-j}^{(n)}\right\rangle}{\sqrt{2}} & \text{for } j \leq \frac{n}{2} \\ \left|E_j^{(n)}\right\rangle & \text{for } j = \frac{n+1}{2} \\ \frac{\left|E_j^{(n)}\right\rangle + \left|E_{n-j}^{(n)}\right\rangle}{\sqrt{2}} & \text{for } j \geq \frac{n}{2} + 1 \end{cases}. \tag{6.30}$$

The action of such transformation, that is also real and symmetric, on the components in the local basis can be expressed for even $n = 2h$ and odd $n = 2h+1$ in terms of the $h \times h$ identity matrix $\mathbb{1}_h$ and reflection matrix $\mathbb{J}_h$ (i.e. the matrix with ones in the anti-diagonal as the only nonvanishing elements) as

$$\mathcal{U}_n = \frac{1}{\sqrt{2}} \begin{pmatrix} \mathbb{1}_h & -\mathbb{J}_h \\ \mathbb{J}_h & \mathbb{1}_h \end{pmatrix} \tag{6.31}$$

and

$$\mathcal{U}_n = \frac{1}{\sqrt{2}} \begin{pmatrix} \mathbb{1}_h & 0 & -\mathbb{J}_h \\ 0 & \sqrt{2} & 0 \\ \mathbb{J}_h & 0 & \mathbb{1}_h \end{pmatrix}, \tag{6.32}$$

respectively. The transformation $\mathcal{U}_n$ generalizes the change from the local basis to the Bell basis for $n = 2$ emitters [41].

In the new representation, the self-energy and the propagator turn out to be block diagonal:

$$\mathcal{U}_n A_n \mathcal{U}_n^\dagger = A_n^- \oplus A_n^+, \tag{6.33}$$

where $A_n^-(\theta, \chi, \boldsymbol{b})$ is the $\lfloor n/2 \rfloor \times \lfloor n/2 \rfloor$ matrix acting on the antisymmetric amplitude vectors of the emitters, with

$$a_j = -a_{n+1-j}, \qquad j = 1, \dots, n, \tag{6.34}$$

and $A_n^+(\theta, \chi, \boldsymbol{b})$ is the $\lceil n/2 \rceil \times \lceil n/2 \rceil$ matrix acting on the symmetric amplitude vectors, with

$$a_j = a_{n+1-j}, \qquad j = 1, \dots, n. \tag{6.35}$$

Therefore, the eigenvalue equation (6.13) can be reduced to the quest for nontrivial solutions of the two decoupled linear systems

$$A_n^{\pm}\Big(\theta(E), \chi(E), \boldsymbol{b}(E)\Big)\, \boldsymbol{a}^{\pm} = 0. \tag{6.36}$$

Eigenvectors with no reflection symmetry are allowed only if the same energy E is an eigenvalue for both systems (6.36) for the same set of parameters ε, m, d and γ. Examples of eigenstates with definite symmetry, whose relevance will be discussed in the following, are shown in Fig. 6.2.

Throughout this section, we will first analyze bound states by neglecting $O(\mathrm{e}^{-md})$ terms in the self-energy, and then discuss the consequences of including all the $b_{j>0}$ terms in the cases $n = 2, 3, 4$.

6.3.2 General properties of the eigenvalue equation

The method used to characterize resonant bound states for a system of n emitters in the case of general n is based on the decomposition (6.36) in decoupled parity sectors. In Section 6.3.3, we will prove that, neglecting the $b_{j>0}$ terms, the eigenvalue equation reduces to $\chi(E) = 0$, yielding $(n-1)$-times degenerate eigenvalues $E_\nu(d)$, with $\nu \in \mathbb{N}$, corresponding to eigenvectors whose atomic excitation amplitudes are constrained by (6.53) or (6.54) according to the sign $(-1)^\nu$. Here, we prove that the resonant energies $E_\nu(d)$ persist as exact eigenvalues even after the introduction of cut integration terms, for some value of the excitation energy ε.

The reduction to a block-diagonal form provided by the transformations (6.31) and (6.32) enables one to recast the eigenvalue equation into the decoupled problems

$$\det[A_n^{\pm}(\theta(E), \chi(E), \boldsymbol{b}(E))] = 0. \tag{6.37}$$

For definiteness, let us first consider the case of even $n = 2h$. Let us introduce for convenience the quantities

$$\beta_j^\nu = \begin{cases} \chi(E_\nu(d)) & \text{if } j = 0 \\ b_j(E_\nu(d)) & \text{if } j > 0 \end{cases} \tag{6.38}$$

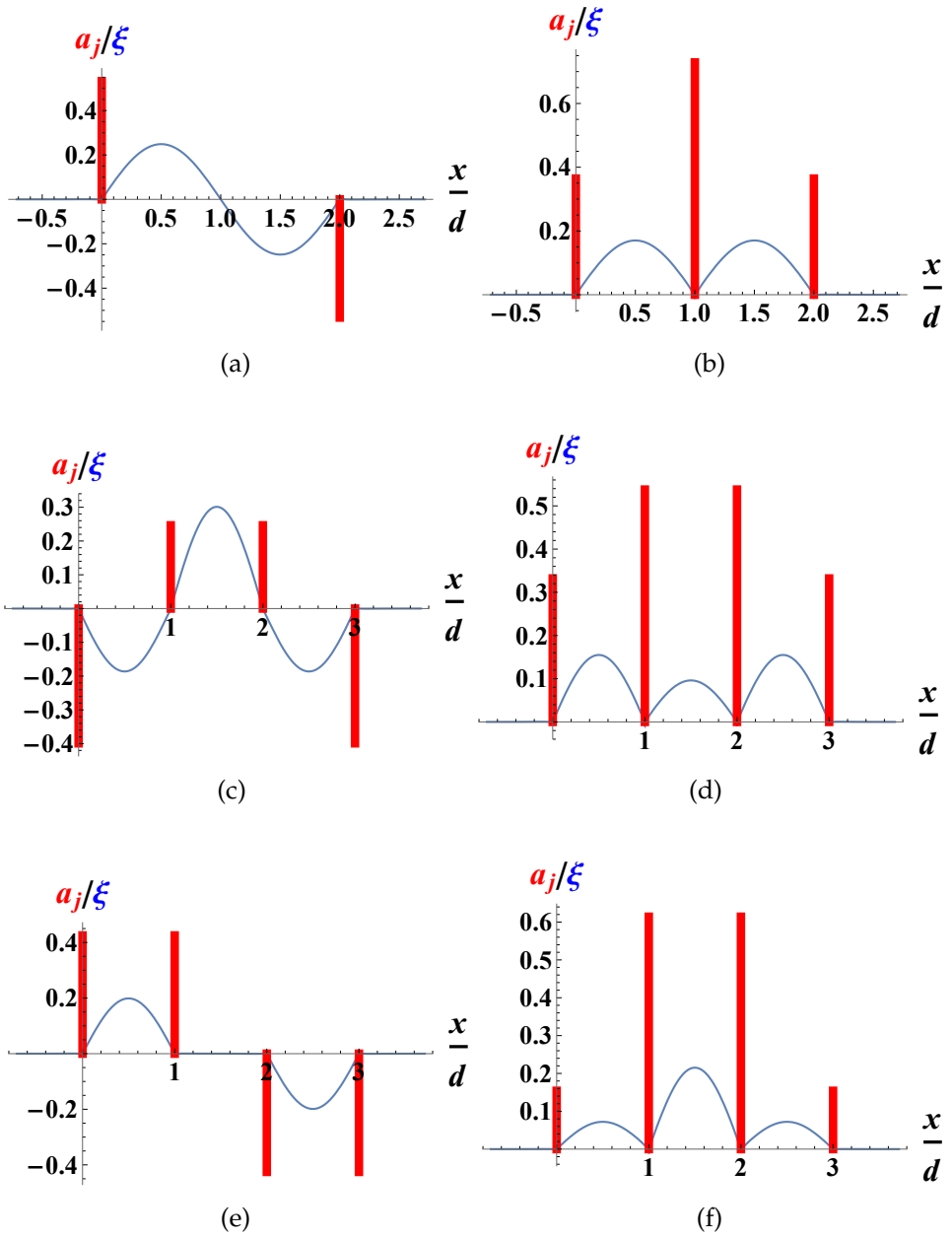

Figure 6.2: Atomic excitation amplitudes a_j, with $1 \leq j \leq n$, represented as (red) bars localized at the emitter positions, and field wavefunctions $\xi(x)$, represented as solid (blue) lines, for different bound states in the continuum of a system of $n = 3$ (panels (a)–(b)) and $n = 4$ (panels (c)–(f)) emitters with $md = 7$ and $\gamma = 10^{-2}m^2$. In panel (a), $a_1 = -a_3$ and $a_2 = 0$; in panel (b), $a_1 = a_3$ and $a_2/a_1 \simeq 2$; in panel (c), $a_1 = a_4$, $a_2 = a_3$ and $a_1/a_2 \simeq -(1 + \sqrt{5})/2$; in panel (d), $a_1 = a_4$, $a_2 = a_3$ and $a_1/a_2 \simeq (\sqrt{5} - 1)/2$; in panel (e), $a_1 = a_2$, $a_3 = a_4$ and $a_2 = -a_3$; in panel (f), $a_1 = a_4$, $a_2 = a_3$ and $a_1/a_2 \simeq 0.25$.

and the real and symmetric matrices

$$\mathcal{A}_q^\nu = \begin{pmatrix} \beta_0^\nu & \beta_1^\nu & \beta_2^\nu & \cdots & \beta_{q-1}^\nu \\ \beta_1^\nu & \beta_0^\nu & \beta_1^\nu & \cdots & \beta_{q-2}^\nu \\ \beta_2^\nu & \beta_1^\nu & \beta_0^\nu & \cdots & \beta_{q-3}^\nu \\ \vdots & \vdots & \vdots & \ddots & \vdots \\ \beta_{q-1}^\nu & \beta_{q-2}^\nu & \beta_{q-3}^\nu & \cdots & \beta_0^\nu \end{pmatrix}, \tag{6.39}$$

$$\mathcal{B}_{q,p}^\nu = \begin{pmatrix} \beta_q^\nu & \beta_{q-1}^\nu & \beta_{q-2}^\nu & \cdots & \beta_{q-p}^\nu \\ \beta_{q-1}^\nu & \beta_{q-2}^\nu & \beta_{q-3}^\nu & \cdots & \beta_{q-p-1}^\nu \\ \beta_{q-2}^\nu & \beta_{q-3}^\nu & \beta_{q-4}^\nu & \cdots & \beta_{q-p-2}^\nu \\ \vdots & \vdots & \vdots & \ddots & \vdots \\ \beta_{q-p}^\nu & \beta_{q-p-1}^\nu & \beta_{q-p-2}^\nu & \cdots & \beta_{q-2p}^\nu \end{pmatrix}, \tag{6.40}$$

and $C_q^\pm$ as the $q \times q$ matrix characterized by the elements

$$\left[C_q^\pm\right]_{j\ell} = (\pm 1)^{j+\ell}. \tag{6.41}$$

If ν is even, then

$$-\mathrm{i}A_{2h}^-(\nu\pi, \chi(E_\nu(d)), \boldsymbol{b}(E_\nu(d))) = \mathcal{A}_h^\nu - \mathcal{B}_{2h-1,h-1}^\nu, \tag{6.42}$$

and

$$-\mathrm{i}A_{2h}^+(\nu\pi, \chi(E_\nu(d)), \boldsymbol{b}(E_\nu(d))) = \mathcal{A}_h^\nu + \mathcal{B}_{2h-1,h-1}^\nu - 2\mathrm{i}C_h^+, \tag{6.43}$$

while, for odd ν,

$$-\mathrm{i}A_{2h}^+(\nu\pi, \chi(E_\nu(d)), \boldsymbol{b}(E_\nu(d))) = \mathcal{A}_h^\nu + \mathcal{B}_{2h-1,h-1}^\nu, \tag{6.44}$$

and

$$-\mathrm{i}A_{2h}^-(\nu\pi, \chi(E_\nu(d)), \boldsymbol{b}(E_\nu(d))) = \mathcal{A}_h^\nu + \mathcal{B}_{2h-1,h-1}^\nu - 2\mathrm{i}C_h^-. \tag{6.45}$$

Fixing $E = E_\nu(d)$ and considering the expression of $\chi(E)$, (6.37) can be generally recast in the form

$$\det(\mathcal{M} - \varepsilon \mathbb{1}) = 0, \tag{6.46}$$

implying that $E_\nu(d)$ is an eigenvalue of the system if and only if ε is the *real* eigenvalue of some matrix $\mathcal{M}$. From the expressions (6.42)–(6.44), one can notice that, in the antisymmetric sector for even ν and in the symmetric sector for odd ν, the matrix $\mathcal{M}$ is Hermitian, entailing the existence of n values of ε, real and *generally distinct*, corresponding to physical systems in which a bound state with energy $E_\nu(d)$ is present. Those values of ε collapse to a single degenerate value in the $\mathrm{e}^{-d} \to 0$ limit. In the cases (6.43)–(6.45), insteads, $\mathcal{M}$ is

not Hermitian, its eigenvalues are generally no longer real, and the bound state energies displace from the resonant values.

The case of odd $n = 2h + 1$ is slighlty different. There, for all resonance orders ν, in the antisymmetric sector

$$-\mathrm{i}A^{-}_{2h+1}(\nu\pi, \chi(E_\nu(d)), \boldsymbol{b}(E_\nu(d))) = \mathcal{A}^\nu_h - \mathcal{B}^\nu_{2h,h-1}, \tag{6.47}$$

leading to a condition (6.46) with a Hermitian $\mathcal{M}$, which implies that all the $E_\nu(d)$ are eigenvalues corresponding to antisymmetric bound states for generally different physical systems. On the other hand, the matrix $\mathcal{M}$ corresponding to all resonances in the symmetric sector is never Hermitian, since it features an imaginary and symmetric contribution proportional to $C^{\pm}_{h+1}$.

6.3.3 Large spacing approximation

When md is large, the terms b_j, with $j > 0$, in the self-energy are exponentially suppressed and will be neglected as a first approximation, namely

$$\boldsymbol{b} = \boldsymbol{0}. \tag{6.48}$$

Both matrices $A^{\pm}_n(\theta, \chi, \boldsymbol{0})$ are singular if and only if

$$\theta = \nu\pi \quad (\nu \in \mathbb{N}), \qquad \text{and} \quad \chi = 0. \tag{6.49}$$

The former condition,

$$\bar{k} = \frac{\nu\pi}{d}, \tag{6.50}$$

selects the possibile eigenvalues in terms of the spacing d

$$E = E_\nu(d) = \sqrt{\frac{\nu^2\pi^2}{d^2} + m^2}, \tag{6.51}$$

which will be called *resonant energies* in the following. Notice that (6.50) implies that the emitters should be at a distance d which is an exact multiple of half wavelengths of the trapped photon $\bar{\lambda} = 2\pi/\bar{k}$, that is $d = \nu\bar{\lambda}/2$.

The second condition in (6.49),

$$\varepsilon = E_\nu(d) - \frac{\gamma d}{\nu\pi} b_0(E_\nu(d)) = E_\nu(d) + \frac{\gamma d}{\nu\pi} \operatorname{Log}\left(\frac{E_\nu(d)}{m} - \frac{\nu\pi}{md}\right), \tag{6.52}$$

provides a constraint involving the excitation energy, the spacing and the order ν of the resonance. A discrete family of curves in the (ε, d) plane is defined

by (6.52), identifying the values ε for which a bound state in the continuum exists.

The emitter configurations associated with the eigenvalues (6.51) satisfy the constraint (6.11), which yields two different conditions according to the parity of the resonance. For even ν, for all the eigenvectors, the atomic excitation amplitudes must sum to zero

$$\sum_{j=1}^{n} a_j = 0; \tag{6.53}$$

while for odd ν one obtains

$$\sum_{j=1}^{n} (-1)^j a_j = 0. \tag{6.54}$$

Hence, each eigenvalue $E_\nu(d)$ is characterized by an $(n-1)$-fold degeneracy. It is worth observing that, since both matrices $A_n^{\pm}$ are characterized by the same singularity conditions at this level of approximation, the same eigenvalue can occur in both the symmetric and antisymmetric sector. In such cases, the bound states are not characterized by a well-defined symmetry.

The photon wavefunction associated with the eigenstates can be derived according to (6.22), considering $E = E_\nu(d)$. Neglecting the η contribution in (6.23), the single-emitter contribution to the field is given by the oscillating function

$$\xi_1(x) \propto \sin\left(\frac{\nu\pi|x|}{d}\right), \tag{6.55}$$

whose half-wavelength coincides with d/ν. The photon wavefunction in the same approximation thus reads

$$\xi(x) \propto \sum_{\ell=1}^{n} a_\ell \,\mathrm{sign}\,(x-(\ell-1)d)\, \sin\left(\frac{\nu\pi x}{d}\right), \tag{6.56}$$

for even ν, and

$$\xi(x) \propto \sum_{\ell=1}^{n} a_\ell\, (-1)^{\ell-1} \mathrm{sign}\,(x-(\ell-1)d)\, \sin\left(\frac{\nu\pi x}{d}\right); \tag{6.57}$$

for odd ν. The field has nodes at the emitter positions $x = jd$ and in both cases, due to conditions (6.53) and (6.54), respectively, it vanishes identically for $x < 0$ and $x > nd$, and is therefore confined inside the emitter array.

Finally, it is worth observing that all possible n-emitter eigenstates can be obtained as linear combinations of two-emitter eigenstates at different positions. However, we will show in the following that $O(\mathrm{e}^{-md})$ effects, however small, remove this degeneracy, and imply selection rules related to the reflection symmetry of the atomic eigenstates.

6.3.4 Full form of the self-energy

The degeneracy obtained in the previous subsection by approximating the self-energy by setting $\boldsymbol{b} = \mathbf{0}$ is lifted by considering the terms b_j, with $j > 0$. We now discuss in detail this phenomenon. The effect of these terms can be summarized in the following points:

i) At given d and $E_\nu(d)$, only one of the two matrices $A_n^\pm(\nu\pi, \chi(E_\nu(d)), \boldsymbol{b}(E_\nu(d)))$, namely the one for which

$$A_n^\pm(\nu\pi, 0, \mathbf{0}) = 0, \tag{6.58}$$

continues to be singular for some values of ε and γ. The matrix satisfying the property (6.58) is the antisymmetric one for odd n and the one with symmetry $(-1)^{\nu+1}$ for even n. Details on this general result are given in Section 6.3.2.

ii) The values of $\chi(E)$ (and hence of ε, through Eq. (6.52)) corresponding to the eigenstates with energy $E_\nu(d)$ will depend on the eigenstate. For any fixed ε, only one stable state with energy $E_\nu(d)$ can generally be found, with the orthogonal states becoming unstable (although possibly long-lived).

iii) If $A_n^\pm(\nu\pi, 0, \mathbf{0})$ does not satisfy condition (6.58), then $A_n^\pm(\nu\pi, \chi(E_\nu(d)), \boldsymbol{b}(E_\nu(d)))$ is in general no longer singular. However, the corresponding stable states do not entirely disappear, but undergo a slight change in their amplitude and energy, which is now displaced with respect to $E_\nu(d)$. Such states must be studied numerically.

Here, we will explicitly examine these effects in the three cases of $n = 2, 3, 4$ emitters. Moreover we shall focus on eigenstates connected by continuity to the resonant bound states discussed in the previous subsection, and postpone to Section 6.4 the study of strong-coupling eigenstates, distant from the resonant values, and characterized by extremely high energies, $E \gtrsim 10^2 m$.

$n = 2$ emitters

With respect to the inclusion of the cut terms $\boldsymbol{b}$ in the self-energy, $n = 2$ represents an oversimplified case, since the linear systems $A_n^\pm(\theta, \chi, \boldsymbol{b})$ reduce to single equations, and the singularity conditions read

$$A_2^\pm(\theta, \chi, b_1) = 1 \pm \mathrm{e}^{\mathrm{i}\theta} + \mathrm{i}(\chi \pm b_1) = 0, \tag{6.59}$$

corresponding to eigenstates in which the emitter excitation amplitudes exactly satisfy

$$a_2 = \pm a_1. \tag{6.60}$$

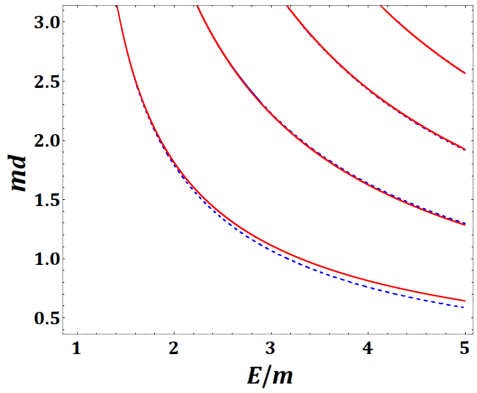

Figure 6.3: Spectral lines in the (E, d) plane for a system of $n = 3$ equally spaced emitters. Solid (red) lines correspond to antisymmetric configurations, while dashed (blue) lines to symmetric ones. For larger values of the distance, the curves follow with excellent approximation the resonant values in (6.51). For $md \lesssim 2$, the difference between the eigenvalues of the lowest-energy symmetric and antisymmetric state becomes appreciable.

The peculiarity of $n = 2$ lies in the fact that the condition $\theta = \nu\pi$, with odd ν in the symmetric sector and even ν in the antisymmetric sector, still holds for both symmetries, yielding a resonant eigenenergy (6.51). The second condition in (6.49) is generalized to

$$\chi = (-1)^{\nu} b_1, \tag{6.61}$$

so that the emitter excitation energy is constrained by

$$\varepsilon = E_\nu(d) - \frac{\gamma d}{\nu\pi}\Big[b_0(E_\nu(d)) - (-1)^{\nu} b_1(E_\nu(d))\Big]. \tag{6.62}$$

In this case, the inclusion of $b_1 = O(\mathrm{e}^{-md})$ in the self-energy does not shift energies away from the resonant values and does not remove any degeneracy, since the symmetric and antisymmetric eigenstates already occurred for different ν's [41].

$n = 3$ emitters

For a system of three emitters, the eigenvalue equation breaks down into a single equation for the antisymmetric sector and a system of two equations for the symmetric sector. In the former case, the eigenvalues are determined by the solution of

$$A_3^-(\theta, \chi, \boldsymbol{b}) = 1 - \mathrm{e}^{2\mathrm{i}\theta} + \mathrm{i}(\chi - b_2) = 0. \tag{6.63}$$

As in the $n = 2$ case, the real part of the above equation is sufficient to ensure that the resonance condition $\theta = \nu\pi$, here with any $\nu \in \mathbb{N}$, is still valid, and the corresponding energy must be resonant (6.51). The constraint on ε for the existence of an antisymmetric eigenstate, with the atomic excitation proportional to $\left(\left|E_3^{(1)}\right\rangle - \left|E_3^{(3)}\right\rangle\right)/\sqrt{2}$, is now determined by the equation

$$\chi = b_2, \tag{6.64}$$

which yields

$$\varepsilon = E_\nu(d) - \frac{\gamma d}{\nu\pi}\Big[b_0(E_\nu(d)) - b_2(E_\nu(d))\Big]. \tag{6.65}$$

Instead, in the symmetric sector, where the eigenenergies are determined by the equation

$$0 = \det A_3^+(\theta, \chi, \boldsymbol{b}) = \det\begin{pmatrix} 1 + i\chi & \sqrt{2}(e^{i\theta} + ib_1) \\ \sqrt{2}(e^{i\theta} + ib_1) & 1 + e^{2i\theta} + i(\chi + b_2) \end{pmatrix}, \tag{6.66}$$

one can easily check that there are no solutions for $\theta = \nu\pi$ with integer ν, as their existence would imply at least one of the conditions $b_2(E) = \pm 3\sqrt{b_1(E)^2 \pm 2b_1(E)}$. Actually, the energy of the symmetric bound state in the continuum

$$E = E_\nu(d) + (-1)^\nu \frac{\bar{k}(E_\nu(d))}{d\, E_\nu(d)} b_1(E_\nu(d)) + O(\mathrm{e}^{-2md}) \tag{6.67}$$

is shifted by an amount of $O(\mathrm{e}^{-md})$ with respect to the resonant value $E_\nu(d)$, corresponding to a shift $\delta\theta \approx (-1)^\nu b_1(E_\nu(d))$ in the phase. The values of (ε, d) at which the symmetric bound states occur can now be derived from the condition

$$\chi(E) = 2(-1)^\nu b_1(E_\nu(d)) + O(\mathrm{e}^{-2md}), \tag{6.68}$$

with E given by (6.67). For the lowest-order resonances $\nu = 1$, one can observe that the energy of the symmetric state is shifted downwards with respect to the value $E_1(d)$, that is exact for the antisymmetric state. This effect is evident in Figure 6.3, in which the behavior of the eigenvalues corresponding to bound states in the continuum for both parity sector is represented in terms of d. The trajectories of the bound states are displayed in Figure 6.4.

While the excitation amplitudes of antisymmetric bound states are constrained to the values

$$a_2 = 0, \quad a_3 = -a_1, \tag{6.69}$$

the amplitudes of the symmetric states depend on the parameters and on the magnitude of the cut contributions. If the terms $b_{j>0}$ are neglected, the symmetric bound state is characterized by

$$a_3 = a_1, \quad a_2 \approx 2(-1)^{\nu+1} a_1, \tag{6.70}$$

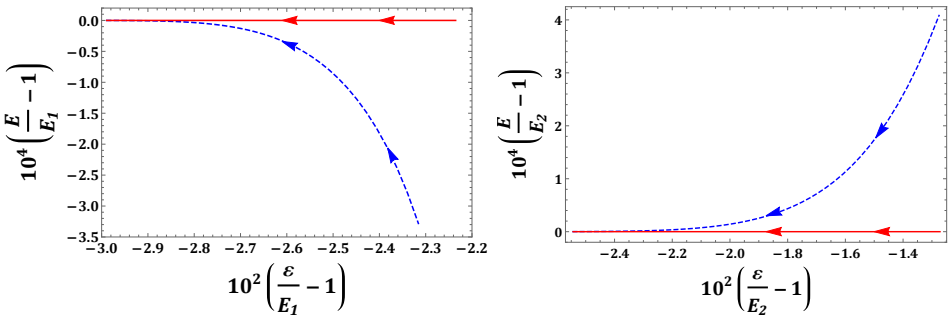

(a) (b)

Figure 6.4: Behavior of the bound state energies E in the vicinity of the resonant values $E_1(d)$ (upper panel) and $E_2(d)$ (lower panel) for $n = 3$, as a function of ε. In both panels, the trajectories for symmetric (dashed blue lines) and antisymmetric states (solid red lines) are shown with the arrows pointing towards increasing emitter separation d. Notice that the antisymmetric bound state corresponds in both cases to the resonant energy, while the energy of the symmetric state approaches the resonant value as d increases (as ε decreases).

with the second value sensitive to $O(\mathrm{e}^{-md})$ corrections when the b_j's are included. These states are represented in the top panels (a)-(b) of Figure 6.2, for some values of the parameters d and γ. In the following Section, we will find that bound states with different amplitudes, not connected by continuity to the ones described above, can emerge in the case $\varepsilon \gg m$, a regime in which, however, the validity of the one-dimensional approximation on which our model is based becomes questionable.

A relevant parameter that characterizes the features of bound states in the continuum is the total probability of atomic excitations

$$p = \boldsymbol{a}^\dagger \boldsymbol{a} = 1 - \int \mathrm{d}k |\xi(k)|^2, \tag{6.71}$$

that "measures" how the single excitation is shared between the emitters and the field. In this case, the probabilities $p_\nu^{(3)\pm}$ for the symmetric (+) and antisymmetric (−) eigenstates read

$$p_\nu^{(3)+} \approx \left(1 + \frac{2\gamma d E_\nu}{3(E_\nu^2 - m^2)} + \frac{\gamma}{\pi m (E_\nu + m)}\right)^{-1}, \tag{6.72}$$

$$p_\nu^{(3)-} \approx \left(1 + \frac{2\gamma d E_\nu}{E_\nu^2 - m^2} + \frac{\gamma}{\pi m (E_\nu + m)}\right)^{-1}, \tag{6.73}$$

up to order $O(\mathrm{e}^{-md})$.

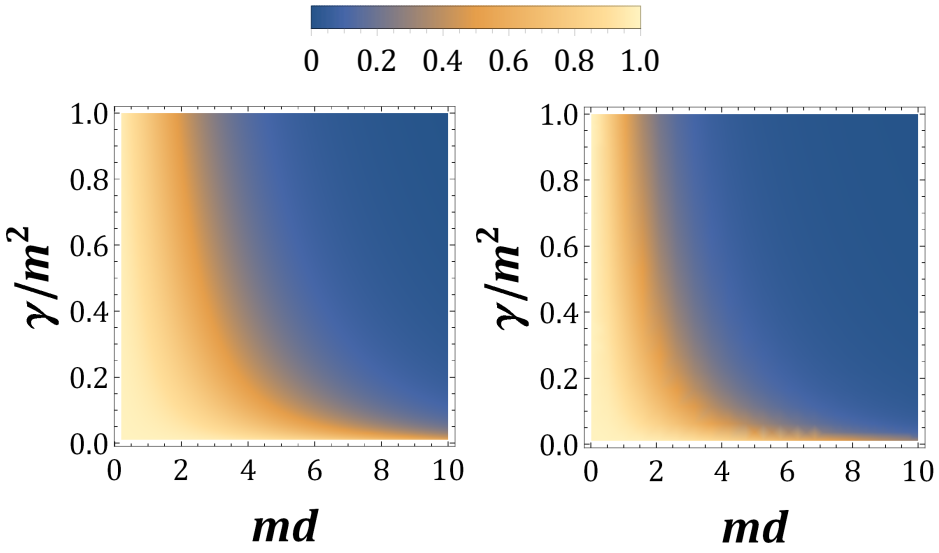

Figure 6.5: Total atomic excitation probability $p = \boldsymbol{a}^\dagger \boldsymbol{a}$, for $n = 3$ emitters, for the symmetric (left panel) and antisymmetric bound states with energy close to $E_1(d)$. In panel (a), $a_3 = a_1$ and $a_2/a_1 \approx 2$; in panel (b), $a_3 = -a_1$ and $a_2 = 0$. The color scale is reported above the plots. We used the expressions (6.72)–(6.73).

As in the case of $n = 2$ emitters [41], the emitter excitation decreases with coupling and distance and increases with energy. In Figure 6.5 we show the probabilities for the symmetric and antisymmetric states with $\nu = 1$, computed from the approximate expressions (6.72)–(6.73) as a function of d and γ. In the whole parameter range, the approximate expressions provide, even for small d, a very good estimate of the exact values, which differ by less than 10^{-3} in the symmetric case and less than 2.5×10^{-2} in the antisymmetric case.

$n = 4$ emitters

For a system made up of $n = 4$ emitters, the eigenvalues in both symmetry sectors are determined by the singularity conditions of the 2×2 matrices

$$A_4^{\pm} = \begin{pmatrix} 1 \pm e^{i\theta} + i(\chi \pm b_1) & e^{i\theta} \pm e^{2i\theta} + i(b_1 \pm b_2) \\ e^{i\theta} \pm e^{2i\theta} + i(b_1 \pm b_2) & 1 \pm e^{3i\theta} + i(\chi \pm b_3) \end{pmatrix}. \tag{6.74}$$

If the cut contributions are neglected, $\boldsymbol{b} = \boldsymbol{0}$, the singularity conditions yield $\theta = \nu\pi$ and $\chi = 0$ as in (6.49), and two complementary pictures emerge according to the parity of ν. For even ν, the three-dimensional subspace corresponding to

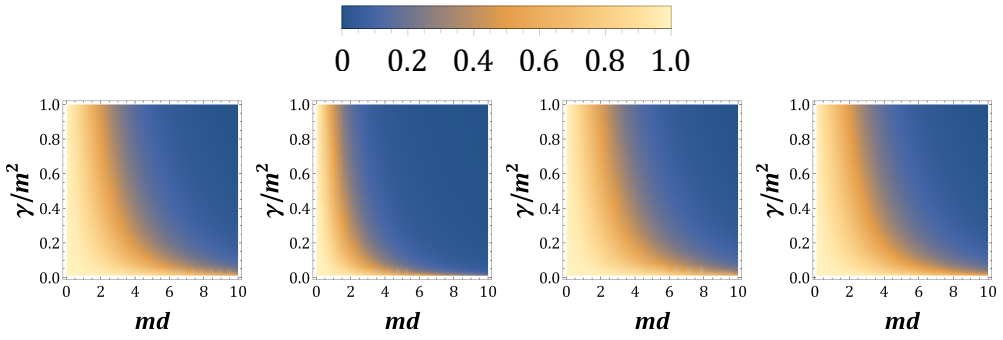

Figure 6.6: Total atomic excitation probability $p = \boldsymbol{a}^\dagger \boldsymbol{a}$, when $n = 4$, for the eigenstates defined by (6.78)–(6.82), characterized by a resonant energy $E_1(d)$ (upper panels), and for the two stable states (6.76) and (6.85), with $E < E_1(d)$ (lower panels). In panel (a) $a_1 = a_4$, $a_2 = a_3$ and $a_1/a_2 \approx -(1+\sqrt{5})/2$; in panel (b), $a_1 = a_4$, $a_2 = a_3$ and $a_1/a_2 \approx -(1-\sqrt{5})/2$; in panel (c), $a_1 = -a_4$, $a_2 = -a_3$ and $\frac{a_1}{a_2} \approx 1$; in panel (d), $a_1 = a_4$, $a_2 = a_3$ and $a_1/a_2 \approx 0.33$. The color scale is reported above the plots.

the eigenvalue $E_\nu(d)$ is spanned by the whole antisymmetric sector and by the symmetric state with

$$a_1 = -a_2 = -a_3 = a_4. \tag{6.75}$$

For odd ν, the eigenspace of $E_\nu(d)$ is still three-dimensional, spanned by the whole symmetric sector and by the antisymmetric state with

$$a_1 = a_2 = -a_3 = -a_4. \tag{6.76}$$

When the $b_{j>0}$ terms are included, there are still eigenstates with resonant energy $E_\nu(d)$ in the antisymmetric sector for even ν and in the symmetric sector for odd ν. In the former case, such states occur when the parameters $(\varepsilon, d, \gamma, m)$ satisfy

$$\Big(\chi(E_\nu) - b_1(E_\nu)\Big)\Big(\chi(E_\nu) - b_3(E_\nu)\Big) = \Big(b_1(E_\nu) - b_2(E_\nu)\Big)^2, \tag{6.77}$$

which yields the two antisymmetric eigenstates characterized, at the lowest order in b_j, by the amplitudes

$$a_1 = -\frac{1 \pm \sqrt{5}}{2} a_2 = \frac{1 \pm \sqrt{5}}{2} a_3 = -a_4 \tag{6.78}$$

and the atomic excitation probabilities

$$p_\nu^{(4)}(\alpha) \approx \left(1 + \alpha \frac{\gamma d E_\nu}{E_\nu^2 - m^2} + \frac{\gamma}{\pi m (E_\nu + m)}\right)^{-1}, \tag{6.79}$$

where the value of α is found to be

$$\alpha = \frac{9 \pm \sqrt{5}}{5 \pm \sqrt{5}}. \tag{6.80}$$

In the case of odd ν, if the parameters satisfy

$$\Big(\chi(E_\nu) + b_1(E_\nu)\Big)\Big(\chi(E_\nu) + b_3(E_\nu)\Big) = \Big(b_1(E_\nu) + b_2(E_\nu)\Big)^2 \tag{6.81}$$

one finds symmetric eigenstates with $E = E_\nu(d)$, amplitudes

$$a_1 = -\frac{1 \pm \sqrt{5}}{2} a_2 = -\frac{1 \pm \sqrt{5}}{2} a_3 = a_4 \tag{6.82}$$

and atomic excitation probabilities $p_\nu^{(4)}(\alpha)$ in (6.79), with

$$\alpha = \frac{13 \pm 5\sqrt{5}}{5 \pm \sqrt{5}}. \tag{6.83}$$

These states are represented in the lower panels (c)–(f) of Figure 6.2, for some values of the parameters d and γ. The atomic probabilities of the four classes of eigenstates defined by (6.78)–(6.82) are shown in Figure 6.6.

The states defined by the amplitudes (6.75)–(6.76) persist as eigenstates even after the introduction of the cut integration terms, $\boldsymbol{b} \neq \mathbf{0}$. However, their energies and the ratios between local amplitudes are shifted by a quantity $O(\mathrm{e}^{-md})$ with respect to $E_\nu(d)$ and to the values in (6.75)–(6.76), respectively. Specifically, at a fixed distance d, the antisymmetric state with amplitudes connected by continuity to (6.76) is characterized by an eigenvalue $E < E_\nu(d)$, slightly smaller than the resonant value. The total atomic probabilities corresponding to states in this class is given by $p_\nu^{(4)}(\alpha)$ in (6.79), with

$$\alpha = 1, \tag{6.84}$$

with even ν, for the symmetric state, and odd ν, for the antisymmetric one.

A numerical analysis of the determinant of the matrices (6.74) reveals the existence of a new class of nondegenerate bound states, characterized, in the distance range $2 \lesssim md \lesssim 6$, by the amplitudes

$$a_1 = a_4, \qquad a_2 = a_3 \approx 3a_1, \tag{6.85}$$

with energy close to $E_\nu(d)$ for odd ν, and

$$a_1 = -a_4, \qquad a_2 = -a_3 \approx -3a_1, \tag{6.86}$$

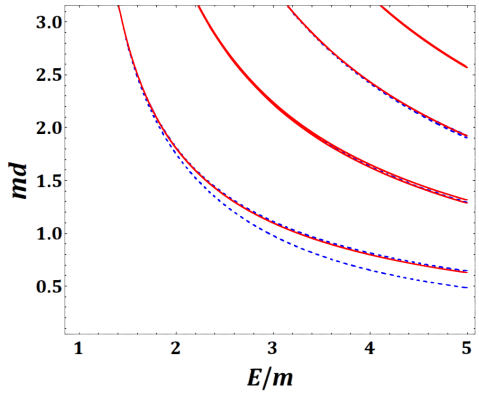

Figure 6.7: Spectral lines in the (E, d) plane for a system of $n = 4$ equally spaced emitters. The solid (red) lines correspond to antisymmetric configurations, while dashed (blue) lines to symmetric ones. As in the $n = 3$ case, the approximation of the resonant values in (6.51) becomes more and more effective for larger values of the distance. For $md \lesssim 2$, the difference between the eigenvalues of the lowest-energy symmetric and antisymmetric states becomes appreciable, with a symmetric state characterized by the amplitudes (6.85) being related to the lowest eigenvalue at a fixed d.

with energy close to $E_\nu(d)$ for even ν. The energy of such states is shifted with respect to the resonant values. In particular, one of the symmetric states (6.85) is characterized by an eigenvalue slighlty smaller than $E_1(d)$, which makes it the lowest-energy bound state in the continuum for a system of $n = 4$ emitters at a fixed spacing d, as can be observed in Figure 6.7. The states (6.85) and (6.86) are characterized by an emitter excitation probability $p_\nu^{(4)}(\alpha)$ in (6.79), with

$$\alpha = \frac{3}{5}. \tag{6.87}$$

The behavior of the lowest-energy bound states in the continuum is shown in detail in Figure 6.8.

6.3.5 Atomic populations

The prediction of bound states populations is the result of complex plane integration, as already implemented in Section 4.1.3. Their analytic expressions are fixed by the excitation amplitude ratios coming from the eigenvalue equation, combined with the normalization condition.

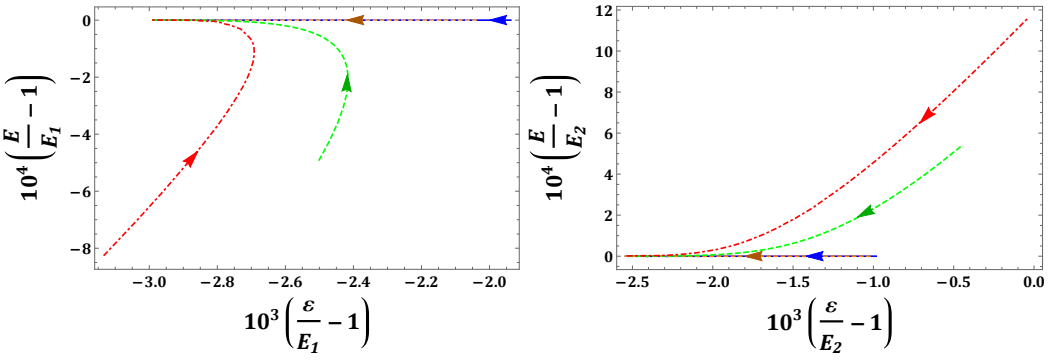

(a) (b)

Figure 6.8: Behavior of the bound state energies E in the vicinity of the resonant values $E_1(d)$ (upper panel) and $E_2(d)$ (lower panel) for $n = 4$, as a function of ε. The two variables have been accordingly rescaled to show the most relevant details in the two panels. The solid (blue) and dotted (brown) lines, that are in practice superposed, are relative to the states defined by the amplitudes (6.82), the dashed (green) lines describe the energy of the states (6.76) in the upper panel and (6.75) in the lower panel, while the dot-dashed (red) lines coincide with the energy of the configurations (6.85) in the upper panel and (6.86) in the lower panel. In all curves, the arrows point towards increasing distance d. While the energy of states (6.82) are equal to the closest resonant value for all spacings, the eigenvalues related to the other states approach the resonant energies as d increases.

$n = 3$ emitters

The proof for the antisymmetric eigenstate (6.73) mimics the initial expression obtained in Section 4.1.3 with $p_v^{(3)-} = |a_1|^2 + |a_3|^2$ in the following way:

$$p_v^{(3)-} = \left(1 + \frac{\gamma}{4\pi}\int \mathrm{d}k \frac{2 - \mathrm{e}^{\mathrm{i}2kd_v} - \mathrm{e}^{-\mathrm{i}2kd_v}}{\omega(k)(E-\omega(k))^2}\right)^{-1} = \left(1 + \frac{\gamma}{4\pi}\mathcal{K}^{(3)-}(E)\right)^{-1}, \tag{6.88}$$

where, applying the half-sum procedure (4.23), we obtain:

$$\mathcal{K}^{(3)-}(E) = \int_{-\infty+\mathrm{i}0^+}^{\infty+\mathrm{i}0^+} \frac{\mathrm{d}k}{\omega(k)} \frac{1-\mathrm{e}^{\mathrm{i}2kd_v}}{(E-\omega(k))^2} + \int_{-\infty-\mathrm{i}0^+}^{\infty-\mathrm{i}0^+} \frac{\mathrm{d}k}{\omega(k)} \frac{1-\mathrm{e}^{\mathrm{i}2kd_v}}{(E-\omega(k))^2} = \mathcal{K}_1^{(3)-}(E) + \mathcal{K}_2^{(3)-}(E). \tag{6.89}$$

The contour deformation introduced in Section 4.1.3 is involved again, thus providing two second order poles in $\pm\bar{k}(E) = \pm\sqrt{E^2 - m^2}$ with associated residue

contribution

$$2\pi\mathrm{i}\lim_{k\to\pm\bar{k}(E)}\frac{\mathrm{d}}{\mathrm{d}k}\left[\left(k\mp\sqrt{E^2-m^2}\right)^2\frac{1-\mathrm{e}^{\mathrm{i}2kd_\nu}}{\sqrt{k^2+m^2}\left(E-\sqrt{k^2+m^2}\right)^2}\right] \tag{6.90}$$

$$=2\pi\mathrm{i}\lim_{k\to\pm\bar{k}(E)}\frac{\mathrm{d}}{\mathrm{d}k}\left[\frac{\left(1-\mathrm{e}^{\mathrm{i}2kd_\nu}\right)\left(E+\sqrt{k^2+m^2}\right)^2}{\sqrt{k^2+m^2}\left(k\pm\sqrt{E^2-m^2}\right)^2}\right]=4\pi d_\nu\frac{E}{E^2-m^2},$$

such that the integral reads

$$\mathcal{K}^{(3)-}(E)=2\mathcal{K}_1^{(3)-}(E)+8\pi d_\nu\frac{E}{E^2-m^2}. \tag{6.91}$$

The cut contribution has the expression

$$\mathcal{K}_1^{(3)-}(E)=2\int_m^\infty\mathrm{d}y\,\frac{\left(1-\mathrm{e}^{-2yd_\nu}\right)(E^2-y^2+m^2)}{\sqrt{y^2-m^2}\,(E^2+y^2-m^2)^2}, \tag{6.92}$$

which is decomposed according to the strategy implemented in (4.31), yielding the same result of (4.32) up to the exponentially suppressed term. This result is again well approximated by (4.33) in the limit of energies near the cutoff m, such that the atomic population (6.73) is obtained.

The same procedure is replied for the study of symmetric bound state populations (6.72), defined as $p_\nu^{(3)+}=|a_1|^2+|a_2|^2+|a_3|^2$, where $a_2/a_1=2(-1)^{\nu+1}$ such that

$$p_\nu^{(3)+}=\left(1+\frac{\gamma}{12\pi}\mathcal{K}^{(3)+}(E)\right)^{-1}, \tag{6.93}$$

with

$$\mathcal{K}^{(3)+}(E)=\int\mathrm{d}k\frac{\mathrm{e}^{\mathrm{i}2kd_\nu}+\mathrm{e}^{-\mathrm{i}2kd_\nu}-4(-1)^\nu(\mathrm{e}^{\mathrm{i}kd_\nu}+\mathrm{e}^{-\mathrm{i}kd_\nu})+6}{\omega(k)(E-\omega(k))^2}. \tag{6.94}$$

The trick (4.23) provides $\mathcal{K}^{(3)+}(E)=\mathcal{K}_1^{(3)+}(E)+\mathcal{K}_2^{(3)+}(E)$, with

$$\mathcal{K}_{1/2}^{(3)+}(E)=\int_{-\infty\pm\mathrm{i}0^+}^{\infty\pm\mathrm{i}0^+}\mathrm{d}k\,\frac{3-4(-1)^\nu\mathrm{e}^{\mathrm{i}kd_\nu}+\mathrm{e}^{\mathrm{i}2kd_\nu}}{\omega(k)(E-\omega(k))^2}, \tag{6.95}$$

whose residue reads

$$2\pi\mathrm{i}\lim_{k\to\pm\bar{k}(E)}\frac{\mathrm{d}}{\mathrm{d}k}\left[\left(k\mp\sqrt{E^2-m^2}\right)^2\frac{3-4(-1)^\nu\mathrm{e}^{\mathrm{i}kd_\nu}+\mathrm{e}^{\mathrm{i}2kd_\nu}}{\sqrt{k^2+m^2}\left(E-\sqrt{k^2+m^2}\right)^2}\right] \tag{6.96}$$

$$=2\pi\mathrm{i}\lim_{k\to\pm\bar{k}(E)}\frac{\mathrm{d}}{\mathrm{d}k}\left[\frac{\left(3-4(-1)^\nu\mathrm{e}^{\mathrm{i}kd_\nu}+\mathrm{e}^{\mathrm{i}2kd_\nu}\right)\left(E+\sqrt{k^2+m^2}\right)^2}{\sqrt{k^2+m^2}\left(k\pm\sqrt{E^2-m^2}\right)^2}\right]=4\pi d_\nu\frac{E}{E^2-m^2},$$

included in the result after contour deformation:

$$\mathcal{K}^{(3)+}(E) = 2\mathcal{K}_1^{(3)+}(E) + 8\pi d_v \frac{E}{E^2 - m^2}. \tag{6.97}$$

Considering that $\mathcal{K}_1^{(3)+}(E) \approx 3\mathcal{K}_1^{(3)-}(E)$, the expression (6.72) is obtained. This latter population shows in Figure 6.5 a more robust behavior with respect to variation of parameters: this phenomenology is understood in Figure 6.12(a), whose inset reveals a higher stability of the symmetric pole trajectory in tangential points with the real axis, signaling the presence of the bound state in the continuum. More precisely, poles trajectories in Figure 6.12 are obtained varying the excitation energy ε parameter and spanning the lower half-plane by changing the coupling constant γ. This means that the variation in the rescaled parameter md in Figure 6.5 has to be interpreted as a modification of the energy scale m, which changes the resonant distance, so that the relative stability between eigenstates is uniquely determined by the inset in Figure 6.12(a).

$n = 4$ emitters

Let us start the study of this wider variety of cases by defining $p_v^{(4)} = |a_1|^2 + |a_2|^2 + |a_3|^2 + |a_4|^2$. Eigenstates belonging to the antisymmetric sector with excitation amplitudes ratios (6.78) provide

$$p_v^{(4)}(\alpha) = \left(1 + \frac{2\gamma}{\pi(5 \pm \sqrt{5})}\mathcal{K}^{(4)}(\alpha, E)\right)^{-1}, \tag{6.98}$$

with

$$\mathcal{K}^{(4)}(\alpha, E) = \int \mathrm{d}k \frac{\frac{3\pm\sqrt{5}}{2}\sin^2\left(\frac{3kd_v}{2}\right) + \sin^2\left(\frac{kd_v}{2}\right) + \frac{1\pm\sqrt{5}}{2}\left(\cos\left(2kd_v\right) - \cos\left(kd_v\right)\right)}{\omega(k)(E - \omega(k))^2}. \tag{6.99}$$

Our familiar integration strategy (4.23) yields

$$\mathcal{K}_{1/2}^{(4)}(\alpha, E) = \int_{-\infty \pm \mathrm{i}0^+}^{\infty \pm \mathrm{i}0^+} \mathrm{d}k \, \frac{\frac{3\pm\sqrt{5}}{4}\left(1 - \mathrm{e}^{\mathrm{i}3kd_v}\right) + \frac{1}{2}\left(1 - \mathrm{e}^{\mathrm{i}kd_v}\right) + \frac{1\pm\sqrt{5}}{2}\left(\mathrm{e}^{\mathrm{i}2kd_v} - \mathrm{e}^{\mathrm{i}kd_v}\right)}{\omega(k)(E - \omega(k))^2}, \tag{6.100}$$

where $\mathcal{K}^{(4)}(\alpha,E) = \frac{1}{2}\left(\mathcal{K}_1^{(4)}(\alpha,E)+\mathcal{K}_2^{(4)}(\alpha,E)\right)$, expressed according to involved residues

$$2\pi\mathrm{i}\lim_{k\to\pm\bar{k}(E)}\frac{\mathrm{d}}{\mathrm{d}k}\left[\left(k\mp\sqrt{E^2-m^2}\right)^2\frac{\frac{5\pm\sqrt{5}}{4}-\frac{3\pm\sqrt{5}}{4}\mathrm{e}^{\mathrm{i}3kd_v}-\frac{1}{2}\mathrm{e}^{\mathrm{i}kd_v}+\frac{1\pm\sqrt{5}}{2}\left(\mathrm{e}^{\mathrm{i}2kd_v}-\mathrm{e}^{\mathrm{i}kd_v}\right)}{\sqrt{k^2+m^2}\left(E-\sqrt{k^2+m^2}\right)^2}\right]$$
$$=2\pi\mathrm{i}\lim_{k\to\pm\bar{k}(E)}\frac{\mathrm{d}}{\mathrm{d}k}\left[\frac{\left(\frac{5\pm\sqrt{5}}{4}-\frac{3\pm\sqrt{5}}{4}\mathrm{e}^{\mathrm{i}3kd_v}-\frac{1}{2}\mathrm{e}^{\mathrm{i}kd_v}+\frac{1\pm\sqrt{5}}{2}\left(\mathrm{e}^{\mathrm{i}2kd_v}-\mathrm{e}^{\mathrm{i}kd_v}\right)\right)\left(E+\sqrt{k^2+m^2}\right)^2}{\sqrt{k^2+m^2}\left(k\pm\sqrt{E^2-m^2}\right)^2}\right]$$
$$=\frac{9\pm\sqrt{5}}{2}\pi d_v\frac{E}{E^2-m^2}, \tag{6.101}$$

as

$$\mathcal{K}^{(4)}(\alpha,E)=\mathcal{K}_1^{(4)}(\alpha,E)+\frac{9\pm\sqrt{5}}{2}\pi d_v\frac{E}{E^2-m^2}. \tag{6.102}$$

Up to the exponentially suppressed terms, the cut contribution obeys the approximation $\mathcal{K}_1^{(4)}(\alpha,E)=\frac{5\pm\sqrt{5}}{4}\mathcal{K}_1^{(3)-}(E)$, thus revealing the associated value of α expressed in (6.80).

The positive parity sector is characterized by the ratios (6.82), whose expression corresponds to (6.98) with

$$\mathcal{K}^{(4)}(\alpha,E)=\int\mathrm{d}k\frac{\frac{3\pm\sqrt{5}}{2}\cos^2\left(\frac{3kd_v}{2}\right)+\cos^2\left(\frac{kd_v}{2}\right)-\frac{1\pm\sqrt{5}}{2}\left(\cos\left(2kd_v\right)+\cos\left(kd_v\right)\right)}{\omega(k)(E-\omega(k))^2}. \tag{6.103}$$

where the half-sum provides $\mathcal{K}^{(4)}(\alpha,E)=\frac{1}{2}\left(\mathcal{K}_1^{(4)}(\alpha,E)+\mathcal{K}_2^{(4)}(\alpha,E)\right)$:

$$\mathcal{K}_{1/2}^{(4)}(\alpha,E)=\int_{-\infty\pm\mathrm{i}0^+}^{\infty\pm\mathrm{i}0^+}\mathrm{d}k\,\frac{\frac{3\pm\sqrt{5}}{4}\left(1+\mathrm{e}^{\mathrm{i}3kd_v}\right)+\frac{1}{2}\left(1+\mathrm{e}^{\mathrm{i}kd_v}\right)-\frac{1\pm\sqrt{5}}{2}\left(\mathrm{e}^{\mathrm{i}2kd_v}+\mathrm{e}^{\mathrm{i}kd_v}\right)}{\omega(k)(E-\omega(k))^2}. \tag{6.104}$$

Contour deformation involves residues in the form

$$2\pi\mathrm{i}\lim_{k\to\pm\bar{k}(E)}\frac{\mathrm{d}}{\mathrm{d}k}\left[\left(k\mp\sqrt{E^2-m^2}\right)^2\frac{\frac{5\pm\sqrt{5}}{4}+\frac{3\pm\sqrt{5}}{4}\mathrm{e}^{\mathrm{i}3kd_v}+\frac{1}{2}\mathrm{e}^{\mathrm{i}kd_v}-\frac{1\pm\sqrt{5}}{2}\left(\mathrm{e}^{\mathrm{i}2kd_v}+\mathrm{e}^{\mathrm{i}kd_v}\right)}{\sqrt{k^2+m^2}\left(E-\sqrt{k^2+m^2}\right)^2}\right]$$
$$=2\pi\mathrm{i}\lim_{k\to\pm\bar{k}(E)}\frac{\mathrm{d}}{\mathrm{d}k}\left[\frac{\left(\frac{5\pm\sqrt{5}}{4}+\frac{3\pm\sqrt{5}}{4}\mathrm{e}^{\mathrm{i}3kd_v}+\frac{1}{2}\mathrm{e}^{\mathrm{i}kd_v}-\frac{1\pm\sqrt{5}}{2}\left(\mathrm{e}^{\mathrm{i}2kd_v}+\mathrm{e}^{\mathrm{i}kd_v}\right)\right)\left(E+\sqrt{k^2+m^2}\right)^2}{\sqrt{k^2+m^2}\left(k\pm\sqrt{E^2-m^2}\right)^2}\right]$$
$$=\frac{13\pm5\sqrt{5}}{2}\pi d_v\frac{E}{E^2-m^2}, \tag{6.105}$$

such that the integral becomes:

$$\mathcal{K}^{(4)}(\alpha, E) = \mathcal{K}_1^{(4)}(\alpha, E) + \frac{13 \pm 5\sqrt{5}}{2} \pi d_\nu \frac{E}{E^2 - m^2}. \tag{6.106}$$

The cut contribution yields the same approximation of the negative parity sector, thus proving the expression (6.83). Concerning the population extension represented in Figure 6.6(a)-(b), the stability description reported in Figure 6.12(b) still holds. The non-perturbative state in Figure 6.6(d) misses this characterization because of the absent analytic description of the associated pole trajectory, up to a numerical root research made difficult by the nearby "perturbative" poles basin of attraction.

The non-perturbative eigenstate is described by ratios (6.85)-(6.86), whose population reads

$$p_\nu^{(4)}(\alpha) = \left(1 + \frac{9\gamma}{10\pi} \mathcal{K}^{(4)}(\alpha, E)\right)^{-1}, \tag{6.107}$$

where we assumed to consider the distance regime with a constant ratio, such that for odd ν

$$\mathcal{K}^{(4)}(\alpha, E) = \int \mathrm{d}k \frac{\frac{1}{9}\cos^2\left(\frac{3kd_\nu}{2}\right) + \cos^2\left(\frac{kd_\nu}{2}\right) + \frac{1}{3}\left(\cos\left(2kd_\nu\right) + \cos\left(kd_\nu\right)\right)}{\omega(k)(E - \omega(k))^2}, \tag{6.108}$$

while for even ν

$$\mathcal{K}^{(4)}(\alpha, E) = \int \mathrm{d}k \frac{\frac{1}{9}\sin^2\left(\frac{3kd_\nu}{2}\right) + \sin^2\left(\frac{kd_\nu}{2}\right) + \frac{1}{3}\left(\cos\left(2kd_\nu\right) - \cos\left(kd_\nu\right)\right)}{\omega(k)(E - \omega(k))^2}. \tag{6.109}$$

Following the usual procedure (4.23) we obtain

$$\mathcal{K}_{1/2}^{(4)}(\alpha, E) = \int_{-\infty \pm \mathrm{i}0^+}^{\infty \pm \mathrm{i}0^+} \mathrm{d}k \, \frac{\frac{1}{18}\left(1 \pm \mathrm{e}^{\mathrm{i}3kd_\nu}\right) + \frac{1}{2}\left(1 \pm \mathrm{e}^{\mathrm{i}kd_\nu}\right) - \frac{1}{3}\left(\mathrm{e}^{\mathrm{i}2kd_\nu} \pm \mathrm{e}^{\mathrm{i}kd_\nu}\right)}{\omega(k)(E - \omega(k))^2}, \tag{6.110}$$

where the integral is again the same for both contours, whose deformation gives the following residue contribution:

$$\begin{aligned}
&2\pi\mathrm{i} \lim_{k \to \pm\bar{k}(E)} \frac{\mathrm{d}}{\mathrm{d}k} \left[\left(k \mp \sqrt{E^2 - m^2}\right)^2 \frac{\frac{1}{18}\left(1 \pm \mathrm{e}^{\mathrm{i}3kd_\nu}\right) + \frac{1}{2}\left(1 \pm \mathrm{e}^{\mathrm{i}kd_\nu}\right) - \frac{1}{3}\left(\mathrm{e}^{\mathrm{i}2kd_\nu} \pm \mathrm{e}^{\mathrm{i}kd_\nu}\right)}{\sqrt{k^2 + m^2}\left(E - \sqrt{k^2 + m^2}\right)^2} \right] \\
&= 2\pi\mathrm{i} \lim_{k \to \pm\bar{k}(E)} \frac{\mathrm{d}}{\mathrm{d}k} \left[\frac{\left(\frac{1}{18}\left(1 \pm \mathrm{e}^{\mathrm{i}3kd_\nu}\right) + \frac{1}{2}\left(1 \pm \mathrm{e}^{\mathrm{i}kd_\nu}\right) - \frac{1}{3}\left(\mathrm{e}^{\mathrm{i}2kd_\nu} \pm \mathrm{e}^{\mathrm{i}kd_\nu}\right)\right)\left(E + \sqrt{k^2 + m^2}\right)^2}{\sqrt{k^2 + m^2}\left(k \pm \sqrt{E^2 - m^2}\right)^2} \right] \\
&= \frac{2}{3}\pi d_\nu \frac{E}{E^2 - m^2}.
\end{aligned} \tag{6.111}$$

The complete integral is expressed by

$$\mathcal{K}^{(4)}(\alpha, E) = \mathcal{K}_1^{(4)}(\alpha, E) + \frac{2}{3}\pi d_\nu \frac{E}{E^2 - m^2}, \tag{6.112}$$

with a cut contribution $\mathcal{K}_1^{(4)}(\alpha, E) = \frac{5}{9}\mathcal{K}_1^{(3)-}(E)$ in the regime we are interested in to prove (6.87).

The last case is represented by the dimerized eigenstates, that obey (6.75)-(6.76), whose population reads

$$p_\nu^{(4)}(\alpha) = \left(1 + \frac{\gamma}{2\pi}\mathcal{K}^{(4)}(\alpha, E)\right)^{-1} \tag{6.113}$$

for odd ν with

$$\mathcal{K}^{(4)}(\alpha, E) = \int \mathrm{d}k \frac{\sin^2\left(\frac{3kd_\nu}{2}\right) + \sin^2\left(\frac{kd_\nu}{2}\right) - (\cos(2kd_\nu) - \cos(kd_\nu))}{\omega(k)(E - \omega(k))^2}, \tag{6.114}$$

while for even ν

$$\mathcal{K}^{(4)}(\alpha, E) = \int \mathrm{d}k \frac{\cos^2\left(\frac{3kd_\nu}{2}\right) + \cos^2\left(\frac{kd_\nu}{2}\right) - (\cos(2kd_\nu) + \cos(kd_\nu))}{\omega(k)(E - \omega(k))^2}. \tag{6.115}$$

Half-sums are given by

$$\mathcal{K}_{1/2}^{(4)}(\alpha, E) = \int_{-\infty \pm \mathrm{i}0^+}^{\infty \pm \mathrm{i}0^+} \mathrm{d}k \, \frac{\frac{1}{2}\left(1 \mp \mathrm{e}^{\mathrm{i}3kd_\nu}\right) + \frac{1}{2}\left(1 \mp \mathrm{e}^{\mathrm{i}kd_\nu}\right) \mp \left(\mathrm{e}^{\mathrm{i}2kd_\nu} \mp \mathrm{e}^{\mathrm{i}kd_\nu}\right)}{\omega(k)(E - \omega(k))^2}, \tag{6.116}$$

whose residues are ruled by the following limit:

$$\begin{aligned}
&2\pi\mathrm{i} \lim_{k \to \pm\bar{k}(E)} \frac{\mathrm{d}}{\mathrm{d}k}\left[\left(k \mp \sqrt{E^2 - m^2}\right)^2 \frac{\frac{1}{2}\left(1 \mp \mathrm{e}^{\mathrm{i}3kd_\nu}\right) + \frac{1}{2}\left(1 \mp \mathrm{e}^{\mathrm{i}kd_\nu}\right) \mp \left(\mathrm{e}^{\mathrm{i}2kd_\nu} \mp \mathrm{e}^{\mathrm{i}kd_\nu}\right)}{\sqrt{k^2 + m^2}\left(E - \sqrt{k^2 + m^2}\right)^2}\right] \\
&= 2\pi\mathrm{i} \lim_{k \to \pm\bar{k}(E)} \frac{\mathrm{d}}{\mathrm{d}k}\left[\frac{\left(\frac{1}{2}\left(1 \mp \mathrm{e}^{\mathrm{i}3kd_\nu}\right) + \frac{1}{2}\left(1 \mp \mathrm{e}^{\mathrm{i}kd_\nu}\right) \mp \left(\mathrm{e}^{\mathrm{i}2kd_\nu} \mp \mathrm{e}^{\mathrm{i}kd_\nu}\right)\right)\left(E + \sqrt{k^2 + m^2}\right)^2}{\sqrt{k^2 + m^2}\left(k \pm \sqrt{E^2 - m^2}\right)^2}\right] \\
&= 2\pi d_\nu \frac{E}{E^2 - m^2}.
\end{aligned} \tag{6.117}$$

The last population is obtained using the integral expression

$$\mathcal{K}^{(4)}(\alpha, E) = \mathcal{K}_1^{(4)}(\alpha, E) + 2\pi d_\nu \frac{E}{E^2 - m^2}, \tag{6.118}$$

whose cut is well approximated for the considered parameters by $\mathcal{K}_1^{(4)}(\alpha, E) = \mathcal{K}_1^{(3)-}(E)$, yielding (6.84). The population stability is evident by looking at Figure 6.6(c), whose robust behavior with respect to parameters variation resides in poles trajectories shown in Figure 6.12(c), where the dimerized antisymmetric state is in proximity of the real axis for a large interval of excitation energies ε.

n	4	6	8	10	12
$m\,d_c$	0.05	0.18	0.26	0.30	0.33
E_c/m	101	28	20	16	15

Table 6.1: Critical values of the distance d_c at which the nonperturbative eigenvalue pair between the resonant energies E_1 and E_2 appears, and corresponding energy E_c, for arrays with different number of equally spaced emitters.

6.4 Non-perturbative eigenstate pairs

Condition (6.17), which determines the eigenvalues of the system, is a complicated equation in E, featuring the functions $\theta(E)$, $\chi(E)$ and $\boldsymbol{b}(E)$. In the previous section, we have analyzed the solutions that can be connected by continuity to the resonant energies (6.51) in the limit $\mathrm{e}^{-md} \to 0$. However, the non-polynomial character of (6.17) can generally give rise to new solutions at finite d, which are unrelated to the resonant eigenvalues and eigenspaces. In particular, this phenomenon is facilitated for very small md, when the magnitude of all the $b_{j>0}$ is relevant and comparable to that of b_0.

Figures 6.9 and 6.10 display general features of such nonperturbative states, for $n = 3$ and $n = 4$ emitters, respectively. These features are confirmed for higher n. At a sufficiently high value of the distance, all the eigenvalues are connected by continuity to the resonant energies $E_\nu(d)$, with $\nu \in \mathbb{Z}_+$. When distance decreases, additional eigenvalues start appearing in the (E, d) plane, between $E_\nu(d)$ and $E_{\nu+1}(d)$, immediately branching in two distinct eigenvalues, whose energy increases when distance is further decreased. The observed processes of pair formation in the cases $n = 3, 4$ occur roughly at the same value of d. To quantify the range in which the phenomenon occurs we define the critical distance $d_c^{(n)}$ as the value which marks the appearence of the first eigenstate of this class between $E_1(d)$ and $E_2(d)$. We obtain the values $md_c = 0.063$ for $n = 3$ emitters and $md_c = 0.052$ for $n = 4$ emitters. Notice that no state of this kind is observed with energy below $E_1(d)$. The value of energy E_c corresponding to the critical distance is $E_c \approx 79m$ for $n = 3$ and $E_c \approx 101m$ for $n = 4$. Thus, independently of the values of the parameters ε and γ, the energy of such states exceeds the mass m by at least two orders of magnitude, an energy range in which the validity of our model, at least in a waveguide QED context, is far from being ensured. However, as one can observe from Table 6.1, the critical energy decreases to an order 10 for larger systems.

The nonperturbative eigenvalues always correspond to symmetric eigenstates, with a photon half-wavelength that is far from multiple integers of the interatomic spacing, as can be observed in both Figure 6.9–6.10. From the ex-

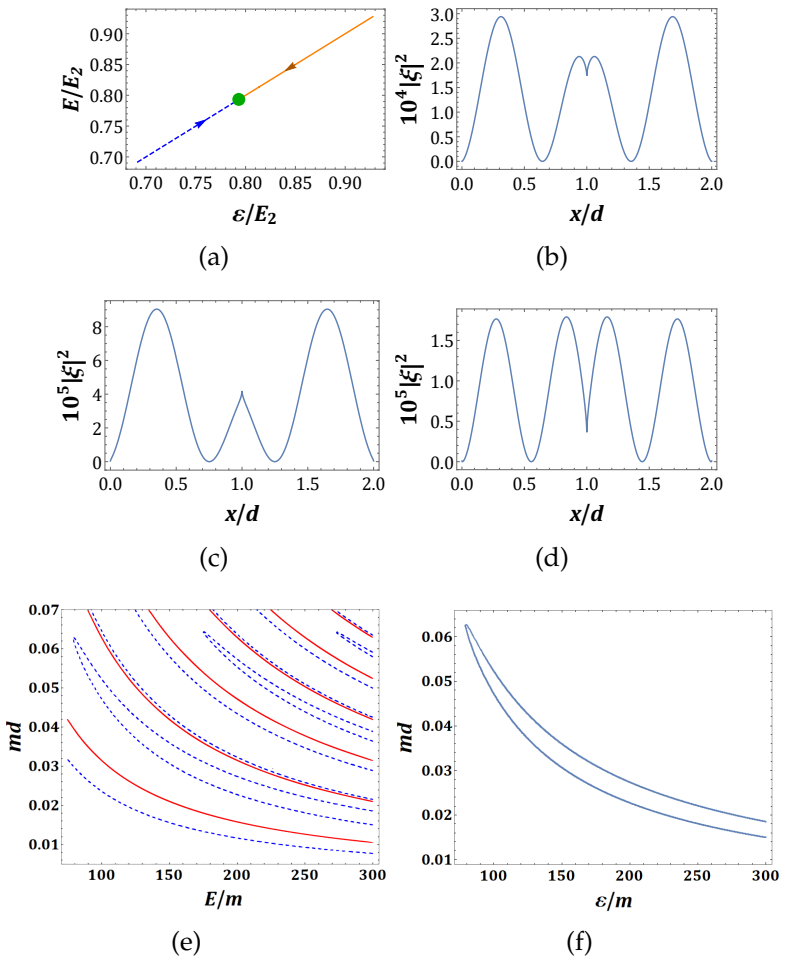

Figure 6.9: Nonperturbative high-energy eigenstates for $n = 3$. Panel (a): energy trajectory of the pair of eigenstates with energy between E_1 and E_2 in the (ε, E) plane (in units of E_2), with the arrows pointing towards increasing values the distance d. At $md = md_c = 0.063$, the two eigenvalues coalesce and disappear. Panel (b): field probability density $|\xi(x)|^2$ corresponding to the critical case. Panels (c)-(d): field probability density $|\xi(x)|^2$ for the pair of bound states corresponding to the (very) small distance $md = 10^{-2}$. Panel (e): spectral lines in the (E, d) plane, with solid (red) lines representing antisymmetric states and dashed (blue) lines representing the symmetric ones; three branching points of eigenvalue pairs are visible. Panel (f): Emitter excitation energies of the lowest-energy nonperturbative eigenstate pair as a function of d for $\gamma = 10^{-2}m^2$.

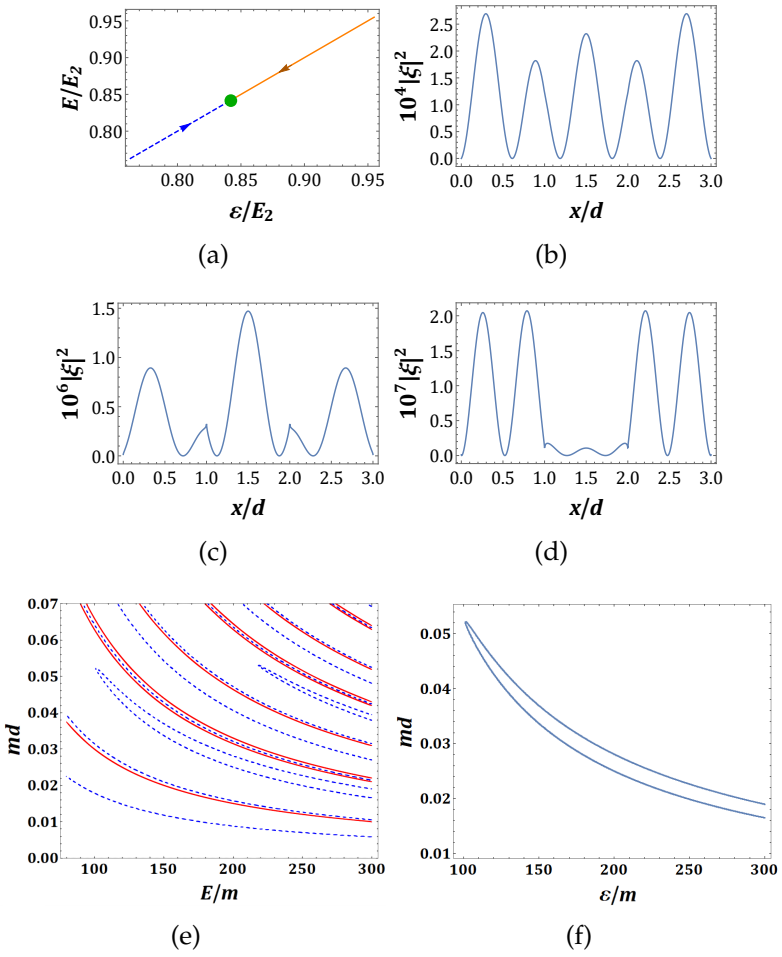

Figure 6.10: Nonperturbative high-energy eigenstates for $n = 4$. Panel (a): energy trajectory of the pair of eigenstates with energy between E_1 and E_2 in the (ε, E) plane (in units of E_2), with the arrows pointing towards increasing values the distance d. At $md = md_c = 0.052$, the two eigenvalues coalesce and disappear. Panel (b): field probability density $|\xi(x)|^2$ corresponding to the critical case. Panels (c)-(d) field probability density $|\xi(x)|^2$ for the pair of bound states corresponding to the (very) small $md = 10^{-4}$. Panel (e): spectral lines in the (E, d) plane, with solid (red) lines representing antisymmetric states and dashed (blue) lines representing the symmetric ones; three branching points of eigenvalue pairs are visible. Panel (f): Emitter excitation energies of the lowest-energy nonperturbative eigenstate pair as a function of d for $\gamma = 10^{-2}m^2$.

pression (6.9) one infers that, in such high-energy states, the field wavefunction is suppressed and the single excitation is almost entirely shared by the emitters. Finally, for $n > 4$, we have found the existence of more than one pair of nonperturbative eigenstates between E_ν and $E_{\nu+1}$.

6.4.1 Cut expansion

A complete characterization of cut contributions allows us to unveil the role of non confined electromagnetic field. For clarity, we will adopt the rescaled quantities $y \to y/m$ and $E \to E/m$. The first step regards the separation of the integral in (6.19) over two different regions: $\left[1, \sqrt{E^2+1}\right)$, where the geometric series associated with the denominator converges, and the remaining $\left[\sqrt{E^2+1}, \infty\right)$. Thus

$$b_j(E) = b_j^c(E) + b_j^{nc}(E), \tag{6.119}$$

with the first term reading

$$b_j^c(E) = \frac{\bar{k}(E)}{\pi} \sum_{\ell=0}^{\infty} \frac{(-1)^\ell}{E^{2\ell+1}} \int_1^{\sqrt{E^2+1}} \mathrm{e}^{-jyd} (y^2-1)^{\ell-\frac{1}{2}} \mathrm{d}y, \tag{6.120}$$

which can be extended up to infinity to recover the integral expression of the modified Bessel functions of the second kind:

$$K_\ell(z) = \frac{\sqrt{\pi}\left(\frac{z}{2}\right)^\ell}{\Gamma\left(\ell+\frac{1}{2}\right)} \int_1^{\infty} \mathrm{e}^{-yz} (y^2-1)^{\ell-\frac{1}{2}} \mathrm{d}y, \tag{6.121}$$

valid for $\mathrm{Re}(\ell) > -\frac{1}{2}$. This expression represents the ℓ-th moment in the form factor measure associated to the energy lying in the k imaginary part distribution, thus related to a realization of coupling transmittance, expressed in the cut resummation:

$$b_j(E) = \frac{\bar{k}(E)}{\pi} \sum_{\ell=0}^{M-1} \frac{(-1)^\ell}{E^{2\ell+1}} \frac{\Gamma(\ell+\frac{1}{2})}{\sqrt{\pi}\left(\frac{jd}{2}\right)^\ell} K_\ell(jd) + \Delta_j(E), \tag{6.122}$$

a series evaluated numerically in its truncated version up to the $(M-1)$-th term, implementing a useful computational complexity reduction with respect to numerical integrations, where Γ is the Euler gamma function and $\Delta_j(E)$ represents an error function.

Adding a new contribution covering the same interval of the second term in (6.119), the definition of the error function in (6.122) is obtained:

$$\frac{\pi}{\bar{k}(E)}\Delta_j(E) = \frac{1}{E}\int_{\sqrt{E^2+1}}^{\infty} \mathrm{d}y\, \frac{\mathrm{e}^{-jyd}}{\sqrt{y^2-1}}\left(\sum_{\ell=0}^{M-1}\left(-\frac{y^2-1}{E^2}\right)^{\ell} - \frac{E^2}{E^2+y^2-1}\right), \tag{6.123}$$

which, in the same spirit of (6.121), is interpreted as a measure of moments fluctuation, further eloborated by means of the partial sum estimation, involving annealed series:

$$\begin{aligned}\frac{\pi}{\bar{k}(E)}\Delta_j(E) &= \frac{(-1)^M}{E^{2M-1}}\int_{\sqrt{E^2+1}}^{\infty} \mathrm{d}y\, \frac{\mathrm{e}^{-jdy}(y^2-1)^{M-\frac{1}{2}}}{E^2+y^2-1} \\ &= \sum_{\ell=0}^{\infty}\frac{(-1)^{M+\ell}}{E^{2(M-\ell)-1}}\int_{\sqrt{E^2+1}}^{\infty} \mathrm{d}y\, \mathrm{e}^{-jdy}(y^2-1)^{M-\ell-\frac{3}{2}}.\end{aligned} \tag{6.124}$$

Applying again the strategy to introduce the expression (6.121), the following result holds:

$$\begin{aligned}\frac{\pi}{\bar{k}(E)}\Delta_j(E) = &\sum_{\ell=0}^{\infty}\frac{(-1)^{M+\ell}}{E^{2(M-\ell)-1}}\frac{\Gamma\left(M-\ell-\frac{1}{2}\right)}{\sqrt{\pi}\left(\frac{jd}{2}\right)^{M-\ell-1}}K_{M-\ell-1}(jd) \\ &- \sum_{\ell=0}^{\infty}\frac{(-1)^{M+\ell}}{E^{2(M-\ell)-1}}\int_{1}^{\sqrt{E^2+1}} \mathrm{d}y\, \mathrm{e}^{-jdy}(y^2-1)^{M-\ell-\frac{3}{2}},\end{aligned} \tag{6.125}$$

where the integral in the second term is further elaborated by means of successive substitutions $y \to y-1$ and $y \to y/2$:

$$\begin{aligned}&\int_1^{\sqrt{E^2+1}} \mathrm{d}y\, \mathrm{e}^{-jdy}(y^2-1)^{M-\ell-3/2} = \int_0^{\frac{\sqrt{E^2+1}-1}{2}} \mathrm{d}y\, \mathrm{e}^{-(2y+1)jd}\,\frac{(4y(y+1))^{M-\ell-\frac{3}{2}}}{2} \\ &= \frac{\left(2\left(\sqrt{E^2+1}-1\right)\right)^{M-\ell-\frac{1}{2}}}{2}\,\mathrm{e}^{-jd}\int_0^1 \mathrm{d}q\, \mathrm{e}^{-jd\left(\sqrt{E^2+1}-1\right)q}\left(\frac{\sqrt{E^2+1}-1}{2}q^2+q\right)^{M-\ell-\frac{3}{2}}.\end{aligned} \tag{6.126}$$

The series expansion of the exponential in the last integral allows us to pursue the integral representation of the hypergeometric function:

$${}_2F_1(n_1,n_2;c;w) = \frac{\Gamma(c)}{\Gamma(n_2)\Gamma(c-n_2)}\int_0^1 \mathrm{d}q\, q^{n_2-1}(1-q)^{c-n_2-1}(1-wq)^{-n_1} \tag{6.127}$$

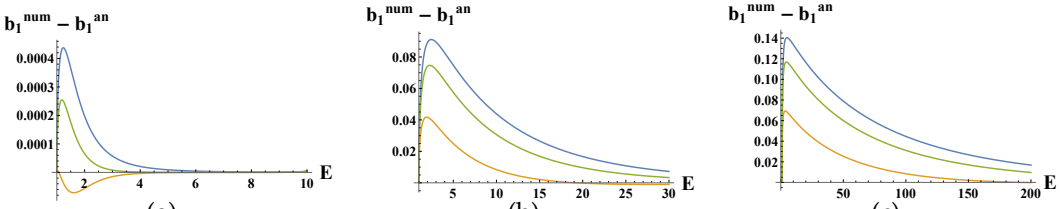

Figure 6.11: Deviations from the exact numerical expression (6.19) (with $j = 1$) of (6.122) making use of (6.128). Blue curves are associated with $M = 2$, the orange ones with $M = 3$ and remaining green ones with $M = 4$. Distance parameter is fixed to $d = 3$ in panel (a), $d = 0.1$ in (b) and $d = 0.01$ in (c).

such that

$$\begin{aligned}\frac{\pi}{\bar{k}(E)}\Delta_j(E) = &\sum_{\ell=0}^{\infty}\frac{(-1)^{M+\ell}}{E^{2(M-\ell)-1}}\frac{\Gamma\left(M-\ell-\frac{1}{2}\right)}{\sqrt{\pi}\left(\frac{jd}{2}\right)^{M-\ell-1}}K_{M-\ell-1}(jd)\\ &-e^{-jd}\sum_{\ell=0}^{\infty}\frac{(-1)^{M+\ell}}{E^{2(M-\ell)-1}}\frac{\left(2\left(\sqrt{E^2+1}-1\right)\right)^{M-\ell-\frac{1}{2}}}{2}\sum_{i=0}^{\infty}\frac{\left(-jd\left(\sqrt{E^2+1}-1\right)\right)^{i}}{\left(M+i-\ell-\frac{1}{2}\right)i!}\\ &\times {}_2F_1\left(\frac{3}{2}+\ell-M, M+i-\ell-\frac{1}{2}, M+i-\ell+\frac{1}{2}; -\frac{\sqrt{E^2+1}-1}{2}\right),\end{aligned} \tag{6.128}$$

In (6.128) there is an implicit constraint linked to the definition of modified Bessel functions $K_{M-\ell-1}(d)$, consisting in $M > \ell + 1$; thus, the series needs a truncation with at least one less term with respect to the partial sum.

The computational complexity perspective, exploited for the use of analytical expressions implemented through Bessel functions, helps us in determining well matching estimations just considering terms up to K_1 near resonant eigenvalues, whose energy scale grows rapidly for small distances. Figure 6.11 shows the deviation from the analytical expression (6.122), caused by series truncation: the estimation of energy scales exploits the expression $E_\nu(d)$, thus verifying the convergence in regions of interest already with a low number of terms. The oscillating behavior with respect to the retained number of terms is caused by the alternating nature of the series. Moreover, looking for the convergence radius r_c of (6.122), without the error function in (6.128), as a Laurent series

$$r_c = \frac{jd}{2}\lim_{\ell}\left|\frac{K_\ell(jd)}{\left(\ell+\frac{1}{2}\right)K_{\ell+1}(jd)}\right| = \begin{cases}\infty \text{ if } d\to 0,\\ \frac{1}{2} \text{ if } d\to\infty,\end{cases} \tag{6.129}$$

it is straightforward the breakthrough in understanding the well behaved series for rapidly growing energy scales.

Without the presented cut expansion (6.128) it is impossible to reach a feasible time for numerical integrations concerning systems with more than four two-level atoms, as presented in Table 6.1. In the regime of distances allowing for these kind of non-perturbative eigenstates cut contributions are dominant and well approximated by this efficient procedure.

6.4.2 Unstable states

The resolvent formalism, employed to evaluate the existence and properties of bound states, also provides information on the lifetime of unstable states. The step required to perform this kind of analysis is the analytic continuation of the self-energy to the second Riemann sheet

$$\Sigma^{\mathrm{II}}_{j\ell}(z) = \Sigma_{j\ell}(z) - \frac{2\mathrm{i}\gamma}{\sqrt{z^2 - m^2}} \cos\left(|j-\ell|\theta(z)\right), \tag{6.130}$$

where z is a complex energy. The lifetimes of unstable states are determined by the solutions $z_p = E_p - \mathrm{i}\gamma_p/2$ of the equation

$$\det\left[\left(\mathrm{G}^{\mathrm{II}}\right)^{-1}\left(E_p - \mathrm{i}\frac{\gamma_p}{2}\right)\right] = 0 \quad \text{with } \gamma_p > 0, \tag{6.131}$$

with

$$\left(\mathrm{G}^{\mathrm{II}}\right)^{-1}(z) = (z-\varepsilon)\mathbb{1} - \Sigma^{\mathrm{II}}(z). \tag{6.132}$$

We are now going to consider the properties of the complex poles of the propagator.

n=3 emitters

The block-diagonalization procedure applied to a system of three emitters implies the singularity conditions:

$$\chi(z) = -\frac{i}{2}\left(2 + e^{-2i\theta(z)}\right) - \frac{b_2(z)}{2} \pm \frac{1}{2}\sqrt{f_3(\theta(z), \boldsymbol{b}(z))}, \tag{6.133}$$

for symmetric states and

$$\chi(z) = \; b_2(z) - i\left(1 - e^{-2i\theta(z)}\right), \tag{6.134}$$

for antisymmetric states, with

$$f_3(\theta, \boldsymbol{b}) = 8b_1^2 + b_2^2 + 16\mathrm{i}b_1\mathrm{e}^{-\mathrm{i}\theta} - 8\mathrm{e}^{-2\mathrm{i}\theta} + 2\mathrm{i}b_2\mathrm{e}^{-2\mathrm{i}\theta} - \mathrm{e}^{-4\mathrm{i}\theta}. \tag{6.135}$$

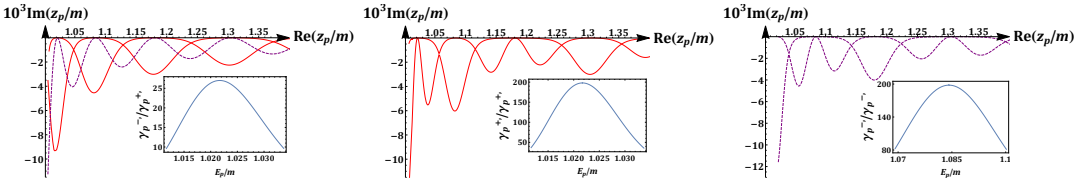

Figure 6.12: Pole trajectories in the lower half-plane of complex energy for $n = 3$ in panel (a) and $n = 4$ in panels (b)-(c). The parameters are set to $md = 15$ and $\gamma = 2\pi \times 10^{-4} m^2$, while ε varies between m and $1.4m$. Solid (red) lines are associated with symmetric eigenstates, while dashed (purple) lines refer to antisymmetric states. In the insets, we report the ratios between the first derivatives $\mathrm{dIm}(z_p)/\mathrm{dRe}(z_p)$ related to two different curves, both approaching the real axis (i.e. corresponding to a stable bound state) at the same point, corresponding to the lowest-energy resonance in the plots. Notice that, close to the resonance points, the imaginary parts of the unstable poles scale linearly with n.

Introducing the functions $R_3(\theta, \boldsymbol{b}) = \mathrm{Re}(f_3(\theta, \boldsymbol{b}))$, $S_3(\theta, \boldsymbol{b}) = \mathrm{Im}(f_3(\theta, \boldsymbol{b}))$, the real and imaginary part of roots of the complex poles for the two blocks read

$$E_p^+ \approx \varepsilon + \frac{\gamma}{2\bar{k}(E_p^+)} \Big(2b_0(E_p^+) + b_2(E_p^+) + \sin\left(2\theta(E_p^+)\right) \mp \sqrt{\frac{R_3(\theta, \mathbf{b}) + \sqrt{R_3^2(\theta, \mathbf{b}) + S_3^2(\theta, \mathbf{b})}}{2}} \Big), \tag{6.136}$$

$$\frac{\gamma_p^+}{2} \approx \frac{\gamma}{2\bar{k}(E_p^+)} \left(2 + \cos\left(2\theta(E_p^+)\right) \pm \sqrt{\frac{-R_3(\theta, \mathbf{b}) + \sqrt{R_3^2(\theta, \mathbf{b}) + S_3^2(\theta, \mathbf{b})}}{2}} \right), \tag{6.137}$$

$$E_p^- \approx \varepsilon + \frac{\gamma}{\bar{k}(E_p^-)} \Big(b_0(E_p^-) + b_2(E_p^-) + \sin\left(2\theta(E_p^-)\right) \Big), \tag{6.138}$$

$$\frac{\gamma_p^-}{2} \approx \frac{\gamma}{\bar{k}(E_p^-)} \Big(1 - \cos\left(2\theta(E_p^-)\right) \Big), \tag{6.139}$$

with $\bar{k}(E) = \sqrt{E^2 - m^2}$. The behavior of the complex poles of the propagator for $n = 3$ is reported in panel (a) of Fig. 6.12.

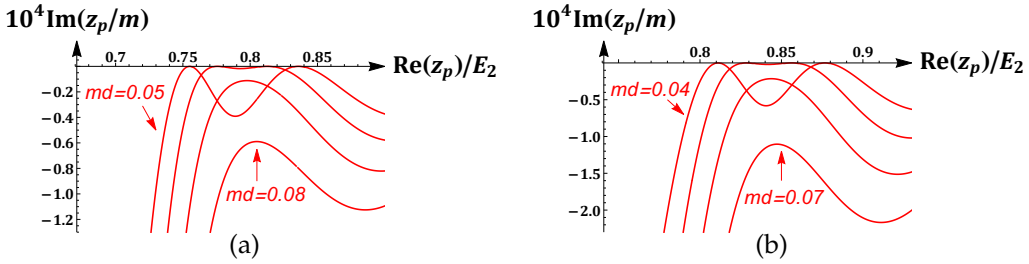

Figure 6.13: Trajectories of poles with real part between $E_1(d)$ and $E_2(d)$ in the complex lower half-plane, for different values of d in a system of $n = 3$ (left) and $n = 4$ (right). The emergence of nonperturbative eigenstates is related to the pole trajectory touching the real axis at a critical distance. Below the critical distance, the trajectories are tangent to the real axis in two points.

n=4 emitters

The singularity condition for the symmetric and antisymmetric blocks in the $n = 4$ system read

$$\chi(z) = -\frac{\mathrm{i}}{2}\left(2 + \mathrm{e}^{-\mathrm{i}\theta(z)} + \mathrm{e}^{-3\mathrm{i}\theta(z)}\right) - \frac{b_1(z) + b_3(z)}{2} \pm \frac{1}{2}\sqrt{f_4^+(\theta(z), \boldsymbol{b}(z))}, \tag{6.140}$$

$$\chi(z) = \frac{\mathrm{i}}{2}\left(-2 + \mathrm{e}^{-\mathrm{i}\theta(z)} + \mathrm{e}^{-3\mathrm{i}\theta(z)}\right) + \frac{b_1(z) + b_3(z)}{2} \pm \frac{1}{2}\sqrt{f_4^-(\theta(z), \boldsymbol{b}(z))}, \tag{6.141}$$

respectively, with

$$\begin{aligned} f_4^+(\theta, \boldsymbol{b}) =& 4(b_1 + b_2)^2 + (b_1 - b_3)^2 + \mathrm{i}(10b_1 + 8b_2 - 2b_3)\mathrm{e}^{-\mathrm{i}\theta} + \mathrm{i}(5\mathrm{i} + 8b_1 + 8b_2)\mathrm{e}^{-2\mathrm{i}\theta} \\ &+ \mathrm{i}(8\mathrm{i} - 2b_1 + 2b_3)\mathrm{e}^{-3\mathrm{i}\theta} - 2\mathrm{e}^{-4\mathrm{i}\theta} - \mathrm{e}^{-6\mathrm{i}\theta}, \end{aligned} \tag{6.142}$$

$$\begin{aligned} f_4^-(\theta, \boldsymbol{b}) =& 4(b_1 - b_2)^2 + (b_1 - b_3)^2 + \mathrm{i}(10b_1 - 8b_2 - 2b_3)\mathrm{e}^{-\mathrm{i}\theta} + \mathrm{i}(5\mathrm{i} - 8b_1 + 8b_2)\mathrm{e}^{-2\mathrm{i}\theta} \\ &- \mathrm{i}(8\mathrm{i} + 2b_1 - 2b_3)\mathrm{e}^{-3\mathrm{i}\theta} - 2\mathrm{e}^{-4\mathrm{i}\theta} - \mathrm{e}^{-6\mathrm{i}\theta}, \end{aligned} \tag{6.143}$$

where we have defined $R_4^{\pm}(\theta, \boldsymbol{b}) = \mathrm{Re}(f_4^{\pm}(\theta, \boldsymbol{b}))$, $S_4^{\pm}(\theta, \boldsymbol{b}) = \mathrm{Im}(f_4^{\pm}(\theta, \boldsymbol{b}))$. In this way approximate decoupled solutions are

$$\begin{aligned} E_p^+ \approx \varepsilon + \frac{\gamma}{2\bar{k}(E_p^+)}\Big(&2b_0(E_p^+) + b_1(E_p^+) + b_3(E_p^+) + \sin(\theta) + \sin(3\theta) \\ &\mp \sqrt{\frac{R_4^+(\theta, \boldsymbol{b}) + \sqrt{R_4^{+2}(\theta, \boldsymbol{b}) + S_4^{+2}(\theta, \boldsymbol{b})}}{2}}\Big), \end{aligned} \tag{6.144}$$

$$\frac{\gamma_p^+}{2} \approx \frac{\gamma}{2\bar{k}(E_p^+)}\left(2+\cos(\theta)+\cos(3\theta) \pm \sqrt{\frac{-R_4^+(\theta,\boldsymbol{b})+\sqrt{R_4^{+2}(\theta,\boldsymbol{b})+S_4^{+2}(\theta,\boldsymbol{b})}}{2}}\right), \tag{6.145}$$

$$E_p^- \approx \varepsilon + \frac{\gamma}{2\bar{k}(E_p^-)}\left(b_0(E_p^-)-b_1(E_p^-)-b_3(E_p^-)-\sin(\theta)-\sin(3\theta) \mp \sqrt{\frac{R_4^-(\theta,\boldsymbol{b})+\sqrt{R_4^{-2}(\theta,\boldsymbol{b})+S_4^{-2}(\theta,\boldsymbol{b})}}{2}}\right), \tag{6.146}$$

$$\frac{\gamma_p^-}{2} \approx \frac{\gamma}{2\bar{k}(E_p^-)}\left(2-\cos(\theta)-\cos(3\theta) \pm \sqrt{\frac{-R_4^-(\theta,\boldsymbol{b})+\sqrt{R_4^{-2}(\theta,\boldsymbol{b})+S_4^{-2}(\theta,\boldsymbol{b})}}{2}}\right), \tag{6.147}$$

with $\bar{k}(E) = \sqrt{E^2-m^2}$. The behavior of the complex poles of the propagator for $n = 4$ in the symmetric and antisymmetric sectors is shown in panels (b)-(c) of Figure 6.12.

We finally comment on the phenomenon of emergence of nonperturbative eigenstates for small values of md. Such poles appear when one of the complex poles with negative imaginary part in the second Riemann sheet approaches the real axis (see Figure 6.13). Due to the analytic properties of the resolvent, there is a symmetric pole of the analytic continuation

$$\Sigma_{j\ell}^{\mathrm{III}}(z) = \Sigma_{j\ell}(z) + \frac{2\mathrm{i}\gamma}{\sqrt{z^2-m^2}}\cos(|j-\ell|\theta(z)) \tag{6.148}$$

in the upper half-plane. At $d = d_c$ the two poles collide and coalesce at a point of the real axis. By further decreasing the spacing d, the two poles split up along the real axis and increase their energy difference.

The propagator analytic continuation yields a complete knowledge of metastable and unstable states decay rate through associated simple poles trajectories. In the regime of small distances, the no more negligible cut contribution in (6.137) and (6.145) allow us to observe the emergence of new eigenstates. The importance of high-energy eigenstate pairs should concern $n \gg 4$, which will be investigated in further develpments of the model including the coupling with more than a single bosonic mode.

Chapter 7

Spin waves and multimerization for many-body bound states

The unmanifest world is simple and linear, it is the manifest world which is 'folded' and nonlinear

Giuseppe Marmo,
XXI International Workshop on
Differential Geometric Methods
in Theoretical Mechanics, 2006

The Friedrichs-Lee model introduced with the Hamiltonian (1.18) is extended to an arbitrary number n of equally spaced qubits embedded in one-dimension with (6.1)-(6.3). It obeys the matricial structure in the one-excitation sector

$$H = \begin{pmatrix} \mathcal{E} & \langle \boldsymbol{F}| \\ |\boldsymbol{F}\rangle & \Omega \end{pmatrix}, \qquad |\psi\rangle = \begin{pmatrix} |\boldsymbol{a}\rangle \\ |\xi\rangle \end{pmatrix} \in \mathscr{H}^{(1)} = \mathbb{C}^n \oplus L^2(\mathbb{R}), \tag{7.1}$$

where $\mathcal{E} = \mathrm{diag}(\varepsilon, \ldots, \varepsilon)$ are excitation energies of the n identical two-level emitters, whose excitation amplitudes are expressed as $|\boldsymbol{a}\rangle = (a_1, \ldots, a_n) \in \mathbb{C}^n$ and $|\boldsymbol{F}\rangle$ is a row of form factors including plane wave phases in (6.3).

Actual experimental realizations of this model, like waveguide QED presented in Section 1.4, exploit the coupling with a single mode based on sufficiently large qubit spacing d. In this Chapter we provide a characterization of eigenstates in proximity of resonant eigenvalues, taking in account just the first cut contribution of the self-energy, according to their exponential suppression in the physical distance regime required for the model. In this approximation the self-energy matrix consists in a Laplacian of a regular graph associated with the one-dimensional lattice for diagonal blocks associated with the parity not

moving from the exact resonant condition. Instead, the remaining block will be displaced from the latter eigenvalues, whose matrix includes the projector onto the unstable state. In both cases the steady excitation amplitude profiles $|\boldsymbol{a}\rangle$ are expressed in terms of spin waves. The modes of these eigenstates have acoustic and optical branches, if nearest-neighbor qubits amplitudes are in phase and in its opposition respectively. Finally, the phenomenon of multimerization for systems consisting of an odd number of emitters is characterized according to the definition of subsystems separated by two lattice spacings not filled by the bosonic field and based on factorizations of the singularity condition.

7.1 Self-energy as a Toeplitz-Hankel matrix

The extension of the model for any number of qubit n is based on looking at (6.15) according to a complex integration perspective: to perform integration in the complex plane we can choose a closed contour lying in a half-plane, which guarantees convergence. This freedom of choice translates in a formulation of the self-energy matrix according to a symmetric Toeplitz pattern [62]

$$\Sigma_{j\ell}(z) = \Sigma_{|j-\ell|}(z), \tag{7.2}$$

where the definition of level shift operator (2.58) entails that interactions between each qubits pair, mediated by the electromagnetic field, only depends on their distance when they are equally spaced.

The original parity invariance of the Hamiltonian (6.3) translates into the introduction of a reflection matrix $\mathbb{J}$, defined with ones in the anti-diagonal, in the inverse propagator kernel (6.13) for the reduced qubit system. Indeed, given the property $\mathbb{J}\mathbb{J}^T = \mathbb{1}$, the reflected amplitudes array $\mathbb{J}\,|\boldsymbol{a}\rangle$ must belong to the kernel of the Hankel matrix $\mathrm{G}^{-1}\mathbb{J}$. This approach represents an algebraic way to perform the parity sector diagonalization (6.36) by exploiting the central symmetry of Toeplitz-Hankel eigenvectors [20].

The rearranged propagator expression (6.25) is valid in general for even dispersion relation $\omega(k)$ and form factor $F(k)$, whose complex extensions are analytic in a strip of the complex plane $\mathbb{R} \times (-m, m)$, with $m > 0$. In our particular case, when $\omega(k)$ is a monotone function for positive k, for energies in the continuum lying above the minimum value of $\omega(k)$, the pole equation $\omega(k) = E$ admits a single positive solution $k(E)$ [44].

To take into account the constraint (6.11) for eigenstates, let us introduce the following unit vectors, functions of the phase parameter that in waveguide QED reads $\theta(E) = d\sqrt{E^2 - m^2}$ and appearing in (6.25):

$$\left|\boldsymbol{e}^{\pm}(\theta)\right\rangle = \frac{1}{\sqrt{n}}\left(1, \mathrm{e}^{\pm \mathrm{i}\theta}, \mathrm{e}^{\pm 2\mathrm{i}\theta}, \ldots, \mathrm{e}^{\pm(n-1)\mathrm{i}\theta}\right), \tag{7.3}$$

such that (6.11) reads

$$\left\langle \boldsymbol{a} \middle| \boldsymbol{e}^{\pm}(\theta) \right\rangle = 0. \tag{7.4}$$

The vectors labeled by (±) in (7.3) coincide in resonance condition $\theta = \nu\pi, \nu \in \mathbb{N}$, representing the parity invariance for unstable super-radiant states characterized in Section 6.4.2. Making use of the constraint (7.4), we are free to subtract to $A_n(\theta, \chi, \boldsymbol{b})$ any matrix containing $|\boldsymbol{a}\rangle$ in its kernel, as:

$$\mathrm{i}\widetilde{A}_n(\theta, \chi, \boldsymbol{b}) = A_n(\theta, \chi, \boldsymbol{b}) - \frac{n}{2} \sum_{s=\pm} |\boldsymbol{e}^s(\theta)\rangle \langle \boldsymbol{e}^s(\theta)|, \tag{7.5}$$

yielding the real symmetric matrix

$$\left[\widetilde{A}_n(\theta, \chi, \boldsymbol{b})\right]_{j\ell} = \begin{cases} \chi, & \text{for } j = \ell \\ \sin\left(\left|j-\ell\right| \theta\right) + b_{|j-\ell|}, & \text{for } j \neq \ell \end{cases} \tag{7.6}$$

which by construction is characterized by a real eigensystem. In particular, the two constraints (7.4) are not independent, since one is the complex conjugate of the other. It is possible to use them singularly following the approach (7.5), as

$$\mathrm{i}\widetilde{A}^{u(l)}_n(\theta, \chi, \boldsymbol{b}) = A_n(\theta, \chi, \boldsymbol{b}) - n \left|\boldsymbol{e}^{\pm}(\theta)\right\rangle \left\langle \boldsymbol{e}^{\pm}(\theta)\right|, \tag{7.7}$$

such that an upper (lower) triangular transfer matrix is obtained in frequency representation, with the exception of unchanged cut contribution elements:

$$\left[\widetilde{A}^{u(l)}_n(\theta, \chi, \boldsymbol{b})\right]_{j\ell} = \begin{cases} \chi, & \text{for } j = \ell \\ 2\Theta\left(\pm\left(j-\ell\right)\right) \sin\left(\left|j-\ell\right| \theta\right) + b_{|j-\ell|}, & \text{for } j \neq \ell \end{cases} \tag{7.8}$$

thus providing a measure for the computational complexity in the determination of the eigensystem, with respect to the lowest one corresponding to triangular matrices, proportional to the number of included cut contributions and accompanied by the numerical integration resource demanding described in Section 6.4.1.

For $b_j \neq 0$, matrices in (6.36) are generally not simultaneously singular, thus implying that stable states in the system are either symmetric or antisymmetric under a reflection around the center of the array. This property is ultimately due to the presence of the b_j's and hence to the finite width of the analiticity strip [44]. Physically, this is caused by the presence of the exponential tails of the photon wavefunctions, which couple with all the qubits of the system, generally causing instability unless proper symmetry conditions are fulfilled. Moreover, depending on n being even or odd, one of the two blocks will still

be singular only if $e^{i\theta} = 1$ or $e^{i\theta} = -1$, i.e. in the same resonance condition of the case not endowed with cut contributions, whilst the other one will have singular elements displaced with respect to exact resonances.

In Section 7.2 we will prove that just the first cut term is sufficient to obtain the degeneracy lifting, with respect to the lowest complexity condition of triangular matrices not endowed with it, described in Section 6.3.3, which contains also less informations. In the description of the large distance regime, the exponentially suppressed behavior of (6.19) allows for applying a local interaction approximation, only involving nearest-neighbor qubits

$$\boldsymbol{b} = (b_1, \dots, b_{n-1}) \to (b, 0, \dots, 0). \tag{7.9}$$

Hence, in the following, we will omit the first cut contribution index. Through the definition of the kernel $\widetilde{A}_n |\boldsymbol{a}\rangle = 0$, it is possible to derive the recurrence relation

$$b(a_{j-1} + a_{j+1}) + \sum_{\ell=1}^{n} \left(g_{\ell-j} + f_{j-\ell}\right) a_\ell = -\chi a_j, \tag{7.10}$$

where $g_{\ell-j} = \Theta(\ell - j)\sin((\ell - j)\theta)$ and $f_{j-\ell} = \Theta(j - \ell - 1)\sin((j - \ell)\theta)$. In a practical perspective, the intrinsic appearance of convolutions leads us to the interpretation of the physical states constraint (6.11) as applied to the discrete Fourier transform (DFT)

$$\left\langle \boldsymbol{a} \middle| e^{\pm}(\theta) \right\rangle = \frac{1}{\sqrt{n}} \sum_{j=1}^{n} a_j \, e^{\pm i(j-1)\theta} = \hat{\boldsymbol{a}}(\theta), \tag{7.11}$$

whose vanishing value corresponds to a specific angle $\bar{\theta}$ associated with each non-degenerate eigenstate. The diagonalization procedure makes use of the presented transformation

$$a_{j-1} + a_{j+1} \xrightarrow{DFT} 2\cos(\theta)\hat{\boldsymbol{a}}(\theta) - \frac{1}{\sqrt{n}}\left(e^{\pm in\theta} a_n + e^{\mp i\theta} a_1\right), \tag{7.12}$$

obtained applying Dirichlet boundaries $a_0 = a_{n+1} = 0$ corresponding to fictitious nodes. Convolutions are reduced to simple products

$$\hat{f}(\theta) = \sum_{k=1}^{n} \sin(k\theta)\, e^{\pm i(k-1)\theta} = i\, \frac{e^{\mp i\theta} n \sin(\theta) - e^{\pm in\theta} \sin(n\theta)}{2\sin(\theta)}, \tag{7.13}$$

$$\hat{g}(\theta) = \sum_{k=-1}^{-n} \sin(k\theta)\, e^{\pm i(k-1)\theta} = i\, \frac{e^{\mp i\theta} n \sin(\theta) - e^{\mp in\theta} \sin(n\theta)}{2\sin(\theta)} - e^{\mp i(n+1)\theta} \sin(n\theta), \tag{7.14}$$

finally yielding

$$\hat{\boldsymbol{a}}(\theta) = \frac{b(e^{\pm in\theta}a_n + e^{\mp i\theta}a_1)}{2b\sqrt{n}\cos(\theta) + \sqrt{n}\,\chi + \hat{f}(\theta) + \hat{g}(\theta)}. \tag{7.15}$$

In case of eigenstates corresponding to resonances $\bar{\theta} = \nu\pi$, the functions in (7.13)-(7.14) vanish, such that the constraint $\hat{\boldsymbol{a}}(\nu\pi) = 0$ imposes $a_1 = -a_n$ for odd n, while, for even n, $a_1 = a_n$ ($a_1 = -a_n$) for odd (even) ν. Setting a vanishing cut contribution, this last characterization disappears, consistently with the degenerate nature of eigenspaces described in Section 6.3.3.

The inversion of the DFT is made according to

$$a_j = \int_0^{2\pi} \frac{\mathrm{d}\theta}{2\pi}\,\hat{\boldsymbol{a}}(\theta)\mathrm{e}^{\mp \mathrm{i}(j-1)\theta}, \tag{7.16}$$

which can be evaluated by analytic extension for $\theta \in \mathbb{C}$. The calculation of the residue is a hard task, given the required transcendental equation solution, even if it is possible to focus on eigenstates whose angle $\bar{\theta}$ coincides with an exact resonance, a familiar condition for experimental platforms as waveguide QED in its single mode realizations [4]. Neglecting the presence of vanishing convolutions for these eigenvalues, we obtain the following equation for poles

$$2b\cos\theta = \frac{\theta}{\gamma d}\left(\sqrt{\left(\frac{\theta}{d}\right)^2 + m^2} - \varepsilon\right) - \frac{\mathrm{sgn}\,(\mathrm{Re}(\theta))}{\pi}\mathrm{Log}\left(\frac{\mathrm{sgn}\,(\mathrm{Re}(\theta))\,\sqrt{\left(\frac{\theta}{d}\right)^2 + m^2} - \frac{\theta}{d}}{m}\right) \tag{7.17}$$

still belonging to the transcendental type. Some approximations, valid near the resonance condition, could simplify the solution, by neglecting the logarithm. We will apply algebraic methods which provide the exact eigensystem, thus circumventing these obstacles.

7.2 Spin waves

Eigenstates excitation amplitude profiles are ruled by spin waves, provided by the finite differences Laplacian of a one-dimensional lattice [22] associated with equally spaced qubits, whose spectrum defines a set of modes. In exact resonances they are related to the same eigenvalue, with negative parity for odd n and positive (negative) for odd (even) ν in case of even n. These states are always accompanied by eigenstates which will move from resonant conditions towards lower (higher) energies for odd (even) ν: each of them will be associated

with a different non-degenerate eigenvalue, showing a deformed spin wave profile. This mismatch is measured according to

$$\delta = 1 - \left\langle \boldsymbol{a} \middle| \tilde{\boldsymbol{a}} \right\rangle = \frac{1}{2} \|\tilde{\boldsymbol{a}} - \boldsymbol{a}\|_{\ell^2}\,, \tag{7.18}$$

where $|\tilde{\boldsymbol{a}}\rangle$ is the exact numerical eigenstate. As shown in Figure 7.1(a-b), it is characterized by a saturation behavior with respect to the number of quantum emitters, choosing a reference unit norm for spin waves. The mismatch is the same for each mode once they are ordered according to their sequence in moving from resonance conditions, so independently on the integer label ν and following the same curve in the variation of n. In a mean field perspective, based on the average of (7.18) per emitter, a convergence to undeformed spin waves is obtained, since $\delta/n \overset{n\to\infty}{\longrightarrow} 0$ [4].

A relevant characterization regards the presence of both acoustic and optical modes, swapping their role for the parity block moving from exact resonance condition: as shown in Figure 7.1(c-f), when we consider a subsequent resonance integer label ν, the first moving optical mode becames an acoustic one for even n, while viceversa for odd n. Their association with lower or higher energies is entailed by parity boundary conditions imposed at the chain center, as we will analyze in Section 7.2.1.

The spin-wave deformation in amplitude, shown in Figure 7.1 for exact eigenvectors $|\tilde{\boldsymbol{a}}\rangle$, is explained according to the physical states constraint. Applying the result of (7.5) concerning $|\tilde{\boldsymbol{a}}\rangle \in \mathbb{R}^n$, we can focus on the imaginary part of (6.11) and expand it for perturbations $\delta\theta$ close to the exact resonances, yielding

$$\sum_{j=1}^{n} \tilde{a}_j (j-1)\delta\theta = 0, \quad \sum_{j=1}^{n} \tilde{a}_j (-1)^{j-1}(j-1)\delta\theta = 0, \tag{7.19}$$

respectively for even (odd) ν. Imposing the parity symmetry, these results motivate the linearly increasing profile mismatch from chain extrema, followed by a number of oscillations corresponding to the mode ordering with respect to the "angular" distance from exact resonance (see Figure 7.1(g-h)).

7.2.1 One-dimensional regular graph Laplacian matrix

The structure of the self-energy diagonal block, associated with eigenstates in resonance condition, stable with respect to the introduction of the cut contribution and obtained through the nearest-neighbors interaction (7.9), corresponds to the one defined by the Laplacian matrix for a one-dimensional regular graph [22, 27]. This description allows us to study the excitation amplitude profile $|\boldsymbol{a}\rangle$ in the spin waves framework, thus including acoustic and optical modes.

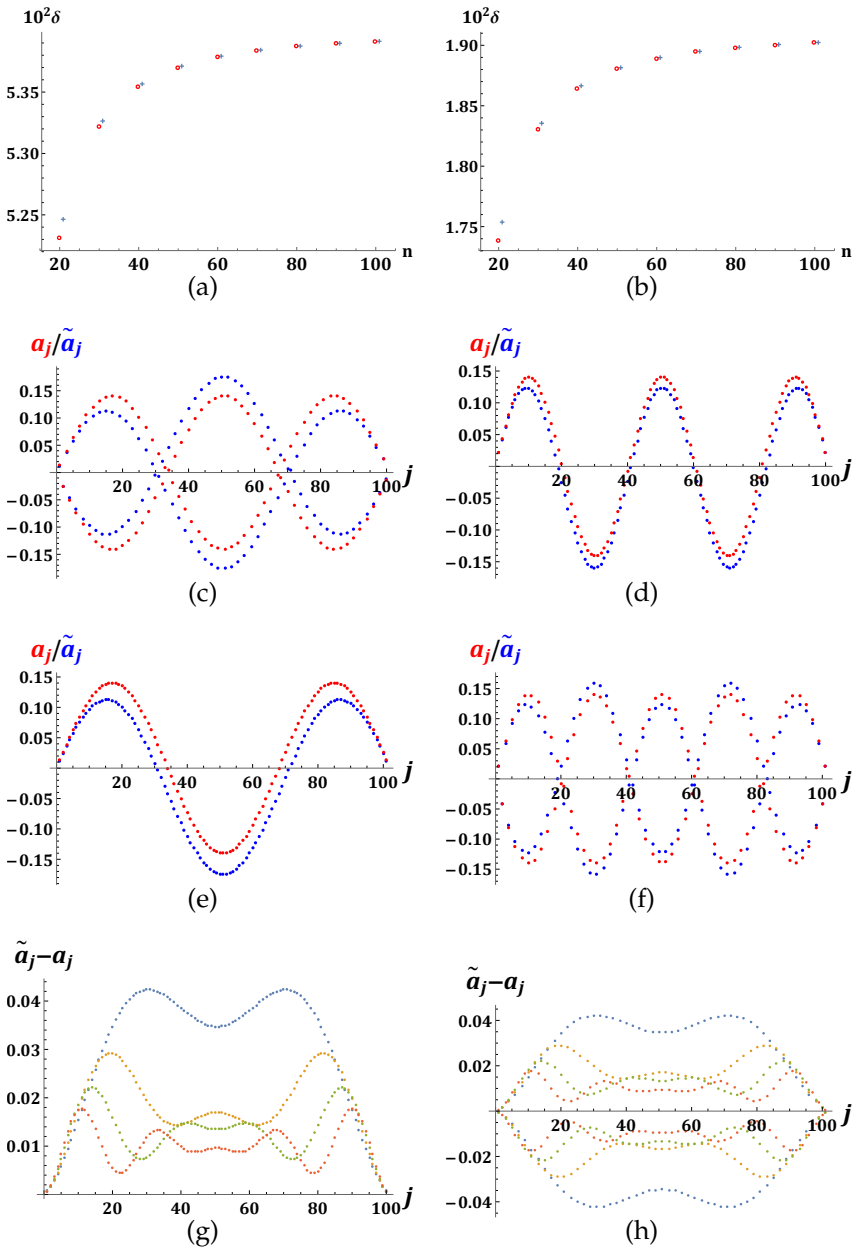

Figure 7.1: Panels (a)-(b): Eigenstates mismatch (7.18), respectively for the first and second mode in (7.25)-(7.30)-(7.35): red circles represent even n and blue crosses odd n. Panels (c)-(d): first and second mode for $n = 100$ and $\nu = 1$ and $\nu = 2$, while viceversa concerning panels (e)-(f) for $n = 101$ with first and second mode in $\nu = 2$ and $\nu = 1$ respectively. Panel (g) mismatches of the first (blue), second (orange), third (green) and fourth mode (red), with $n = 100$ and $\nu = 2$, where the absolute value coincides for $\nu = 1$, as verified for $n = 101$ in panel (h). Model parameters are $md = 7$ and $\gamma/m^2 = 2\pi \times 10^{-4}$.

As already characterized for the inverse propagator (6.33), also the self-energy matrix decomposes according to

$$\mathcal{U}_n \, \Sigma_n(\varphi) \, \mathcal{U}_n^\dagger = \Sigma^-_{\lfloor n/2 \rfloor}(\varphi) \oplus \Sigma^+_{\lceil n/2 \rceil}(\varphi), \tag{7.20}$$

where we define $\Sigma_n(\varphi) = -\frac{\mathrm{i}}{b}\Sigma(E)$, with $\varphi = \frac{b_0}{2b}$, thus considering a matrix with elements measured according to the energy scale of the first cut contribution b, whose stable blocks in case $n = 2h+1$ correspond to $\Sigma^-_h(\varphi)$ in resonance conditions, while, in case $n = 2h$, $\Sigma^\pm_h(\varphi)$ for respectively $\mathrm{e}^{\mathrm{i}\theta} = \mp 1$. Now we are looking at the reduced system composed by emitters in its associated amplitude profiles, which is not influenced by the considered eigenvalue E_ν, but just by the associated "stable" parity.

The Laplacian matrix Δ acts on functions a_ℓ, with $\ell = 1, \ldots, h$, sampled in a one-dimensional lattice, with the aim of implementing finite differences

$$\Delta a_\ell = a_{\ell+1} + a_{\ell-1} - 2a_\ell, \tag{7.21}$$

where the lattice spacing is the unit. Boundary conditions are implemented by means of fictitious nodes corresponding to $\ell = 0, h+1$ [78], in order to preserve the notion of regular graph. The antisymmetric block for a system consisting of an odd number of emitters mimics pure Dirichlet boundary conditions in both lattice ends, $a_0 = a_{h+1} = 0$, while blocks for even n implement mixed Dirichlet-(anti)Neumann boundaries, $a_0 = 0$ and $a_{\frac{n}{2}} = a_{\frac{n}{2}+1}$ ($a_{\frac{n}{2}} = -a_{\frac{n}{2}+1}$), alternatively in the stable parity, thus concerning odd (even) ν.

The translation of (7.21) into the graph framework encodes in an adiacency matrix the super- and sub-diagonal elements implementing the excitation hopping, so taking into account the edge number between each pair of vertices, in our system corresponding to quantum emitters, minus a diagonal matrix whose elements report each vertex degree, which is equal to its number of edges.

Let us start with the analysis of systems endowed with $n = 2h+1$, where the rescaled self-energy antisymmetric block reads

$$\Sigma^-_h(\varphi) = \begin{pmatrix} 2\varphi & 1 & & & \\ 1 & 2\varphi & 1 & & \\ & \ddots & \ddots & \ddots & \\ & & 1 & 2\varphi & 1 \\ & & & 1 & 2\varphi \end{pmatrix}, \tag{7.22}$$

which implements a recurrence relation for the associated eigenfunctions, solved by Chebyshev polynomials of the second kind [126], thus yielding

$$a^{(j)}_\ell = U_{\ell-1}\left(-\varphi + \frac{\lambda_j}{2}\right). \tag{7.23}$$

Given the absence of a singularity condition involving the positive parity block, the action of the considered "stable in resonance" block involves excitation amplitudes associated with the first h qubits, with the $(h+1)$-th qubit working as a dynamical mirror, thus implementing a Dirichlet boundary because it represents a fictitious node. Indeed, the spectrum is provided by the encoded boundary in the last diagonal element, translated in $a^{(j)}_{h+1} = U_h\left(\frac{\lambda_j}{2}\right) = 0$, assuming $\varphi = 0$, which represents just a translation for the spectrum, in correspondence with the associated singularity condition of the inverse propagator, analyzed in Section 7.3. The degeneracy lifting made by cut contributions, results here in a straightforward relation with simple roots of Chebyshev polynomials.

In the case of Dirichlet condition on both the extreme ficititious nodes of a lattice with h sites ($a_0 = a_{h+1} = 0$), eigenvalues and eigenvectors of the Laplacian matrix are given by

$$\lambda_j = -4\sin^2\left(\frac{j\pi}{2(h+1)}\right), \tag{7.24}$$

$$a^{(j)}_\ell = \sqrt{\frac{2}{h+1}}\sin\left(\frac{j\pi}{h+1}\ell\right), \tag{7.25}$$

with $j, \ell = 1, \ldots, h$ and where the excitation amplitude profile has been normalized to unity in its ℓ^2 norm on the half chain [22]. These expressions map exactly our acoustic and optical spin waves spectrum, just imposing a translation equal to 2 for eigenvalues λ_j to remove the "potential" caused by lattice vertices degree. This appraoch has straightforward extensions concerning sublattices involved in cases with an odd h, where the excitation may be trapped in multi-excitations sectors, thus giving rise to multimers [103] (see Section 7.3).

The same analysis is applied for systems characterized by $n = 2h$, even if new boundary conditions have to be included, according to the self-energy matrix:

$$\Sigma^{\pm}_h(\varphi) = \begin{pmatrix} 2\varphi & 1 & & & \\ 1 & 2\varphi & 1 & & \\ & \ddots & \ddots & \ddots & \\ & & 1 & 2\varphi & 1 \\ & & & 1 & 2\varphi \pm 1 \end{pmatrix}, \tag{7.26}$$

up to the overall spectrum translation φ, translated in:

$$a^{(j)}_{h+1} \mp a^{(j)}_h = U_h\left(\frac{\lambda_j}{2}\right) \mp U_{h-1}\left(\frac{\lambda_j}{2}\right) = 0, \tag{7.27}$$

which provides the spectrum. The parity of the stable block is imposed by $e^{i\theta} = \pm 1$: antisymmetric eigenstates are associated with $e^{i\theta} = 1$, while the

symmetric case concerns the remaining value. The latter is described by $\Sigma_h^+(\varphi)$ in (7.26), encoding a mixed Dirichlet-Neumann boundary condition for the Laplacian, implemented through $a_0 = 0$, $a_h = a_{h+1}$:

$$\Delta a_h = a_{h-1} - a_h, \tag{7.28}$$

whose eigensystem reads as follows:

$$\lambda_j = -4\sin^2\left(\frac{\left(j-\frac{1}{2}\right)\pi}{2h+1}\right), \tag{7.29}$$

$$a_\ell^{(j)} = \sqrt{\frac{2}{h+\frac{1}{2}}}\sin\left(\frac{2\left(j-\frac{1}{2}\right)\pi}{2h+1}\ell\right), \tag{7.30}$$

again requiring a translation equal to 2 for the spectrum to balance nodes degree potential. This spectrum is provided by the Neumann condition:

$$U_h\left(\frac{\lambda_j}{2}\right) - U_{h-1}\left(\frac{\lambda_j}{2}\right) = \frac{4\cos\left((h+\frac{1}{2})\arccos\frac{\lambda_j}{2}\right)\sin\left(\frac{1}{2}\arccos\frac{\lambda_j}{2}\right)}{\sqrt{4-\lambda_j^2}} = 0. \tag{7.31}$$

The analysis of antisymmetric blocks, regarding $\Sigma_h^-(\varphi)$ in (7.26), is less trivial because the Laplacian now includes $a_0 = 0$, $a_h = -a_{h+1}$ such that:

$$\Delta a_h = a_{h-1} - 3a_h, \tag{7.32}$$

which we are calling the anti-Neumann boundary condition, encoded in the first antisymmetric qubit of the second half of the chain. The Laplacian is endowed with an opposite spectrum with respect to the latter case, because of the new boundary condition:

$$U_h\left(\frac{\lambda_j}{2}\right) + U_{h-1}\left(\frac{\lambda_j}{2}\right) = \frac{4\sin\left((h+\frac{1}{2})\arccos\frac{\lambda_j}{2}\right)\cos\left(\frac{1}{2}\arccos\frac{\lambda_j}{2}\right)}{\sqrt{4-\lambda_j^2}} = 0, \tag{7.33}$$

which implies the opposite spectrum by means of decreasing eigenvalues ordering

$$\lambda_j = 2\cos\left(\frac{2\pi(h+1-j)}{2h+1}\right) = -2\cos\left(\frac{2\pi(j-\frac{1}{2})}{2h+1}\right). \tag{7.34}$$

This sign causes the appearance of an alternating sign factor in (7.30) for Dirichlet-anti-Neumann eigenvectors:

$$a_\ell^{(j)} = \sqrt{\frac{2}{h+\frac{1}{2}}}(-1)^{\ell+1}\sin\left(\frac{2\left(j-\frac{1}{2}\right)\pi}{2h+1}\ell\right), \tag{7.35}$$

thus acoustic spin waves will present a node between central qubits, while optical modes easily obey to the anti-Neumann boundary.

The knowledge of Laplacian spectra allows us to deduce a one to one correspondence between eigenvalues λ_j and the bare emitters energy ε through the definition of the inverse propagator kernel, with fixed coupling constant γ

$$\varepsilon = E_\nu + \frac{\gamma b(E_\nu)}{\sqrt{E_\nu^2 - m^2}}\lambda_j + \frac{\gamma b_0(E_\nu)}{\sqrt{E_\nu^2 - m^2}}, \tag{7.36}$$

thus selecting each spin wave mode.

7.2.2 Rank-one modification of the symmetric eigenproblem

The self-energy diagonal block associated with states moving from exact resonance conditions consists in the Laplacian endowed of a certain boundary induced by parity plus a dyadic product, which corresponds to the projector on the unstable super-radiant state [15, 57].

Let us consider the system with $n = 2h$ and the associated self-energy matrix decomposition in parity sectors as a function of the first cut contribution parameter b

$$\widetilde{\Sigma}^{\mp}(b) = b\Sigma^{\mp}(\varphi) - 2h\mathrm{i}\,\left|\boldsymbol{u}^{\mp}\right\rangle\left\langle\boldsymbol{u}^{\mp}\right| = b\begin{pmatrix} 2\varphi \mp 1 & 1 & & & \\ 1 & 2\varphi & 1 & & \\ & \ddots & \ddots & \ddots & \\ & & 1 & 2\varphi & 1 \\ & & & 1 & 2\varphi \end{pmatrix} - 2h\mathrm{i}\,\left|\boldsymbol{u}^{\mp}\right\rangle\left\langle\boldsymbol{u}^{\mp}\right|, \tag{7.37}$$

where $\Sigma^{\pm}(\varphi)$ corresponds to the Laplacian matrix for stable in resonance eigenstates, while $\widetilde{\Sigma}^{\mp}(b)$ describes eigenstates associated with eigenvalues moving from resonance and $|\boldsymbol{u}^{\pm}\rangle = \frac{1}{\sqrt{h}}(1, \pm 1, \dots)^T$ represents the unstable super-radiant W state, thus corresponding to $|\boldsymbol{e}(\nu\pi)\rangle$ respectively for odd (even) ν. The last block is an approximation because we are neglecting phase perturbation in $\theta(E) = d\sqrt{E^2 - m^2}$ from the exact resonance condition. We recognize that, in absence of perturbations, $\widetilde{\Sigma}^{\mp}(0)$ shows $h-1$ degenerate eigenstates, thus corresponding to an exceptional point $b = 0$ [80]. We will see that the computation of

the eigensystem for rank-one modifications [15, 57] is characterized analytically according to a well approximating ansatz for the secular equation.

Eigenpairs obtained in the approximate exact resonance condition are deduced according to formulas in [15, 57], whose calculations are based on a real parameter weighting the dyadic product contribution, while we adapt the scheme for the purely imaginary case. To deduce our extended approach let us start with the equivalent system, dealing with the more general inverse problem [15]

$$\begin{pmatrix} \Lambda - \tilde{\lambda}_j \mathbb{1} & |\boldsymbol{z}\rangle \\ \langle \boldsymbol{z}| & \frac{1}{\mathrm{i}n} \end{pmatrix} \begin{pmatrix} \left|\boldsymbol{\alpha}_j\right\rangle \\ \beta \end{pmatrix} = \begin{pmatrix} |\boldsymbol{v}\rangle \\ 0 \end{pmatrix}, \tag{7.38}$$

where Λ is a diagonal matrix, whose elements are eigenvalues λ_j associated with eigenvectors $\left|\boldsymbol{\alpha}_j\right\rangle$. The solution is expressed by

$$\left|\boldsymbol{\alpha}_j\right\rangle = \left[\frac{1}{\Lambda - \tilde{\lambda}_j \mathbb{1}} - \left(\left\langle \boldsymbol{z}\right| \frac{1}{\Lambda - \tilde{\lambda}_j \mathbb{1}} \left|\boldsymbol{z}\right\rangle - \frac{1}{\mathrm{i}n}\right)^{-1} \frac{1}{\Lambda - \tilde{\lambda}_j \mathbb{1}} |\boldsymbol{z}\rangle \langle \boldsymbol{z}| \frac{1}{\Lambda - \tilde{\lambda}_j \mathbb{1}}\right] |\boldsymbol{v}\rangle . \tag{7.39}$$

To avoid a vanishing eigenvector in our case, which concerns $|\boldsymbol{v}\rangle = 0$, we have to examine the propagator:

$$\widetilde{G}\left(\tilde{\lambda}_j\right) = \left(\Lambda - \tilde{\lambda}_j \mathbb{1} - \mathrm{i}\, n\ |\boldsymbol{z}\rangle \langle \boldsymbol{z}|\right)^{-1}, \tag{7.40}$$

corresponding to its poles. This translates in the determination of a singularity condition, given the research for eigenvectors belonging to its kernel. Eigenvalues satisfying this requirement are deduced exploiting the matrix determinant lemma [57]

$$\det \widetilde{G}\left(\tilde{\lambda}_j\right) = \prod_{i=1}^{n} \left(\lambda_i - \tilde{\lambda}_j\right) \left(1 - \mathrm{i}\, n \sum_{i=1}^{n} \frac{\zeta_i^2}{\lambda_i - \tilde{\lambda}_j}\right), \tag{7.41}$$

thus providing the secular equation. Eigenvectors are expressed by (7.39), where the first term is absent for $|\boldsymbol{v}\rangle = 0$, while the second one is indeterminate when examined corresponding to eigenvalues given by (7.41). In this way it is possible to consider directly the solution given by (7.38), defined up to a normalization constant:

$$\left|\boldsymbol{\alpha}_j\right\rangle = -\beta \left(\Lambda - \tilde{\lambda}_j \mathbb{1}\right)^{-1} |\boldsymbol{z}\rangle , \tag{7.42}$$

representing the Bunch-Nielsen-Sørensen formula [15].

This approach will be applied in a straightforward way to obtain spin waves deformation, keeping in mind that we measured Laplacian eigenvalues in cut contribution units, as expressed in (7.36). The latter energy scale will be adopted also for eigenvalues perturbation, so from now on $\widetilde{\Sigma}$ will not dependend on it.

The self-energy Laplacian in (7.37) is diagonalized according to:

$$\Sigma^{\pm}(\varphi) = \Xi^{\pm}\Lambda^{\pm}\left(\Xi^{\pm}\right)^{T}, \tag{7.43}$$

which induces the same rotation for unstable super-radiant state involved in the dyadic product:

$$\widetilde{\Sigma}^{\pm} = \Xi^{\pm}\left(\Lambda^{\pm} - 2h\mathrm{i}\,\left|z^{\pm}\right\rangle\left\langle z^{\pm}\right|\right)\left(\Xi^{\pm}\right)^{T} = \widetilde{\Xi}^{\pm}\widetilde{\Lambda}^{\pm}\left(\widetilde{\Xi}^{\pm}\right)^{T}, \tag{7.44}$$

where $|z^{\pm}\rangle = \left(\Xi^{\pm}\right)^{T}|u^{\pm}\rangle = \left(\zeta_1^{\pm}, \zeta_2^{\pm}, \ldots\right)$, with components:

$$\zeta_{\ell}^{\pm} = \left\langle u^{\pm}\middle|a_{\ell}^{\pm}\right\rangle = \pm\sqrt{\frac{2}{h\left(h+\frac{1}{2}\right)}}\,U_h\left(\cos\left(\frac{\pi\left(\ell-\frac{1}{2}\right)}{2h+1}\right)\right)\sin\left(\frac{\pi\left(\ell-\frac{1}{2}\right)}{2h+1}h\right). \tag{7.45}$$

The determination of eigenvalues resides in the solution of the secular equation

$$w(\mu_j^{\pm}) = 1 - 2h\mathrm{i}\sum_{\ell=1}^{h}\frac{\left(\zeta_{\ell}^{\pm}\right)^2}{\lambda_{\ell}^{\pm} - \tilde{\lambda}_j^{\pm}} = 0, \tag{7.46}$$

where $\tilde{\lambda}_j^{\pm} = \lambda_j^{\pm} - 2h\mathrm{i}\,\mu_j^{\pm}$. Eigenvectors of $\tilde{\Lambda}^{\pm}$ obey the expression

$$\left|\alpha_j^{\pm}\right\rangle = \left(\Lambda^{\pm} - \tilde{\lambda}_j^{\pm}\mathbb{1}\right)^{-1}\left|z^{\pm}\right\rangle, \tag{7.47}$$

with $\left|\tilde{a}_j^{\pm}\right\rangle = \Xi^{\pm}\left|\alpha_j^{\pm}\right\rangle$ [15, 57]. Our ansatz assumes solutions of (7.46) in the form

$$\bar{\mu}_j^{\pm} = \pm\mathrm{i}\,\frac{\sin\left(\frac{2\pi\left(j-\frac{1}{2}\right)}{2h+1}(h+1)\right)\sin\left(\frac{2\pi\left(j-\frac{1}{2}\right)}{2h+1}h\right)}{2h^2\left(h+\frac{1}{2}\right)}, \tag{7.48}$$

with the plus (minus) sign holding for even (odd) ν. The application of (7.48) in (7.47) provides $\left|\bar{\alpha}_j^{\pm}\right\rangle$, whose rotation is composed by spin wave modes associated with exact resonances in Ξ is

$$\begin{aligned}\left|\bar{a}_j^{\pm}\right\rangle = \sum_{k=1}^{h}(\pm1)^{k+1}\Bigg(&\mp2\sqrt{h}\frac{U_h\left(\cos\left(\frac{\pi\left(j-\frac{1}{2}\right)}{2h+1}\right)\right)\sin\left(\frac{\pi\left(j-\frac{1}{2}\right)}{2h+1}h\right)}{\sin\left(\frac{2\pi\left(j-\frac{1}{2}\right)}{2h+1}(h+1)\right)\sin\left(\frac{2\pi\left(j-\frac{1}{2}\right)}{2h+1}h\right)}\sin\left(\frac{2\pi\left(j-\frac{1}{2}\right)}{2h+1}k\right)\\ &\mp\sum_{\ell\neq j}\frac{U_h\left(\cos\left(\frac{\pi\left(\ell-\frac{1}{2}\right)}{2h+1}\right)\right)\sin\left(\frac{\pi\left(\ell-\frac{1}{2}\right)}{2h+1}h\right)\frac{1}{\sqrt{h}\left(h+\frac{1}{2}\right)}\sin\left(\frac{2\pi\left(\ell-\frac{1}{2}\right)}{2h+1}k\right)}{\sin\left(\frac{\pi\left(\ell+j-1\right)}{2h+1}\right)\sin\left(\frac{\pi\left(\ell-j\right)}{2h+1}\right) - \frac{1}{2h\left(h+\frac{1}{2}\right)}\sin\left(\frac{2\pi\left(j-\frac{1}{2}\right)}{2h+1}(h+1)\right)\sin\left(\frac{2\pi\left(j-\frac{1}{2}\right)}{2h+1}h\right)}\Bigg)|E_k\rangle,\end{aligned} \tag{7.49}$$

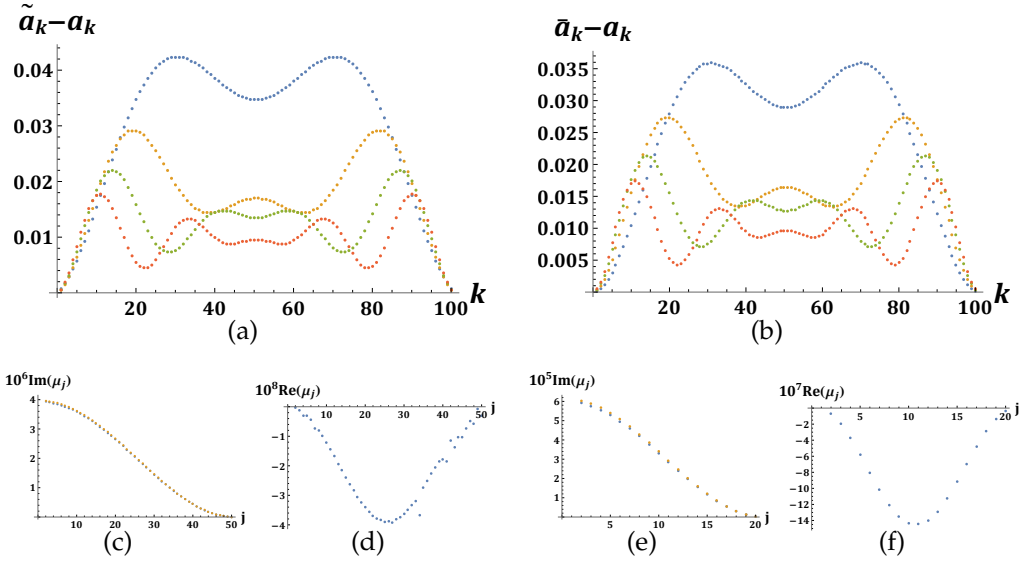

Figure 7.2: In panel (c) orange points coincide with (7.48), while the underlying blue ones represent exact imaginary parts of numerical roots for μ_j in (7.46), whose much smaller real parts is plotted in (d). The real part of the distance of associated eigenvectors (7.50) with respect to spin waves (7.30) for $j = 2, 3, 4, 5$ (blue, orange, green, red) is shown in panel (b), which coincide with Figure 7.1(g). Same eigenvectors distance with purely imaginary numerical μ_j is shown in (a). A more stable numerical research for $h = 20$ is plotted in (e-f).

representing deformed spin waves, up to an overall normalization constant.

As discussed in Appendix B, the numerical root research for (7.46) through the Newton method allows us to implement exact eigenpairs: in this way it is possible to check how much the hypothesis concerning super-radiant eigenvectors involved in the dyadic product without any phase perturbation is correct. At the basis of (7.48) there is the imposition of real eigenvectors, but this is not true even at the numerical step in Figure 7.1, where we are neglecting a much smaller imaginary contribution, weighted by the neglected phase perturbation in the dyadic product. Finally, we verified numerically that solutions of (7.46) coincide with the ones associated with just the sum in it, thus neglecting the unit, which guarantee a safe measure of eigenvalue in cut contribution units.

Let us consider the general formula for eigenvectors associated with a rank-one modification of a Laplacian eigenproblem with $n = 2h$:

$$\left|\tilde{a}_j^{\pm}\right\rangle = \sqrt{\frac{2}{h+\frac{1}{2}}} \sum_{k=1}^{h} \left(\frac{\zeta_j^{\pm}}{2hi\mu_j^{\pm}} \sin\left(\frac{2\left(j-\frac{1}{2}\right)\pi}{2h+1} k \right) + \sum_{\ell \neq j} \frac{\zeta_\ell^{\pm} \sin\left(\frac{2\left(\ell-\frac{1}{2}\right)\pi}{2h+1} k \right)}{\lambda_\ell - \lambda_j + 2hi\mu_j^{\pm}} \right) |E_k\rangle\,, \quad (7.50)$$

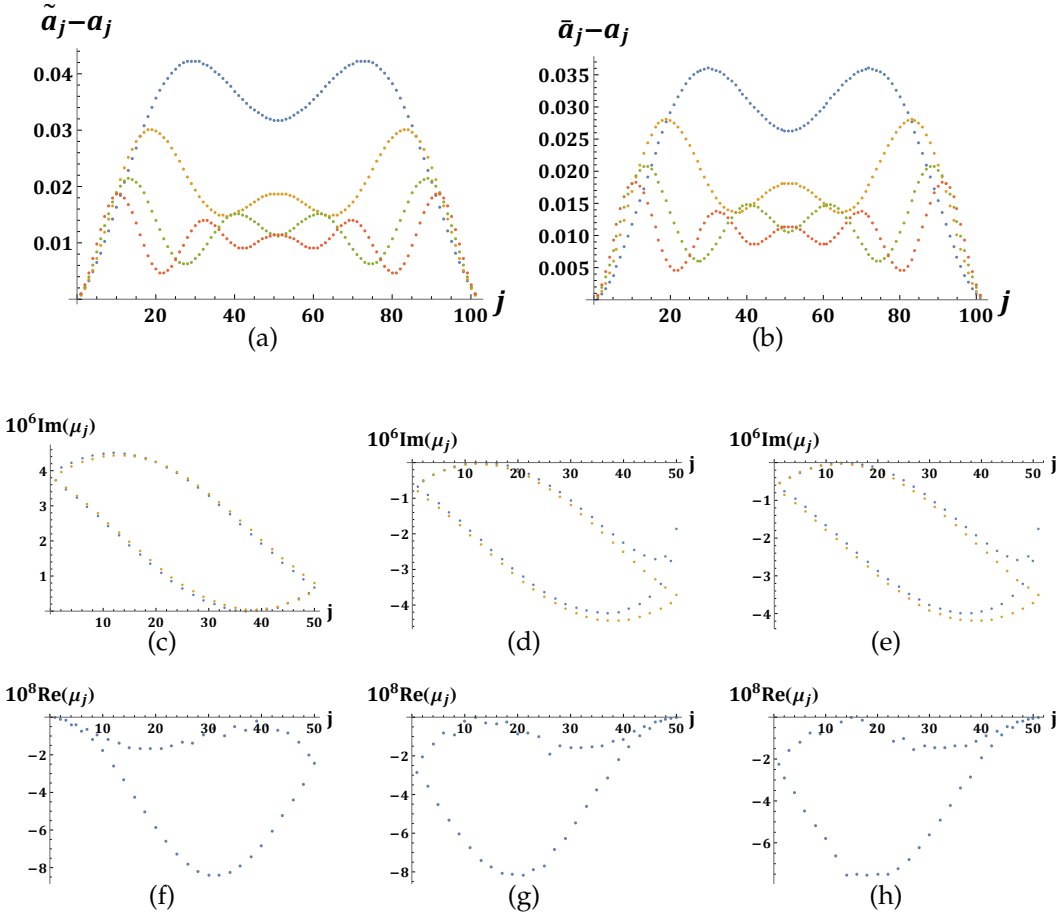

Figure 7.3: In panel (c) orange points coincide with (7.58), while the underlying blue ones represent exact imaginary parts of numerical roots for μ_j in (7.46), whose much smaller real parts is plotted in (f), for even ν, $h = 50$. The real part of the distance of associated eigenvectors (7.56) with respect to spin waves (7.25) for $j = 2, 3, 4, 5$ (blue, orange, green, red) is shown in panel (a), which coincide with exact diagonalization results. Same eigenvectors distance with purely imaginary numerical μ_j is shown in (b). The same spectrum in (c) and (f) is plotted in (d-g) for odd ν, $h = 50$, while for odd ν, $h = 51$ in (e-h).

which, for exact $\mu_j \in \mathbb{C}$, coincides with the result of numerical diagonalization, as shown in Figure 7.2. In this analysis $j = 1$ is associated with the super-radiant eigenvector. Neglecting real parts of numerical μ_j results in eigenvectors approximately identical to the ones obtained through the ansatz (7.48), as shown in Figure 7.2(d) and Figure 7.4(a), because imaginary parts of μ_j are well represented in particular for higher values of n.

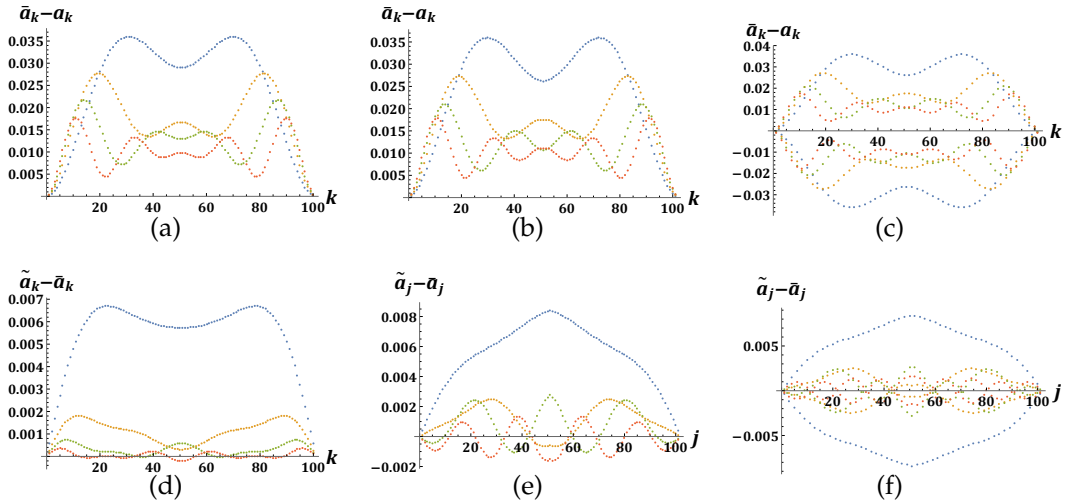

Figure 7.4: Deformed spin waves mismatch, respectively for the ansatz and spin waves in exact resonance conditions in panels (a-c) or numerical exact eigenvectors in panels (d-f), of the first (blue), second (orange), third (green) and fourth mode (red). In (a)-(d) $n = 100$ and $\nu = 2$, $n = 101$ and $\nu = 2$ in (b)-(e), $n = 101$ and $\nu = 1$ in (c)-(f). Model parameters are $md = 7$ and $\gamma/m^2 = 2\pi \times 10^{-4}$.

This framework is applied for systems with $n = 2h + 1$, whose self-energy diagonal block $\widetilde{\Sigma}^+ = \Sigma^+_{h+1}(\varphi) - (2h+1)\,\mathrm{i}\,|\boldsymbol{u}^\nu\rangle\langle\boldsymbol{u}^\nu|$, with the Laplacian part in the form (as the inverse propagator (7.74))

$$\Sigma^+_{h+1}(\varphi) = \begin{pmatrix} 2\varphi & 1 & & & & & \\ 1 & 2\varphi & 1 & & & & \\ & \ddots & \ddots & \ddots & & & \\ & & 1 & 2\varphi & 1 & & \\ & & & 1 & 2\varphi & \sqrt{2} & \\ & & & & \sqrt{2} & 2\varphi \end{pmatrix}, \tag{7.51}$$

and with $|\boldsymbol{u}^\nu\rangle = \frac{1}{\sqrt{n}}\left(\sqrt{2}, \pm\sqrt{2}, \ldots, (\pm 1)^{h-1}\sqrt{2}, (\pm 1)^h\right)^T$ depending on even (odd) ν, with matching dimensions $(h+1)\times 1$.

The eigensystem of the Laplacian (7.51) is easily characterized considering the known structure for the $h\times h$ block not including the central qubit: eigenvectors are determined up to the global spectrum translation φ, with a boundary condition skipping the central emitter, in such a way to mimic the singularity condition of (7.74)

$$T_{h+1}\left(\frac{\lambda_j}{2}\right) = U_{h+1}\left(\frac{\lambda_j}{2}\right) - U_{h-1}\left(\frac{\lambda_j}{2}\right) = 0, \tag{7.52}$$

which allows us to deduce eigenvalues through the imposition of a boundary intrinsincally present in the singularity condition:

$$\frac{4\cos\left((h+1)\arccos\frac{\lambda_j}{2}\right)\sin\left(\arccos\frac{\lambda_j}{2}\right)}{\sqrt{4-\lambda_j^2}}=0. \tag{7.53}$$

Applying again the translation to avoid vertices degree potential, eigenpairs are determined as follows:

$$\lambda_j = -4\sin^2\left(\frac{\left(j-\frac{1}{2}\right)\pi}{2h+2}\right), \tag{7.54}$$

$$a_\ell^{(j)} = \sqrt{\frac{2}{h+1}}\sin\left(\frac{\left(j-\frac{1}{2}\right)\pi}{h+1}\ell\right), \tag{7.55}$$

with a symmetric reflection just involving the first h amplitudes (see Figure 7.1(e-f)), thus following (7.29)-(7.30) for the even n case.

The Laplacian eigensystem is determined to apply the procedure for rank-one modifications, whose eigenvectors are expressed in the general form (7.47), which explicitly reads

$$\left|\tilde{\boldsymbol{a}}_j^{\nu,h}\right\rangle = \sqrt{\frac{2}{h+1}}\sum_{k=1}^{h+1}\left(\frac{\zeta_j^{\nu,h}\sin\left(\frac{\left(j-\frac{1}{2}\right)\pi}{h+1}k\right)}{(2h+1)\mathrm{i}\mu_j^{\nu,h}}+\sum_{\ell\neq j}\frac{\zeta_\ell^{\nu,h}\sin\left(\frac{\left(\ell-\frac{1}{2}\right)\pi}{h+1}k\right)}{\lambda_\ell-\lambda_j+(2h+1)\mathrm{i}\mu_j^{\nu,h}}\right)|E_k\rangle \tag{7.56}$$

where there is a dependence in both ν and h for the odd n case. The ratio between spin waves and deformations is strongly influenced by eigenvalues corrections $\mu_j^{\nu,h}$. Components of rotated vectors in the dyadic product are

$$\zeta_\ell^{\nu,h} = \sqrt{\frac{2}{(2h+1)(h+1)}} \tag{7.57}$$
$$\times\left[(\pm1)^h\sin\left(\left(\ell-\frac{1}{2}\right)\pi\right)+\sqrt{2}\begin{cases}U_h\left(\cos\left(\frac{\pi\left(\ell-\frac{1}{2}\right)}{2h+2}\right)\right)\sin\left(\frac{\pi\left(\ell-\frac{1}{2}\right)}{2h+2}h\right) & \text{even } \nu,\\ -\frac{\sin\left(\frac{\pi\left(\ell-\frac{1}{2}\right)}{2h+2}h\right)\cos\left(\frac{\pi}{2}\left(\ell-\frac{1}{2}\right)\right)}{\cos\left(\frac{\pi\left(\ell-\frac{1}{2}\right)}{2h+2}\right)} & \text{odd } \nu,\ \text{even } h,\\ \frac{\cos\left(\frac{\pi\left(\ell-\frac{1}{2}\right)}{2h+2}h\right)\sin\left(\frac{\pi}{2}\left(\ell-\frac{1}{2}\right)\right)}{\cos\left(\frac{\pi\left(\ell-\frac{1}{2}\right)}{2h+2}\right)} & \text{odd } \nu,\ \text{odd } h,\end{cases}\right],$$

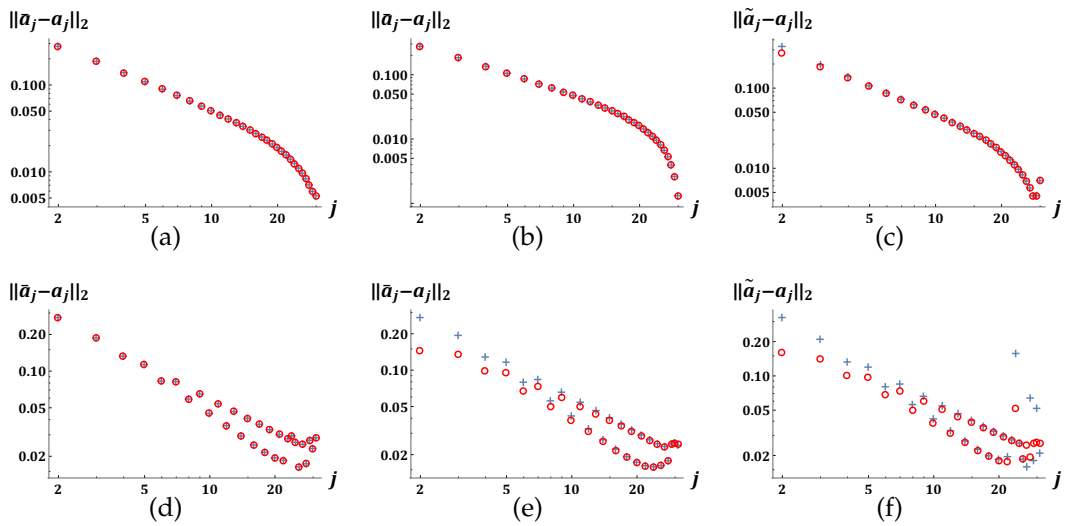

Figure 7.5: Distance between our conjectured deformed spin-waves (using (7.48)) and the eigenvectors in exact resonance condition, for $\nu = 1$ (disks) and $\nu = 2$ (crosses) of a system with $h = 30$ in panel (a) for $n = 2h$. In (b) the same behavior is plotted for (7.50) with purely imaginary numerical μ_j, while exact complex solutions are involved in (c). Same case are plotted in (d-f) for $n = 2h + 1$, where (d) is based on (7.58).

for respectively even (odd) ν. These expressions are much more hard to be analyzed with respect to the even n case, our ansatz for the odd n case reads

$$\mu_j^{\nu,h} = -\frac{81}{100}\frac{(-1)^j \cos\left(\frac{h+\frac{1}{2}}{h+1}\left(2j-\frac{1}{2}\right)\pi\right) - \cos\left(\frac{2j-\frac{1}{2}}{2h+2}\pi\right) - \frac{36}{25}}{(h+1)(2h+1)^2} \tag{7.58}$$

where for odd ν we have just to take the opposite sign in the reverse j ordering (see Figure 7.3). The requirement for an explicit mode label j dependence, instead of a constant estimation, is annealed in the research of an higher precision for modes moving less fastly from exact resonance conditions. These algebraic expressions aim at providing an easier experimental interface with respect to the application of numerical complex functions $w(\mu_j)$ roots research through Newton method, even if this will be the preferred way for system consisting of low number of emitters (up to approximately $h = 20$). The different behavior in Figure 7.5 for even and odd n concerning even or odd ν is primarily caused by numerical precision in Newton method (see Figure 7.2-7.3).

In Figure 7.2 it is observed the reduction of μ_j real parts for increasing n: we already characterized the appearance of a new pole for $n = 4$, whose number increases with n, such that mutual poles interaction [39] limits phase

perturbation in resonance conditions eigenstates in the considered distance regime. In conclusion the energetic behavior for acoustic and optical modes is:

- for $n = 2h + 1$ the antisymmetric diagonal block is associated with exact resonances, thus imposing the central qubit as a dynamical mirror to obtain the desired Dirichlet boundary in both chain extrema, which provides the lowest energy mode as an acoustic one whose wavelength coincides with the whole system, as the envelope of the highest energy optical mode;

- for $n = 2h + 1$ symmetric eigenstates displace from exact resonances towards lower (higher) energies if ν is odd (even), with a first moving mode consisting in a deformed optical (acoustic) one, whose envelope wavelength equals to $2/3$ of the lattice length;

- for $n = 2h$ in odd ν exact resonances involve symmetric eigenstates, whose lowest energy mode is acoustic, with half wavelength equal to the lattice length because of Neumann boundaries at the chain center, while the first moving antisymmetric eigenstate towards lower energies is a deformed optical mode whose envelope wavelength is $2/3$ of the whole lattice;

- for $n = 2h$ in even ν optical modes correspond to lower energies in exact resonances because of the anti-Neumann boundary, whose lowest one is endowed with an envelope half wavelength covering the lattice, while the first moving symmetric eigenstate towards higher energies is a deformed acoustic mode with a wavelength equal to $2/3$ of the lattice length.

7.2.3 Nonlinear matrix pencils

The technique implemented in Section 7.2.2 provides analytical results for eigenpairs associated with parity blocks not stable in exact resonance conditions with respect to the inclusion of cut terms, even if in our distance regimes we neglect perturbations in $\theta(E)$, thus causing the appearance of much smaller imaginary component for amplitudes profile $|\boldsymbol{a}\rangle$. To obtain exact real eigenvectors the dyadic product should involve generally $|\boldsymbol{e}(\theta)\rangle$: here we will consider a linear expansion near resonances, even if these result will hold true also in the general case.

Without including parity indices for clarity, the generalized eigenvalue problem analyzed in Section 7.2.2 reads:

$$\left(\Sigma - \mathrm{i}\, n \, \left|\boldsymbol{e}(\theta_j)\right\rangle \left\langle \boldsymbol{e}(\theta_j)\right|\right) \left|\tilde{\boldsymbol{a}}_j\right\rangle = \tilde{\lambda}_j \left|\tilde{\boldsymbol{a}}_j\right\rangle, \tag{7.59}$$

where $\theta_j = \{\pi - \delta\theta_j, 2\pi + \delta\theta_j\}$ with $\delta\theta_j \ll 1$, such that it is possible to expand

$$\mathrm{i}\, n \left(\left|e(\theta_j)\right\rangle\left\langle e(\theta_j)\right| - |u\rangle\langle u|\right) \approx \delta\theta_j\, \mathfrak{M}, \tag{7.60}$$

where $\mathfrak{M}$ is a skew-symmetric Toeplitz matrix with linearly increasing entries as follows:

$$\mathfrak{M} = \begin{pmatrix} 0 & \mp 1 & -2 & \dots \\ \pm 1 & 0 & \mp 1 & \\ 2 & \pm 1 & 0 & \\ \vdots & & & \ddots \end{pmatrix}, \tag{7.61}$$

for respectively odd (even) ν, satisfying the condition required for the application of Gershgorin theorem, which consists in vanishing diagonal elements. More precisely, it states that if the diagonalization of a matrix A, using a similarity transformation X, yields $X^{-1}AX = D + F$, where $D = \mathrm{diag}(d_1, \dots, d_n)$ and $F = (f_{i,j})$ has zero diagonal entries, then the spectrum $\sigma(A) \subseteq \bigcup_{i=1}^{n} D_i$ with $D_i = \left\{z \in \mathbb{C} : |z - d_i| \leq \sum_{j=1}^{n} \left|f_{i,j}\right|\right\}$ [58].

At this stage it is useful to introduce a common tool of linear algebra, named linear matrix pencil and defined as a linear combination of a pair of matrices $A - \lambda B$. Solutions of the generalized eigenvalue problem $\det(A - \lambda B) = 0$ define the eigenvalues λ of the pencil [58]. We can obtain a congruence with another equivalent pair of matrices, as already made in the diagonalization procedure of Bunch-Nielsen-Sørensen for the pencil $\widetilde{\Sigma} - \tilde{\lambda}\mathbb{1}$, by means of the orthogonal transformation Ξ, which maintains $\mathfrak{M}^R = \Xi^T \mathfrak{M} \Xi$ with vanishing diagonal elements.

The complete version of the eigenvalue problem (7.59) corresponds to a nonlinear matrix pencil according to the expansion (7.60), where the successive linear approximation method is applied to obtain a generalized eigenvalue problem [76]

$$\left[\Sigma - \mathrm{i}n\,|u\rangle\langle u| - \left(\delta\theta\left(\tilde{\lambda}_j^{(i)}\right) - \delta\theta'\Big|_{\tilde{\lambda}_j^{(i)}}\, \tilde{\lambda}_j^{(i)}\right)\mathfrak{M}\right]\left|\tilde{a}_j^{(i+1)}\right\rangle = \tilde{\lambda}_j^{(i+1)}\left[\mathbb{1} - \delta\theta'\left(\tilde{\lambda}_j^{(i)}\right)\mathfrak{M}\right]\left|\tilde{a}_j^{(i+1)}\right\rangle. \tag{7.62}$$

To motivate the appearance of numerical eigenstates, as the one for the system with $n = 4$ qubits in Chapter 6, we can observe that more than n solution may be involved if the rank of the right hand side of (7.62) is less than n [58]. In a more general perspective we can include an arbitrary number of orders in the Taylor expansion for $\delta\theta(\tilde{\lambda}_j)$, such that the generalized eigenvalue problem becomes:

$$\left(\Lambda - \mathrm{i}\, n\, |z\rangle\langle z| - \delta\theta(\tilde{\lambda}_j)\mathfrak{M}^R\right)\left|\alpha_j\right\rangle = \tilde{\lambda}_j \left|\alpha_j\right\rangle, \tag{7.63}$$

whose property resides in the complete knowledge of eigenpairs associated with the rank-one modification analyzed in Section 7.2.2. The inclusion of the

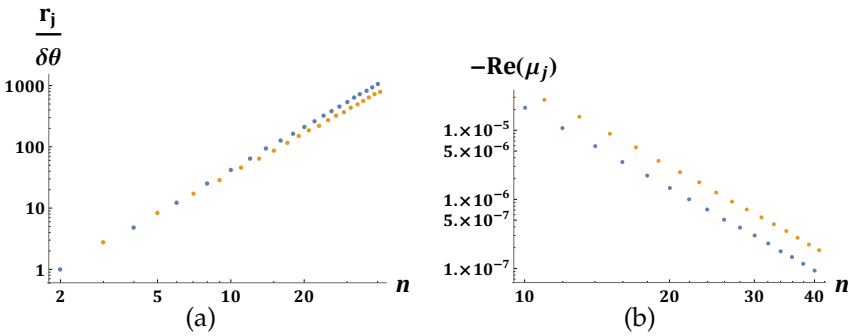

Figure 7.6: Behavior with respect to n for (7.65) in panel (a) regarding the mode j with largest contribution. Linear interpolation in the log-log plot provides a slope for even n equal to 2.33, while for the odd case 2.17. Panel (b) shows the same behavior for the mode j endowed with the largest real part: slopes for linear interpolations in log-log plot are -3.91 for even n and -3.84 for odd n.

perturbation in $\delta\theta(\tilde{\lambda}_j)$ will shift eigenvalues inside Gershgorin disks:

$$\mathcal{G}_j^q = \{z \in \mathbb{C} : |z - \tilde{\lambda}_j| \leq r_j^q(z) c_j^{1-q}(z)\}, \tag{7.64}$$

as defined in their nonlinear extension, named j-th generalized Gershgorin region [10], for every $0 \leq q \leq 1$, where:

$$r_j(z) = \delta\theta(z_j) \sum_{k=1}^{\lceil n/2 \rceil} \left| \mathfrak{M}_{jk}^R \right|, \tag{7.65}$$

$$c_j(z) = \delta\theta(z_j) \sum_{i=1}^{\lceil n/2 \rceil} \left| \mathfrak{M}_{ij}^R \right|. \tag{7.66}$$

In Figure 7.6(a), the behavior in the variation of n for $r_j(z)/\delta\theta(z)$ (for $q = 1$) shows approximately a super-quadratic growth in both cases regarding mode with maximum row contribution. In Figure 7.6(b), the maximum real part of μ_j is endowed with a sub-quartic suppression, such that it lies in Gershgorin regions and it provides an estimation for the upper bound of phase perturbation. These perturbations decrease with n, thus signaling the appearance of new poles, whose Coulomb interaction [39] maintains the analyzed eigensystem in proximity of exact resonance conditions.

Experimental platform interested in the knowledge of the excitation amplitude profile to predict string encoded in the system, without including phase perturbation of the super-radiant state, can obtain important informations using the bound of Gershgorin regions to control the error.

7.3 Multimerization

The research for fragmentation mechanisms in quantum emitters arrays has been investigated prevalently in multi-excitations sectors. It consists in the definition of product states for multipartite subsets of emitters, called multimers, where excitations are stored [103]. Our analysis is constrained in the one-excitation sector, where the product state of multimers is no more valid: it translates in a multipartite global state characterized by annealed singularity conditions of the inverse propagator. The multimerization phenomenon is provided by the determinant factorization, included in the Laplacian matrix structure in iterated block diagonalizations, holding true also concerning their associated sublattices.

The presence of unexcited emitters, working as dynamical mirrors, leads at the hearth of this phenomenon: they yield a double lattice spacing between elements which result decoupled in our approximation. In a physical perspective this motivates exact multimerizations referred only to systems with an odd n, given the presence of a central emitter as a dynamical mirror for every antisymmetric eigenstate. Iterating this procedure to obtain lattice subdivision translates automatically in the research of natural number partitions, causing that only odd numbers obtained in decompositions can be further partitioned.

Let's consider the definition of diagonal blocks presented in Section 7.2. Considering a lattice endowed with $n = 2h + 1$ sites:

$$A_h^-(\eta) = \begin{pmatrix} 2\eta & 1 & & & \\ 1 & 2\eta & 1 & & \\ & \ddots & \ddots & \ddots & \\ & & 1 & 2\eta & 1 \\ & & & 1 & 2\eta \end{pmatrix}, \tag{7.67}$$

where this matrix $A_h^-(\eta) \to -\frac{\mathrm{i}}{b} A_h^-(\eta)$ includes in its definition the cut contribution, with $\eta = \frac{\chi}{2b}$. The determinant of this matrix is $\det A_h^-(\eta) = U_h(\eta)$, consisting in Chebyshev polynomials of the second kind

$$U_h(\eta) = \frac{\left(\eta + \sqrt{\eta^2 - 1}\right)^{h+1} - \left(\eta - \sqrt{\eta^2 - 1}\right)^{h+1}}{2\sqrt{\eta^2 - 1}}, \tag{7.68}$$

obtained imposing $U_1(\eta) = 2\eta$, $U_2(\eta) = 4\eta^2 - 1$ in the recurrence relation $U_{h+1}(\eta) = 2\eta U_h(\eta) - U_{h-1}(\eta)$ [96].

Implementing the diagonalization iteration for $h = 2p$

$$\mathcal{U}_h A_h^-(\eta) \mathcal{U}_h^\dagger = B_p^+(\eta) \oplus B_p^-(\eta), \tag{7.69}$$

yields diagonal blocks

$$B_p^{\pm}(\eta) = \begin{pmatrix} 2\eta & 1 & & & \\ 1 & 2\eta & 1 & & \\ & \ddots & \ddots & \ddots & \\ & & 1 & 2\eta & 1 \\ & & & 1 & 2\eta \pm 1 \end{pmatrix}, \tag{7.70}$$

which is not true when $n = 2h$ becuase the two blocks migrate in different resonance conditions. The associated determinant $L_p^{\pm}(\eta)$ works as a irriducible factor and it is endowed with the same recurrence relation of (7.67), but with new initial conditions $L_1^{\pm}(\eta) = 2\eta \pm 1$, $L_2^{\pm}(\eta) = 4\eta^2 \pm 2\eta - 1$, thus yielding

$$\begin{aligned} L_p^{\pm}(\eta) &= \frac{\left(\eta \pm 1 + \sqrt{\eta^2-1}\right)\left(\eta + \sqrt{\eta^2-1}\right)^p - \left(\eta \pm 1 - \sqrt{\eta^2-1}\right)\left(\eta - \sqrt{\eta^2-1}\right)^p}{2\sqrt{\eta^2-1}} \\ &= U_p(\eta) \pm U_{p-1}(\eta), \end{aligned} \tag{7.71}$$

which represents the factorization:

$$U_h(\eta) = L_{\frac{h}{2}}^{+}(\eta) L_{\frac{h}{2}}^{-}(\eta) = U_{\frac{h}{2}}^2(\eta) - U_{\frac{h}{2}-1}^2(\eta), \tag{7.72}$$

whose proof is given straightforwardly by means of the property $U_m(\eta)U_l(\eta) = \sum_{k=0}^{l} U_{m-l+2k}(\eta)$, applied for the expansion of the right hand side of (7.72), using $m = l = \frac{h}{2}, \frac{h}{2} - 1$. In a similar way we can consider the case of odd h:

$$\mathcal{U}_h A_h^{-}(\eta) \mathcal{U}_h^{\dagger} = C_{\lceil h/2 \rceil}(\eta) \oplus A_{\lfloor h/2 \rfloor}^{-}(\eta), \tag{7.73}$$

thus involving the diagonal block:

$$C_{\lceil h/2 \rceil}(\eta) = \begin{pmatrix} 2\eta & 1 & & & & \\ 1 & 2\eta & 1 & & & \\ & \ddots & \ddots & \ddots & & \\ & & 1 & 2\eta & 1 & \\ & & & 1 & 2\eta & \sqrt{2} \\ & & & & \sqrt{2} & 2\eta \end{pmatrix}. \tag{7.74}$$

The determinant $\det C_{\lceil h/2 \rceil}(\eta) = 2T_{\lceil h/2 \rceil}(\eta)$ works as the irriducible factor

$$T_{\lceil h/2 \rceil}(\eta) = \frac{1}{2}\left(\left(\eta + \sqrt{\eta^2-1}\right)^{\lceil h/2 \rceil} + \left(\eta - \sqrt{\eta^2-1}\right)^{\lceil h/2 \rceil}\right), \tag{7.75}$$

represented by Chebyshev polynomials of the first kind [126], again ruled by the recurrence equation $T_{h+1}(\eta) = 2\eta T_h(\eta) - T_{h-1}(\eta)$ but obtained with initial conditions $T_1(\eta) = 2\eta$, $T_2(\eta) = 4\eta^2 - 2$. This result completes the analysis of determinant factorization for $n = 2h+1$, because of the property $2T_m(\eta)U_l(\eta) = U_{m+l}(\eta) + U_{l-m}(\eta)$, holding true for $l \geq m-1$, where we have to impose $m = \lceil h/2 \rceil$ and $l = \lfloor h/2 \rfloor$ to obtain the desired result, given that $U_{-1}(\eta) = 0$. At each iteration step the factor $U_{\lfloor h/2 \rfloor}(\eta)$ may be further decomposed in a product of the form (7.72) or in the presented mixed product of Chebyshev polynomials of the first and second kind, depending respectively on even or odd $\lfloor h/2 \rfloor$. The procedure stops when diagonal blocks in the form $B^{\pm}$ are obtained. This factorization is exact in the regime of exponentailly small, but non-vanishing first cut contribution b, which lifts the eigenspace degeneracy and allows for a one to one correspondence between qubits energy gap ε and each eigenstate, with fixed coupling constant γ. In the limit of vanishing nearest-neighbor tail interaction any pair of excited emitters is an eigenstate belonging to the $(n-1)$-times degenerate eigenspace, thus losing the factorization description, while the degenaracy lifting is obtained by simple roots of orthogonal polynomials.

A recurrence relation is available also in case $n = 2h$, for the diagonal block associated with eigenstates displaced with respect to the resonant ones, according to a small eigenstate dependent phase perturbation $\delta\theta$. We define again the matrix $\widetilde{B}_h^{\pm}(\eta) \to -\frac{\mathrm{i}}{b}\widetilde{B}_h^{\pm}(\eta)$ and expand up to $O(\delta\theta)$, which reads:

$$\widetilde{B}_h^{\pm}(\eta) = A_h^{-}(\eta) - \frac{2h\mathrm{i}}{b}\left|\boldsymbol{u}^{\pm}\right\rangle\left\langle\boldsymbol{u}^{\pm}\right| + \delta\theta\,\mathfrak{P}, \tag{7.76}$$

where

$$\mathfrak{P} = \begin{pmatrix} \pm(n-1) & n-1 & & \dots & & (\pm 1)^{h+1}(n-1) \\ n-1 & \pm(n-3) & n-3 & & & \\ & n-3 & \pm(n-5) & n-5 & & \\ \vdots & & \ddots & \ddots & \ddots & \vdots \\ & & & 7 & \pm 5 & 5 \\ & & & & 5 & \pm 3 & 3 \\ (\pm 1)^{h+1}(n-1) & & & \dots & 3 & \pm 1 \end{pmatrix}, \tag{7.77}$$

whose determinant $\det \widetilde{B}_h^{\pm} = \widetilde{L}_h^{\pm} + O(\delta\theta)$ is decomposed in the following way:

$$J_h^{\pm}(\eta) = \frac{\widetilde{L}_h^{\pm} - L_h^{\pm}}{2\mathrm{i}/b}. \tag{7.78}$$

This quantity is ruled by the recurrence relation:

$$J_{h+1}^{\pm}(\eta) = \mp J_h^{\pm}(\eta) - (h+1)U_h(\eta), \tag{7.79}$$

where the imposition of $J_1^{\pm}(\eta) = -1$ provides the solution:

$$J_h^{\pm}(\eta) = \frac{\mp(h+1)U_{h-1}(\eta) - hU_h(\eta)}{2(\eta \pm 1)}, \tag{7.80}$$

which imposes a constraint for a real characteristic equation, differing from exact resonance conditions because of a term suppressed for $h \gg 1$ as h^{-1}. These diagonal blocks associated with states displaced from the the resonance condition display a behavior already found in Chapter 6, linked with the definition of two multimers endowed with a half-chain extension, as discussed for the dimerization characterizing the system composed by $n = 4$ qubits. This phenomenon is not linked with annealed singularity condition for sublattices because there is not a double edge separating multimers, but it is driven just by destructive interference.

The multimerization phenomenon works effectively (if possible) as a subdivision of boundary conditions at the extrema of sublattices, under the partitioning condition for the odd n case, by means of the iterated diagonalization procedure. Spin waves characterized in Section 7.2.1 automatically include these properties, thus relating boundary conditions of the lattice, as sublattices obtained in the iterative procedure, with singularity conditions factorization.

Conclusions and Outlook

A conjecture thought to be sound
was that every circle was round

Paul Erdös,
"The magician of Budapest"

Bound states in the continuum emerged in this thesis as a characterizing feature of the Friedrichs-Lee model simulators, thus providing a promising platform in the framework of quantum computing for noise-free memories, able to implement quantum registers [23]. Their description has been achieved by means of propagator poles in the second Riemann sheet and algebraic properties of Chebyshev polynomials for the many-body generalization, based on the graph Laplacian. This structure is related to the interaction among two-level emitters composing the system, imposed by the analytic expression of the self-energy matrix characterizing the reduced system, given by the integration on the complex energy plane. Entangled bound states generation requires a vanishing pole contribution, while remaining cut terms, named tail interactions, lift the degeneracy even if they are exponentially suppressed with distance. According to this characterization we truncated them up to the first cut term, thus implementing a nearest-neighbors approximation, so yielding the regular graph structure associated with vertices of degree equal to two. A careful analysis concerning the estimation for eigenvectors correction in phase perturbations coming from Toeplitz matrices with linearly increasing entries with known eigensystem [16] could provide useful predictions.

Experimental realizations in waveguide QED mimicking the coupling with a single mode should obey this description. Further develpments will concern other kind of bosonic field, as in trapped ions setups involving phonons [12, 23, 29, 86, 99, 100, 105, 118]. In this framework the extension for two-dimensional systems [17] has to be develped, exploiting results concerning graphs Cartesian product, where the Laplacian spectrum is given by linear combination of all possible eigenvalues pairs, thus getting a special attention to associated eigenvectors [4]. Moreover implementations of the Friedrichs-Lee model with

a generic bosonic field will include a physical realization of thermal baths [100], whose inclusion will provide a more suitable description for experimental applications.

The extension of the model for the coupling with more than a single mode of the electromagnetic field provides the possibility of studying higher energies of eigenstates, thus including system size reduction implemented with lower values for interatomic distances. In this condition the emerged new eigenstates below some critical distances could be resilient with respect to the introduction of new decay channels.

Appendix A

Waveguide modes

Let us consider a waveguide of infinite length, parallel to the x axis, characterized by a rectangular cross section with $y \in [0, L_y]$ and $z \in [0, L_z]$. We conventionally assume that $L_y > L_z$. A common choice is $L_y/L_z = 2$. In a generic guide made of a linear dielectric with uniform density and coated by a conducting material, the boundary conditions for the electric and magnetic fields on the surface S read

$$E_x|_S = 0 \qquad \text{and} \qquad \left.\frac{\partial B_x}{\partial n}\right|_S = 0, \tag{A.1}$$

with $\partial/\partial n$ denoting the normal derivative with respect to the surface. Transverse electric (TE) modes are characterized by $E_x = 0$ everywhere in the guide and obtained by imposing $\partial B_x/\partial n = 0$ on the surface. On the other hand, transverse magnetic (TM) modes have $B_x = 0$ identically. If the waveguide is rectangular, the boundary conditions for TE modes reduce to

$$\left.\frac{\partial B_x}{\partial y}\right|_{y=0} = \left.\frac{\partial B_x}{\partial y}\right|_{y=L_y} = \left.\frac{\partial B_x}{\partial z}\right|_{z=0} = \left.\frac{\partial B_x}{\partial z}\right|_{z=L_z} = 0, \tag{A.2}$$

which limits the form of the longitudinal magnetic field to the real part of

$$B_x = B_0 \cos\left(\frac{\ell\pi y}{L_y}\right)\cos\left(\frac{n\pi z}{L_z}\right)e^{i(kx-\omega_{\ell,n}(k)t)}, \tag{A.3}$$

with $(\ell, n) \in \mathbb{N}^2\backslash\{(0,0)\}$ and B_0 a constant.
The integers ℓ and n label the mode $\mathrm{TE}_{\ell,n}$. The dispersion relation with respect to the longitudinal momentum has the same form as a massive relativistic particle,

$$\omega_{\ell,n}(k) = \sqrt{(vk)^2 + \omega_{\ell,n}(0)^2}, \tag{A.4}$$

with $\omega_{\ell,n}(0) = v\left[\left(\frac{\ell\pi}{L_y}\right)^2 + \left(\frac{n\pi}{L_z}\right)^2\right]^{\frac{1}{2}}$, where the mass term is called the *cutoff frequency* of the mode, and $v = (\mu\epsilon)^{-1/2}$ is the phase velocity in the waveguide, assumed isotropic and nondispersive with magnetic permeability μ and dielectric constant ϵ. Since $L_y > L_z$, the $TE_{1,0}$ mode has the lowest cutoff frequency. It can be proved [79] that $\omega_{1,0}(0)$ is also lower than the cutoffs of all TM modes. Thus, at sufficiently low energy the contribution of the higher energy modes can be neglected, and propagation occurs effectively in one dimension.

The $TE_{1,0}$ mode is characterized by the following behavior of the fields

$$B_x = B_0 \cos\left(\frac{\pi y}{L_y}\right) e^{\mathrm{i}(kx-\omega_{1,0}(k)t)}, \tag{A.5}$$

$$B_y = -\mathrm{i}\frac{kL_yB_0}{\pi} \sin\left(\frac{\pi y}{L_y}\right) e^{\mathrm{i}(kx-\omega_{1,0}(k)t)}, \tag{A.6}$$

$$E_z = \mathrm{i}\frac{\omega_{1,0}(k)L_yB_0}{\pi} \sin\left(\frac{\pi y}{L_y}\right) e^{\mathrm{i}(kx-\omega_{1,0}(k)t)}, \tag{A.7}$$

with the other three components vanishing. These fields can be derived from the (transverse) vector potential

$$A_z = \frac{L_yB_0}{\pi} \sin\left(\frac{\pi y}{L_y}\right) e^{\mathrm{i}(kx-\omega_{1,0}(k)t)}. \tag{A.8}$$

Appendix B

Iterative methods

Newton's method

Newton's method, also called the Newton-Raphson method, is a root-finding algorithm used in numerical analysis, with gradually improving approximation. Using the Taylor series of a differentiable function $f(x)$ of one real variable in the vicinity x_0

$$f(x_0 + \epsilon) = f(x_0) + f'(x_0)\,\epsilon + \frac{1}{2}\,f''(x_0)\,\epsilon^2 + \dots \tag{B.1}$$

which, at first order in ϵ, reads

$$f(x_0 + \epsilon) \approx f(x_0) + f'(x_0)\,\epsilon. \tag{B.2}$$

The intersection of this line with the x-axis is $(x_1, 0)$, so setting $f(x_0 + \epsilon) = 0$ and solving for $\epsilon = \epsilon_0$

$$\epsilon_0 = -\frac{f(x_0)}{f'(x_0)}, \tag{B.3}$$

which is the first-order adjustment to the root's position. By letting $x_1 = x_0 + \epsilon_0$, calculating a new ϵ_1, and so on, the process can be repeated until it converges to a fixed point (which is a root) using

$$\epsilon_n = -\frac{f(x_n)}{f'(x_n)}. \tag{B.4}$$

Unfortunately, this procedure can be unstable near a horizontal asymptote or a local extremum. However, with a good initial choice of the root's position, the algorithm can be applied iteratively to obtain

$$x_{n+1} - x_n = -\frac{f(x_n)}{f'(x_n)}, \tag{B.5}$$

which is called the Newton step.

Halley's method

In numerical analysis, Halley's method is a root-finding algorithm used for functions of one real variable with a continuous second derivative. This last condition is needed for the use of the tangent hyperbolas, a second-order tangent which represents an osculating curve.

The second-order Taylor series in the neighbourhood of the point x_n subject to the imposition of $f(x_{n+1}) = 0$, where we exploit Newton's iteration $x_{n+1} = x_n - f(x_n)/f'(x_n)$ yields

$$x_{n+1} - x_n = -\frac{2\, f(x_n)\, f'(x_n)}{2\,[f'(x_n)]^2 - f''(x_n)\, f(x_n)}. \tag{B.6}$$

This expression is called Halley's step and it may also be derived by using an osculating curve of the hyperbola form:

$$h(x) = b + \frac{a}{x - c}, \tag{B.7}$$

where a, b, c are parameters derived by means of the conditions provided by the nature of second-order tangent in the point x_n such that

$$\left\{ a = -4\,\frac{[f'(x_n)]^3}{[f''(x_n)]^2}, b = f(x_n) - 2\,\frac{[f'(x_n)]^2}{f''(x_n)}, c = x_n + 2\,\frac{f'(x_n)}{f''(x_n)} \right\}. \tag{B.8}$$

These parameters have to be inserted in the condition expressing a zero for the hyperbola $h(x_{n+1}) = 0$ to obtain (B.6).

The employment of second-order tangents hyperbolas is translated in a less chaotic behaviour of the Halley's method than the Newton's one: the trajectory, made of the iterations sequence, is less unstable with respect to the choice of the initial point. This approach can be viewed using the extension of these iterative methods in the complex plane, where the basins of attraction are defined by the modulus of the complex function $f(z)$, with $z \in \mathbb{C}$. In practice each set of the form:

$$C_n = \{z \in \mathbb{C} : |h(z)| = |h(z_n)|\}, \tag{B.9}$$

represents the osculating circumference of the level curve:

$$S_n = \{z \in \mathbb{C} : |f(z)| = |f(z_n)|\}, \tag{B.10}$$

endowed with the same curvature of C_n, because of its definition, in the point $z_n = (x_n, y_n)$, where x_n is the real part and y_n the imaginary one.

The uniqueness of the point z_{n+1} as a zero for the hyperbola $h(z)$ is ensured by this latter nature of Möbius transformation, which is a bijection [140].

Bibliography

[1] C. Addis, F. Ciccarello, M. Cascio, G. M. Palma, and S. Maniscalco. "Dynamical decoupling efficiency versus quantum non-Markovianity". In: *New J. Phys.* 17.123004 (2015).

[2] H. Araki, Y. Munakata, M. Kawaguchi, and T. Goto. "Quantum field theory of unstable particles". In: *Progress of Theoretical Physics* 17.3 (1957).

[3] M. O. Araújo, I. Krešić, R. Kaiser, and W. Guerin. "Superradiance in a Large and Dilute Cloud of Cold Atoms in the Linear-Optics Regime". In: *Phys. Rev. Lett.* 117.073002 (2016).

[4] A. Asenjo-Garcia, M. Moreno-Cardoner, A. Albrecht, H. J. Kimble, and D. E. Chang. "Exponential Improvement in Photon Storage Fidelities Using Subradiance and "Selective Radiance" in Atomic Arrays". In: *Phys. Rev. X* 7.031024 (2017).

[5] O. Astafiev, A. M. Zagoskin, A. A. Abdumalikov, Yu. A. Pashkin, T. Yamamoto, K. Inomata, Y. Nakamura, and J. S. Tsai. "Resonance Fluorescence of a Single Artificial Atom". In: *Science* 327.840 (2010).

[6] M. Bajcsy, S. Hofferberth, V. Balic, T. Peyronel, M. Hafezi, A. S. Zibrov, V. Vuletic, and M. D. Lukin. "Efficient All-Optical Switching Using Slow Light within a Hollow Fiber". In: *Phys. Rev. Lett.* 102.203902 (2009).

[7] M. Bello, G. Platero, J. I. Cirac, and A. González-Tudela. "Unconventional quantum optics in topological waveguide QED". In: *Science Advances* 5.7 (2019).

[8] P. R. Berman, D. R. Bates, and B. Bederson(eds.) "Cavity Quantum Electrodynamics". In: *Adv. At. Mol. Opt. Phys., Suppl. 2* (1994).

[9] H. Bernien et al. "Probing many-body dynamics on a 51-atom quantum simulator". In: *Nature* 579 (2017).

[10] D. Bindel and A. Hood. "Localization theorems for nonlinear eigenvalue problems". In: *SIAM J. Matrix Anal. Appl.* 34 (2013).

[11] A. Blais, A. Huang R. S.and Wallraff, S. M. Girvin, and R. J. Schoelkopf. "Cavity quantum electrodynamics for superconducting electrical circuits: An architecture for quantum computation". In: *Phys. Rev. A* 69.062320 (2004).

[12] R. Blatt, J. I. Cirac, A. S. Parkins, and P. Zoller. "Quantum Motion of Trapped Ions". In: *Physica Scripta* T59 (1995), pp. 294–302.

[13] J. Bleuse, J. Claudon, M. Creasey, N. S. Malik, J. M. Gerard, I. Maksymov, J. P. Hugonin, and P. Lalanne. "Inhibition, Enhancement, and Control of Spontaneous Emission in Photonic Nanowires". In: *Phys. Rev. Lett.* 106.103601 (2011).

[14] O. Bratteli and D. W. Robinson. *Operator Algebras and Quantum Statistical Mechanics 2*. Springer-Verlag (Berlin Heidelberg New York), 2002.

[15] J. R. Bunch, C. P. Nielsen, and D. C. Sorensen. "Rank-one modification of the symmetric eigenproblem". In: *Numerische Mathematik* 31.1 (1978), 31–48.

[16] F. Bünger. "Inverses, determinants, eigenvalues, and eigenvectors of real symmetric Toeplitz matrices with linearly increasing entries". In: *Linear Algebra and its Applications* 459 (2014), 595–619.

[17] G. Calajò, M. J. A. Schuetz, H. Pichler, M. D. Lukin, P. Schneeweiss, J. Volz, and P. Rabl. "Quantum acousto-optic control of light-matter interactions in nanophotonic networks". In: *Phys. Rev. A* 99.053852 (2019).

[18] G. Calajó, F. Ciccarello, D. Chang, and P. Rabl. "Atom-field dressed states in slow-light waveguide QED". In: *Phys. Rev. A* 93.033833 (2016).

[19] G. Calajó, Y.-L. L. Fang, H. U. Baranger, and F. Ciccarello. "Exciting a Bound State in the Continuum through Multiphoton Scattering Plus Delayed Quantum Feedback". In: *Phys. Rev. Lett.* 122.073601 (2019).

[20] A. Cantoni and P. Butler. "Eigenvalues and Eigenvectors of Symmetric Centrosymmetric Matrices". In: *Linear Algebra and its Applications* 13 (1976), pp. 275–288.

[21] N. Cherroret, M. Hemmerling, V. Nador, J. T. M. Walraven, and R. Kaiser. "Robust coherent transport of light in multi-level hot atomic vapors". In: *Phys. Rev. Lett.* 122.183203 (2019).

[22] F. Chung and S. T. Yau. "Discrete Green's Functions". In: *Journal of Combinatorial Theory* A 91 (2000), pp. 191–214.

[23] J. I. Cirac and P. Zoller. "Quantum Computations with Cold Trapped Ions". In: *Phys. Rev. Lett.* 74.20 (1995).

[24] J. Clarke and A. I. Braginski. *The SQUID Handbook, Vol. 1, Fundamentals and Technology of SQUIDS and SQUID Systems*. WILEY-VCH Verlag GmbH & Co. KGaA, Weinheim, 2004.

[25] C. Cohen-Tannoudji, J. Dupont-Roc, and G. Grynberg. *Atom-Photon Interactions: Basic Processes and Applications*. Wiley-VCH Verlag GmbH (Weinheim), 1998.

[26] L. N. Cooper. "Bound electron pairs in a degenerate Fermi gas". In: *Phys. Rev.* 104.4 (1956).

[27] D. M. Cvetković, M. Doob, and H. Sachs. *Spectra of Graphs: Theory and Applications*. Wiley (New York), 1998.

[28] B. Dayan, A. S. Parkins, Takao Aoki, E. P. Ostby, K. J. Vahala, and H. J. Kimble. "A Photon Turnstile Dynamically Regulated by One Atom". In: *Science* 319.1062 (2008).

[29] X. Deng. *Entanglement States in Ion Traps: Properties and Applications*. Ph.D thesis, University of München, Germany, 2007.

[30] R. H. Dicke. "Coherence in Spontaneous Radiation Processes". In: *Phys. Rev.* 93.99 (1954).

[31] F. Dinc, A. M. Brańczyk, and I. Ercan. "Real-space time dynamics in waveguide QED: bound states and single-photon-pulse scattering". In: *arXiv:1809:05164* (2018).

[32] P. A. M. Dirac. "The Fundamental Equations of Quantum Mechanics". In: *Proceedings of the Royal Society A: Mathematical, Physical and Engineering Sciences* 109.752 (1925), pp. 642–653.

[33] P. A. M. Dirac. "The Quantum Theory of the Emission and Absorption of Radiation". In: *Proceedings of the Royal Society* A.114 (1927).

[34] H. Dong, Z. R. Gong, H. Ian, L. Zhou, and C. P. Sun. "Intrinsic cavity QED and emergent quasinormal modes for a single photon". In: *Phys. Rev. A* 79.063847 (2009).

[35] Y. Dong, Y.-S. Lee, and K. S. Choi. "Waveguide QED toolboxes for synthetic quantum matter with neutral atoms". In: *arXiv:1712.02020* (2018).

[36] U. Dorner and P. Zoller. "Laser-driven atoms in half-cavities". In: *Phys. Rev. A* 66.023816 (2002).

[37] J. S. Douglas, H. Habibian, C. L. Hung, A. V. Gorshkov, H. J. Kimble, and D. E. Chang. "Quantum many-body models with cold atoms coupled to photonic crystals". In: *Nat. Photonics* 9.326 (2015).

[38] F. P. Dyson. "The S Matrix in Quantum Electrodynamics". In: *Phys. Rev.* 75.1736 (1949).

[39] F. P. Dyson. "A Brownian-Motion Model for the Eigenvalues of a Random Matrix". In: *J. of Math. Phys.* 3.6 (1962).

[40] P. Facchi. *Quantum time evolution: free and controlled dynamics*. Ph.D thesis, Università di Bari, Italy, 2000.

[41] P. Facchi, M. S. Kim, S. Pascazio, F. V. Pepe, D. Pomarico, and T. Tufarelli. "Bound states and entanglement generation in waveguide quantum electrodynamics". In: *Physical Review A* 94.043839 (2016).

[42] P. Facchi, M. Ligabò, and D. Lonigro. "Spectral properties of the singular Friedrichs-Lee Hamiltonian". In: *arXiv:1910.05957* (2019).

[43] P. Facchi, D. Lonigro, S. Pascazio, F. V. Pepe, and D. Pomarico. "Bound states in the continuum for an array of quantum emitters". In: *Physical Review A* 100.023834 (2019).

[44] P. Facchi, D. Lonigro, S. Pascazio, F. V. Pepe, and D. Pomarico. "Spin waves and multimerization for many-body bound states in the continuum". In: *in preparation* (2019).

[45] P. Facchi and S. Pascazio. *La regola d'oro di Fermi*. Bibliopolis (Napoli), 1999.

[46] P. Facchi, S. Pascazio, F. V. Pepe, and D. Pomarico. "Correlated photon emission by two excited atoms in a waveguide". In: *Physical Review A* 98.063823 (2018).

[47] P. Facchi, S. Pascazio, F. V. Pepe, and K. Yuasa. "Long-lived entanglement of two multilevel atoms in a waveguide". In: *J. Phys. Commun.* 2.035006 (2018).

[48] Y. L. L. Fang and H. U. Baranger. "Waveguide QED: Power spectra and correlations of two photons scattered off multiple distant qubits and a mirror". In: *Phys. Rev. A* 91.053845 (2015).

[49] Y. L. L. Fang, H. Zheng, and H. U. Baranger. "One-dimensional waveguide coupled to multiple qubits: photon-photon correlations". In: *EPJ Quantum Technol* 1 (2014).

[50] A. Faraon, E. Waks, D. Englund, I. Fushman, and J. Vučković. "Efficient photonic crystal cavity-waveguide couplers". In: *Appl. Rev. Lett.* 90.073102 (2007).

[51] E. Fermi. "Quantum theory of radiation". In: *Reviews of Modern Physics* 4 (1932).

[52] E. Fermi. "Tentativo di una teoria dei raggi β". In: *La Ricerca Scientifica* 2.12 (1933).

[53] K. O. Friedrichs. "On the Perturbation of Continuous Spectra". In: *Communications on Pure and Applied Mathematics* 1 (1948), pp. 361–406.

[54] C. Gardiner and P. Zoller. *Quantum Noise: A Handbook of Markovian and Non-Markovian Quantum Stochastic Methods with Applications to Quantum Optics*. Springer-Verlag (Berlin Heidelberg), 2000.

[55] T. Giamarchi. *Quantum Physics in One Dimension*. Oxford University Press, 2004.

[56] A. Goban, C. L. Hung, J. D. Hood, S. P. Yu, J. A. Muniz, O. Painter, and H. J. Kimble. "Superradiance for Atoms Trapped along a Photonic Crystal Waveguide". In: *Phys. Rev. Lett.* 115.063601 (2015).

[57] G. H. Golub. "Some modified matrix eigenvalue problems". In: *Siam Rev.* 15.2 (1973), 318–334.

[58] G. H. Golub and C. F. van Loan. *Matrix Computations*. Johns Hopkins University Press, 2013.

[59] C. Gonzalez-Ballestero, F. J. Garcia-Vidal, and E. Moreno. "Non-Markovian effects in waveguide-mediated entanglement". In: *New J. Phys.* 15.073015 (2013).

[60] A. Gonzalez-Tudela, D. Martin-Cano, E. Moreno, L. Martin-Moreno, C. Tejedor, and F. J. Garcia-Vidal. "Entanglement of Two Qubits Mediated by One-Dimensional Plasmonic Waveguides". In: *Phys. Rev. Lett.* 106.020501 (2011).

[61] A. González-Tudela, V. Paulisch, H. J. Kimble, and J. I. Cirac. "Efficient Multiphoton Generation in Waveguide Quantum Electrodynamics". In: *Phys. Rev. Lett.* 118.213601 (2017).

[62] R. M. Gray. "Toeplitz and Circulant Matrices: A Review". In: *Foundations and Trends in Communications and Information Theory* 2.3 (2006), pp. 155–239.

[63] W. Greiner and J. Reinhardt. *Field quantization*. Springer-Verlag (Berlin Heidelberg New York), 1996.

[64] M. Gross and S. Haroche. "Superradiance: An essay on the theory of collective spontaneous emission". In: *Phys. Rep.* 93.301 (1982).

[65] X. Gu, A. F. Kockum, A. Miranowicz, Y.-X. Liu, and F. Nori. "Microwave photonics with superconducting quantum circuits". In: *Phys. Rep.* 1 (2017), pp. 718–719.

[66] P. Guimond, H. Pichler, A. Rauschenbeutel, and P. Zoller. "Chiral quantum optics with V-level atoms and coherent quantum feedback". In: *Phys. Rev. A* 94.033829 (2016).

[67] Q. Guo et al. "Dephasing-Insensitive Quantum Information Storage and Processing with Superconducting Qubits". In: *Physical Review Letters* 121.130501 (2018).

[68] N. J. Hale N. Higham and L. N. Trefethen. "Computing A^α, log(A), and related matrix functions by contour integrals". In: *SIAM J. Numer. Anal.* 46.5 (2008), 2505–2523.

[69] B. C. Hall. *Quantum Theory for Mathematicians*. Springer-Verlag (Berlin Heidelberg Dordrecht London), 2013.

[70] B. C. Hall. *Lie Groups, Lie Algebras, and Representations: An Elementary Introduction*. Springer-Verlag (Berlin Heidelberg Dordrecht London), 2015.

[71] S. Haroche, (eds.) J. Dalibard, J.-M. Raimond, and J. Zinn-Justin. "Fundamental Systems in Quantum Optics". In: *Proceedings of the Les Houches Summer School of Theoretical Physics* (1992), p. 767.

[72] E. A. Hinds. "Cavity Quantum Electrodynamics". In: *Adv. At. Mol. Opt. Phys.* 28.237 (1990).

[73] I. C. Hoi, A. F. Kockum, L. Tornberg, A. Pourkabirian, G. Johansson, P. Delsing, and C. M. Wilson. "Probing the quantum vacuum with an artificial atom in front of a mirror". In: *Nat. Phys.* 11.1045 (2015).

[74] C. K. Hong, Z. Y. Ou, and L. Mandel. "Measurement of subpicosecond time intervals between two photons by interference". In: *Phys. Rev. Lett.* 59.2044 (1987).

[75] C. W. Hsu, B. Zhen, A. D. Stone, J. D. Joannopoulos, and Marin Soljačić. "Bound states in the continuum". In: *Nat. Rev. Mater.* 1.16048 (2016).

[76] X. Huang, Z. Bai, and Y. Su. "Nonlinear rank-one modification of the symmetric eigenvalue problem". In: *J. of Comp. Math.* 28 (2010).

[77] A. Imamoglu, D. D. Awschalom, G. Burkard, D. P. DiVincenzo, D. Loss, M. Sherwin, and A. Small. "Quantum Information Processing Using Quantum Dot Spins and Cavity QED". In: *Phys. Rev. Lett.* 83.20 (1999).

[78] N. Sh. Izmailian and R. Kenna. "A generalised formulation of the Laplacian approach to resistor networks". In: *J. of Stat. Mech.: Th. and Exp.* (2014).

[79] J. D. Jackson. *Classical Electrodynamics*. John Wiley & Sons (New York), 1999.

[80] T. Kato. *Perturbation Theory for Linear Operators*. Springer-Verlag (Berlin Heidelberg), 1995.

[81] A. F. Kockum, G. Johansson, and F. Nori. "Decoherence-Free Interaction between Giant Atoms in Waveguide Quantum Electrodynamics". In: *Phys. Rev. Lett.* 120.140404 (2018).

[82] Y. Kuramoto and K. Kato. *Dynamics of One-Dimensional Quantum Systems: Inverse-Square Interaction Models*. Cambridge University Press, 2009.

[83] M. Laakso and M. Pletyukhov. "Scattering of Two Photons from Two Distant Qubits: Exact Solution". In: *Phys. Rev. Lett.* 113.183601 (2014).

[84] K. Lalumière, B. C. Sanders, A. F. van Loo, A. Fedorov, A. Wallraff, and A. Blais. "Input-output theory for waveguide QED with an ensemble of inhomogeneous atoms". In: *Phys. Rev. A* 88.043806 (2013).

[85] T. D. Lee. "Some special examples in renormalizable field theory". In: *Physical Review* 95.5 (1954).

[86] D. Leibfried, R. Blatt, C. Monroe, and D. Wineland. "Quantum dynamics of single trapped ions". In: *Rev. Mod. Phys.* 75 (2003).

[87] Y. Li, O. Voskoboynikov, C.P. Lee, and S.M. Sze. "Computer simulation of electron energy levels for different shape InAs/GaAs semiconductor quantum dots". In: *Comp. Phys. Comm.* 141 (2001), 66–72.

[88] N. Lindlein, R. Maiwald, H. Konermann, M. Sondermann, U. Peschel, and G. Leuchs. "A new 4π geometry optimized for focusing on an atom with a dipole-like radiation pattern". In: *Laser Phys.* 17.927 (2007).

[89] P. Lodahl, S. Mahmoodian, and S. Stobbe. "Interfacing single photons and single quantum dots with photonic nanostructures". In: *Rev. Mod. Phys.* 87.347 (2015).

[90] P. Lodahl, S. Mahmoodian, S. Stobbe, A. Rauschenbeutel, P. Schneeweiss, and J. Volz. "Chiral quantum optics". In: *Nature* 541.473 (2017).

[91] F. Lombardo F. Ciccarello and G. M. Palma. "Photon localization versus population trapping in a coupled-cavity array". In: *Phys. Rev. A* 89.053826 (2014).

[92] D. Lonigro, P. Facchi, and M. Ligabò. "The Friedrichs-Lee Model and Its Singular Coupling Limit". In: *Proceedings IQIS 2018* 12.1 (2019).

[93] A. F. van Loo, A. Fedorov, K. Lalumière, B. C. Sanders, A. Blais, and A. Wallraff. "Photon-Mediated Interactions Between Distant Artificial Atoms". In: *Science* 342.1494 (2013).

[94] W. H. Louisell. *Quantum Statistical Properties of Radiation*. John Wiley & Sons (New York), 1973.

[95] H. Nakazato, M. Namiki, and S. Pascazio. "Temporal behavior of quantum mechanical systems". In: *Int. J. Mod. Phys. B* 10.247 (1996).

[96] P. L. Nash. "Chebyshev polynomials and quadratic path integral". In: *Journal of Mathematical Physics* 27.2963 (1986).

[97] O. Nikodym. "Sur une généralisation des intégrales de M. J. Radon". In: *Fundamenta Mathematicae* 15 (1930), 131–179.

[98] G. Oreg Y. Refael and F. von Oppen. "Helical Liquids and Majorana Bound States in Quantum Wires". In: *Physical Review Letters* 115.177002 (2010).

[99] M. Orszag. *Quantum Optics, Including Noise Reduction, Trapped Ions, Quantum Trajectories and Decoherence*. Springer Verlag Berlin-Heidelberg, 2008.

[100] G. M. Palma, K.-A. Suominen, and A. K. Ekert. "Quantum computers and dissipation". In: *Proc. R. Soc. Lond. A* 452 (1996), pp. 567–584.

[101] V. Paulisch, H. Kimble, and A. González-Tudela. "Universal quantum computation in waveguide QED using decoherence free subspaces". In: *New J. Phys.* 18.043041 (2016).

[102] M. E. Peskin and D. V. Schroeder. *An Introduction to Quantum Field Theory*. Addison-Wesley Publishing Company, 1995.

[103] H. Pichler, T. Ramos, A. J. Daley, and P. Zoller. "Quantum optics of chiral spin networks". In: *Phys. Rev. A* 91.042116 (2015).

[104] H. Pichler and P. Zoller. "Photonic Circuits with Time Delays and Quantum Feedback". In: *Phys. Rev. Lett.* 116.093601 (2016).

[105] D. Porras and J. I. Cirac. "Bose–Einstein Condensation and strong correlation behavior of phonons in ion traps". In: *Phys. Rev. Lett.* 93 (2004).

[106] M. Pulvirenti. *Scaling Limits and Effective Equations in Kinetic Theory*. Lectures in Gran Sasso Science Institute (L'Aquila), 2017.

[107] J. M. Raimond, M. Brune, and S. Haroche. "Manipulating quantum entanglement with atoms and photons in a cavity". In: *Rev. Mod. Phys.* 73.565 (2001).

[108] J. M. Raimond, P. Facchi, B. Peaudecerf, S. Pascazio, C. Sayrin, I. Dotsenko, S. Gleyzes, M. Brune, and S. Haroche. "Quantum Zeno dynamics of a field in a cavity". In: *Physical Review A* 86.032120 (2012).

[109] T. Ramos, H. Pichler, A. Daley, and P. Zoller. "Quantum Spin Dimers from Chiral Dissipation in Cold-Atom Chains". In: *Phys. Rev. Lett.* 113.237203 (2014).

[110] T. Ramos, B. Vermersch, P. Hauke, H. Pichler, and P. Zoller. "Non-Markovian dynamics in chiral quantum networks with spins and photons". In: *Phys. Rev. A* 93.062104 (2016).

[111] E. S. Redchenko and V. I. Yudson. "Decay of metastable excited states of two qubits in a waveguide". In: *Phys. Rev. A* 90.063829 (2014).

[112] M. Reed and B. Simon. *Methods of Modern Mathematical Physics I: Functional Analysis*. Academic Press, 1980.

[113] M. E. Reimer, G. Bulgarini, N. Akopian, M. Hocevar, M. B. Bavinck, M. A. Verheijen, E. P. A. M. Bakkers, L. P. Kouwenhoven, and V. Zwiller. "Bright single-photon sources in bottom-up tailored nanowires". In: *Nat. Commun.* 3.737 (2012).

[114] A. Rosario Hamann, C. Müller, M. Jerger, M. Zanner, J. Combes, M. Pletyukhov, M. Weides, T. M. Stace, and A. Fedorov. "Nonreciprocity Realized with Quantum Nonlinearity". In: *Phys. Rev. Lett.* 121.123601 (2018).

[115] C. M. Roy D. Wilson and Firstenberg O. "Colloquium: Strongly interacting photons in one-dimensional continuum". In: *Rev. Mod. Phys.* 89.021001 (2017).

[116] J. J. Sakurai. *Modern Quantum Mechanics*. Addison-Wesley Publishing Company, 1994.

[117] E. Sanchez-Burillo, D. Zueco, L. Martin-Moreno, and J. J. Garcia-Ripoll. "Dynamical signatures of bound states in waveguide QED". In: *Phys. Rev. A* 96.023831 (2017).

[118] C. Schneider, D. Porras, and T. Schaetz. "Experimental quantum simulations of many-body physics with trapped ions". In: *Rep. Prog. Phys.* 75 (2012).

[119] E. Schrödinger. "An undulatory theory of the mechanics of atoms and molecules". In: *Physical Review* 28.6 (1926).

[120] J. Schwinger. "On Green's functions of quantized fields". In: *PNAS* 37 (1951), 452–459.

[121] J. Schwinger. "Field theory of unstable particles". In: *Annals of physics* 9 (1960).

[122] E. Shahmoon and G. Kurizki. "Nonradiative interaction and entanglement between distant atoms". In: *Phys. Rev. A* 87.033831 (2013).

[123] J. T. Shen and S. Fan. "Coherent Single Photon Transport in a One-Dimensional Waveguide Coupled with Superconducting Quantum Bits". In: *Phys. Rev. Lett.* 95.213001 (2005).

[124] T. Shi, D. E. Chang, and J. I. Cirac. "Multiphoton-scattering theory and generalized master equations". In: *Phys. Rev. A* 92.053834 (2015).

[125] T. Shi, Y. H. Wu, A. Gonzalez-Tudela, and J. I. Cirac. "Bound States in Boson Impurity Models". In: *Phys. Rev. X* 6.021027 (2015).

[126] M. A. Snyder. *Chebyshev methods in numerical approximation*. Prentice-Hall Inc., 1966.

[127] P. Solano, J. A. Grover, J. E. Hoffman, S. Ravets, F. K. Fatemi, L. A. Orozco, and S. L. Rolston. "Optical Nanofibers: A New Platform for Quantum Optics". In: *Advances In Atomic, Molecular, and Optical Physics* 51 (2017), 439–505.

[128] G. Teschl. *Mathematical Methods in Quantum Mechanics*. 2005.

[129] T. S. Tsoi and C. K. Law. "Quantum interference effects of a single photon interacting with an atomic chain inside a one-dimensional waveguide". In: *Phys. Rev. A* 78.063832 (2008).

[130] T. Tufarelli, F. Ciccarello, and M. S. Kim. "Dynamics of spontaneous emission in a single-end photonic waveguide". In: *Phys. Rev. A* 87.013820 (2013).

[131] P. J. Ungar, D. S. Weiss, E. Riis, and S. Chu. "Optical molasses and multilevel atoms: theory". In: *J. Opt. Soc. Am. B* 6.11 (1989).

[132] E. Vetsch, D. Reitz, G. Sague, R. Schmidt, S. T. Dawkins, and A. Rauschenbeutel. "Optical Interface Created by Laser-Cooled Atoms Trapped in the Evanescent Field Surrounding an Optical Nanofiber". In: *Phys. Rev. Lett.* 104.203603 (2010).

[133] A. Wallraff, D. I. Schuster, A. Blais, L. Frunzio, R. S. Huang, J. Majer, S. Kumar, S. M. Girvin, and R. J. Schoelkopf. "Strong coupling of a single photon to a superconducting qubit using circuit quantum electrodynamics". In: *Nature* 431.162 (2004).

[134] Z.R. Wasilewski, S. Fafard, and J.P. McCaffrey. "Size and shape engineering of vertically stacked self-assembledquantum dots". In: *Journal of Crystal Growth* 201/2021.1131 (1999).

[135] A.-M. Wazwaz. *Linear and Nonlinear Integral Equations: Methods and Applications*. Springer Verlag Berlin-Heidelberg, 2011.

[136] S. Weinberg. *The Quantum Theory of Fields, Volume I: Foundations*. Cambridge University Press, 1995.

[137] E. P. Wigner. "Random matrices in physics". In: *SIAM Review* (1967).

[138] D. Witthaut and A. S. Sørensen. "Photon scattering by a three-level emitter in a one-dimensional waveguide". In: *New J. Phys.* 12.043052 (2010).

[139] W. K. Wootters. "Entanglement of Formation of an Arbitrary State of Two Qubits". In: *Phys. Rev. Lett.* 80.2245 (1998).

[140] L. Yau and A. Ben-Israel. "The Newton and Halley Methods for Complex Roots". In: *The American Mathematical Monthly* 105 (1998), 806–818.

[141] J. Q. You and F. Nori. "Atomic physics and quantum optics using superconducting circuits". In: *Nature* 474.589 (2011).

[142] V. I. Yudson. "Dynamics of the integrable one-dimensional system "photons + two-level atoms"". In: *Phys. Lett. A* 129.17 (1988).

[143] V. I. Yudson and P. Reineker. "Multiphoton scattering in a one-dimensional waveguide with resonant atoms". In: *Phys. Rev. A* 78.052713 (2008).

[144] X. H. H. Zhang and H. U. Baranger. "Heralded Bell State of Dissipative Qubits Using Classical Light in a Waveguide". In: *Phys. Rev. Lett.* 122.140502 (2019).

[145] H. Zheng and H. U. Baranger. "Persistent Quantum Beats and Long-Distance Entanglement from Waveguide-Mediated Interactions". In: *Phys. Rev. Lett.* 110.113601 (2013).

[146] G. Zumofen, N. M. Mojarad, V. Sandoghdar, and M. Agio. "Perfect Reflection of Light by an Oscillating Dipole". In: *Phys. Rev. Lett.* 101.180404 (2008).

Acknowledgements

During last years I have benefited from teachings given by Saverio Pascazio, Paolo Facchi and Francesco Pepe, driving me both professionally and temperamentally. In particular I want to express my gratitude for their support, based on a continuous invitation at interpreting what mathematics means in physics. Following the same line I thank Hiromichi Nakazato, Kazuya Yuasa, Giuseppe Florio and Marilena Ligabò whose experience helped me in multiple aspects of the PhD. A sincere acknowledgement is addressed to Davide Lonigro for our fruitful collaboration driven by our supervisors, essential in targeting topics presented in this thesis. Let me thank also Giovanni Gramegna and Giovanni Scala for the exploration of complementary knowledge of equal importance. It is also a pleasure to thank the "extended" group I met in Vietri, San Rufo-Policeta, Bologna, Trieste, Torun and Milano for keeping me dreaming about mathematical physics, as the medical physics group who enriched me with completely new perspectives.

A special acknowledgement is reserved for the friendships with Margherita Altamura, Alessandro Cataldi, Stefano Dello Russo, Lino Digregorio, Giuseppe Negro, Francesco Pavese, Pasquale Ricci, Roberta Sergio, Daniela Trisciuzzi, Alessandro Vitale and everyone who helped me in growing up during the PhD experience. My gratitude is referred to Adi and Link, constantly seen in supporting students hungry for culture.

I will always be grateful to my parents for letting me meet science from my childhood and driving me in its exploration. At the same time I will always recognize the central role played by them together with my sister, brother, grandparents, aunts, uncles, cousins and all friends in my hometown, in never giving up with their fundamental help.

Thanks very much to all of you, including all those are not explicitly mentioned: this thesis is "entangled" with each experience we shared!